Engineering and structural characterization of cross-reactive, pH-sensitive antibodies against the long-chain α-neurotoxins

Wade, Jack

Publication date:
2023

Document Version
Publisher's PDF, also known as Version of record

Engineering and structural characterization of cross-reactive, pH-sensitive antibodies against the long-chain α-neurotoxins

PhD thesis by Jack Wade
Main supervisor: Andreas H. Laustsen-Kiel
Co-supervisor: Jens Preben Morth
Department of Biotechnology and Biomedicine
The Technical University of Denmark
February 2023

Contents

Preface

The work presented in this thesis was carried out from March 1st 2020 to February 28th 2023, at the Technical University of Denmark (DTU) in the Department of Biotechnology and Biomedicine, under the supervision of Professor Andreas Hougaard Laustsen-Kiel and co-supervisor Professor Jens Preben Morth.

This thesis describes the development and structural characterization of neutralizing antibodies against long-chain α-neurotoxins. The research is presented in the form of manuscripts and has involved multiple interactions with different collaborations. My contributions to each of the articles are outlined below.

Paper 1. 'Advances in antibody phage display technology'
Contribution: I wrote the phage display library types and designs section.

Manuscript 1. Discovery and optimization of a broadly-neutralizing human monoclonal antibody against long-chain α-neurotoxins from snakes
In this manuscript, I characterized the antibodies used in the main body of this thesis by surface plasmon resonance. I was involved in writing parts of the manuscript related to antibody characterization and responding to reviewer feedback.

Manuscript 2. Structure of a neurotoxin-neutralizing antibody reveals determinants for broad reactivity and a pH-responsive allosteric switch
I designed the study and performed all experiments, analysis, writing and preparation of figures. The antibody Fab fragments used for screening in manuscript 3 were produced at the National Biologics Facility, DTU. I produced all other protein for crystallography.

Manuscript 3. An antibody framework module that confers modular pH-dependent antigen binding properties
I co-conceptualized the study, designed and produced the phage display library, and conducted an initial test phage display selection round, which was up-scaled in the library validation presented in the manuscript, and involved a multi-collaborative effort with scientists in the Centre for Antibody Technologies.

Manuscript 4. Generation of Multivalent Nanobody-Based Proteins with Improved Neutralization of Long α-Neurotoxins from Elapid Snakes
In collaboration with Charlotte Rimbault, I characterized different multivalent nanobody fusion proteins by DLS, FIDA, and SEC. Characterization by ITC was performed in Prof. Maher Abou Hachem lab with Esperanza Rivera De Torre in the Department of Biotechnology and Biomedicine. Functional testing and antibody production was performed by external collaborators stated in the article affiliations. I was responsible for writing the manuscript and preparing figures, mediating external collaborations, and addressing reviewer feedback.

Acknowledgements

Firstly, I would like to thank Andreas for giving me the opportunity to pursue a PhD in your group. It was a tough start at the beginning of the pandemic, but the video calls during that time whilst I was in living in the 'trash cans' at the university (as you described them – correctly) helped make the time more bearable. The freedom you allow to pursue different ideas, no matter how crazy, and the culture you have created in the group has collectively made my time in Denmark one I will look back on fondly.

I would like to thank my co-supervisor Preben, for your genuine passion, positivity and ideas in the different projects. Seeing your rigorous approach to science and the pride you take in your work has shaped my own outlook. I'm really proud of the results and there have also been some great laughs doing it, especially making Jenkins errors.

I'm grateful to all my work colleagues, past and present, in the Center for Antibody Technologies for how collaborative and supportive everyone has been throughout the last three years. Special thanks go to Charlotte and Esperanza, not only for the work we have done together on different projects but for keeping the storm that can be the CAT lab at times functional. Thanks to the structure folks: Markus, Giang, Tine and Suzanna for your input and to Nina for your work in laying the groundwork for the crystallography project. Also thanks to Tom for your input into the scaffold project, and to Anne for your feedback with writing. Lastly, thanks to Maher for providing easy access to your equipment at various points.

For making sure that I didn't become too much of a recluse, special thanks to Line and Anna (for hosting so many parties, all of which were great), Cecilie Knudsen, Yessica, and Tulika (for the less wild social events, walks, food and movies), Cecilie Clausen and Helen (for a mix of everything, but mainly for not taking offence to me sleeping whilst hanging out, or for taking pictures of me doing it -_-), Kostas (BBQs, long may they continue), Tim and Chris (mainly for preventing my late night biking excursions back from Copenhagen), Maike and Charlotte Christensen (for organising and always being down for socialising, no matter the scale), and Christina for the best adventures here in Denmark (xD).

I'd also like to thank some people outside of DTU, Anne Knudsen (for the sanity checks) and Billy and Puneet with coding.

Lastly, I would like to thank my family for all the encouragement and support you have given me, not just in the past three years but throughout. No matter what it was, you have always believed in me. There were some updates in the end, this work is for you.

Abstract

Antibodies are proteins secreted by immune cells during the immune response to a pathogen. By binding to the surfaces of pathogens with high affinity and specificity, antibodies both neutralize pathogens and coordinate the immune response. To generate an effective antibody immune response, the immune system samples over 10^8 unique antibodies in the naïve antibody repertoire, which expands exponentially following a pathogenic challenge. For over a century, the treatment of snakebite envenomings has taken advantage of the ability of the immune system to generate highly potent, broadly neutralizing antibodies by immunizing large animals with snake venoms and extracting the antibodies for treatment. This forms modern-day antivenom and validates the capability of antibodies to neutralize the venom of different snakes. However, as the antibodies are of non-human origin, they have an increased likelihood of causing adverse reactions when used to treat snakebite victims due to their heterologous nature, which is associated with high immunogenicity. Therefore, developing an antivenom that consists of human antibodies is one approach to improving snakebite treatment.

Antibodies are both highly potent and specific for their target and are heavily used as therapeutics, accounting for over half of the approved biopharmaceuticals in the last 4 years. Beyond their high affinity and specificity, antibodies have been engineered to have different mechanisms of action. For example, a generation of antibodies has been developed to bind non-stoichiometrically, to neutralize more than one target molecule in their lifetime, allowing them to be administered at a lower dose than a conventional antibody. These antibodies require their binding affinity to be pH-dependent, specifically to have a low affinity at acidic pH, allowing the antibodies to release antigens for lysosomal degradation whilst being exposed to low pH during cellular recycling. As a result, antibodies are returned to the bloodstream unbound and ready to bind to another target molecule at neutral pH. This property could potentially help lower the dose and economic feasibility of a more efficacious antivenom for developing countries affected by snakebite. Further, developing antibodies that are cross-reactive, and therefore can bind to structurally similar toxins in different snakes, would broaden the usage (polyvalence) of a prospective antivenom and lower the number of antibodies required for treatment.

This thesis focuses on the development of neutralizing human monoclonal antibodies against long-chain α-neurotoxins from elapid snakes and understanding the molecular determinants underpinning pH-dependent antigen binding in antibodies. We began by discovering antibodies from a naïve human antibody phage display library and optimizing them for improved cross-reactivity through light chain shuffling. By doing so, we enhanced the neutralization capacity of one antibody *in vivo*, showcasing the use of phage display technology and light chain shuffling as an approach to discovering broadly neutralizing antibodies against this toxin family (Chapter 4).

Building further upon the abovementioned study, we report the crystal structure of one of these antibodies bound to a long-chain α-neurotoxin, determined at 1.6 Å, and elucidate the basis for the neutralization mechanism of this lineage of antibodies. Through the antibody heavy chain complementary determining region 3, these antibodies mimicked conserved interactions between long-chain α-neurotoxins and the acetylcholine receptor to neutralize long-chain α-neurotoxins and achieve broad cross-reactivity. This antibody also bound pH-dependently to all long-chain α-neurotoxins tested, initiating further structural studies to investigate the pH-dependent binding mechanism. Determining the structures of the antibody bound to long-chain α-neurotoxin at different pH identified a network of residues that respond in concert to low pH in the antibody structure, located at the interface

between the antibody heavy and light chain (Chapter 5). Thus, these data provide an indication of a paratope-independent, pH-sensitive binding mechanism.

The discovery of pH-dependent antibodies is low throughput and necessitates multiple engineering steps and discovery campaigns to tune the antibody affinity at both neutral and acidic pH. This thesis aimed to improve the discovery of pH-dependent antibodies using *in vitro* display technology. We had observed that pH-dependent antigen binding could be encoded exclusively away from the paratope, potentially in the heavy-light chain interface, and used this insight to conceptualize an approach to engineer a generic pH switch into the antibody variable domain. We designed and validated a phage display library targeting the antibody heavy-light chain interface framework region to introduce a generic pH switch into the antibody variable domain. With pH-dependent binding engineered as a pre-determined feature into antibodies, we envisage a high throughput approach to discovering and/or engineering pH-dependent antibodies using *in vitro* display technologies *a priori* (Chapter 6).

Lastly, we employed a self-assembly protein domain to expand the valence and neutralization capacity of nanobodies targeting long-chain α-neurotoxins and validated parameters important for their application (Chapter 7). We produced stable, multivalent nanobody-based proteins engineered to contain up to sixteen binding domains that display enhanced neutralization potency of long-chain α-neurotoxins *in vitro*, and were able to be recycled in a cellular assay when engineered to contain IgG-Fc.

Overall, this work defines the molecular determinants of antibody recognition and neutralization of long-chain α-neurotoxins, which will be useful to guide the engineering of these antibodies to improve their neutralization potency for use in a recombinant antivenom. I have also developed an approach to enhance the neutralization capacity of nanobodies and expand their half-life and effector function properties, which might facilitate the use of nanobodies in the treatment of different diseases. Furthermore, the molecular insights gained through the work behind this thesis on pH-dependent antigen binding can be used to guide the engineering of this property into antibodies. This will have utility in improving the pharmacology of antibodies that suffer from target-mediated clearance, improve their cost-effectiveness by having a longer duration of action and a lower administration dose, and potentially yield therapies with better patient compliance (due to more infrequent dosing). Lastly, the insights acquired into how antibodies bind pH-dependently to their target due to properties lying outside of the paratope and epitope interface may have many further implications in the *de novo* discovery of antibodies with pH-dependent binding properties. One example includes the design of specialized *in vitro* display antibody libraries with pre-established pH-dependent binding properties that could be used in a generic fashion to discover recycling antibodies and/or antibodies that engage with their target antigen at exact anatomical locations at the right time. My hope is that this will one day lead to more efficient development of therapies against snakebite envenoming, but also beyond in areas such as oncology, infectious diseases, and autoimmune diseases.

Sammenfatning

Antistoffer er proteiner, der dannes af immunsystemet som reaktion på patogener. Som en del af immunresponset udskilles antistoffer af B-celler og binder sig til patogener med høj affinitet og specificitet for at neutralisere dem og koordinere immunresponset. For at antistoffer i princippet kan genkende ethvert patogen, udtager immunrepertoiret over 108 unikke antistoffer i det naive antistofrepertoire, som eksponentielt udvides efter en patogen påvirkning. I over et århundrede har man ved behandlingen af slangebidforgiftninger draget fordel af immunsystemets evne til at generere meget potente, bredt neutraliserende antistoffer ved at immunisere store dyr med slangegift og udvinde antistofferne med henblik på behandling. Dette udgør den nuværende modgift og bekræfter antistoffernes evne til at neutralisere giften fra forskellige slanger. Da antistofferne imidlertid er af ikke-menneskelig oprindelse, er der større risiko for bivirkninger, når de anvendes til behandling af slangebidsofre på grund af deres høje immunogenicitet. Derfor er udvikling af en modgift, der består af menneskelige antistoffer, en af metoderne til at forbedre behandlingen af slangebid.

En generation af antistoffer er blevet udviklet til at binde mere end ét målmolekyle og derfor kan administreres i en lavere dosis end et konventionelt antistof, som kun kan binde et enkelt molekyle én gang. Disse antistoffer kræver, at deres bindingsaffinitet er pH-afhængig, således at antistoffet binder med høj affinitet ved neutral pH, men med lav affinitet ved en sur pH-værdi. Dette gør det muligt for antistoffer at frigive antigener til nedbrydning, mens antistofferne udsættes for en lav pH-værdi under den cellulære genanvendelse. Antistofferne returneres efterfølgende til blodbanen og er klar til at binde sig til et andet målmolekyle ved neutral pH-værdi. Denne egenskab kan sænke den dosis, der er nødvendig for behandlingen med antistoffer, hvilket er relevant for udviklingslande, der er plaget af slangebid. Endvidere vil udvikling af antistoffer, der er krydsreaktive og derfor kan binde til strukturelt ens toksiner i forskellige slanger, kunne udvide anvendelsen af en fremtidig modgift og reducere antallet af antistoffer, der er nødvendige for behandlingen.

Denne afhandling indledes med udviklingen af neutraliserende humane monoklonale antistoffer mod langkædede α-neurotoksiner fra elapideslanger. Antistofferne blev fundet fra et naivt humant antistof-fagdisplay-bibliotek og optimeret med henblik på forbedret krydsreaktivitet ved hjælp af udskiftning af de lette kæder. Ved at optimere antistoffets lette kæde transformerede vi et antistofs neutraliseringskapacitet *in vivo* og viste derved brugen af phage display-teknologi og udskiftningen af de lette kæder som en metode til at finde bredt neutraliserende antistoffer mod denne toksinfamilie (Manuskript II). Vi rapporterer krystalstrukturen af et af disse antistoffer (2555_01_A01) bundet til α-cobratoksin ved 1,6 Å og belyser neutraliseringsmekanismen for denne type antistoffer, der er opdaget ved hjælp af phage display, ved hjælp af receptormimikering. Der blev foretaget yderligere strukturelle undersøgelser for at undersøge den pH-afhængige bindingsmekanisme for dette antistof, som binder pH-afhængigt til alle testede langkædede α-neurotoksiner. Ved at bestemme strukturen af 2555_01_A01 bundet til α-cobratoksin mellem pH 6,0 - pH 4,5 blev der identificeret et netværk af aminosyrerester placeret ved grænsefladen mellem antistoffets tunge og lette kæde, der reagerer i samspil ved lav pH-værdi i antistofstrukturen (Manuskript III). Dette giver således en indikation for en paratop-uafhængig, pH-følsom bindingsmekanisme.

Konceptet om en paratop-uafhængig, pH-følsom bindingsmekanisme blev videreudviklet ved at konceptualisere et pH-følsomt antistofstillads med henblik på at forbedre opdagelsen af antistoffer med denne bindingsegenskab *in vitro*. Med henblik herpå har vi designet og valideret et phage display-bibliotek til afprøvning af denne fremgangsmåde (Manuskript IV).

Endelig har vi anvendt et selvsamlingsdomæne til at udvide valens- og neutraliseringskapaciteten af langkædede α-neurotoksiner og valideret parametre, der er vigtige for deres anvendelse (Manuskript V). Dette arbejde definerer samlet set de molekylære determinanter for antistofgenkendelse og neutralisering af langkædede α-neurotoksiner, som sammen med evalueringen af forskellige multivalente formater vil være retningsgivende for udviklingen af neutraliserende antistoffer mod denne familie af toksiner. Endelig vil den molekylære indsigt i pH-determinanter, der fører til pH-afhængig antigenbinding, give grundlag for den fremtidige udvikling og opdagelse af pH-afhængige antistoffer.

Publications

Papers included in the thesis

1. Advances in antibody phage display technology
Line Ledsgaard, Anne Ljungars, Charlotte Rimbault, Christoffer V. Sørensen, Tulika Tulika, **Jack Wade**, Yessica Wouters, John McCafferty, Andreas H. Laustsen
Drug Discov Today. 2022;27(8):2151-2169.

2. Discovery and optimization of a broadly-neutralizing human monoclonal antibody against long-chain α-neurotoxins from snakes
Line Ledsgaard, **Jack Wade**, Timothy P. Jenkins, Kim Boddum, Irina Oganesyan, Julian A. Harrison, Pedro Villar, Rachael A. Leah, Renato Zenobi, Sanne Schoffelen, Bjørn Voldborg, Anne Ljungars, John McCafferty, Bruno Lomonte, José M. Gutiérrez, Andreas H. Laustsen & Aneesh Karatt-Vellatt
Nature Communications 2023, 14 (1), 682

3. Structure of a neurotoxin-neutralizing antibody reveals determinants for broad reactivity and a pH-responsive allosteric switch
Manuscript draft

4. Antibody framework engineering to introduce conditional pH binding properties into antibody paratopes
Manuscript draft

5. Generation of Multivalent Nanobody-Based Proteins with Improved Neutralization of Long α-Neurotoxins from Elapid Snakes
Jack Wade[#], Charlotte Rimbault[#], Hanif Ali, Line Ledsgaard, Esperanza Rivera-de-Torre, Maher Abou Hachem, Kim Boddum, Nadia Mirza, Markus-Frederik Bohn, Siri A. Sakya, Fulgencio Ruso-Julve, Jan Terje Andersen, and Andreas H. Laustsen
Bioconjugate Chemistry **2022** *33* (8), 1494-1504

Papers related to the thesis

***In vitro* discovery of a human monoclonal antibody that neutralizes lethality of cobra snake venom**
Ledsgaard L[#], Laustsen AH[#], Pus U, **Wade J,** Villar P, Boddum K, Slavny P, Masters EW, Arias AS, Oscoz S, Griffiths DT, Luther AM, Lindholm M, Leah RA, Møller MS, Ali H, McCafferty J, Lomonte B, Gutiérrez JM, Karatt-Vellatt A
MAbs. 2022 Jan-Dec;14(1):2085536

[#]These authors contributed equally

Abbreviations

3FTx	Three-finger toxin
α-cbtx	α-cobratoxin
BLI	Bio-layer interferometry
α-bgtx	α-bungarotoxin
CDRs	Complementarity determining regions
DELFIAs	Dissociation-enhanced lanthanide fluorescence immunoassays
DLS	Dynamic Light Scattering
ENC	Expression-normalized capture
α-eptx	α-elapitoxin
Fab	Fragment antigen-binding
FIDA	Flow-Induced Dispersion Analysis
FcγRIIb	Fcγ receptor IIb
Fc region	Fragment crystallizable region
FcRn	Neonatal Fc receptor
Ig	Immunoglobulin
ITC	Isothermal Titration Calorimetry
mAb	Monoclonal antibody
nAChR	Nicotinic acetylcholine receptor
Quads	Multivalent nanobody fusion proteins
scFvs	Single-chain variable fragment
SEC	Size Exclusion Chromatography
SPR	Surface Plasmon Resonance
WHO	World Health Organization

1. Introduction

1.1. Snakebite envenoming

Each year, snakebite envenoming causes significant harm and death with more than 50 000 fatalities and 400 000 permanent injuries.[1,2] As a response, snakebite envenoming was enlisted as a neglected tropical disease in 2017 by the World Health Organisation (WHO), with an aim set to halve snakebite fatalities by 2030.[3] However, developing a treatment for snakebite envenoming poses a unique set of challenges in comparison to other diseases. In contrast to infectious diseases, such as viruses, there is only a short incubation time before disease onset, as snake venom is injected at a high dose and the toxin constituents of venom are often highly potent and fast-acting. Additionally, snake venoms often contain more than 40 different toxins that act in concert to target the nervous and circulatory systems, as well as organs and tissues, providing snakes with a powerful weapon for defence and predation purposes.[4] To successfully relieve symptoms, neutralizing multiple toxins is a prerequisite for the majority of snake venoms. Further, of the 700+ venomous snakes known most are located in Asia, Africa, Oceania, and Latin America, intersecting with societies that have a limited healthcare capacity for treating the clinical manifestations of envenoming's. As a therapeutic challenge, this places a burden not only on a quick intervention, but also financially in order to make therapies accessible to people in the developing countries where the majority of snakebites occur.[1]

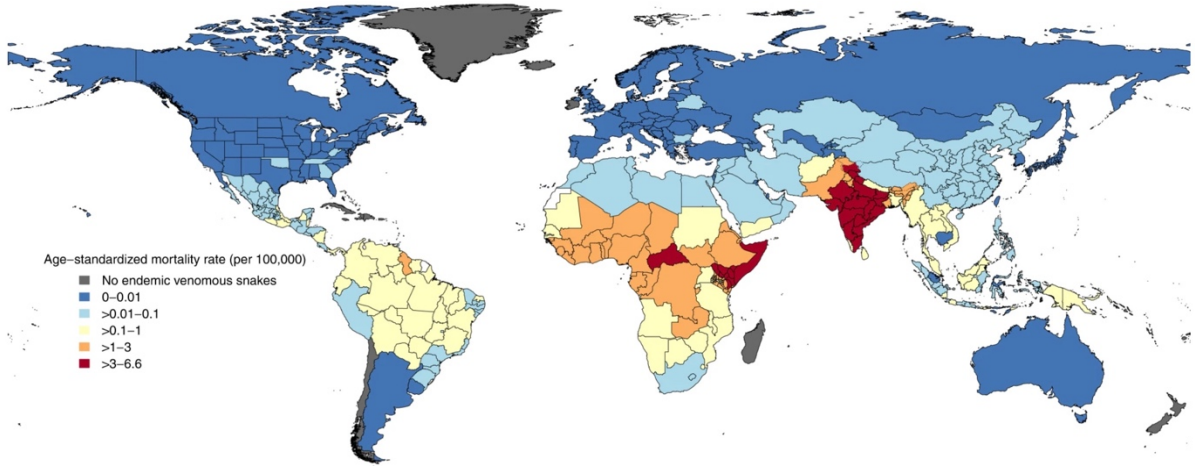

Figure 1. Snakebite epidemiology. Age standardized mortality rates of snakebite envenoming's in 2019. Figure adopted from[1]

1.1.1. Antivenom

Serum-based antivenoms have been the mainstay treatment for snakebite for over a century, and are derived from animals that have developed immunity against snake venoms over time through repeated immunizations (Fig. 2).[5] Although effective, antivenoms come at risk of severe allergic side-reactions due to their non-human origin,[6] the likelihood of which is increased due to the high doses required for efficacy. The activity of antivenoms is hampered by their purity due to a lack of use of specialised chromatography equipment[7] and the non-selective purification of the venom-specific neutralizing components in plasma – antibodies. As a consequence, antivenom compositions vary and reflect the entire antibody repertoire of the production animal (including non-neutralizing and non-venom specific antibodies), diluting their activity.[8]

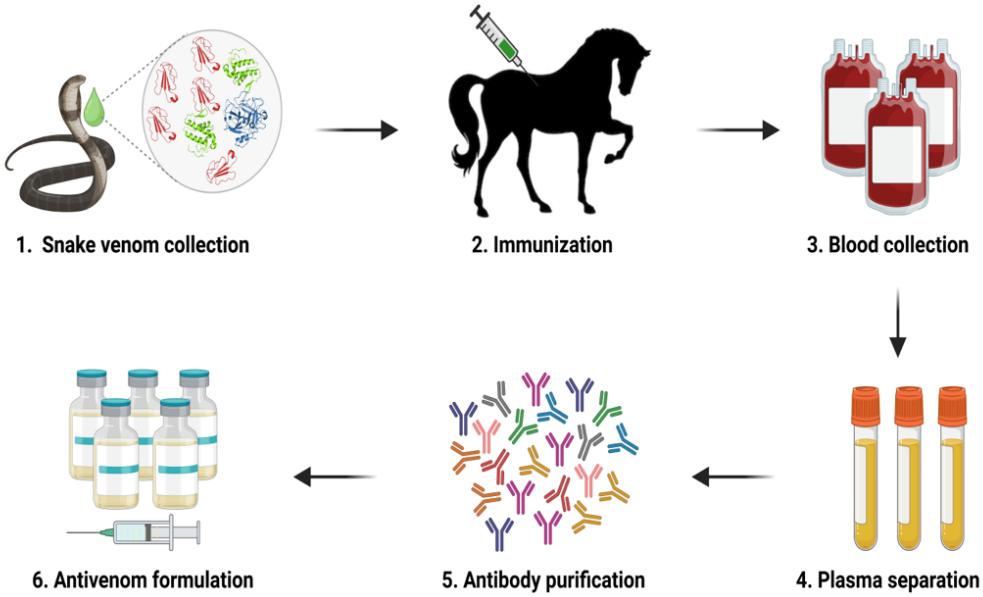

Figure 2. Antivenom production. Traditional antivenom production. (1) The most prevalent snakes in a region are chosen to raise an antivenom against. (2) Immunization of large mammals with venom. (3) The blood drawn from the animal, plasma separated (4) and the antibodies (5) purified. The final antivenom (6) has a mixture of both snake venom-specific and non-specific antibodies.

Despite these drawbacks, antivenoms validate the use of antibodies as a drug format to neutralize whole venoms.[9] Modern biotechnology has developed manufacturing pipelines to produce human antibodies as recombinant proteins of a known sequence from a single cell.[10] Produced as pharmaceutical products of a defined composition to treat cancer, autoimmune, and infectious diseases, such technology pipelines could address the purity and immunogenicity related limitations of plasma-derived products.[11] In a step towards this aim, discovery workflows have been implemented to discover recombinant human antibodies against medically relevant snake toxins *in vitro*, and have proven able to also neutralize *in vivo* (Chapter 5). Because the sequences of recombinantly produced antibodies are known, they can be further engineered to tune the natural biology of antibodies to have improved safety profiles,[12] therapeutic properties and be produced as oligoclonal mixtures for broader usage (Fig 3).[13]

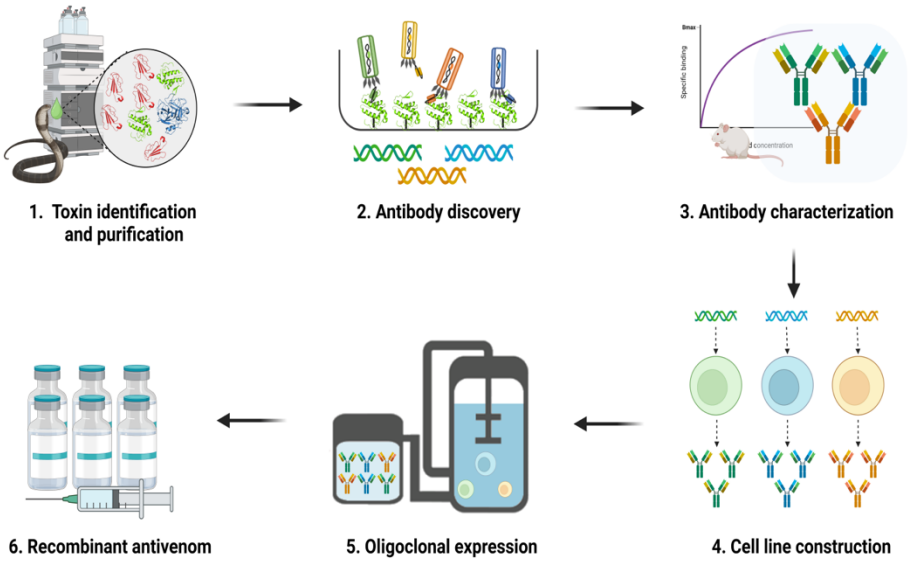

Figure 3. Recombinant antivenom. Recombinantly produced antivenom. (1) The most important toxins to neutralize in a snake venom are identified and purified. (2) Human antibodies able to recognise toxins are displayed on phages and discovered *in vitro*, and (3) verified functionally.(4) Production cell lines are generated from the DNA of identified neutralizing antibodies and (5) produced at a large scale in fermenters before being formulated as a biopharmaceutical product (6).

1.2. Antibodies

Antibodies, or immunoglobulins (Igs), are glycoproteins secreted by plasma and memory B cells that bind to pathogens with high affinity. The immune system has five distinct antibody subclasses that differ in their functional properties to enable the immune system to detect and mount an effective immune response (Fig 4).[16] The most common antibody isotype in the serum is the IgG isotype, and is secreted in high titres by B cells into the bloodstream to find and eliminate pathogens and different disease-causing molecules.[1] IgGs are assembled from four polypetide chains, two heavy chains and two light chains. Both chains are used to form two fragment antigen binding (Fab) domains, which each bind to a specific surface of a pathogen known as the antibody epitope. The specific region of the antibody within the Fab domain that facilitates the interaction is known as the variable region, and is unique to each antibody secreted by a B cell. In the fully assembled IgG molecule, the two heavy chains are dimerized and form a fragment crystallizable (Fc) domain, which is covalently connected to the Fab domains by a flexible hinge (Fig. 4). The Fc domain interacts with Fc receptors (FcRs) to confer a set of effector functions to the antibody.[2]

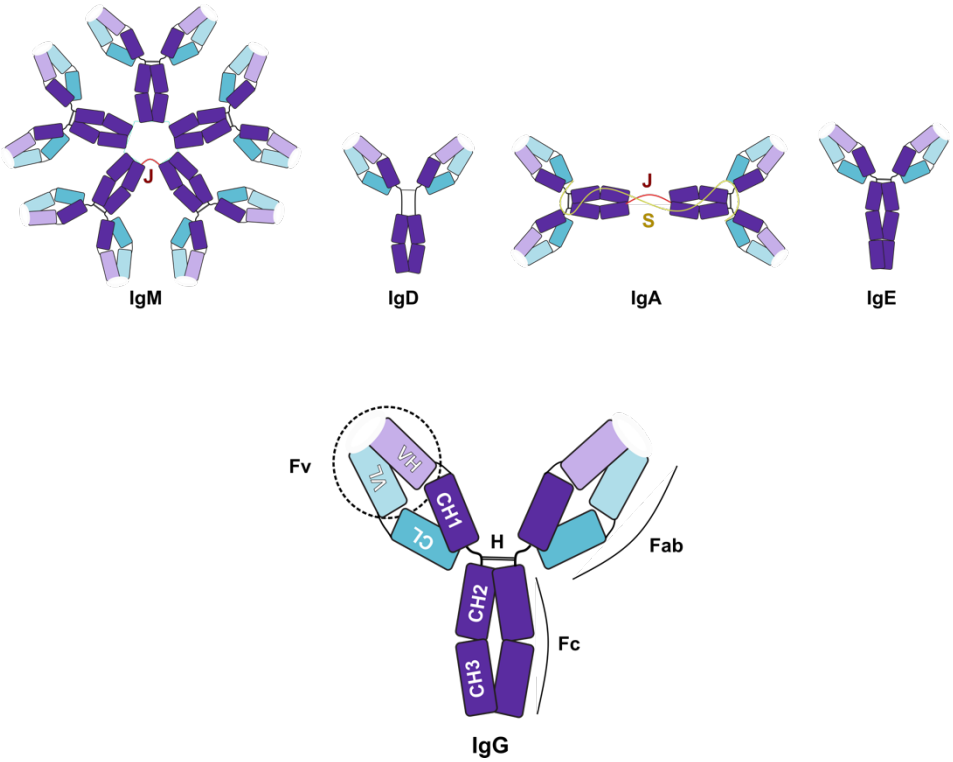

Figure 4. Antibody isotypes. Structure of the five antibody isotypes found in humans, each assembled from Fab and Fc domains in a 'Y' shape architecture. IgM and IgA exist as pentamers and dimers linked by a join (J) chain. The IgG subclass is the most abundant isotype in serum, established therapeutically and used in this thesis. Formed from 4 chains, 2 heavy (purple) composed of 3 constant domains (CH1-CH3) domains and a variable domain (V_H) and 2 light chains (cyan) composed of a constant (C_L) and variable (V_L) domain. An IgG can interact with two antigen molecules simultaneously through its Fragment variable region (Fv) assembled from variable light V_L and variable heavy V_H domains from each chain. The heavy chain Fc mediates interactions with receptors through the CH3 & CH2 and hinge (H) domains. With Fab and Fc domains positioned at opposite ends of the molecule, IgGs are well positioned to bridge cell types and form multivalent complexes through binding avidly to targets.

Antibodies function to protect the host from different pathogenic challenges.[17] By binding to specific sites on a pathogen surface, antibodies can neutralize the pathogen. One example is through binding to a site on the pathogen surface important for function, such as blocking a virus from binding to host cell receptors to prevent infection.[3] Secondly, antibodies binding to pathogens decorate the surface of pathogens with antibodies, labelling them for recognition and elimination by cells in the immune system. The component of the antibody recognised by immune cells is the antibody Fc domain, which interacts with specific FcRs on the immune cell to modulate their activity. The structure of the antibody is well suited for the recruitment of immune cells to a pathogen, principally by having the Fab arms and Fc domains located at opposite ends of the IgG molecule in a 'Y' shaped structure. In this structural arrangement, the Fab arms localize the antibody to the pathogen, and the Fc is presented away from the cell surface, accessible to an immune cell receptor. Thus, antibodies home the immune response to different pathogens and can either neutralize a pathogen due to their epitope or by recruiting immune cells that eliminate the pathogen independently of the epitope through their Fc domain.[2]

1.2.1. Antibody specificity

Antibodies bind with high affinity to protect against pathogens and can reach affinities up to 10^{-10} mol l^{-1} [4] and are consequently very potent. The effects of their activity are most keenly felt in autoimmune diseases, when pathogenic antibodies exhibit an off-target toxicity and bind to self-molecules, reacting with host cells, tissues and organs.[5] Under normal circumstances, antibodies bind to pathogens and are highly conformationally specific to their target to avoid interacting with self-molecules or leading to off-target effects.

Over 1000 structures of antibodies bound to an antigen have been determined, predominantly through X-ray crystallography and cryo-EM, and describe the structure-function relationship of the antibody variable region. The variable region is assembled from two domains that form the antigen binding site, one contributed by the antibody heavy chain (variable heavy V_H) and one from the light chain (variable light V_L domain). These domains pair together to form the variable region of an antibody,[26] which contains six loops called complementary determining regions (CDRs) connected by beta-sheets (Fig. 5). The CDR loops are different lengths and sequence compositions to form a surface on the antibody that has a unique topology and biochemical composition. Should the antibody surface be complementary to the surface of a pathogen, then an interface is formed between the antibody and the pathogen (known as the antigen) facilitated by numerous molecular interactions. The residues in the antibody that interact with the antigen are called the paratope, and interact with corresponding residues on the antigen called the epitope.

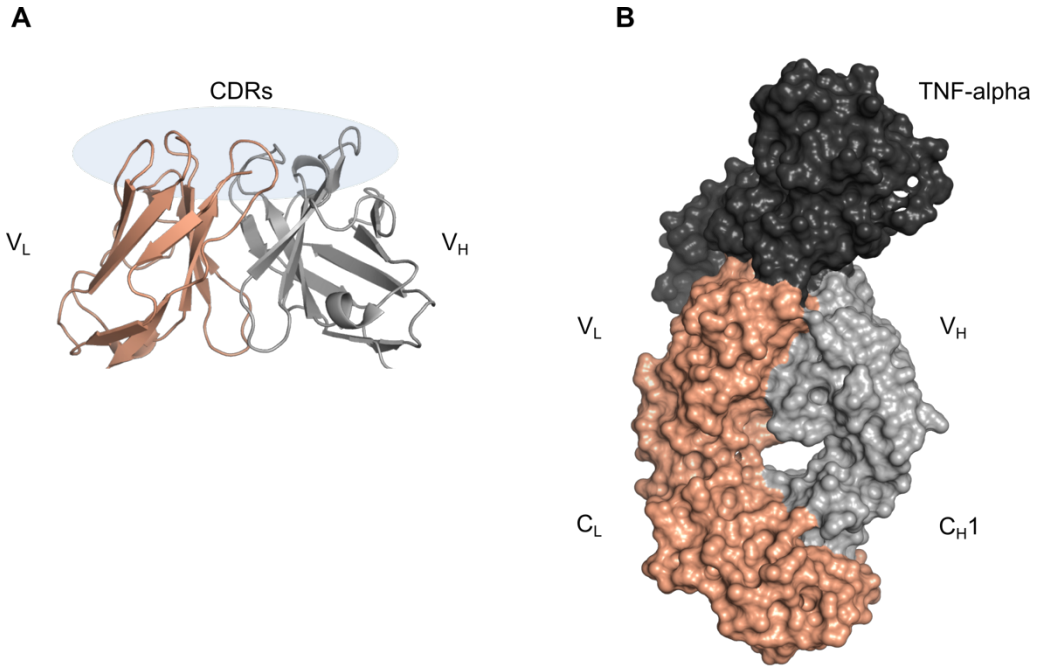

Figure 5. Antigen recognition. (A) Cartoon depiction of the antibody variable region. V_L (red) V_H (grey), CDR loops at the apex of the region are solvent exposed and available to form interactions with an antigen, supported by a framework region formed from β-sheets. (B) Surface depiction of the full fragment antigen binding domain (Fab), highlighting the structural complementarity between antibody and antigen. The CDR and framework residues (FWR) both contribute to the formation of the binding site; the latter may also be a site for engineering new binding properties. Structure taken from PDB: 3wd5.

The immune system samples a huge structural diversity of antibodies in order to recognise in principle, any target. Antibodies can recognise large molecules and form interfaces with their target with large surface areas (400-1000 Å^2) [24,25] and are able to discriminate single amino acid differences or post-translation modifications [6,7] The large surface area not only affords antibodies to be highly conformationally specific but allows them to facilitate high-affinity interactions through an extensive interaction network between the paratope and epitope.

1.2.2. Framework residue effects on antigen binding

The framework region (FWR) in the antibody variable region is located beneath the CDRs, composed of beta sheets and hairpin loops that support the CDR loops to facilitate binding. The importance of these FWR residues in binding was observed when engineering antibodies derived from mice for therapeutic use in humans.[8] To be used as therapeutics in humans, mouse antibodies are usually engineered to contain a higher content of human sequence, to avoid being rejected by the human immune system. In these engineering efforts, framework residues in the mouse antibody were required to retain binding.[27] As framework residues are located in the beta-sheets of the antibody variable domain, they rarely form the antibody paratope, and highlight the importance of residues outside the paratope in facilitating binding.

The importance of the framework region has been further illustrated in the development of broadly neutralizing anti-HIV-1 antibodies.[29–31] Broadly neutralizing HIV-1 antibodies are subjected to prolonged somatic hypermutations *in vivo* from chronic exposure to HIV-1, and therefore have acquired rare mutations in the framework region beneficial for broad neutralization. Specifically, these rare mutations mainly occur in the V_H-to-V_L chain interface region within the framework, leading to a reconfiguration of the antibody paratope by changing the V_H and V_L orientation.[9] This reconfiguration facilitates binding to conserved epitopes on the HIV-env protein. Further characterization of these antibodies by molecular dynamic simulations has been used to analyse the effect these mutations have on their conformational ensemble in solution. The effect associates the framework mutations in chain interface with an increase in flexibility, important for accommodating subtle structural differences in the HIV-1 envelope protein as it acquires mutations to escape the immune system. The importance of the antibody framework for binding suggests that it could be an engineerable feature in antibodies to alter their binding properties.

1.2.3. Antibody avidity

Antibodies are able to bind multivalently. An antibody has two Fab arms, which bind to the antigen, and the Fc domain is composed of two heavy chains, affording interactions to two FcRs. Partaking in multivalent interactions enables IgGs to bind avidly to antigens and FcRs on immune cells. Avidity refers to the cumulative strength of multiple non-covalent interactions, which results in an increase in affinity by lowering the dissociation rate of a molecule (Fig. 6A).[10] A slower dissociation rate is important for the activity of antibodies. For example, antibodies have a more sustained effect when blocking viral entry into cells, preventing infection, and staying bound to FcRs on immune cells for a sufficient amount of time to activate the immune cell. Secondly, in combination with antibody specificity, it gives conditionality to the antibody function, as the ability to bind bivalently is dependent on the target abundance. Therefore immune cells, for example, are only activated when a sufficient level of antibodies are bound to cluster their FcRs, avoiding off-target effects.[20] Avidity can be enhanced by increasing the antibody valence, for example, by fusing binding domains to self-assembly proteins (Fig. 6B),[21,22] or by adding binding domains as tandem repeats (Manuscript III).[23] In this thesis the effect of valence on both binding and Fc domains is investigated.

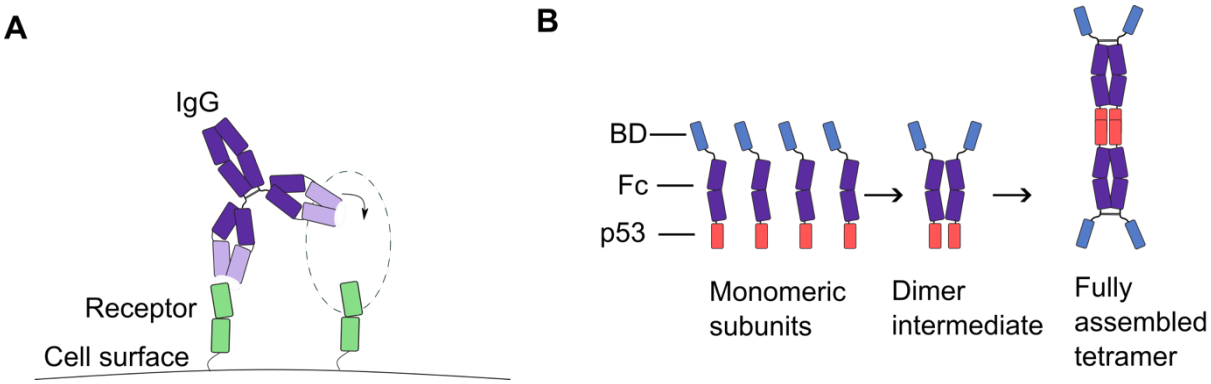

Figure 6. Avidity engineering. (A) Schematic of an IgG binding avidly to a cell surface receptor. The local concentration of the antibody is higher on the receptor when one arm of the antibody remains bound. If the on rate is faster than the off rate, the antibody can rebind and stay localized on the cell surface. (B) Avidity engineering by increasing valence, by using self-assembly proteins. The p53 tetramerization domain is used to assemble four monomeric building blocks and create various multivalent formats. BD stands for binding domain.

1.2.4. Antibody recycling

In addition to being highly specific and binding avidly, antibodies have a prolonged duration of action due to their inherently long serum half-life relative to other proteins (except albumin).[11] This is due to binding to the neonatal Fc receptor (FcRn), which prevents IgG isotype antibodies from entering the lysosomal degradation system during cellular recycling.[12]

Antibodies naturally enter the cell through pinocytosis, and are transferred into the acidic environment of the endosome. Here, an Fc receptor called the neonatal Fc receptor, FcRn, binds to the Fc domain preventing the IgG from progressing to the lysosome. Through FcRn antibodies are recycled back to the cell surface, where a lower affinity to FcRn releases the IgG back into the extracellular space.[33,34] The interaction between the IgG Fc and FcRn is strictly pH-dependent, enabling antibodies to be bound in the endosome and returned into the plasma (Fig. 6), giving IgGs a half-life of around 3 weeks.[35] As a result, IgGs are the most prominent antibody isotype in the serum, providing intracellular and extracellular immunity in response to pathogens.[32]

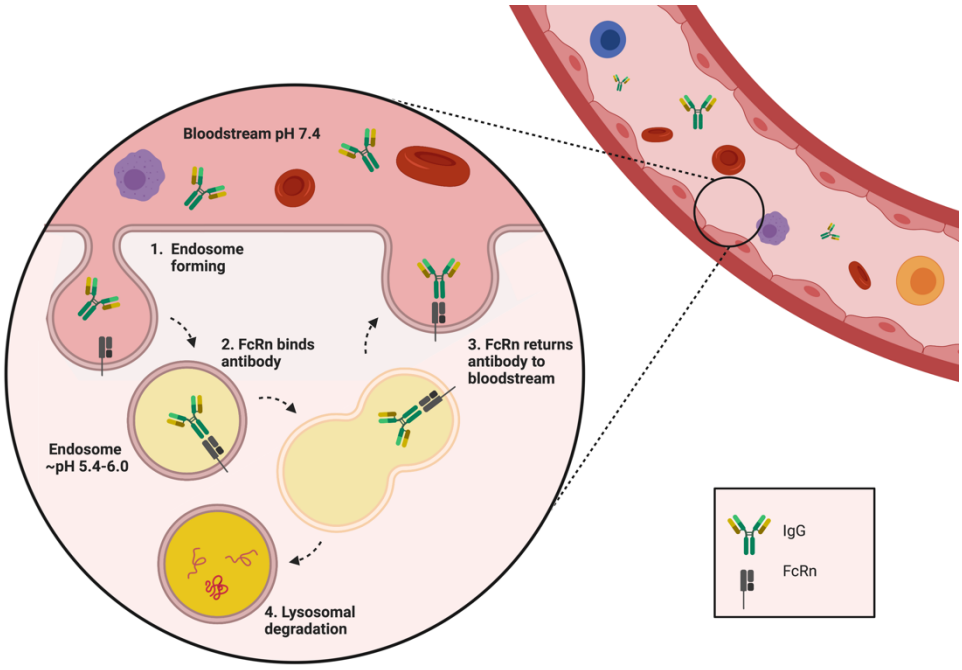

Figure 6. Antibody recycling. Antibodies enter a cell from the bloodstream through fluid-phase pinocytosis and enter into endosomes (1). In the low pH of the endosomes, IgG antibodies bind to FcRn (2) and are transported back to the cell surface (3) and are rescued from entering the lysosome and being degraded (4). At the higher pH on the cell surface, the antibody is released back into circulation. Figure modified from Tulika.

1.2.5. Recycling antibodies

Even though antibodies have a naturally long half-life, certain targets can reduce their half-life to just a few days, thereby reducing the pharmacodynamic effect of an antibody and requiring more frequent dosing. One of the causes of this is target-mediated degradation.[13] When an antibody binds to cell surface receptors, it can induce receptor internalization and be transported by the receptor to the lysosome.[14] Similarly, some extracellular proteins can promote lysosomal degradation of IgGs, speculated to be a result of altered interactions of IgG with FcRn.[36] To overcome this issue, antibodies can be engineered to release their target at the point in the endosome, where FcRn is present and can rescue the antibody and recycle is back into circulation. This causes the target, but not the antibody, to be degraded, and therefore the antibody is recycled unbound and able to bind to another target molecule (Fig. 7, recycling antibody).[37,38]

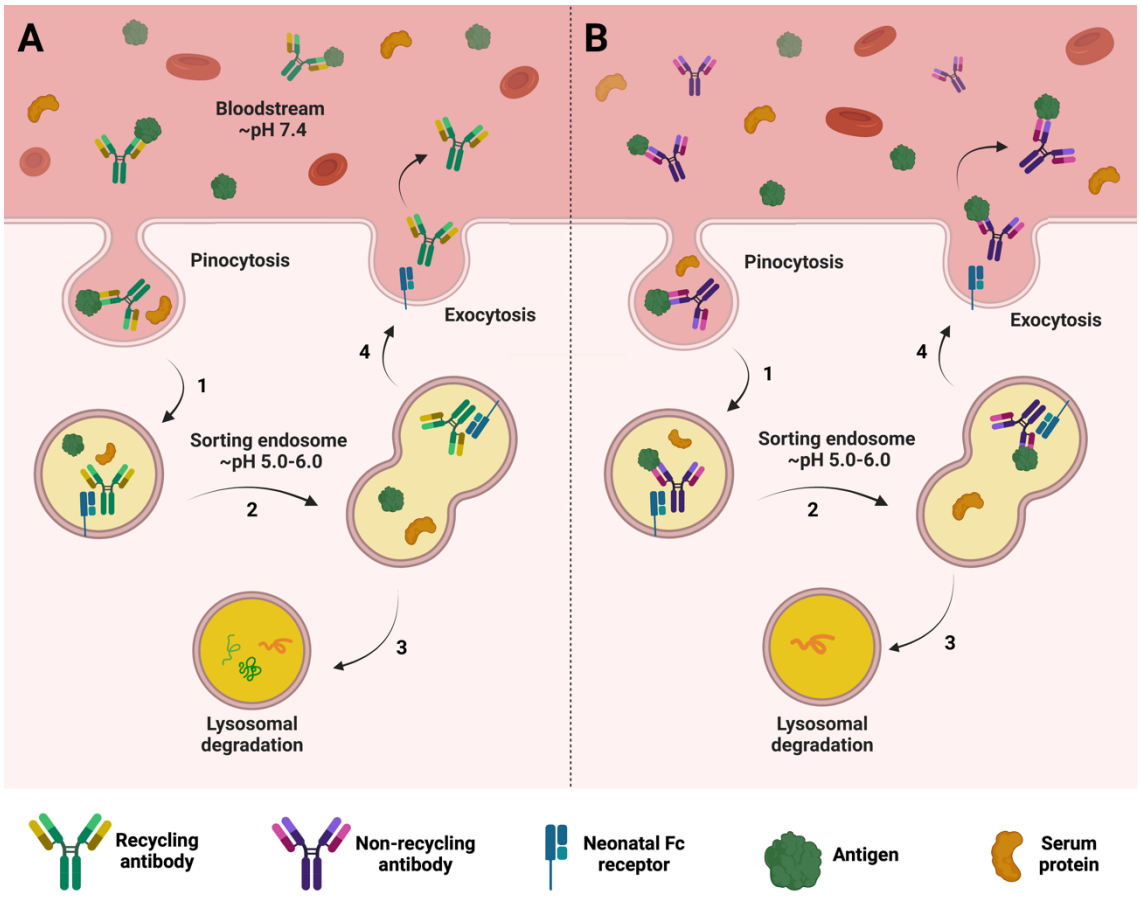

Figure 7. Recycling antibodies. (A) Antibodies with a low affinity for their antigen at acidic pH release their antigen following entry into the endosome (1) before being transported back to the cell surface unbound (2), whilst the antigen is degraded by the lysosome (3). (B) In contrast, antibodies that bind non-pH-dependently stay bound to their antigen, which is transported back to the cell surface with the antibody. Antibodies that bind with low affinity at endosomal acidic pH are recycled back unbound and are able to bind another antigen, and therefore have the potential to neutralize multiple antigens in their lifetime, called recycling antibodies. The rate of antibody recycling can be tuned by adjusting the affinity of IgG-Fc for FcRn, giving a customizable rate of antigen degradation.

Recycling antibodies, therefore, degrade the target and re-instate the IgG half-life by preventing target-mediated degradation. In certain indications, however, targets such as cytokines or toxins are produced chronically and require a sustained duration of degradation to treat with an antibody.[15] To increase the duration of action of an antibody, Fc mutations are engineered into the IgG Fc domain to increase the affinity of IgG-Fc for FcRn at acidic pH. In this way, the IgG is more efficiently rescued from lysosomal degradation by FcRn and more antibody is returned to the bloodstream, extending the antibody half-life.[16,17] Combining such Fc modifications with pH-dependent antigen binding concomitantly extends the IgG half-life and the duration of antigen degradation, lowering the administration frequency of the antibody and prolonging the antibody pharmacology.[39,40]

Lastly, tuning the affinity of IgG-Fc to FcRn at neutral pH gives a customizable rate of antibody recycling and target degradation by pH-dependent antibodies.[18] Called 'sweeping' antibodies, these antibodies bind with a higher affinity to FcRn at neutral pH, and therefore have a greater rate of cellular internalization by binding to FcRn at the cell surface. The antibodies are still released into circulation, but the balance between recycling and time in circulation is adjusted through the affinity and pH-dependent binding to FcRn to increase the recycling rate (Fig. 8).[41]

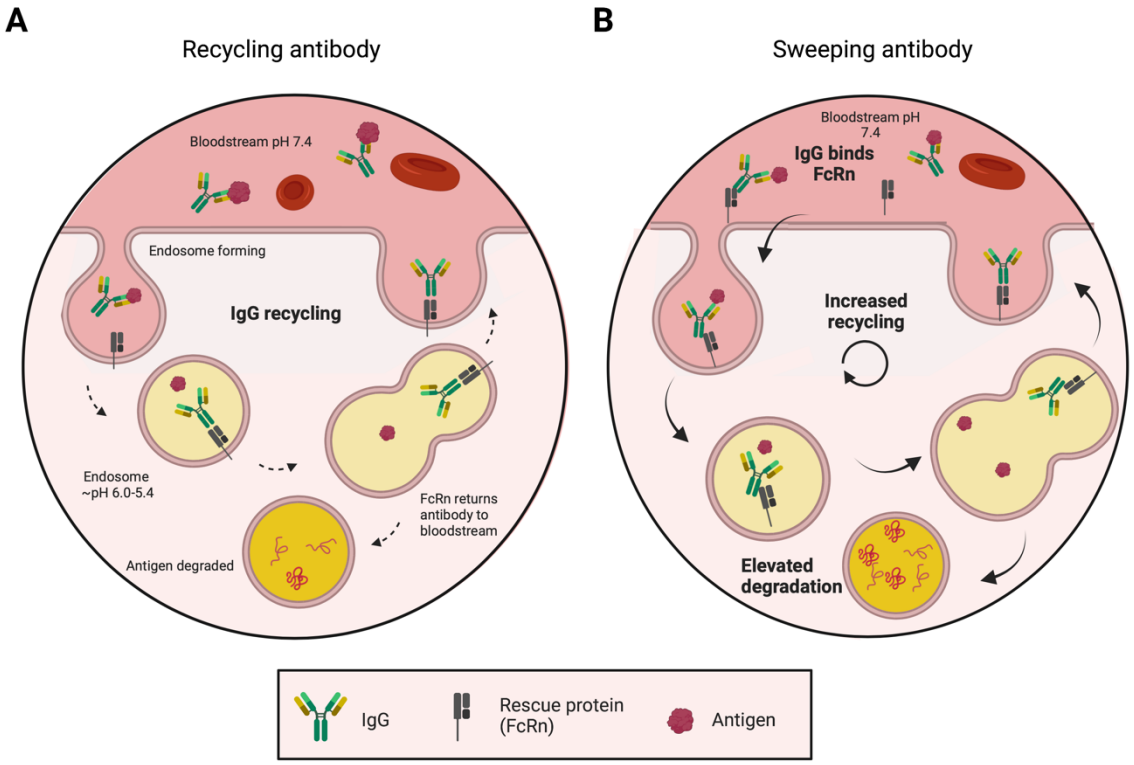

Figure 8. Sweeping antibodies. In contrast to a recycling antibody, (A) sweeping antibodies are designed for an enhanced rate of antigen degradation by increasing the affinity for the FcRn receptor at pH 7.4 (B), which results in an increased cellular uptake and increased rate of recycling.

1.3. pH-dependent interactions

Changes in environmental pH are sensed by proteins and are important for facilitating biological processes. For example, viral fusion proteins undergo structural re-arrangements in the endosome to mediate viral escape and infection,[44–46] and antibodies are reliant on the formation of a pH-dependent interface with FcRn for their recycling.[44] In relation to the Fc-FcRn interaction, pH-dependent binding is conferred through complementary electrostatic interactions between positively charged, protonated histidine residues, and negatively charged acidic residues in the interaction interface.[19,20] Upon entering the endosome, salt bridges are formed between protonated histidines and negatively charged acidic residues to facilitate binding, which is broken at neutral pH when histidine is deprotonated. Histidine is known to facilitate pH-dependent interactions in the pH range of biological systems due to having a pKa value of 6.0, which denotes the pH value at which the protonation of a compound is 50 percent (Equation 1). At the acidic pH of 5.5 in the endosome, histidine residues with a pKa value of 6.0 will predominantly be double protonated and charged, allowing for complementary charged electrostatics to facilitate pH-dependent interactions between FcRn and the Fc region of the antibody.[47]

$$pH = pKa$$

$$-log[H^+] = -log[H^+][A^-]/[HA] \quad (1)$$

$$[H^+] = [H^+][A^-]/[HA] \quad (2)$$

$$1 = [A^-]/[HA] \quad (3)$$

$$[A^-] = [HA] \quad (4)$$

Equation 1. pH effects on protonation dissociation equilibrium. To illustrate that when the pKa value is equal to the pH of the solution 50% of the compound is protonated, we set pH equal to the pKa. The impact of pH on protonation dissociation equilibrium (pKa) can be explained by defining pH as the concentration of protons and pKa as the equilibrium position of ionizable forms of a compound in solution (1). Re-arranging the -log (2) and concentration of protons (3) results in the ratio of ionizable to non-ionizable forms being equal to 1. By rearranging equation 3, it becomes clear that the concentrations of both ionizable and non-ionized forms are equal only when the pH equals the pKa. As a result, when the pH value is equal to the pKa value of a compound, it is in a state of half protonation, and when the pH value is above the pKa, the compound is in a predominantly non-protonated form.

The protonation probability of amino acid residues is dependent on their surrounding environment, which includes other amino acids, metals, and is dynamic in proteins as they sample different conformational states.[21] Antibodies for example have been associated with pH-dependent equilibriums during their characterization, attributed to the change in charge state of acidic residues in hydrophobic environments.[22] However, because hisitidne has a pKa value of 6, this residue is chosen for engineering pH switches into antibodies to introduce the pH-dependent binding required for recycling and antigen-sweeping applications. Engineering pH-dependent antigen binding is presented in the Chapter 3 in the form of a review article.

2. Project Aims

This thesis is split into two themes, pH-dependent antibody binding characterization and antibody engineering. Both themes are approached from the context of snakebite envenoming, using neutralizing antibodies to long-chain α-neurotoxins.

1. The mechanisms by which antibodies bind pH-dependently to their antigen are rarely reported. The aim of this thesis was to investigate how antibodies can interact pH-dependently with their antigen by structurally characterizing a pH-dependent antibody using X-ray crystallography.

2. The discovery of pH-dependent antibodies directly from *in vitro* display libraries normally demands multiple follow-up engineering steps to optimize their binding affinity. The aim of this thesis was to improve the discovery of pH-dependent antibodies from *in vitro* display libraries by engineering a pH-sensitive antibody framework, to use as a scaffold to design phage display libraries with pH-dependent binding properties pre-determined into antibodies. This was approached by using phage display to introduce pH-dependent binding in a non-pH-dependent antibody selectively through the antibody framework region.

3. Approaches to enhance both the neutralization capacity of nanobodies and their half-life are typically centred around genetically fusing nanobodies to IgG scaffolds, which limits the neutralization potency that can be achieved. The aim of the thesis was to expand the valence and half-life of nanobodies by employing a self-assembly protein, p53.

3. Advances in antibody phage display technology

This scientific review is a continuation of the thesis introduction and reviews the different aspects of phage display technology used to engineer and discover antibodies for different therapeutic applications. We begin by reviewing the different antibody formats used in phage display for antibody discovery and engineering, and review different antigen presentation and selection strategies and library designs.

This article highlights the utility of phage display to discover antibodies with tailored antigen binding properties. As an example, antibodies can be selected for improved cross-reactivity by cross-panning between different antigens between phage display selection rounds. Additionally, libraries can be designed to favour antibodies with specific binding properties before conducting a phage display antibody discovery campaign, such as by enriching phage display libraries with the histidine amino acid residue to increase the potential of discovering antibodies that interact pH-dependently with their antigen. Alternatively, libraries can be designed to maximise antibody diversity to discover antibodies to a broad range of targets. These libraries can be produced by acquiring antibody sequences from the human immune system, and therefore utilize the immune system's ability to recognise a diverse range of target classes.

This scientific review is published in Drug Discovery Today:
Line Ledsgaard, Anne Ljungars, Charlotte Rimbault, Christoffer V. Sørensen, Tulika Tulika, Jack Wade, Yessica Wouters, John McCafferty, Andreas H. Laustsen, Advances in antibody phage display technology, Drug Discovery Today, Volume 27, Issue 8, 2022, Pages 2151-2169, ISSN 1359-6446, https://doi.org/10.1016/j.drudis.2022.05.002.

ELSEVIER

Advances in antibody phage display technology

Line Ledsgaard [a,*], Anne Ljungars [a], Charlotte Rimbault [a], Christoffer V. Sørensen [a], Tulika Tulika [a], Jack Wade [a], Yessica Wouters [a], John McCafferty [b,c], Andreas H. Laustsen [a,*]

[a] Department of Biotechnology and Biomedicine, Technical University of Denmark, DK-2800 Kongens Lyngby, Denmark
[b] Department of Medicine, Addenbrookes Hospital, Box 157, Hills Road, Cambridge CB2 0QQ, UK
[c] Department of Medicine, Cambridge Institute of Therapeutic Immunology and Infectious Disease, University of Cambridge, Addenbrooke's Hospital, Hills Road, Cambridge CB2 0QQ, UK

Phage display technology can be used for the discovery of antibodies for research, diagnostic, and therapeutic purposes. In this review, we present and discuss key parameters that can be optimized when performing phage display selection campaigns, including the use of different antibody formats and advanced strategies for antigen presentation, such as immobilization, liposomes, nanodiscs, virus-like particles, and whole cells. Furthermore, we provide insights into selection strategies that can be used for the discovery of antibodies with complex binding requirements, such as targeting a specific epitope, cross-reactivity, or pH-dependent binding. Lastly, we provide a description of specialized phage display libraries for the discovery of bispecific antibodies and pH-sensitive antibodies. Together, these methods can be used to improve antibody discovery campaigns against all types of antigens.

Keywords: Phage display; Antibody discovery; Antigen presentation; Selection strategy; Library design

Line Ledsgaard Line Ledsgaard has a BSc Eng. (2016) and MSc Eng. (2018) in biotechnology from the Technical University of Denmark (DTU). She holds a PhD from the Department of Biotechnology and Biomedicine at DTU, and her research centers on the discovery of antibodies against snake venom toxins with the aim of replacing current antivenoms with next-generation antivenoms, based on human recombinant monoclonal antibodies. Her work especially focuses on using phage display technology to discover broadly neutralizing antibodies with the ability to bind and neutralize the toxic effects of groups of similar toxins from different snake species.

Andreas Hougaard Laustsen-Kiel Andreas Hougaard Laustsen-Kiel heads the Center for Antibody Technologies in the Department of Biotechnology and Biomedicine at DTU and is specialized in antibody technologies. He is also the CTO of Bactolife ApS, where he is responsible for nanobody technology and discovery. Andreas is a Fellow of the Danish Academy of Technical Sciences, the Young Academy of Denmark, and the Young Academy of Europe. He holds a PhD from the University of Copenhagen (2016) and an M.Sc.Eng. from DTU (2012). Andreas is a co-founder of the companies, Biosyntia, VenomAb, Antag Therapeutics, Chromologics, VenomAid Diagnostics, and Bactolife.

John McCafferty John McCafferty was one of the founders of Cambridge Antibody Technology (CAT) and a co-inventor of antibody phage display. In 2012, he formed IONTAS, an innovative biotechnology company using phage display to develop novel antibody therapeutics. During this period John developed IONTAS's proprietary mammalian display technology. John is also an inventor of a novel molecular fusion format (KnotBody™), wherein naturally occurring, venom-derived cysteine-rich peptides are inserted into peripheral CDR loops of an antibody. He recently formed Maxion Therapeutics to take advantage of this drug development opportunity with a particular focus on modulation of ion channels and GPCRs. Interspersed within this company formation John has held academic positions at the Wellcome Trust Sanger Institute and the University of Cambridge. This includes establishment in 2022 of a group in the Department of Medicine to develop recombinant antivenoms.

* *Corresponding authors.Ledsgaard, L. (liljen@dtu.dk), Laustsen, A.H. (ahola@bio.dtu.dk).*

1359-6446/
https://doi.org/10.1016/j.drudis.2022.05.002

Introduction

Phage display technology was first invented in 1985[1] for the display of peptides and, later, in 1990, the first antibody fragment was displayed on phages.[2] Since then, the technology has been used successfully for the discovery of many hundreds of antibodies for research, diagnostic, and therapeutic applications, including more than 14 antibodies that are clinically approved.[3] All aspects of the phage display methodology have been refined and advanced to enable the discovery of antibodies against challenging targets and antibodies with certain binding properties. One of the advantages of phage display, compared with other display technologies, such as ribosome,[4,5] yeast,[6] or mammalian display,[7,8] is that large libraries (diversity of $> 10^{11}$ unique clones) can be created and stored ready for selections, which allows for high-affinity antibodies to be discovered against a wide range of antigens. In this review, we address four major parameters that can be optimized to improve the outcome of antibody discovery campaigns: the choice of antibody display format, antigen presentation, selection strategy, and library construction.

Antibody formats used in phage display libraries

Phage display libraries can be designed using different bacteriophages, such as filamentous M13, fd, and f1 bacteriophages,[9] to display a variety of different antibody formats. The two most commonly used formats are single-chain variable fragments (scFvs) and antigen-binding fragments (Fabs).[10,11] ScFvs are small (25–27 kDa) monovalent antibody fragments comprising V_H and V_L domains connected by a short peptide linker.[12] Fabs are 50 kDa in size[13] and comprise V_H, V_L, C_L, and C_H1 domains.[14] There is potential for loss of affinity on conversion of scFv to the Fab/IgG format,[11,15] which might be less of an issue for antibodies discovered in the Fab format.[11,15,16] However, Fabs generally do have lower expression yields than scFvs[17] and typically exhibit lower display levels on phages,[18,19] making scFvs a more robust format for libraries, particularly naïve libraries.

Other antibody formats have also been used for the construction of antibody phage display libraries, including human single-domain antibodies (human V_H) and camelid and shark single-domain antibodies (V_HH and V_{NAR}, respectively). V_HHs are small (12–15 kDa[13]) and comprise the antigen-binding fragment from heavy-chain-only antibodies. With conventional antibodies, the interface that mediates pairing of V_H and V_L incorporates hydrophobic residues that are buried in the interface. In V_HHs, these are substituted with more hydrophilic residues, which results in increased water solubility and a decreased tendency to form aggregates.[20] The complementarity-determining region 3 (CDR3) loop in the V_HH is often elongated compared with conventional antibodies, which allows the V_HH to bind antigens that would be inaccessible for conventional antibodies, such as catalytic clefts of enzymes or receptor domains.[21,22] The V_{NAR} antibody fragments are similar to the V_HH antibody fragments in size, with the notable exception that they only have two CDR loops because of a deletion of a large portion of the Fr2-CDR2 region.[23]

Which of the antibody formats to choose for a phage display campaign is dependent on the final application of the discovered antibody. If the application is therapeutic and a long half-life is beneficial or engagement of effector cells is needed, an scFv or Fab library might be optimal, because they allow for easy reformatting to the commonly therapeutically used IgG format. For research reagents and diagnostic applications, or when the cost of large-scale manufacture is a major concern, a format such as the V_HH might be most optimal, although this format can also be fused to an Fc-region to create a V_HH-Fc molecule with similar properties as an IgG in terms of half-life and effector cell engagement. Taken together, it is vital to delineate the requirements for the final antibody product to select the most suitable type of library.

Antigen presentation strategies

For a successful phage display-based antibody discovery program, it is crucial that the conformation of the included antigens resembles the conformation that the antigens will have in the final application. Otherwise, the discovered antibodies could end up only recognizing the antigen in an altered conformation. Therefore, an initial and critical step for a phage display campaign is to determine the optimal strategy for antigen presentation.[24]

Antigen presentation through direct or indirect immobilization

The most widely used antigen presentation strategy is to directly or indirectly immobilize the antigen on a surface (Fig. 1a). In direct immobilization, the antigen is coated on the surface using passive adsorption. This strategy is by far the simplest for antigen presentation; however, it is not well suited for many types of antigen that alter their native conformation upon adsorption.[25] It can be particularly more problematic for small antigens that might not exhibit enough intermolecular attraction forces to exert passive adsorption.[26] For some of these antigens, indirect immobilization can be used instead of direct immobilization.

Through indirect immobilization, the antigen is captured on the surface using a capture molecule. The most popular technique exploits the strong binding between streptavidin/neutravidin and biotin, whereby the surface is coated with streptavidin/neutravidin, and the antigen is conjugated to biotin via a linker or tag.[27,28] This enables an indirect, yet stable, attachment of the antigen to the surface.[27,28] The antigen is more likely to retain its native conformation through indirect immobilization because the antigen is raised from the selection surface. However, it is crucial not to overbiotinylate the antigen, because this can obscure important epitopes or result in antigen aggregation.[29]

Two different strategies for biotinylation exist: site-specific or random biotinylation. Site-specific biotinylation can be achieved using biotinylation acceptor peptides (BAPs) comprising an enzymatic biotinylation site.[30,31] One of the most widely used BAPs is the AviTag, which requires recombinant expression of the target antigen fused to the 15-amino acid peptide tag.[32] The AviTag sequence is biotinylated at its lysine residue by the *Escherichia coli* biotin ligase, BirA.[33] The AviTagged antigen can be co-expressed with BirA in bacterial cells, yeast, and mammalian cells to achieve *in vivo* biotinylation.[34,35] Alternatively, purified AviTagged antigen can be incubated with purified BirA and biotin to achieve *in vitro* biotinylation.[36] Biotinylation using BAPs

results in site-specific addition of a single biotin per antigen, thus controlling the antigen-to-biotin ratio and avoiding overbiotinylation. Nevertheless, it might not be possible to use the AviTag system in all cases, especially when it is difficult/unpractical to express the target antigen recombinantly, or when the AviTag would interfere with a potentially important (terminal) epitope of the antigen.

As an alternative to BAP biotinylation, random chemical biotinylation can be used. In this method, purified antigen and biotinylation reagents, using a variety of possible reaction chemistries, are mixed to achieve a covalent linkage between the antigen and biotin. A variety of linkers are available, making it possible to biotinylate antigens at the primary amines (N terminus or side chain of lysine residues[37]) or sulfhydryl and carboxyl groups.[38,39] Although faster and cheaper than enzymatic biotinylation (by the *E. coli* biotin ligase), chemical biotinylation needs titration to achieve the desired 1:1 antigen-to-biotin ratio.

Indirect immobilization of an antigen can also be used based on different peptide tags and tag-specific capture molecules. This requires the recombinant expression of the antigen in fusion with a peptide tag and the selection surface to be coated with the fusion tag-specific capture molecule. Binding between the tag and the capture molecule results in immobilization of the antigen. Although less popular than the biotin–streptavidin system, His-tags and anti-His antibodies or other His-capturing molecules have been exploited for antigen presentation in phage display selections.[40] Recently, a peptide–protein ligand pair, known as SpyTag/SpyCatcher, derived from fibronectin-binding protein in *Streptococcus pyogenes,* was used for antigen presentation in phage display selections.[41,42] The binding between SpyTag and SpyCatcher occurs via an isopeptide bond and has been reported to be irreversible, specific, and robust to various conditions, such as pH, temperature, and buffer.[41].

Antigen presentation through whole-cell panning

Even though indirect immobilization is suitable for displaying many antigens, it is often not optimal when it comes to presenting antigens such as membrane proteins. Membrane proteins typically contain hydrophobic transmembrane regions and might be a part of a multisubunit protein complex; as a result,

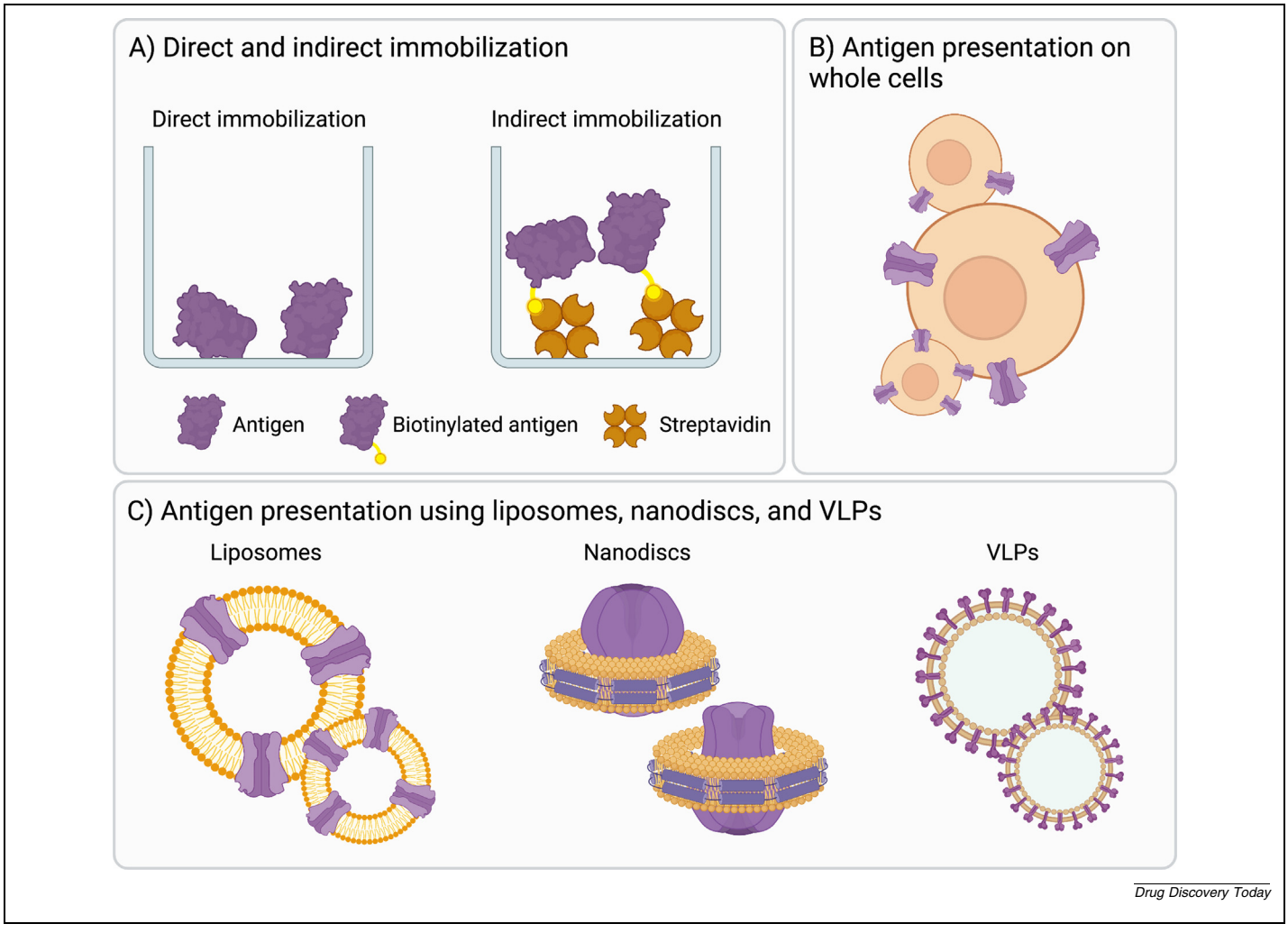

FIG. 1

Antigen presentation strategies. **(a)** Direct and indirect immobilization. **(b)** Antigen presentation on whole cells. **(c)** Antigen presentation on liposomes, nanodiscs, and virus-like particles (VLPs).

they lose their native conformation when isolated from their natural environment.[43] To conserve their conformation, membrane proteins can be expressed on a cell membrane (Fig. 1b). Mammalian cell lines, such as human embryonic kidney (HEK) cells or Chinese hamster ovary (CHO) cells, can be either transiently or stably transfected with a target protein to overexpress it and obtain a high density on the cell surface, while retaining the native conformation of the antigen.[43–46] Although selections are sometimes performed using cultured primary cells, it has been shown that cultured cells can alter their protein expression levels compared with primary cells[47]; to overcome this potential issue,[48] primary cells without culturing can be used for selection.[49] Other cell expression systems, including *E. coli*, yeast, and insect cells, can also be used to express and present membrane proteins.[50–52].

One problem with phage display selection on whole cells is that the target antigen, whether endogenous or recombinantly expressed, will represent only a small proportion of the total protein milieu presented to the library. To overcome this, deselection techniques can be used as described below. In addition, when transfected cells are used, the host cell can be altered between the selection rounds to focus selection on the recombinant antigens present on both cells.[43] Another challenge is that phage particles can nonspecifically adsorb to the cell surface via their coat protein (independently of their displayed antibody fragment). To counteract this, washing using low pH can be applied.[43,53] Furthermore, some phages can bind nonspecifically to dead cells and cell debris in the cell suspension used for panning. To reduce enrichment of such nonspecific binders, it is important to ensure that most of the cells used for selection are viable.[43,54]

Antigen presentation through liposomes, nanodiscs, and VLPs

Membrane proteins can also be presented on amphiphilic structures, such as liposomes, nanodiscs, and virus-like particles (VPLs) (Fig. 1c). Liposomes are spherical vesicles comprising a volume of aqueous solution enclosed by one or more lipid bilayer membranes, usually composed of phospholipid molecules. The phospholipid bilayer membrane mimics the environment of a plasma membrane and creates a suitable platform to present membrane proteins.[55,56] Presenting antigens on liposomes requires the formation of the liposomes, extraction of the antigen from its native membrane environment (whether isolated from natural source or recombinantly expressed), and finally transferring the extracted antigen to the preformed liposomes. When recombinantly expressed, the antigen can be fused with a tag, which can be used later for purification.[57]

Membrane proteins can also be presented on nanodiscs, which are nanometer-sized discoidal structures comprising phospholipid bilayers encircled by two amphipathic helical protein belts, termed 'membrane scaffold proteins' (MSPs).[58] Purified membrane protein can be mixed with phospholipids and MSPs to obtain membrane protein-carrying nanodiscs[59,60] (Fig. 1c). The protein belts constrain the size of the bilayers, resulting in a more monodispersed and consistent size distribution of nanodiscs compared with liposomes. Furthermore, nanodiscs provide a more stable environment for the membrane proteins and can be stored for a longer period compared with liposomes.[61,62] Moreover, because of their discoidal structure, proteins incorporated in the nanodiscs are accessible from both sides of the membrane. This is beneficial when access to both the extracellular and intracellular domains of membrane proteins is required. Both liposomes and nanodiscs can be used to present ion channels and multitransmembrane proteins, such as ion channels and G-protein-coupled receptors, which have until recently proved difficult to express/purify. However, both liposomes and nanodiscs rely on detergents to extract membrane proteins, which can alter the structure of the protein. As an alternative, a detergent-free approach, using styrene maleic acid (SMA) copolymer, can solubilize membranes into lipid nanodiscs, which are nanometer-sized discoidal structures comprising a phospholipid bilayer encircled by SMA copolymer resulting in a structure called a 'styrene maleic acid–lipid particle' (SMALP).[57,63,64] The detergent-free extracted protein can also then be incorporated into liposomes for antigen presentation.[57].

Cytotoxic proteins can cause growth retardation and toxicity to the host cells when overexpressed, making them difficult to express.[65] Cytotoxic and membrane proteins can be synthesized in a cell-free manner in a reaction comprising modified cell lysates, which provide a suitable environment for the target protein expression,[66] potentially combined with membrane-mimicking structures, such as liposomes and nanodiscs, which capture and present the newly synthesized proteins.[67] Membrane protein presentation on nanodiscs has been successfully implemented for phage display.[62,68].

VLPs are another alternative for presentation of membrane proteins suitable for phage display.[69] VLPs are non-infectious, virus-like multiprotein structures that lack the viral genome, but contain the viral capsid proteins.[70,71] Target membrane proteins can be transiently overexpressed on the surface of the capsid-expressing host cell. The self-assembling viral capsid protein directs the budding of the plasma membrane, resulting in the formation of VLPs studded with target antigens (Fig. 1c). It is also possible to first synthesize the VLPs and then covalently attach the target proteins to their surface.[72] Compared with liposomes, VLPs are more stable and can present antigens at higher density. However, VLPs have a high cost, because commercially available VLPs are expensive, and their production in the lab can be laborious.[72].

Advanced phage display selection strategies

An antibody discovery campaign using phage display selection can be conducted using various strategies and protocols. These strategies should be carefully selected to maximize the chance of discovering an antibody with the desired characteristics. Here, we present different strategies that can be used to discover antibodies with binding characteristics, such as cross-reactivity, high selectivity, or pH dependence.

Deselection strategies: Antigen tags and carrier material

During a selection process, binders will potentially be selected against all antigens, including tags or fusion partners, as well support matrices, such as streptavidin beads. To overcome this, a deselection step using a nontarget is typically included to limit

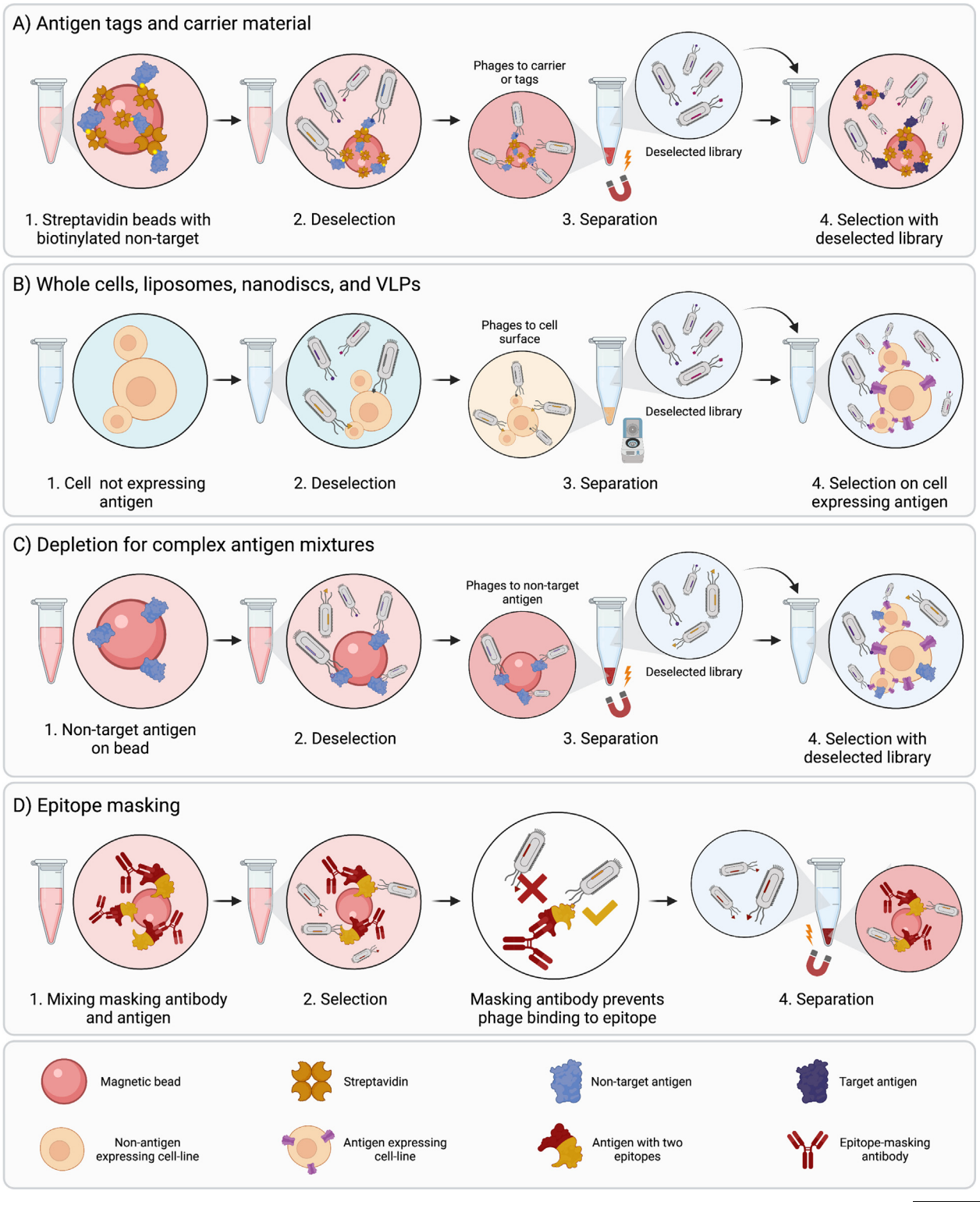

FIG. 2

Deselection strategies. **(a)** Deselection of antibodies against antigen tags or carrier material. **(b)** Deselection when presenting antigens on cells, liposomes, nanodiscs, and virus-like particles (VLPs). **(c)** Depletion of phages when selecting on complex antigen mixtures. **(d)** Using antibodies for masking specific epitopes.

enrichment of antibodies against antigens other than the target. For example, selection on a biotinylated protein using streptavidin beads can be preceded by exposing the library to a biotinylated nontarget protein coupled to streptavidin beads to reduce the proportion of such unwanted binders progressing to the selection step on the intended target[73–75] (Fig. 2a).

Deselection strategies: Whole cells, liposomes, nanodiscs, and VLPs

The same principle can be applied to more complex targets, such as whole cells, liposomes, nanodiscs, or VLPs. When panning on whole cells, a cell transfected to express e.g. a surface receptor of interest is used to display the antigen, and antibodies specific to the receptor can be enriched using a mock-transfected cell or possibly an untransfected cell for deselection.[43,44,54] Moreover, for discovery of antibodies against viral targets, selection can be performed using an infected host cell as antigen and lysate of uninfected host cells for deselection.[76] When cells with an endogenous expression of the target are used, ideally, the same cell knocked down or knocked out for the antigen of interest can be used for deselection (Fig. 2b). For liposomes, nanodiscs, and VLPs, a similar strategy can be used, in which deselection is performed using the particle used for presentation without the antigen embedded, before selection on the antigen-displaying particle.[77]

A more complex scenario is when whole cells are used without knowing the target *a priori* in a phenotypic discovery campaign using mammalian[49] or bacterial cells.[78] Under such circumstances, deselection can be performed on a nontarget cell similar to the target cell to avoid enrichment against common cell surface antigens. However, the perfect match, as in the example with transfected cells, is impossible.[49,79] An example includes deselection on T cells when the goal is to identify antibodies targeting B cells.

Deselection strategies: Depletion for complex antigen mixtures

Deselection through depletion can be used for complex targets, such as whole cells or impure protein samples, also when the target is unknown. An example is selection on whole cells without knowing the target beforehand. In such cases, even though the target antigen is unknown, the nontarget antigens might be known, which allows for protein depletion to be performed. During protein depletion, the phage display library is incubated with recombinant proteins corresponding to nontarget antigens coated or captured on immunotubes or beads. Thereafter, the unbound phages are transferred to the target antigen and used for selection[80–82] (Fig. 2c).

Deselection strategies: epitope-specific deselection

For therapeutic antibodies, it is often crucial which epitope of a target antigen an antibody binds, because this can determine whether the antibody is of therapeutic value. To direct antibody binding to a specific part of the antigen, different techniques can be applied. To find binders against the ligand-binding site of a receptor, the elution step can be performed by adding high concentrations of the ligand, which will elute only antibodies competing with the ligand for binding.[83] However, a major drawback with this strategy is that mainly low-affinity antibodies are eluted, which makes it possible to use the method specifically for the reduction of the amount of low-affinity binders.[84] Antibody blocking,[81] also called epitope masking,[85–88] is another strategy for directing antibodies against a specific part of an antigen. During the selection, previously discovered antibodies binding undesirable epitopes of the antigen are included for blocking. These antibodies bind and block certain epitopes of the antigen, making some epitopes nonaccessible for new antibodies displayed on phages during the selection step. Thereby, antibodies binding new epitopes can be enriched (Fig. 2d). In addition to antibodies, receptor–ligand complexes can also be used in a similar way to deselect binders that do not recognize the same site as the receptor or ligand does.[89]

Selection with competition

In many cases, it is desirable to reduce binding to antigens that are related to the target antigen. Thus, the goal is to focus selections on epitopes that are unique to the target antigen and reduce the proportion of binders to epitopes shared with related antigens. This is achieved by prior deselection on the related antigen.[74] However, deselection is not 100% efficient and is related to the target concentration and the affinity of the binding to the shared epitope. The binding between an antibody and an antigen is an equilibrium reaction following the law of mass action. Therefore, not all antibodies are bound to their antigens at a given time point. Thus, in all deselection strategies, several antibodies that have specificity for an antigen used for deselection will not be bound to the antigen at the time point at which deselection is concluded. Consequently, these antibodies with specificity to the antigen used for deselection will be carried through to the selection phase and might bind the target antigen here. To circumvent this, as an alternative to (or in combination with) deselection, selections can be performed in the presence of competing antigens (selection with competition).

In a selection with competition, target and nontarget antigens are mixed with the antibody library, allowing for competition for antibody binding between the target and nontarget. Use of a large excess of the nontarget antigen drives binding to epitopes shared between target and nontarget antigen, increasing the fraction of recovered antibodies that bind target-specific epitopes. Therefore, after the selection step, antibodies binding to the target antigen are enriched. Strategies to collect the target with binding antibodies include labeling the target with, for example, biotin, while leaving the nontarget unlabeled (Fig. 3a). This strategy can be used both for whole cells and purified proteins.[75] Another alternative is to present the target and nontarget antigens in different ways, such as having the target antigen immobilized or coated on a plastic surface and adding nontarget antigen in solution[90] (Fig. 3b). For whole-cell selections, the nontarget cells can also be presented as membrane particles, resulting in different densities of target and nontarget antigens, which allows for separation through centrifugation.[91].

Antigens that are upregulated in diseased tissue, cells, and fluids compared with healthy samples commonly serve as relevant targets for therapy or diagnosis.[92] An alternative for discovery of both such targets and antibodies targeting these is to use phenotypic discovery. However, in this case, a classical deselection strategy using healthy samples is suboptimal, because binders

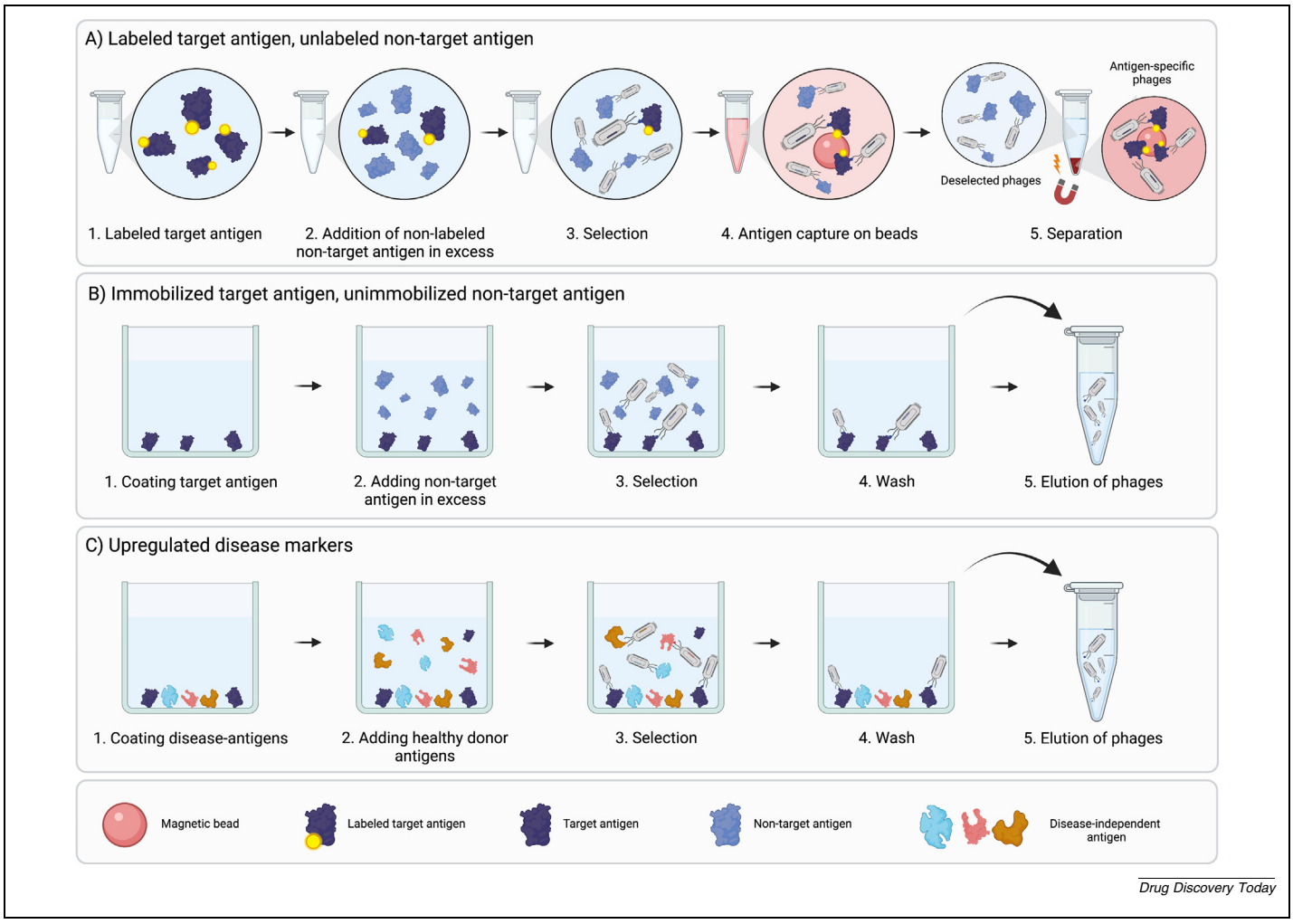

FIG. 3

Selection with competition. **(a)** Competitive selection using labeled target antigen and unlabeled nontarget antigen. **(b)** Competitive selection using immobilized target antigen and non-immobilized nontarget antigen. **(c)** Selecting for upregulated disease markers using competitive selection.

against all antigens present in the deselection step (on the healthy sample) will be reduced. Instead, including a competition during selection allows for the discovery of antibodies against these types of upregulated targets, not only the ones uniquely expressed. By varying the amount of added nontarget antigen for competition, the selection can be guided for the discovery of antibodies against a target that is upregulated to a certain degree.[93] Antibodies will compete for binding to the antigen present on both target and nontarget antigens, and the expression levels will determine whether antibodies are mainly collected and enriched or removed (Fig. 3c).

Strategies to generate cross-reactive antibodies

Antibodies are highly specific molecules, and selections are typically designed to find specific antibodies against one target antigen and avoid any binding to other molecules. However, in many circumstances, although the antibodies must be highly specific for their target, they should preferably also bind homologs or different mutated versions of the same target. For example, preclinical studies of a therapeutic antibody binding a human target will be significantly easier to conduct if the antibody also recognizes the murine and simian version of the antigen. Other examples are infectious diseases and antivenom development, where it is beneficial if broadly neutralizing antibodies recognizing several different viruses, bacteria, or toxins can be discovered.[94]

Cross-panning

A way to achieve cross-reactivity is to perform cross-panning, in which antigens are alternated between the different rounds in the selection process[95] (Fig. 4a). This technique has been used to find antibodies against conserved epitopes of HIV,[96] Influenza A strains,[97] and against cytotoxins in snake venoms from multiple species.[98] Success depends on the degree of conservation between related targets. A requirement for broad cross-reactivity against orthologs or paralogs with low conservation might result in finding low-affinity antibodies, nonspecific binders, or no antibodies.

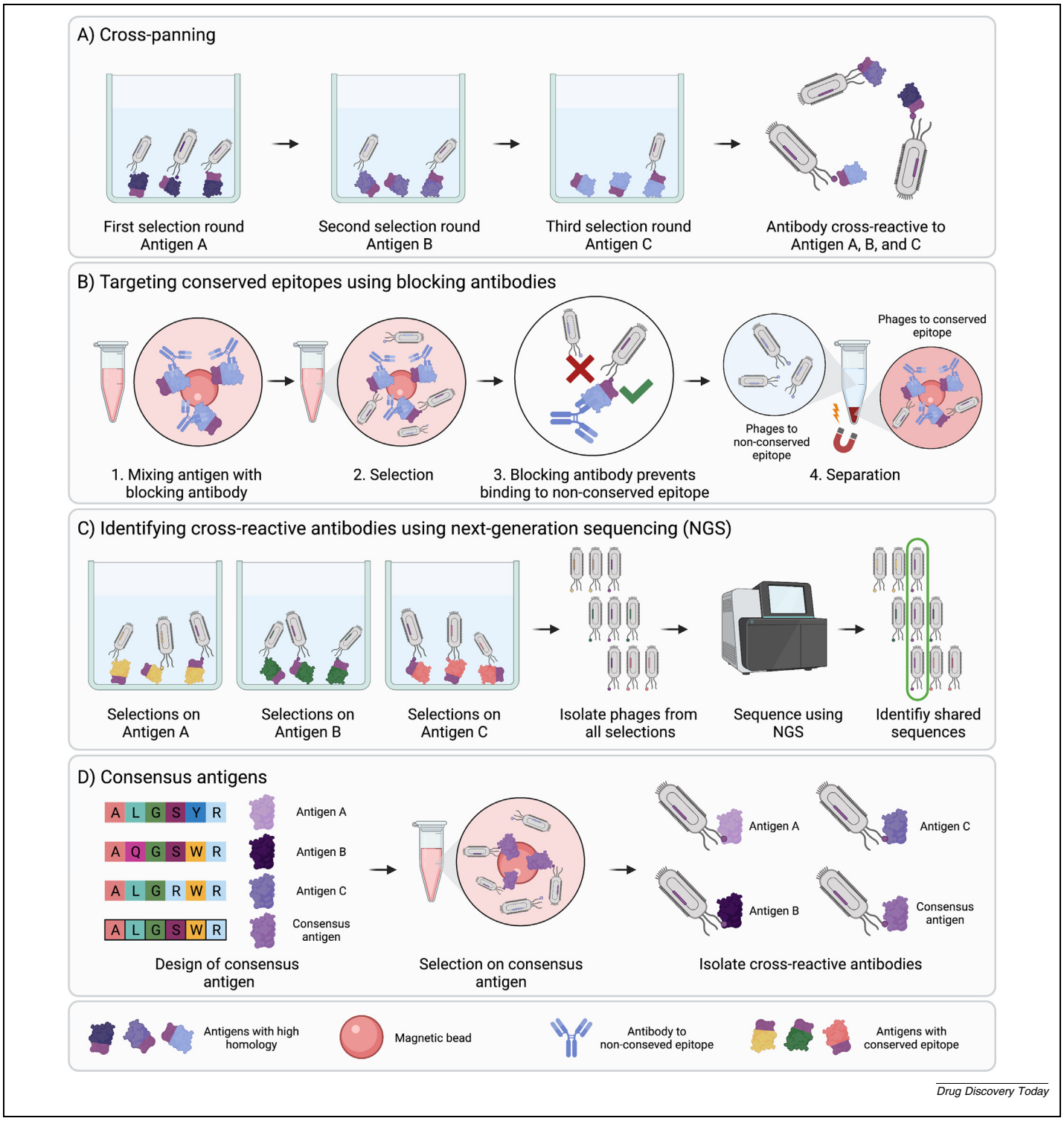

FIG. 4

Strategies to generate cross-reactive antibodies. **(a)** Cross-panning. **(b)** Targeting conserved epitopes using blocking antibodies. **(c)** Using next-generation sequencing (NGS) for identification of cross-reactive antibodies. **(d)** Consensus antigens.

Antibody blocking and next-generation sequencing

For the discovery of cross-reactive antibodies when the same antigen is used in repetitive selection rounds, selections can be guided towards conserved epitopes of the antigen using antibody blocking, as described above (Fig. 4b). Another alternative is to evaluate the output from parallel pannings on different homologous proteins, with next-generation sequencing (NGS) to identify antibodies that are enriched and found in all output pools (Fig. 4c). This has been used to identify binders against serum albumin.[99]

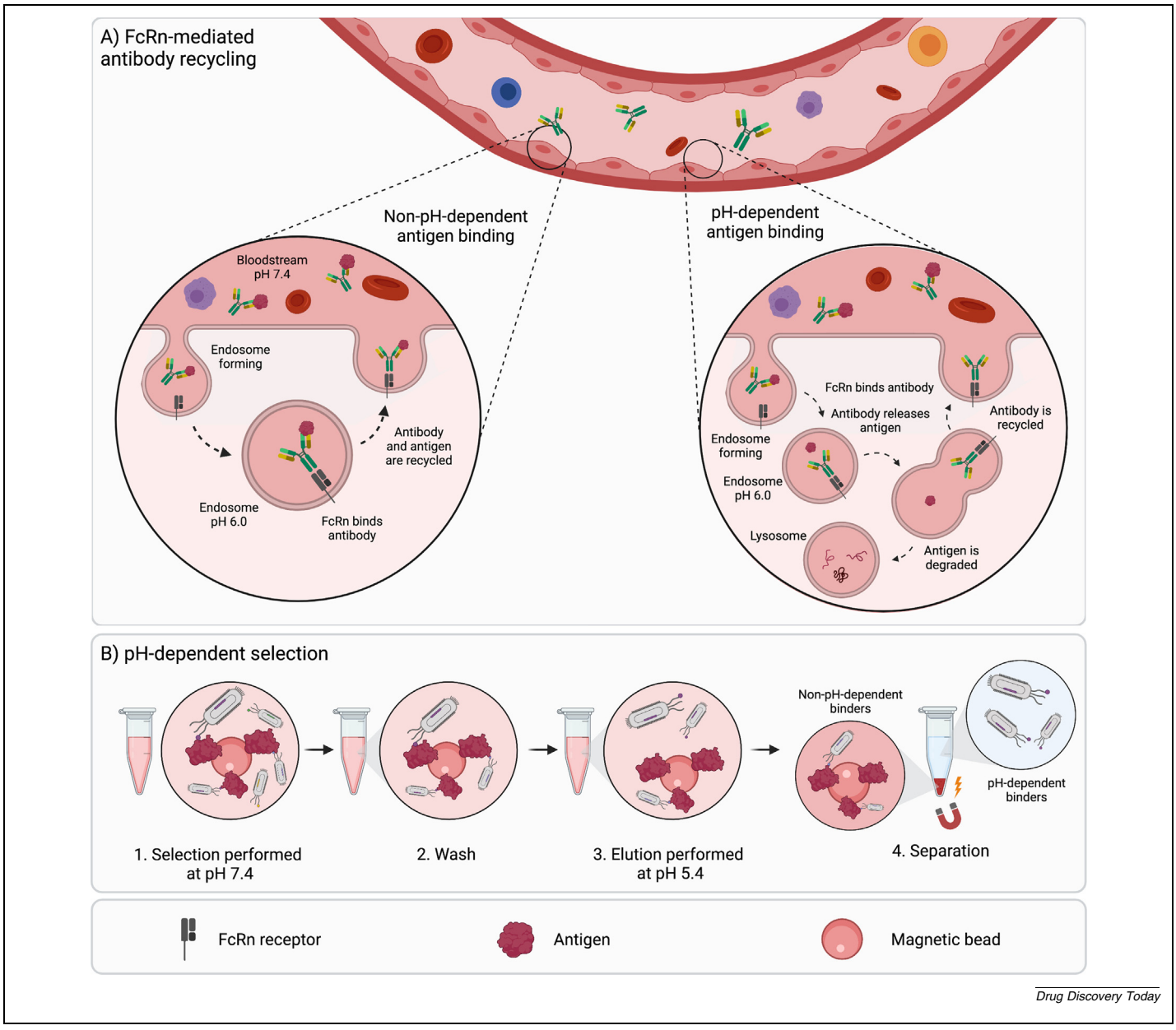

FIG. 5

Environment-sensing antibodies. **(a)** Neonatal Fc receptor (FcRn)-mediated recycling mechanism shown with and without pH-dependent binding to antigen. **(b)** Selection strategy for isolation of antibodies with pH-dependent binding.

Consensus antigens

Another alternative to identify cross-reactive antibodies is to use consensus antigens in the selections (Fig. 4d). A consensus antigen is designed by sequence alignment of multiple homologous antigens and construction of an 'average' consensus antigen, containing the most abundant amino acid in each position. In positions where multiple alternatives exist, different approaches can be taken, such as selecting amino acids based on similar chemical properties or the one with the greatest predicted immunogenicity.[100] Polyclonal broadly neutralizing antibodies against short neurotoxins from various snakes have successfully been generated using consensus toxins for immunization of horses,[101,102] and it has been hypothesized that the use of consensus antigens might also be useful in phage-display-based antibody discovery campaigns.[103]

Selection of environment-sensing antibodies

When administering therapeutic antibodies, the antibodies remain in circulation until they are endocytosed by cells. After endocytosis, the antibodies are directed to the lysosomes, where they can be recycled to the circulation via binding to the neonatal Fc receptor (FcRn). This significantly increases the half-lives of the antibodies.[104] However, when an antibody is bound to an antigen, the antigen-antibody complex is internalized and either degraded in the lysosomal compartment or recycled. To avoid recycling of the antigen as well as unnecessary antibody degrada-

tion, antibodies can be engineered to dissociate from their antigens within the acidic endosomes, allowing the antigen to be degraded while the antibody is recycled[105] (Fig. 5a). For a therapeutic antibody, this enables the antibody to be administered less frequently and/or at a lower dose to the patient. Given that the pH differs between circulation (pH 7.4) and inside endosomes (pH 5.8), antibodies binding their antigens with different affinities at different pH are desirable when the antibody is to be recycled without its cargo. It has been shown that the plasma antigen concentration was decreased by using a pH-dependent antibody, also engineered to have increased FcRn affinity, compared with a conventional antibody.[106,107] In addition, pH-dependent binding can enhance the cytotoxicity of antibody-drug conjugates[108,109] and possibly promote antibody transcytosis across the blood-brain barrier.[109] For discovery of pH-dependent antibodies, the phage selection protocol can be modified to enrich for this property. During the selection, binding is allowed to occur at neutral pH, following elution of pH-dependent binders by decreasing the pH to 5.4.[110] To optimize the chances of finding pH-dependent binders, libraries enriched for histidines can be used, which are described in more detail below.

Another strategy for increasing the half-life of antibodies is to have antibodies with binding properties dependent on the presence of ions. The calcium concentration differs between the environments in the endosomes and the plasma. Therefore, similar to pH dependence, calcium dependence can be used to recycle antibodies from the endosomes. As an example, selections against IL-6R in a calcium-containing buffer, followed by addition of EDTA to chelate Ca^{2+} and thereby elute calcium-dependent antibodies, resulted in the discovery of an antibody with accelerated clearance of the antigen from plasma.[111]

Depending on the final use of the antibodies, enrichment for additional requirements, such as improved stability, or slow off rates, can be achieved during selection. One way to increase the stability is to increase the temperature[112] or add proteases[113] during the selection step for enrichment of antibodies stable to those conditions. For discovery of antibodies with slow off rates, the antigen concentration is typically reduced in consecutive selection rounds,[114] and additional wash steps are added.[115]

In vivo phage display selection

As described previously, using whole cells as antigens for phage display selection is a valid strategy that accommodates many aspects, such as correct folding, post-translational modifications, and functionality of an antigen. However, the complexity and pharmacology of the antigen in a living organism remain lacking. Similar cell types might have completely different expression profiles or post-translational modifications because of variations in tissue microenvironments, both in healthy[116] and diseased tissues.[117]

To fully mimic the *in vivo* profile of the antigen, *in vivo* phage display technology was developed.[118] Here, a phage display library is usually administered intravenously and allowed to circulate, followed by intracardiac perfusion to remove unbound phages. Finally, the phages are rescued from the harvested, homogenized, or lysed target tissues and analyzed by sequencing. If the target of interest is known, the antibodies can be analyzed for binding before sequencing. Enrichment of phages is determined by comparing sequences present in the target tissues

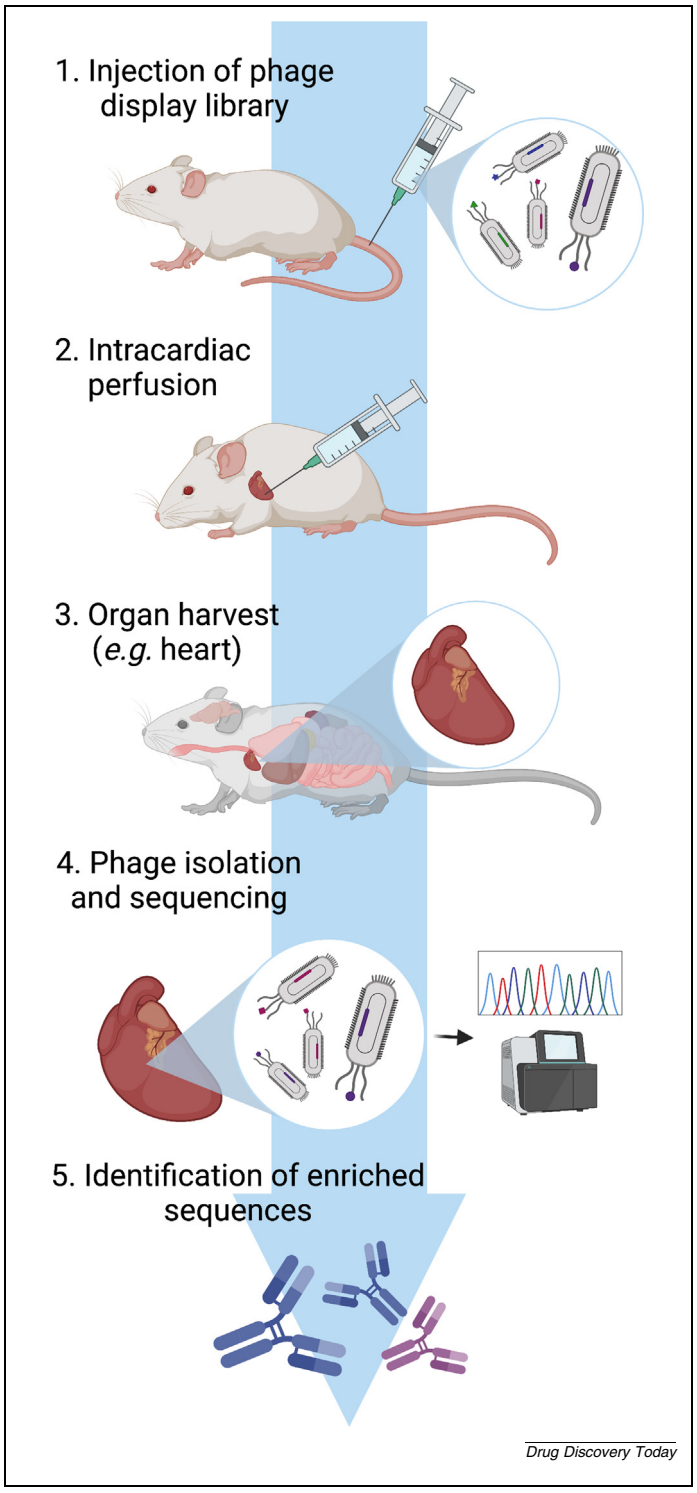

FIG. 6

In vivo phage display selection. (1) Phage display library is injected into the mouse. (2) Intracardiac perfusion is performed before (3) harvesting the organ in question. (4) Phages are isolated from the organ and the DNA is sequenced. (5) Sequences are compared to sequences from phages isolated from other organs or the input to identify enriched sequences.

with sequences present in the input or irrelevant tissues, and enriched sequences are selected for further characterization (Fig. 6).

In the original study describing *in vivo* phage display selection, peptide-based phage display libraries were used for identification of peptides that specifically bound to either brain or kidney blood vessels.[118] Antibodies in the form of scFvs[119,120] and single-domain antibodies (sdAbs)[121,122] have also been discovered using this technology. *In vivo* phage display has mainly been performed using mice or rats, although, a few studies also describe the use of this technology in humans.[123–125] However, it is not possible to perform the intracardiac perfusion step in humans because it leads to the death of the subject. To assign sequences specifically targeting the tissue of interest, phages present in the blood stream are analyzed and used for comparison.

Design of antibody phage display libraries

As described above, selections can be performed using different selection strategies dependent on the final requirements for the desired antibody. In addition to the selection methodologies used, various phage display libraries can also be used to optimize the chances of identifying an antibody with the desired characteristics. Libraries can be based on different antibody formats, on natural or synthetic antibody sequences, and can even be tailored to contain antibodies with specific biophysical or binding characteristics. Different cloning strategies, such as sequential cloning of the light and heavy chain repertoires,[126,127] splicing by overlap extension PCR,[128] or golden gate cloning,[11,129] can be conducted to link V_H and V_L during library construction. Here, we describe some of the general library types, as well as more advanced tailored library designs.

Overall, antibody phage display libraries are divided into two main classes: natural and synthetic libraries, based on the origin of the antibody sequences used for library construction. The sequences are either obtained directly from B cells[73,130,131] or synthetically created using *de novo* synthetic technologies.[131,132]

Natural libraries

Natural libraries capture the antibody repertoire of a donor and can be derived from specifically immunized or non-immunized ('naïve') donors. The immune response following an antigen challenge is accompanied by antibody class-switching from naïve IgM to secreted IgG. Therefore, naïve libraries are typically generated from the IgM repertoire of healthy donors to capture a diverse population of antibodies. By contrast, the IgG repertoire, reflecting the recent immune history of the donor, is used for immune libraries. The immune response is further driven by somatic hypermutations, resulting in improved affinity, expression levels, and antibody specificity.[133] Therefore, on average, antibodies discovered from an immune library have higher affinity than do those directly isolated from naïve libraries. However, antibody-engineering techniques enable optimization of antibodies from naïve libraries to the same or even better performance level compared with antibodies discovered directly from immune libraries.[134] Another difference is that immune libraries are typically smaller in size and can only be effectively used for discovery of antibodies against the antigen used for immunization or closely related antigens, whereas naïve libraries have broader application. For both naïve and immune natural libraries, the diversity of the library goes beyond the natural diversity,[135] because heavy and light chains,[73,127,136] as well as sometimes CDR regions,[137] are combined randomly without consideration for the natural pairing.

Synthetic libraries

Synthetic libraries can be created *de novo* with multiple frameworks and random CDRs[138] or based on natural antibody sequences with synthesis of specific regions of interest in an antibody, typically the CDR loops most likely to be involved in antigen binding.[139] Both synthetic and natural libraries have their pros and cons for use in antibody discovery, some of which will be highlighted below.

Antigen immunogenicity requirements

The creation of an immune library requires immunization with the antigen in question. This requires that the antigen is immunogenic, which is why immune libraries based on human donors cannot be efficiently created against human antigens unless B cells are taken from (naturally) infected patients.[140,141] Therefore, the creation of useful immune libraries against human antigens typically requires the use of orthologous species. For therapeutic purposes, such heterologous antibodies must be 'humanized'[142,143] following discovery. However, humanization can lead to a trade-off with potency, because residues crucial for binding in the original antibody cannot be removed entirely. Alternatively, fully human libraries for self-antigens can now be constructed through immunization of human immunoglobulin transgenic animals.[134]

Naïve libraries, alongside synthetically made libraries, have no antigen immunogenicity requirements and can be used to discover antibodies against all types of antigens, including highly conserved self antigens,[144] as well as those that are toxic to the host.[98]

Library design

Throughout the years, numerous therapeutic antibodies have been discovered through phage display selection campaigns using mainly natural naïve libraries.[145,146] Requirements for a therapeutic antibody include having high stability and a low propensity to aggregate. These traits allow the antibody to be formulated at high concentration, which is often required for administration, and lower the risk of aggregate formation, which is associated with immunogenicity.[147–149] Collectively, biophysical properties of an antibody, that can be used to predict how easy it is to be developed into a therapeutic, are often referred to as the 'developability' of the antibody.[150]

To an extent, the process of B cell maturation eliminates poorly behaved antibodies, because B cell viability is maintained by tonic signaling proportional to the level of surface-expressed B cell receptors.[151] However, the fact that an antibody is from an immune source does not guarantee good developability. Nature does not require individual antibodies to be produced in serum to the level that might be required in antibody drug formulation, where concentrations around 100 mg/ml are typically required. Thus, irrespective of the origin of the antibody, biophysical lia-

bilities sometimes emerge during preclinical/clinical development when higher concentrations are required.[30]

During library construction, developability might be increased through amplification of certain germlines from donor lymphocytes based on the selected primers. However, primer overlap with unfavorable germlines can still occur. In synthetic libraries, developability can be improved by including clinically validated scaffolds and well-paired V_H-V_L germlines.[152] Additionally, germline frameworks not conserved in all humans, such as the VH4b[153], can be omitted in the design.[154]

Finally, removal of sequence liabilities that might influence the antibody homogeneity and downstream manufacturing can be beneficial.[155] Sequence liabilities include NXS glycosylation sites; deamidation NG, NS, and NA motifs; DG isomerization; and M/C oxidation sites.[155] Naturally, the risk that a sequence liability will be important for the binding and functionality of an antibody increases with the number of sequence liabilities that are contained within the antibody paratope. Site-specific control of amino acids within synthetic libraries allow to minimize the occurrence of these motifs relative to natural libraries, which can save time on downstream engineering.

Library diversity

Central to the prospects of discovering a therapeutic antibody against a desired epitope is maximizing the sequence diversity captured within a phage display library. Immune libraries use the natural diversity and affinity maturation process *in vivo* and are enriched for binders specific to the antigen used for immunization, but their use is limited to antibody discovery campaigns directed against only that and closely related antigens. By contrast, unbiased naïve and synthetic libraries can, if they are large enough, be used for discovery of binders against any antigen of interest.[73]

First-generation naïve libraries conventionally approached maximizing diversity by increasing the number of donors used as input into the library. The existence of public clones, antibody sequences that are shared between humans,[156] affects the true diversity of such first-generation naïve libraries. Consequently, the library size, determined by the number of unique sequences, is orders of magnitudes lower than how phage display diversity is measured conventionally (by counting the number of colonies following library transformation).[157] To increase the library size, not only the number of donors used for library construction is of importance, but also simply the amount of genetic starting material used.[158]

When working with synthetic libraries, the researcher has complete control over the input sequences, which means that germlines known to present poorly on phages can be omitted. Furthermore, the use of synthetic technologies can reduce clonal dominance and result in a higher sequence diversity, typically containing > 95% unique clones.[132,154]

Although synthetic libraries are better placed to fill the theoretical sequence space of a phage library with unique clones, it is unknown whether they contain the same level of structural diversity as natural libraries. In particular, the CDR-H3 loop, the most complex and major determinant for antigen specificity,[159] is typically fixed to a narrow loop length in synthetic libraries,[160] which can be a disadvantage for certain targets. Therefore, the theoretical larger size of synthetic libraries might not translate into a more functionally diverse antibody repertoire than those obtained from naïve natural libraries.

Specialized antibody phage libraries

The choice of an appropriate library for a phage display selection campaign is one of the most crucial steps for identifying optimal antibody binders. Factors affecting the library choice include application of the end product, nature of the antigen, and the library availability in the laboratory. The emergence of new molecular methods has allowed laboratories to construct their own combinatorial antibody phage libraries to replicate the natural antibody repertoire offered by the immune system. Many of these libraries are designed with structural and sequence diversity with early-stage drug discovery in mind. However, some applications need libraries comprising antibodies with particular structural- or sequence-based characteristics.

Bispecific antibody libraries

Compared with standard human antibodies, in which both binding sites are directed against the same epitope, bispecific antibodies (bsAbs) are engineered with two binding sites directed to different epitopes. These two binding sites can be directed to the same antigen (biparatopic bsAbs) or two different antigens. In the latter, one paratope could be used to target a specific region or cell, whereas the other one could bind the antigen of interest. The archetypical application of bsAb is T cell redirection in cancer immunotherapy[161] (i.e., the redirection of the cytotoxic activity of effector T cells to specifically eliminate tumor cells), but other disease areas outside cancer are also being explored, such as inflammatory disorders, diabetes, viral and bacterial infections, and Alzheimer's disease.[162]

A huge variety of bispecific antibody formats exists, including bispecific IgGs (bsIgGs), heterodivalent V_HH dimeric constructs, and BiTEs.[162–165] However, some of these antibody formats are not simple to manufacture, such as bsIgGs, which are challenging to produce in a single host cell because co-expression of the heavy and light chains from two different antibodies results in random pairing of the chains and a complex mixture of IgG molecules. Ultimately, this reduces the overall yield of the bsIgG of interest, and the relatively low concentration of the bsIgG among the byproducts (including the incorrectly chain-paired IgGs) results in the need for elaborate purification techniques. To simplify the expression and purification processes, several strategies for chain pairing have been developed, including specialized phage display libraries with common light or heavy chains.[166] This approach allows for the concomitant expression of three different chains (instead of four) in the same cell and results in a mixture containing only two monoclonal antibodies (mAbs) and one bsAb (instead of ten different molecules) (Fig. 7a–c). Moreover, libraries with common light or heavy chains could also be used for the discovery of binding domains that can be used as building blocks to create new antibody formats.[163,167]

Chain pairing with common heavy chains

ScFv-based phage display libraries with a common heavy chain (V_H) and different repertoires of light-chain variable genes (V_L)

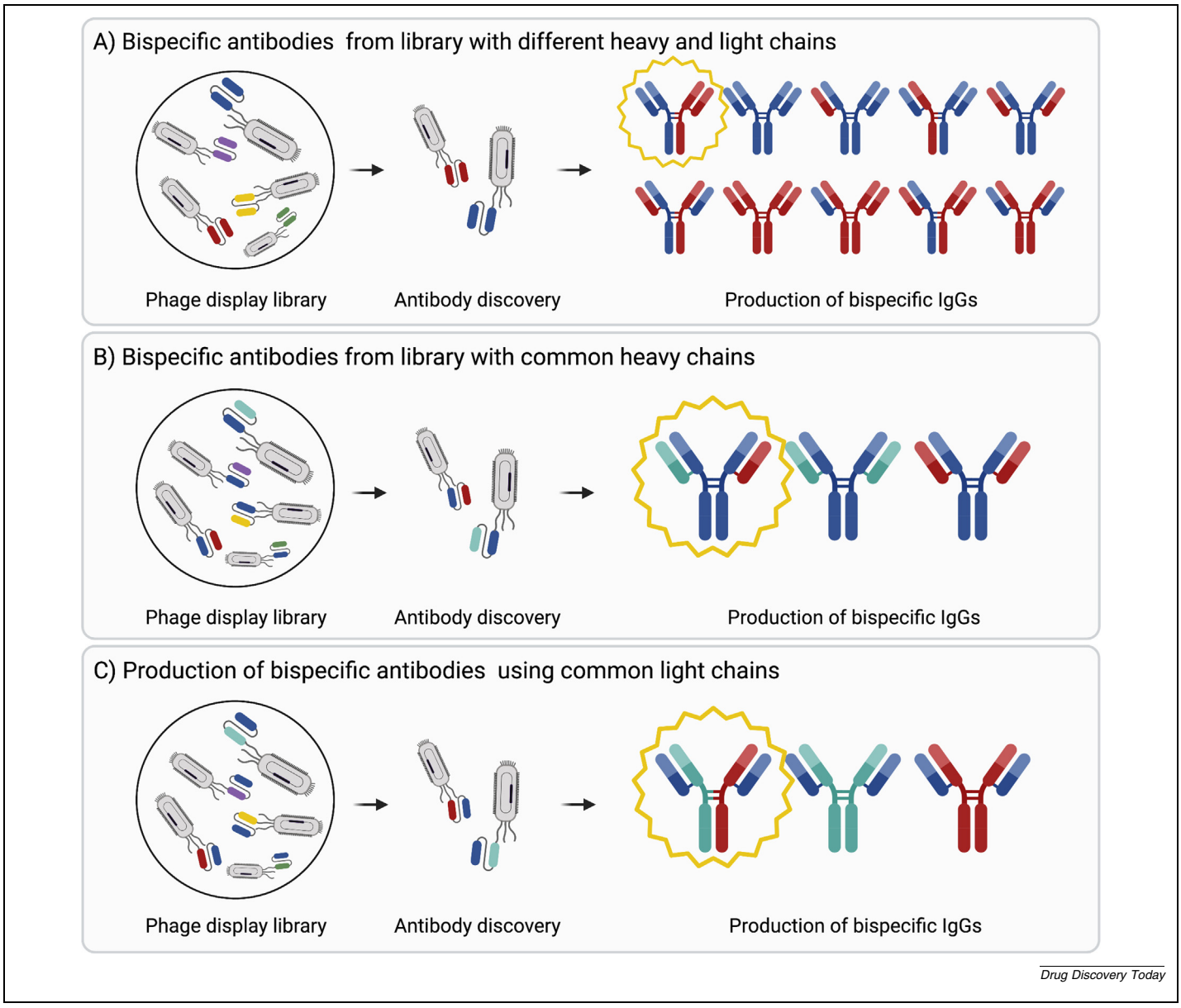

FIG. 7

Production of bispecific antibodies. **(a)** From libraries with different heavy and light chains, resulting in one bispecific antibody and nine incorrect antibody species. **(b)** From libraries with common heavy chains, resulting in one bispecific and only two incorrect antibody species. **(c)** From libraries with common heavy chains, resulting in one bispecific and only two incorrect antibody species.

can be created and used to select antibodies against two different antigens. The fixed V_H could be chosen for its favorable properties for *in vitro* display technologies, its occurrence in natural human antibody repertoires, or intrinsic stability. Alternatively, the V_H could be derived from an already existing mAb. The V_L sequences could either be isolated from circulating B cells from healthy individuals or patients, or diversity could be generated *in vitro* using advanced mutagenesis strategies.[168] This allows for the isolation of candidates with different target specificities that share the same heavy chain but carry either κ or λ light chains. Based on its structure, such a fully human bsIgG format, carrying both a κ and a λ light chain, is referred to as a κλ-body.[168] These specialized libraries have been successfully developed and used against several soluble and cell surface human antigens, resulting in the discovery of high-affinity IgGκ and IgGλ. This confirms that the light chain can be sufficient to drive antibody specificity and has enabled the isolation of high-affinity antibodies that can be used for construction of functional bsIgG for several antigen combinations.[168]

Chain pairing with common light chains

The most common strategy of chain pairing relies on the use of common light chains and distinct diversified heavy chains. This takes advantage of the high diversity in CDR-H3, which tends to dominate binding interactions in many cases.[169,170] Although the first scFv-based phage display libraries with common light chains appeared during the 1990 s,[171,172] subsequent use in bispecifics is more complicated than the corresponding heavy-

light chain pairing with a common heavy chain. Indeed, modification of the heavy chain in the Fc region is necessary to force the heterodimerization of two different heavy chains (e.g., 'knobs-into-holes' technology,[156,172,173] use of opposite electrostatic charges,[174–176] or grafting a heterodimeric interface onto the homodimeric interface of the IgG[177]). However, this strategy has been successfully applied with scFv and Fab libraries, with common light chains extracted from naïve or immune repertoires, as well as from existing therapeutic antibodies.[172,178,179] More recently, complexity has further increased with the generation of bispecific antibodies with histidine-enriched common light chains, allowing the antibody to bind its targets in a pH-dependent manner,[180] as further described below.

Libraries focused on CDR-H3

The CDR3 of the immunoglobulin heavy and light chains are the most important regions involved in antigen contacts in antibody–antigen complexes. In particular, CDR-H3 shows the largest diversity of the CDRs, both in terms of sequence and length,[169] and this diversity is often sufficient for driving the specificity of an antibody.[169,170,181] Therefore, small libraries with relatively large structural diversity can be created by focusing on diversity in the CDR-H3 residues alone.[182]

Researchers have shed light on structural differences in CDR-H3s between antibodies from different species. For example, it was found that the CDR-H3s in antibodies from galline, camelid, and bovine species are longer than the corresponding loop of human antibodies, although examples of long CDR-H3s in humans exist.[183] Galline antibodies contain a high proportion of small amino acids that are associated with flexibility,[184] and high-affinity binding galline antibodies typically have an increased cysteine content, which creates long loops with complex, disulfide-constrained structures. Using yeast display technology,[185] or immunization followed by sorting and NGS of antigen binding B cells,[186] bovine antibodies with CDR-H3s specific against epidermal growth factor receptor (EGFR) and complement component C5, respectively, have been discovered. This highlights the likelihood that long loop binders can also be discovered from bovine antibody libraries using phage display technology. In camelids, the V_HHs tend to bind with protruding loops into concave cavities on the surface of the antigen, whereas, in bovines, ultralong CDR-H3 regions form a 'stalk and knob' independently folding mini domain, similar to a knottin domain, which projects far out from the surface of the antibody and is diverse in both its sequence and disulfide pattern.[187] This 'minifold' has a general shape and dimension similar to several small disulfide-bonded protein families, including protease inhibitors, ion-channel blockers, venom toxins, and G-protein-coupled receptor ligands.[188–190] Thus, these atypical paratopes could provide the ability to interact with different epitopes, particularly recessed or concave surfaces, as exist in many enzymes, pores, and channels, compared with traditional antibodies.[191,192] As a proof of concept, an antibody format, 'KnotBodies', which are similar to the peculiar bovine antibodies and display knottin domains in place of the CDR2 loops,[193] was recently developed. These knottins, which are difficult to engineer and have short *in vivo* half-lives on their own,[194] benefit from the increased stability and extended half-life of the antibody scaffold. Both the knottin and the antibody loop sequences could be engineered and used in phage display selections to optimize binding selectivity and, as an example, the blocking potency of an antibody against an ion-channel.

Altogether, elucidation of other structural features of antibodies from other species has revealed eccentricities that can be used to bind new types of difficult-to-target epitopes, and new specialized phage display libraries with these features are coming to light.[195–198].

Side-and-loop libraries

SdAbs and antibody mimics typically bind antigen clefts via their CDR loops.[199,200] As a consequence, when the antigen epitope is different (i.e., rather convex), it is less likely that an sdAb with a convex paratope will be able to bind. Hence, researchers have generated a new recognition surface on single immunoglobulin-like scaffolds by tailoring the location of amino acid diversity to residues outside the conventional loop positions.

Koide *et al*. observed that an FN3 monobody (an antibody mimic selected from a diversified library of the tenth FN3 domain of human fibronectin), was forming a binding surface via the longest loop and the face of a β-sheet.[201] Based on this observation, they created a monobody 'side-and-loop' library,[201] in which the longest loop and the adjacent β-sheet were carrying diversity. This corresponds, by structural homology, to the CDR3 loop and the β-sheet of an immunoglobulin that mediates heterodimerization between the variable domains of the heavy and light chains. After a few rounds of phage and yeast display selection, using a 'side-and-loop' and a 'loop only' library in parallel, it was demonstrated that the two libraries performed differently against different targets. Indeed, for one target (GFP), the side library clones had higher affinity than the counterparts from the loop library, whereas, for another target (hSUMO1), the trend was the opposite. This demonstrated that alternative library designs focused on the side-and-loop surface could be more effective than conventional loop-based strategies in recognizing epitopes with distinct topography.[202–205]

Histidine-enriched libraries

The pH dependence of antibody–antigen interactions has an effect on subcellular trafficking dynamics and antibody recycling,[206] as described above. The literature has numerous examples of effective engineered antibodies with pH-sensitive binding derived from existing antibodies.[107,207–210] The principle is relatively simple and relies on the incorporation of histidine residues in the binding interface, which are ionizable at pH lower than 6. Upon protonation of these residues in the acidic endosome, structural transitions, caused by altered electrostatic interactions, account for a loss of binding to the antigen. Moreover, the total number of ionizable histidine residues involved in antigen binding impacts the degree of pH sensitivity.[208]

Whereas most examples of engineered antibodies with pH-sensitive binding used histidine scanning alone or combinatorial histidine scanning libraries derived from existing antibodies, there are only a few attempts of *de novo* isolation of pH-dependent antibodies from naïve libraries. The first example took advantage of a synthetic scFv-based phage display library

enriched in histidine residues to find pH-dependent binders to the human chemokine CXCL10.[110] The library was constructed to be histidine enriched by alternating YAT and NHT codons in 8–15 amino acid positions in the CDR-H3. However, after three rounds of selection, the pH dependency of the best clone was too low, and new libraries enriched for histidine in all the CDRs from the light and heavy chains were created. These new scFv-based libraries led to a final reformatted IgG clone with a low nanomolar affinity at pH 7.2 and a 22-fold faster dissociation rate at pH 6.0. Another recent study used a histidine-enriched and CDR3-diversified V_{NAR} domain yeast display library against EpCAM, in which only one pH-dependent binder was found.[211]

The upfront selection of optimal conformations or sequences rather than the re-engineering of an antibody that was not initially selected for pH-dependent binding properties appears an attractive idea. Indeed, it is understandable that already existing antibodies are not always amenable to transformation into pH-dependent antibodies. However, the only two examples of *de novo* isolation of pH-sensitive antibodies might be an indication of the process difficulty, including the need to generate additional sublibraries for pH dependence and affinity maturation. Furthermore, the histidine-mediated pH-dependent binding restricts the number of suitable epitopes because they need to have positively charged, or proton donating residues. In other words, a negatively charged or proton-acceptor epitope is theoretically a difficult target for a pH-dependent binding antibody.

Concluding remarks

In this review, four major parameters that can be altered to tailor an antibody discovery campaign using phage display selections have been presented: antibody format, antigen presentation, selection strategy, and design of phage display library. The information provided in this review can be used individually or in combination for designing an antibody discovery campaign, dependent on the requirements of the desired antibodies.

Declaration of interests

The authors declare that they have no competing interests.

CRediT authorship contribution statement

Line Ledsgaard: Conceptualization, Investigation, Visualization, Writing – original draft, Writing – review & editing. **Anne Ljungars:** Conceptualization, Investigation, Writing – original draft, Writing – review & editing. **Charlotte Rimbault:** Investigation, Writing – original draft, Writing – review & editing. **Christoffer V. Sørensen:** Investigation, Writing – original draft, Writing – review & editing. **Tulika Tulika:** Investigation, Writing – original draft, Writing – review & editing. **Jack Wade:** Investigation, Writing – original draft, Writing – review & editing. **Yessica Wouters:** Investigation, Writing – original draft, Writing – review & editing. **John McCafferty:** Investigation, Writing – review & editing. **Andreas H. Laustsen:** Conceptualization, Investigation, Writing – review & editing.

Acknowledgments

Figures were created using BioRender (BioRender.com). The authors gratefully acknowledge the following sources of funding: Villum Foundation grant 00025302, Wellcome (221702/Z/20/Z), The European Research Council (ERC) under the European Union's Horizon 2020 research and innovation programme grant no. 850974, The Novo Nordisk Foundation (NNF16OC0019248), and The Hørslev Foundation (203866) to A.H.L.; Olsens Mindefold, Marie og M.B. Richters Fond, Niels Bohr Fondet, Torben og Alice Fritmodts Fond, William Demant Fonden, Otto Mønsteds Fond, Knud Højgaards Fond, Rudolph Als Fondet, Augustinus Fonden, and Tranes Fond to L.L.

References

1. G.P. Smith, Filamentous fusion phage: novel expression vectors that display cloned antigens on the virion surface, Science. 228 (1985) 1315–1317.
2. J. McCafferty, A.D. Griffiths, G. Winter, D.J. Chiswell, Phage antibodies: filamentous phage displaying antibody variable domains, Nature. 348 (1990) 552–554.
3. M.A. Alfaleh, H.O. Alsaab, A.B. Mahmoud, A.A. Alkayyal, M.L. Jones, S.M. Mahler, et al., Phage display derived monoclonal antibodies: from bench to bedside, Front Immunol. 11 (2020) 1986.
4. J. Hanes, A. Plückthun, *In vitro* selection and evolution of functional proteins by using ribosome display, Proc Natl Acad Sci USA 94 (1997) 4937–4942.
5. L.C. Mattheakis, R.R. Bhatt, W.J. Dower, An *in vitro* polysome display system for identifying ligands from very large peptide libraries, Proc Natl Acad Sci USA 91 (1994) 9022–9026.
6. E.T. Boder, Wittrup KD Yeast surface display for screening combinatorial polypeptide libraries, Nat Biotechnol. 15 (1997) 553–557.
7. K. Parthiban, R.L. Perera, M. Sattar, Y. Huang, S. Mayle, E. Masters, et al., A comprehensive search of functional sequence space using large mammalian display libraries created by gene editing, mAbs 11 (2019) 884–898.
8. R.R. Beerli, M. Bauer, R.B. Buser, M. Gwerder, S. Muntwiler, P. Mauer, et al., Isolation of human monoclonal antibodies by mammalian cell display, Proc Natl Acad Sci USA 105 (2008) 14336–14341.
9. J.W. Kehoe, B.K. Kay, Filamentous phage display in the New Millennium, Chem. Rev. 105 (2005) 4056–4072.
10. C.E.Z. Chan, A.H.Y. Chan, A.P.C. Lim, Hanson BJ Comparison of the efficiency of antibody selection from semi-synthetic scFv and non-immune Fab phage display libraries against protein targets for rapid development of diagnostic immunoassays, J Immunol Methods 373 (2011) 79–88.
11. K. Chockalingam, Z. Peng, C.N. Vuong, L.R. Berghman, Chen Z Golden Gate assembly with a bi-directional promoter (GBid): a simple, scalable method for phage display Fab library creation, Sci Rep. 10 (2020) 2888.
12. K. Li, K.A. Zettlitz, J. Lipianskaya, Y. Zhou, J.D. Marks, P. Mallick, et al., A fully human scFv phage display library for rapid antibody fragment reformatting, Protein Eng Des Sel. 28 (2015) 307–316.
13. R. Ahamadi-Fesharaki, A. Fateh, F. Vaziri, G. Solgi, S.D. Siadat, F. Mahboudi, et al., Single-chain variable fragment-based bispecific antibodies: hitting two targets with one sophisticated arrow, Mol. Ther. Oncolytics 14 (2019) 38–56.
14. D. Röthlisberger, A. Honegger, A. Plückthun, Domain interactions in the Fab fragment: a comparative evaluation of the single-chain Fv and Fab format engineered with variable domains of different stability, J Mol Biol. 347 (2005) 773–789.
15. M. Steinwand, P. Droste, A. Frenzel, M. Hust, S. Dübel, T. Schirrmann, The influence of antibody fragment format on phage display based affinity maturation of IgG, mAbs 6 (2014) 204–218.
16. V. Quintero-Hernández, V.R. Juárez-González, M. Ortíz-León, R. Sánchez, L.D. Possani, B. Becerril, The change of the scFv into the Fab format improves the stability and *in vivo* toxin neutralization capacity of recombinant antibodies, Mol Immunol. 44 (2007) 1307–1315.
17. A. Frenzel, M. Hust, T. Schirrmann, Expression of recombinant antibodies, Front Immunol. 4 (2013) 217.
18. J.T. Koerber, M.J. Hornsby, J.A. Wells, An improved single-chain Fab platform for efficient display and recombinant expression, J Mol Biol. 427 (2015) 576–586.

19. R.H. Reader, R.G. Workman, B.C. Maddison, K.C. Gough, Advances in the production and batch reformatting of phage antibody libraries, Mol Biotechnol. 61 (2019) 801–815.
20. C. Vincke, R. Loris, D. Saerens, S. Martínez-Rodriguez, S. Muyldermans, K. Conrath, General strategy to humanize a camelid single-domain antibody and identification of a universal humanized nanobody scaffold, J Biol Chem. 284 (2009) 3273–3284.
21. D. Könning, S. Zielonka, J. Grzeschik, M. Empting, B. Valldorf, S. Krah, C. Schröter, et al., Camelid and shark single domain antibodies: structural features and therapeutic potential, Curr. Opin. Struct. Biol. 45 (2017) 10–16.
22. S. Jähnichen, C. Blanchetot, D. Maussang, M. González-Pajuelo, K.Y. Chow, L. Bosch, et al., CXCR4 nanobodies (VHH-based single variable domains) potently inhibit chemotaxis and HIV-1 replication and mobilize stem cells, Proc. Natl. Acad. Sci. U. S. A. 107 (2010) 20565–20570.
23. H. Dooley, M.F. Flajnik, A.J. Porter, Selection and characterization of naturally occurring single-domain (IgNAR) antibody fragments from immunized sharks by phage display, Mol. Immunol. 40 (2003) 25–33.
24. H. Ebersbach, S. Geisse, Antigen generation and display in therapeutic antibody drug discovery – a neglected but critical player, Biotechnol. J. 7 (2012) 1433–1443.
25. J.E. Butler, L. Ni, R. Nessler, K.S. Joshi, M. Suter, B. Rosenberg, et al., The physical and functional behavior of capture antibodies adsorbed on polystyrene, J. Immunol. Methods 150 (1992) 77–90.
26. Z. Duan, H. Siegumfeldt, An efficient method for isolating antibody fragments against small peptides by antibody phage display, Comb. Chem. High Throughput Screen. 13 (2010) 818–828.
27. C.M. Dundas, D. Demonte, S. Park, Streptavidin-biotin technology: improvements and innovations in chemical and biological applications, Appl. Microbiol. Biotechnol. 97 (2013) 9343–9353.
28. V.S. Ivanov, Z.K. Suvorova, L.D. Tchikin, A.T. Kozhich, V.T. Ivanov, Effective method for synthetic peptide immobilization that increases the sensitivity and specificity of ELISA procedures, J. Immunol. Methods 153 (1992) 229–233.
29. L. Ledsgaard, M. Kilstrup, A. Karatt-Vellatt, J. McCafferty, A.H. Laustsen, Basics of antibody phage display technology, Toxins 10 (2018) 236.
30. A.P. Sibler, E. Kempf, A. Glacet, G. Orfanoudakis, D. Bourel, E. Weiss, *In vivo* biotinylated recombinant antibodies: high efficiency of labelling and application to the cloning of active anti-human IgG1 Fab fragments, J. Immunol. Methods 224 (1999) 129–140.
31. E. de Boer, P. Rodriguez, E. Bonte, J. Krijgsveld, E. Katsantoni, A. Heck, et al., Efficient biotinylation and single-step purification of tagged transcription factors in mammalian cells and transgenic mice, Proc. Natl. Acad. Sci. USA 100 (2003) 7480–7485.
32. D. Beckett, E. Kovaleva, Schatz PJA minimal peptide substrate in biotin holoenzyme synthetase-catalysed biotinylation, Protein Sci. 8 (1999) 921–929.
33. M.G. Cull, P.J. Schatz, Biotinylation of proteins *in vivo* and *in vitro* using small peptide tags, Methods Enzymol. 326 (2000) 430–440.
34. B.K. Kay, S. Thai, V.V. Volgina, High-throughput biotinylation of proteins, Methods Mol. Biol. 498 (2009) 185–196.
35. M.D. Scholle, F.R. Collart, B.K. Kay, *In vivo* biotinylated proteins as targets for phage-display selection experiments, Protein Expr. Purif. 37 (2004) 243–252.
36. M. Fairhead, M. Howarth, Site-specific biotinylation of purified proteins using BirA, Methods Mol. Biol. 1266 (2015) 171–184.
37. O. Azim-Zadeh, A. Hillebrecht, U. Linne, M.A. Marahiel, G. Klebe, K. Lingelbach, et al., Use of biotin derivatives to probe conformational changes in proteins, J. Biol. Chem. 282 (2007) 21609–21617.
38. Luna EJ. Biotinylation of proteins in solution and on cell surfaces. *Curr. Protoc. Protein Sci.* 2001; Chapter 3, Unit 3.6.
39. Luna EJ. Biotinylation of proteins in solution and on cell surfaces. *Curr. Protoc. Protein Sci.* 1996; 6; 3.6.1–3.6.15.
40. A. Koide, J. Wojcik, R.N. Gilbreth, A. Reichel, J. Piehler, S. Koide, Accelerating phage-display library selection by reversible and site-specific biotinylation, Protein Eng. Des. Sel. 22 (2009) 685–690.
41. B. Zakeri, J.O. Fierer, E. Celik, E.C. Chittock, U. Schwarz-Linek, V.T. Moy, et al., Peptide tag forming a rapid covalent bond to a protein, through engineering a bacterial adhesin, Proc. Natl. Acad. Sci. USA 109 (2012) E690–E697.
42. J.K. Fierle, J. Abram-Saliba, M. Brioschi, M. deTiani, G. Coukos, S.M. Dunn, Integrating SpyCatcher/SpyTag covalent fusion technology into phage display workflows for rapid antibody discovery, Sci. Rep. 9 (2019) 12815.
43. M.L. Jones, M.A. Alfaleh, S. Kumble, S. Zhang, G.W. Osborne, M. Yeh, et al., Targeting membrane proteins for antibody discovery using phage display, Sci. Rep. 6 (2016) 26240.
44. B.D. Lipes, Y.-H. Chen, H. Ma, H.F. Staats, D.J. Kenan, M.D. Gunn, An entirely cell-based system to generate single-chain antibodies against cell surface receptors, J. Mol. Biol. 379 (2008) 261–272.
45. K.H. Khan, Gene expression in mammalian cells and its applications, Adv. Pharm. Bull. 3 (2013) 257–263.
46. A.D. Bandaranayake, S.C. Almo, Recent advances in mammalian protein production, FEBS Lett. 588 (2014) 253–260.
47. E. Urich, S.E. Lazic, J. Molnos, I. Wells, P.O. Freskgård, Transcriptional profiling of human brain endothelial cells reveals key properties crucial for predictive *in vitro* blood-brain barrier models, PLoS ONE 7 (2012) e38149.
48. P. Uva, A. Lahm, A. Sbardellati, A. Grigoriadis, A. Tutt, E. de Rinaldis, Comparative membranome expression analysis in primary tumors and derived cell lines, PLoS ONE 5 (2010) e11742.
49. A. Ljungars, L. Mårtensson, J. Mattsson, M. Kovacek, A. Sundberg, U.-C. Tornberg, et al., A platform for phenotypic discovery of therapeutic antibodies and targets applied on chronic lymphocytic leukemia, NPJ Precis. Oncol. 2 (2018) 18.
50. K. Kanonenberg, J. Royes, A. Kedrov, G. Poschmann, F. Angius, A. Solgadi, et al., Shaping the lipid composition of bacterial membranes for membrane protein production, Microb. Cell Factories 18 (2019) 131.
51. S.J. Routledge, L. Mikaliunate, A. Patel, M. Clare, S.P. Cartwright, Z. Bawa, et al., The synthesis of recombinant membrane proteins in yeast for structural studies, Methods 95 (2016) 26–37.
52. C. Trometer, P. Falson, Mammalian membrane protein expression in baculovirus-infected insect cells, in: I. Mus-Veteau (Ed.), Heterologous Expression of Membrane Proteins: Methods and Protocols, Totowa; Humana Press, 2010, pp. 105–117.
53. Tur MK, Huhn M, Sasse S, Engert A, Barth S. Selection of scFv phages on intact cells under low pH conditions leads to a significant loss of insert-free phages. *BioTechniques* 2010; 30: 404–408, 410, 412–413.
54. Y. Stark, S. Venet, A. Schmid, Whole cell panning with phage display, Methods Mol. Biol. 1575 (2017) 67–91.
55. A. Jesorka, O. Orwar, Liposomes: technologies and analytical applications, Annu. Rev. Anal. Chem. 1 (2008) 801–832.
56. L.K. Jespersen, A. Kuusinen, A. Orellana, K. Keinänen, J. Engberg, Use of proteoliposomes to generate phage antibodies against native AMPA receptor, Eur. J. Biochem. 267 (2000) 1382–1389.
57. I.A. Smirnova, P. Ädelroth, P. Brzezinski, Extraction and liposome reconstitution of membrane proteins with their native lipids without the use of detergents, Sci. Rep. 8 (2018) 14950.
58. T. Ravula, N.Z. Hardin, A. Ramamoorthy, Polymer nanodiscs: advantages and limitations, Chem. Phys. Lipids 219 (2019) 45–49.
59. I.G. Denisov, S.G. Sligar, Nanodiscs for structural and functional studies of membrane proteins, Nat. Struct. Mol. Biol. 23 (2016) 481–486.
60. T.H. Bayburt, Y.V. Grinkova, S.G. Sligar, Self-assembly of discoidal phospholipid bilayer nanoparticles with membrane scaffold proteins, Nano Lett. 2 (2002) 853–856.
61. A. Nath, W.M. Atkins, S.G. Sligar, Applications of phospholipid bilayer nanodiscs in the study of membranes and membrane proteins, Biochemistry 46 (2007) 2059–2069.
62. M. Pavlidou, K. Hänel, L. Möckel, D. Willbold, Nanodiscs allow phage display selection for ligands to non-linear epitopes on membrane proteins, PLoS ONE 8 (2013) e72272.
63. T.J. Knowles, R. Finka, C. Smith, Y.-P. Lin, T. Dafforn, M. Overduin, Membrane proteins solubilized intact in lipid containing nanoparticles bounded by styrene maleic acid copolymer, J. Am. Chem. Soc. 131 (2009) 7484–7485.
64. K.S. Simon, N.L. Pollock, S.C. Lee, Membrane protein nanoparticles: the shape of things to come, Biochem. Soc. Trans. 46 (2018) 1495–1504.
65. L. Thoring, D.A. Wüstenhagen, M. Borowiak, M. Stech, A. Sonnabend, S. Kubick, Cell-free systems based on CHO cell lysates: optimization strategies, synthesis of 'difficult-to-express' proteins and future perspectives, PLoS ONE 11 (2016) e0163670.
66. S.K. Dondapati, M. Stech, A. Zemella, S. Kubick, Cell-free protein synthesis: a promising option for future drug development, BioDrugs 34 (2020) 327–348.
67. C.E. Hodgman, M.C. Jewett, Cell-free synthetic biology: thinking outside the cell, Metab. Eng. 14 (2012) 261–269.
68. P.K. Dominik, M.T. Borowska, O. Dalmas, S.S. Kim, E. Perozo, R.J. Keenan, et al., Conformational chaperones for structural studies of membrane proteins using antibody phage display with nanodiscs, Structure. 24 (2016) 300–309.
69. B. van der Woning, G. De Boeck, C. Blanchetot, V. Bobkov, A. Klarenbeek, M. Saunders, et al., DNA immunization combined with scFv phage display identifies antagonistic GCGR specific antibodies and reveals new epitopes on the small extracellular loops, mAbs 8 (2016) 1126–1135.

70. Z. Shirbaghaee, A. Bolhassani, Different applications of virus-like particles in biology and medicine: vaccination and delivery systems, Biopolymers 105 (2016) 113–132.
71. A. Zeltins, Construction and characterization of virus-like particles: a review, Mol. Biotechnol. 53 (2013) 92–107.
72. R. Huang, M.M. Kiss, M. Batonick, M.P. Weiner, B.K. Kay, Generating recombinant antibodies to membrane proteins through phage display, Antibodies 5 (2016) 11.
73. D.J. Schofield, A.R. Pope, V. Clementel, J. Buckell, S.D.J. Chapple, K.F. Clarke, et al., Application of phage display to high throughput antibody generation and characterization, Genome Biol. 8 (2007) R254.
74. A. Roghanian, I. Teige, L. Mårtensson, K.L. Cox, M. Kovacek, A. Ljungars, et al., Antagonistic human FcγRIIB (CD32B) antibodies have anti-tumor activity and overcome resistance to antibody therapy *in vivo*, Cancer Cell 27 (2015) 473–488.
75. M. Yeboah, C. Papagregoriou, D.C. Jones, H.T.C. Chan, G. Hu, J.S. McPartlan, et al., LILRB3 (ILT5) is a myeloid cell checkpoint that elicits profound immunomodulation, JCI Insight 5 (2020) 141593.
76. M.I. Kirsch, B. Hülseweh, C. Nacke, T. Rülker, T. Schirrmann, H.-J. Marschall, et al., Development of human antibody fragments using antibody phage display for the detection and diagnosis of Venezuelan equine encephalitis virus (VEEV), BMC Biotechnol. 8 (2008) 66.
77. P.K. Dominik, A.A. Kossiakoff, Phage display selections for affinity reagents to membrane proteins in nanodiscs, Methods Enzymol. 557 (2015) 219–245.
78. A. DiGiandomenico, P. Warrener, M. Hamilton, S. Guillard, P. Ravn, R. Minter, et al., Identification of broadly protective human antibodies to Pseudomonas aeruginosa exopolysaccharide Psl by phenotypic screening, J. Exp. Med. 209 (2012) 1273–1287.
79. J.B. Ridgway, E. Ng, J.A. Kern, J. Lee, J. Brush, A. Goddard, P. Carter, Identification of a human anti-CD55 single-chain Fv by subtractive panning of a phage library using tumor and nontumor cell lines, Cancer Res. 59 (1999) 2718–2723.
80. G.S. Williams, B. Mistry, S. Guillard, J.C. Ulrichsen, A.M. Sandercock, J. Wang, et al., Phenotypic screening reveals TNFR2 as a promising target for cancer immunotherapy, Oncotarget 7 (2016) 68278–68291.
81. A. Ljungars, C. Svensson, A. Carlsson, B. Birgersson, U.-C. Tornberg, B. Frendéus, et al., Deep mining of complex antibody phage pools generated by cell panning enables discovery of rare antibodies binding new targets and epitopes, Front. Pharmacol. 10 (2019) 847.
82. C.C. Lim, P.C.Y. Woo, T.S. Lim, Development of a phage display panning strategy utilizing crude antigens: isolation of MERS-CoV nucleoprotein human antibodies, Sci. Rep. 9 (2019) 6088.
83. S.U. Eisenhardt, M. Schwarz, N. Bassler, K. Peter, Subtractive single-chain antibody (scFv) phage-display: tailoring phage-display for high specificity against function-specific conformations of cell membrane molecules, Nat. Protoc. 2 (2007) 3063–3073.
84. H. Thie, B. Voedisch, S. Dübel, M. Hust, T. Schirrmann, Affinity maturation by phage display, Methods Mol. Biol. 525 (2009) 309–322.
85. H.J. Ditzel, Rescue of a broader range of antibody specificities using an epitope-masking strategy, in: P.M. O'Brien, R. Aitken (Eds.), Antibody Phage Display: Methods and Protocols, Humana Press, Totowa, 2002, pp. 179–186.
86. H.J. Ditzel, J.M. Binley, J.P. Moore, J. Sodroski, N. Sullivan, L.S. Sawyer, et al., Neutralizing recombinant human antibodies to a conformational V2- and CD4-binding site-sensitive epitope of HIV-1 gp120 isolated by using an epitope-masking procedure, J. Immunol. 1995 (154) (1950) 893–906.
87. P.P. Sanna, R.A. Williamson, A.D. Logu, F.E. Bloom, D.R. Burton, Directed selection of recombinant human monoclonal antibodies to herpes simplex virus glycoproteins from phage display libraries, Proc. Natl. Acad. Sci. USA 92 (1995) 6439–6443.
88. K. Even-Desrumeaux, D. Nevoltris, M.N. Lavaut, K. Alim, J.-P. Borg, S. Audebert, et al., Masked selection: a straightforward and flexible approach for the selection of binders against specific epitopes and differentially expressed proteins by phage display, Mol. Cell. Proteomics 13 (2014) 653–665.
89. X. Zeng, L. Li, J. Lin, X. Li, B. Liu, Y. Kong, et al., Isolation of a human monoclonal antibody specific for the receptor binding domain of SARS-CoV-2 using a competitive phage biopanning strategy, Antib. Ther. 3 (2020) 95–100.
90. B. Stausbøl-Grøn, T. Wind, S. Kjaer, L. Kahns, N.J.V. Hansen, P. Kristensen, et al., A model phage display subtraction method with potential for analysis of differential gene expression, FEBS Lett. 391 (1996) 71–75.
91. J. Fransson, U.-C. Tornberg, C.A.K. Borrebaeck, R. Carlsson, B. Frendéus, Rapid induction of apoptosis in B-cell lymphoma by functionally isolated human antibodies, Int. J. Cancer 119 (2006) 349–358.
92. P. Carter, L. Smith, M. Ryan, Identification and validation of cell surface antigens for antibody targeting in oncology, Endocr. Relat. Cancer 11 (2004) 659–687.
93. Frendéus B. Bioinvent International. Method for screening anti-ligand libraries for identifying anti-ligands specific for differentially and infrequently expressed ligands. WO/2004/023140.
94. A.H. Laustsen, How can monoclonal antibodies be harnessed against neglected tropical diseases and other infectious diseases?, Expert Opin Drug Discov. 14 (2019) 1103–1112.
95. A.R.M. Bradbury, S. Sidhu, S. Dübel, J. McCafferty, Beyond natural antibodies: the power of *in vitro* display technologies, Nat. Biotechnol. 29 (2011) 245–254.
96. M.-Y. Zhang, Y. Shu, S. Phogat, X. Xiao, F. Cham, P. Bouma, et al., Broadly cross-reactive HIV neutralizing human monoclonal antibody Fab selected by sequential antigen panning of a phage display library, J. Immunol. Methods 283 (2003) 17–25.
97. D.C. Ekiert, A.K. Kashyap, J. Steel, A. Rubrum, G. Babha, R. Khayat, et al., Cross-neutralization of influenza A viruses mediated by a single antibody loop, Nature. 489 (2012) 526–532.
98. S. Ahmadi, M.B. Pucca, J.A. Jürgensen, R. Janke, L. Ledsgaard, E.M. Schoof, et al., An *in vitro* methodology for discovering broadly-neutralizing monoclonal antibodies, Sci. Rep. 10 (2020) 10765.
99. K.A. Henry, J. Tanha, G. Hussack, Identification of cross-reactive single-domain antibodies against serum albumin using next-generation DNA sequencing, Protein Eng. Des. Sel. 28 (2015) 379–383.
100. A.S. Kolaskar, P.C. Tongaonkar, A semi-empirical method for prediction of antigenic determinants on protein antigens, FEBS Lett. 276 (1990) 172–174.
101. G. de la Rosa, L.L. Corrales-García, X. Rodriguez-Ruiz, E. López-Vera, G. Corzo, Short-chain consensus alpha-neurotoxin: a synthetic 60-mer peptide with generic traits and enhanced immunogenic properties, Amino Acids 50 (2018) 885–895.
102. G. de la Rosa, F. Olvera, I.G. Archundia, B. Lomonte, A. Alagón, G. Corzo, Horse immunization with short-chain consensus α-neurotoxin generates antibodies against broad spectrum of elapid venomous species, Nat. Commun. 10 (2019) 3642.
103. M. Hamza, C. Knudsen, C.A. Gnanathasan, W. Monteiro, M.R. Lewin, A.H. Laustsen, et al., Clinical management of snakebite envenoming: future perspectives, Toxicon X 11 (2021) 100079.
104. D.C. Roopenian, A.S. FcRn, the neonatal Fc receptor comes of age, Nat. Rev. Immunol. 7 (2007) 715–725.
105. T. Igawa, K. Haraya, K. Hattori, Sweeping antibody as a novel therapeutic antibody modality capable of eliminating soluble antigens from circulation, Immunol. Rev. 270 (2016) 132–151.
106. T. Igawa, A. Maeda, K. Karaya, T. Tachibana, Y. Iwayanagi, F. Mimoto, et al., Engineered monoclonal antibody with novel antigen-sweeping activity *in vivo*, PLoS ONE. 8 (2013) e63236.
107. T. Igawa, S. Ishii, T. Tachibana, A. Maeda, Y. Higuchi, S. Shimaoka, et al., Antibody recycling by engineered pH-dependent antigen binding improves the duration of antigen neutralization, Nat. Biotechnol. 28 (2010) 1203–1207.
108. J.C. Kang, W. Sun, P. Khare, M. Karimi, X. Wang, Y. Shen, et al., Engineering a HER2-specific antibody–drug conjugate to increase lysosomal delivery and therapeutic efficacy, Nat. Biotechnol. 37 (2019) 523–526.
109. H. Sade, C. Baumgartner, A. Hugenmatter, E. Moessner, P.-O. Freksgård, J. Niewoehner, A human blood-brain barrier transcytosis assay reveals antibody transcytosis influenced by pH-dependent receptor binding, PLoS ONE 9 (2014) e96340.
110. P. Bonvin, S. Venet, G. Fontaine, U. Ravn, F. Gueneau, M. Kosco-Vilbois, et al., De novo isolation of antibodies with pH-dependent binding properties, mAbs 7 (2015) 294–302.
111. N. Hironiwa, S. Ishii, S. Kadono, F. Mimoto, K. Habu, T. Igawa, et al., Calcium-dependent antigen binding as a novel modality for antibody recycling by endosomal antigen dissociation, mAbs 8 (2015) 65–73.
112. S. Jung, A. Honegger, A. Plückthun, Selection for improved protein stability by phage display, J. Mol. Biol. 294 (1999) 163–180.
113. V. Sieber, A. Plückthun, F.X. Schmid, Selecting proteins with improved stability by a phage-based method, Nat. Biotechnol. 16 (1998) 955–960.
114. Ledsgaard L, Laustsen AH, Puš U, Wade J, Villar P, Boddum K, *et al*. In vitro discovery and optimization of a human monoclonal antibody that neutralizes neurotoxicity and lethality of cobra snake venom. *BioRxiv*. Published online September 7, 2021. http://dx.doi.org/10.1101/2021.09.07.459075.
115. S. Steidl, O. Ratsch, B. Brocks, M. Dürr, E. Thomassen-Wolf, *In vitro* affinity maturation of human GM-CSF antibodies by targeted CDR-diversification, Mol. Immunol. 46 (2008) 135–144.

116. E. Durr, J. Yu, K.M. Krasinska, L.A. Carver, J.R. Yates, J.E. Testa, et al., Direct proteomic mapping of the lung microvascular endothelial cell surface *in vivo* and in cell culture, Nat. Biotechnol. 22 (2004) 985–992.
117. P. Oh, J. Yu, E. Durr, K.M. Krasinska, L.A. Carver, J.E. Testa, et al., Subtractive proteomic mapping of the endothelial surface in lung and solid tumours for tissue-specific therapy, Nature. 429 (2004) 629–635.
118. R. Pasqualini, E. Ruoslahti, Organ targeting *In vivo* using phage display peptide libraries, Nature. 380 (1996) 364–366.
119. K. Deramchia, M.-J. Jacobin-Valat, A. Vallet, H. Bazin, X. Santarelli, S. Sanchez, et al., *In vivo* phage display to identify new human antibody fragments homing to atherosclerotic endothelial and subendothelial tissues, Am. J. Pathol. 180 (2012) 2576–2589.
120. P. Valadon, J.D. Garnett, J.E. Testa, M. Bauerle, P. Oh, J.E. Schnitzer, Screening phage display libraries for organ-specific vascular immunotargeting *in vivo*, Proc. Natl. Acad. Sci. USA 103 (2006) 407–412.
121. P. Stocki, J. Szary, C.L.M. Rasmussen, M. Demydchuk, L. Northall, D.B. Logan, et al., Blood-brain barrier transport using a high affinity, brain-selective VNAR antibody targeting transferrin receptor 1, FASEB J. 35 (2021) e21172.
122. S.A.M. van Lith, I. Roodink, J.J.C. Verhoeff, P.I. Mäkinen, J.P. Lappalainen, S. Ylä-Herttuala, et al., *In vivo* phage display screening for tumor vascular targets in glioblastoma identifies a llama nanobody against dynactin-1-p150 Glued, Oncotarget 7 (2016) 71594–71607.
123. W. Arap, R. Pasqualini, E. Ruoslahti, Cancer treatment by targeted drug delivery to tumor vasculature in a mouse model, Science 279 (1998) 377–380.
124. F.I. Staquicini, M. Cardó-Vila, M.G. Kolonin, M. Trepel, J.K. Edwards, D.N. Nunes, et al., Vascular ligand-receptor mapping by direct combinatorial selection in cancer patients, Proc. Natl. Acad. Sci. USA 108 (2011) 18637–18642.
125. D.N. Krag, G.S. Shukla, G.-P. Shen, S. Pero, T. Ashikaga, S. Fuller, et al., Selection of tumor-binding ligands in cancer patients with phage display libraries, Cancer Res. 66 (2006) 7724–7733.
126. D.J. Schofield, A.R. Pope, V. Clementel, J. Buckell, S.D.J. Chapple, K.F. Clarke, et al., Application of phage display to high throughput antibody generation and characterization, Genome Biol. 8 (2007) R254.
127. J. Kügler, S. Wilke, D. Meier, F. Tomszak, A. Frenzel, T. Schirrmann, et al., Generation and analysis of the improved human HAL9/10 antibody phage display libraries, BMC Biotechnol. 15 (2015) 10.
128. R.S. Nelson, Valadon PA universal phage display system for the seamless construction of Fab libraries, J. Immunol. Methods 450 (2017) 41–49.
129. C. Sellmann, L. Pekar, C. Bauer, E. Ciesielski, S. Krah, S. Becker, et al., A one-step process for the construction of phage display scFv and VHH libraries, Mol. Biotechnol. 62 (2020) 228–239.
130. G. Bullen, J.D. Galson, G. Hall, P. Villar, L. Moreels, L. Ledsgaard, et al., Cross-Reactive SARS-CoV-2 Neutralizing Antibodies From Deep Mining of Early Patient Responses, Front. Immunol. 12 (2021) 2049.
131. J.C. Almagro, M. Pedraza-Escalona, H.I. Arrieta, S.M. Pérez-Tapia, Phage display libraries for antibody therapeutic discovery and development, Antibodies 8 (2019) 44.
132. L. Frigotto, M.E. Smith, C. Brankin, A. Sedani, S.E. Cooper, N. Kanwar, et al., Codon-precise, synthetic, antibody fragment libraries built using automated hexamer codon additions and validated through next generation sequencing, Antibodies 4 (2015) 88–102.
133. N.J. Kräutler, A. Yermanos, A. Pedrioli, S.P.M. Welten, D. Lorgé, U. Greczmiel, et al., Quantitative and qualitative analysis of humoral immunity reveals continued and personalized evolution in chronic viral infection, Cell Rep. 30 (2020) 997–1012.
134. A.H. Laustsen, V. Greiff, A. Karatt-Vellatt, S. Muyldermans, T.P. Jenkins, Animal immunization, *in vitro* display technologies, and machine learning for antibody discovery, Trends Biotechnol. 39 (2021) 1263–1273.
135. C.A.K. Borrebaeck, M. Ohlin, Antibody evolution beyond Nature, Nat. Biotechnol. 20 (2002) 1189–1190.
136. L.J. Schwimmer, B. Huang, H. Giang, R.L. Cotter, D.S. Chemla Vogel, F.V. Dy, et al., Discovery of diverse and functional antibodies from large human repertoire antibody libraries, J. Immunol. Methods 391 (2013) 60–71.
137. E. Söderlind, L. Strandberg, P. Jirholt, N. Kobayashi, V. Alexeiva, A.-M. Åberg, et al., Recombining germline-derived CDR sequences for creating diverse single-framework antibody libraries, Nat. Biotechnol. 18 (2000) 852–856.
138. T. Tiller, I. Schuster, D. Deppe, K. Siegers, R. Strohner, T. Herrmann, et al., A fully synthetic human Fab antibody library based on fixed VH/VL framework pairings with favorable biophysical properties, mAbs 5 (2013) 445–470.
139. R.J. Johnston, L.J. Su, J. Pickney, D. Critton, E. Boyer, A. Krishnakumar, et al., VISTA is an acidic pH-selective ligand for PSGL-1, Nature 574 (2019) 565–570.
140. R.M. Hoet, E.H. Cohen, R.B. Kent, K. Rookey, S. Schoonbroodt, S. Hogan, et al., Generation of high-affinity human antibodies by combining donor-derived and synthetic complementarity-determining-region diversity, Nat. Biotechnol. 23 (2005) 344–348.
141. Y. Pan, J. Du, J. Liu, H. Wu, F. Gui, N. Zhang, et al., Screening of potent neutralizing antibodies against SARS-CoV-2 using convalescent patients-derived phage-display libraries, Cell Discov. 7 (2021) 57.
142. P.T. Jones, P.H. Dear, J. Foote, M.S. Neuberger, G. Winter, Replacing the complementarity-determining regions in a human antibody with those from a mouse, Nature 321 (1986) 522–525.
143. L. Riechmann, M. Clark, H. Waldmann, G. Winter, Reshaping human antibodies for therapy, Nature 332 (1988) 323–327.
144. A. Ascione, C. Arenaccio, A. Mallano, M. Flego, M. Gellini, M. Andreotti, et al., Development of a novel human phage display-derived anti-LAG3 scFv antibody targeting CD8+ T lymphocyte exhaustion, BMC Biotechnol. 19 (2019) 67.
145. A. Frenzel, T. Schirrmann, M. Hust, Phage display-derived human antibodies in clinical development and therapy, mAbs 8 (2016) 1177–1194.
146. R.-M. Lu, Y.-C. Hwang, I.-J. Liu, C.-C. Lee, H.-Z. Tsai, H.-J. Li, et al., Development of therapeutic antibodies for the treatment of diseases, J. Biomed. Sci. 27 (2020) 1.
147. K.D. Ratanji, J.P. Derrick, R.J. Dearman, I. Kimber, Immunogenicity of therapeutic proteins: influence of aggregation, J. Immunotoxicol. 11 (2014) 99–109.
148. M. Nabhan, M. Pallardy, I. Turbica, Immunogenicity of bioproducts: cellular models to evaluate the impact of therapeutic antibody aggregates, Front. Immunol. 11 (2020).
149. M. Sauerborn, V. Brinks, W. Jiskoot, H. Schellekens, Immunological mechanism underlying the immune response to recombinant human protein therapeutics, Trends Pharmacol. Sci. 31 (2010) 53–59.
150. T. Jain, T. Sun, S. Durand, A. Hall, N.R. Houston, J.H. Nett, et al., Biophysical properties of the clinical-stage antibody landscape, Proc. Natl. Acad. Sci. 114 (2017) 944–949.
151. S. Yasuda, Y. Zhou, Y. Wang, M. Yamamura, J.-Y. Wang, A model integrating tonic and antigen-triggered BCR signals to predict the survival of primary B cells, Sci. Rep. 7 (2017) 14888.
152. J. Glanville, W. Zhai, J. Berka, D. Telman, G. Huerta, G.R. Mehta, et al., Precise determination of the diversity of a combinatorial antibody library gives insight into the human immunoglobulin repertoire, Proc. Natl. Acad. Sci. USA 106 (2009) 20216–20221.
153. P.H. Sudmant, T. Rausch, E.J. Gardner, R.E. Handsaker, A. Abyzov, J. Huddleston, et al., An integrated map of structural variation in 2,504 human genomes, Nature 526 (2015) 75–81.
154. W. Zhai, J. Glanville, M. Fuhrmann, L. Mei, I. Ni, P.D. Sundar, et al., Synthetic antibodies designed on natural sequence landscapes, J. Mol. Biol. 412 (2011) 55–71.
155. W.R. Strohl, L.M. Strohl, Therapeutic Antibody Engineering, Woodhead Publishing, Sawston, 2012, pp. 377–595.
156. J.B. Ridgway, L.G. Presta, P. Carter, 'Knobs-into-holes' engineering of antibody CH3 domains for heavy chain heterodimerization, Protein Eng. 9 (1996) 617–621.
157. J. Glanville, S. D'Angelo, T.A. Khan, S.T. Reddy, L. Naranjo, F. Ferrara, et al., Deep sequencing in library selection projects: what insight does it bring?, Curr Opin. Struct. Biol. 33 (2015) 146–160.
158. M.F. Erasmus, S. D'Angelo, F. Ferrara, L. Naranjo, A.A. Teixeira, R. Buonpane, et al., A single donor is sufficient to produce a highly functional *in vitro* antibody library, Commun. Biol. 4 (2021) 1–16.
159. J.L. Xu, M.M. Davis, Diversity in the CDR3 region of VH is sufficient for most antibody specificities, Immunity 13 (2000) 37–45.
160. W. Zhai, J. Glanville, M. Furhmann, L. Mei, I. Ni, P.D. Sundar, et al., Synthetic antibodies designed on natural sequence landscapes, J. Mol. Biol. 412 (2011) 55–71.
161. R.E. Kontermann, U. Brinkmann, Bispecific antibodies, Drug Discov. Today 20 (2015) 838–847.
162. A.F. Labrijn, M.L. Janmaat, J.M. Reichert, P.W.H.I. Parren, Bispecific antibodies: a mechanistic review of the pipeline, Nat. Rev. Drug Discov. 18 (2019) 585–608.
163. U. Brinkmann, R.E. Kontermann, The making of bispecific antibodies. *mAbs* 9 (2017) 182–212.
164. J. Ma, Y. Mo, M. Tang, J. Shen, Y. Qi, W. Zhao, et al., Bispecific antibodies: from research to clinical application, Front. Immunol. 12 (2021) 626616.
165. S. Wang, K. Chen, Q. Lei, P. Ma, A.Q. Yuan, Y. Zhao, et al., The state of the art of bispecific antibodies for treating human malignancies, EMBO Mol. Med. 13 (2021).
166. S. Krah, C. Sellmann, L. Rhiel, C. Schröter, S. Dickgiesser, J. Beck, et al., Engineering bispecific antibodies with defined chain pairing, New Biotechnol. 39 (2017) 167–173.

167. A. Ljungars, T. Schiött, U. Mattson, J. Steppa, B. Hambe, M. Semmrich, et al., A bispecific IgG format containing four independent antigen binding sites, Sci. Rep. 10 (2020) 1546.
168. N. Fischer, G. Elson, G. Magistrelli, E. Dheilly, N. Fouque, A. Laurendon, et al., Exploiting light chains for the scalable generation and platform purification of native human bispecific IgG, Nat. Commun. 6 (2015) 6113.
169. V. Kunik, Y. Ofran, The indistinguishability of epitopes from protein surface is explained by the distinct binding preferences of each of the six antigen-binding loops, Protein Eng. Des. Sel. 26 (2013) 599–609.
170. J.L. Xu, M.M. Davis, Diversity in the CDR3 region of V(H) is sufficient for most antibody specificities, Immunity 13 (2000) 37–45.
171. E.S. Ward, VH shuffling can be used to convert an Fv fragment of anti-hen egg lysozyme specificity to one that recognizes a T cell receptor V alpha, Mol. Immunol. 32 (1995) 147–156.
172. A.M. Merchant, Z. Zhu, J.Q. Yuan, A. Goddard, C.W. Adams, L.G. Presta, et al., An efficient route to human bispecific IgG, Nat. Biotechnol. 16 (1998) 677–681.
173. S. Atwell, J.B. Ridgway, J.A. Wells, P. Carter, Stable heterodimers from remodeling the domain interface of a homodimer using a phage display library, J. Mol. Biol. 270 (1997) 26–35.
174. K. Gunasekaran, M. Pentony, M. Shen, L. Garrett, C. Forte, A. Woodward, et al., Enhancing antibody Fc heterodimer formation through electrostatic steering effects: applications to bispecific molecules and monovalent IgG, J. Biol. Chem. 285 (2010) 19637–19646.
175. C. De Nardis, L.J.A. Hendriks, E. Poirier, T. Arvinte, P. Gros, A.B.H. Bakker, et al., A new approach for generating bispecific antibodies based on a common light chain format and the stable architecture of human immunoglobulin G1, J. Biol. Chem. 292 (2017) 14706–14717.
176. P. Strop, W.-H. Ho, L.M. Boustany, Y.N. Abdiche, K.C. Lindquist, S.E. Farias, et al., Generating bispecific human IgG1 and IgG2 antibodies from any antibody pair, J. Mol. Biol. 420 (2012) 204–219.
177. D. Skegro, C. Stutz, R. Ollier, E. Svensson, P. Wassmann, F. Bourquin, et al., Immunoglobulin domain interface exchange as a platform technology for the generation of Fc heterodimers and bispecific antibodies, J. Biol. Chem. 292 (2017) 9745–9759.
178. J. Jackman, Y. Chen, A. Huang, B. Moffat, J.M. Scheer, S.R. Leong, et al., Development of a two-part strategy to identify a therapeutic human bispecific antibody that inhibits IgE receptor signaling, J. Biol. Chem. 285 (2010) 20850–20859.
179. S. Krah, C. Schröter, C. Eller, L. Rhiel, N. Rasche, J. Beck, et al., Generation of human bispecific common light chain antibodies by combining animal immunization and yeast display, Protein Eng. Des. Sel. 30 (2017) 291–301.
180. J.P. Bogen, S.C. Hinz, J. Grzeschik, A. Ebening, S. Krah, S. Zielonka, et al., Dual function pH responsive bispecific antibodies for tumor targeting and antigen depletion in plasma, Front. Immunol. 10 (2019) 1892.
181. M. Zemlin, M. Klinger, J. Link, C. Zemlin, K. Bauer, J.A. Engler, et al., Expressed murine and human CDR-H3 intervals of equal length exhibit distinct repertoires that differ in their amino acid composition and predicted range of structures, J. Mol. Biol. 334 (2003) 733–749.
182. C.M. Mahon, M.A. Lambert, J. Glanville, J.M. Wade, B.J. Fennell, M.R. Krebs, et al., Comprehensive interrogation of a minimalist synthetic CDR-H3 library and its ability to generate antibodies with therapeutic potential, J. Mol. Biol. 425 (2013) 1712–1730.
183. K. Sankar, K.H. Hoi, I. Hötzel, Dynamics of heavy chain junctional length biases in antibody repertoires, Commun. Biol. 3 (2020) 207.
184. L. Wu, K. Oficjalska, M. Lambert, B.J. Fennell, A. Darmanin-Sheehan, D.N. Shuílleabhaín, et al., Fundamental characteristics of the immunoglobulin VH repertoire of chickens in comparison with those of humans, mice, and camelids, J. Immunol. 188 (2012) 322–333.
185. L. Pekar, D. Klewinghaus, P. Arras, S.C. Carrara, J. Harwardt, S. Krah, et al., Milking the cow: cattle-derived chimeric ultralong CDR-H3 antibodies and their engineered CDR-H3-only knobbody counterparts targeting epidermal growth factor receptor elicit potent NK cell-mediated cytotoxicity, Front. Immunol. 12 (2012) 742418.
186. A. Macpherson, A. Scott-Tucker, A. Spiliotopoulos, C. Simpson, J. Staniforth, A. Hold, et al., Isolation of antigen-specific, disulphide-rich knob domain peptides from bovine antibodies, PLoS Biol. 18 (2020) e3000821.
187. F. Wang, D.C. Ekiert, I. Ahmad, W. Yu, Y. Zhang, O. Bazirgan, et al., Reshaping antibody diversity, Cell 153 (2013) 1379–1393.
188. J.J. Smith, J.M. Hill, M.J. Little, G.M. Nicholson, G.F. King, P.F. Alewood, et al., Unique scorpion toxin with a putative ancestral fold provides insight into evolution of the inhibitor cystine knot motif, Proc. Natl. Acad. Sci. USA 108 (2011) 10478–10483.
189. J. Silverman, Q. Lu, A. Bakker, W. To, A. Duguay, B.M. Alba, et al., Multivalent avimer proteins evolved by exon shuffling of a family of human receptor domains, Nat. Biotechnol. 23 (2005) 1556–1561.
190. D.J. Craik, N.L. Daly, C. Waine, The cystine knot motif in toxins and implications for drug design, Toxicon 39 (2001) 43–60.
191. A. Desmyter, T.R. Transue, M.R. Ghahroudi, M.-H.-D. Thi, F. Poortmans, R. Hamers, et al., Crystal structure of a camel single-domain V H antibody fragment in complex with lysozyme, Nat. Struct. Biol. 3 (1996) 803–811.
192. T. Liu, Y. Liu, Y. Wang, M. Hull, P.G. Schultz, F. Wang, Rational design of CXCR4 specific antibodies with elongated CDRs, J. Am. Chem. Soc. 136 (2014) 10557–10560.
193. D.C. Bell, A. Karratt-Vellatt, S. Surade, T. Luetkens, E.W. Masters, N.M. Sørensen, et al., Knotbodies: a new generation of ion channel therapeutic biologics created by fusing knottin toxins into antibodies, Biophys. J. 114 (2018) 203a.
194. Z. Miao, G. Ren, H. Liu, R.H. Kimura, L. Jiang, J.R. Cochran, et al., An engineered knottin peptide labeled with 18F for PET imaging of integrin expression, Bioconjug. Chem. 20 (2009) 2342–2347.
195. W. Lee, A. Syed Atif, S.C. Tan, C.H. Leow, Insights into the chicken IgY with emphasis on the generation and applications of chicken recombinant monoclonal antibodies, J. Immunol. Methods 447 (2017) 71–85.
196. U.S. Diesterbeck, Construction of bovine immunoglobulin libraries in the single-chain fragment variable (scFv) format, Methods Mol. Biol. 1701 (2018) 113–131.
197. H. Matz, H. Dooley, Shark IgNAR-derived binding domains as potential diagnostic and therapeutic agents, Dev. Comp. Immunol. 90 (2019) 100–107.
198. H. English, J. Hong, M. Ho, Ancient species offers contemporary therapeutics: an update on shark VNAR single domain antibody sequences, phage libraries and potential clinical applications, Antib. Ther. 3 (2020) 1–9.
199. H. Akiba, H. Tamura, M. Kiyoshi, S. Yanaka, K. Sugase, J.M.M. Caaveiro, et al., Structural and thermodynamic basis for the recognition of the substrate-binding cleft on hen egg lysozyme by a single-domain antibody, Sci. Rep. 9 (2019) 15481.
200. K.A. Henry, C.R. MacKenzie, Antigen recognition by single-domain antibodies: structural latitudes and constraints, mAbs 10 (2018) 815–826.
201. A. Koide, J. Wojcik, R.N. Gilbreth, R.J. Hoey, S. Koide, Teaching an old scaffold new tricks: monobodies constructed using alternative surfaces of the FN3 scaffold, J. Mol. Biol. 415 (2012) 393–405.
202. J. Wojcik, A.J. Lamontanara, G. Grabe, A. Koide, L. Akin, B. Gerig, et al., Allosteric inhibition of Bcr-Abl kinase by high affinity monobody inhibitors directed to the Src homology 2 (SH2)-kinase interface, J. Biol. Chem. 291 (2016) 8836–8847.
203. T. Kükenshöner, N.E. Schmit, E. Bouda, F. Sha, F. Pojer, A. Koide, et al., Selective targeting of SH2 domain-phosphotyrosine interactions of Src family tyrosine kinases with monobodies, J. Mol. Biol. 429 (2017) 1364–1380.
204. G. La Sala, C. Michiels, T. Kükenshöner, T. Brandstoetter, B. Maurer, A. Koide, et al., Selective inhibition of STAT3 signaling using monobodies targeting the coiled-coil and N-terminal domains, Nat. Commun. 11 (2020) 4115.
205. E.J. Petrie, R.W. Birkinshaw, A. Koide, E. Denbaum, J.M. Hildebrand, S.E. Garnish, et al., Identification of MLKL membrane translocation as a checkpoint in necroptotic cell death using monobodies, Proc. Natl. Acad. Sci. USA 117 (2020) 8468–8475.
206. S.C. Devanaboyina, S.M. Lynch, R.J. Ober, S. Ram, D. Kim, A. Puig-Canto, et al., The effect of pH dependence of antibody-antigen interactions on subcellular trafficking dynamics, mAbs 5 (2013) 851–859.
207. J. Chaparro-Riggers, H. Liang, R.M. DeVay, L. Bai, J.E. Sutton, W. Chen, et al., Increasing serum half-life and extending cholesterol lowering *in vivo* by engineering antibody with pH-sensitive binding to PCSK9, J. Biol. Chem. 287 (2012) 11090–11097.
208. M.L. Murtaugh, S.W. Fanning, T.M. Sharma, A.M. Terry, J.R. Horn, A combinatorial histidine scanning library approach to engineer highly pH-dependent protein switches, Protein Sci. 20 (2011) 1619–1631.
209. C. Schröter, R. Günther, L. Rhiel, S. Becker, L. Toleikis, A. Doerner, et al., A generic approach to engineer antibody pH-switches using combinatorial histidine scanning libraries and yeast display, mAbs 7 (2014) 138–151.
210. B.J. Tillotson, L.I. Goulatis, I. Parenti, E. Duxbury, E.V. Shusta, Engineering an anti-transferrin receptor ScFv for pH-sensitive binding leads to increased intracellular accumulation, PLoS ONE 10 (2015) e0145820.
211. D. Könning, S. Zielonka, C. Sellmann, C. Schröter, J. Grzeschik, S. Becker, et al., Isolation of a pH-sensitive IgNAR variable domain from a yeast-displayed, histidine-doped master library, Mar. Biotechnol. 18 (2016) 161–167.

4. Development of broadly neutralizing anti-α-neurotoxin antibodies

This research article presents a strategy for developing broadly neutralizing antibodies against long-chain α-neurotoxins through phage display and light chain shuffling. To improve cross-reactivity, an antibody discovered against long-chain α-neurotoxin from *N. kaouthia* was affinity matured by diversifying the antibody light chain with a naïve repertoire of antibody light chains. The light chain shuffled library was cross-panned against long-chain α-neurotoxins from *N. kaouthia* and *D. polylepis* elapids at reducing concentrations to select for clones with improved cross-reactivity and affinity. Affinity measurements of light chain shuffled antibodies using surface plasmon resonance demonstrated the success of this approach, with the light chain improving the affinity of antibodies by an order of magnitude against both neurotoxins used in the phage display selections. The improved affinity translated to enhanced *in vitro* neutralization potency, and antibodies also demonstrated cross-neutralization to long-chain α-neurotoxin from *B. multicinctus* (α-bungarotoxin). The most cross-reactive antibody, 2554_01_D11, was then evaluated for its capacity to neutralize long-chain α-neurotoxins *in vivo* with long-chain α-neurotoxin from different elapids. The results of which accumulated in demonstrating the broad-neutralization capacity of long-chain α-neurotoxins by 2554_01_D11 in both a pre-incubation model (antibody is allowed to bind to neurotoxin before being administered) and in a rescue model when administered after mice were envenomed with whole venom from *N. kaouthia*.

Overall, this research article describes an approach to improve both the neutralization capacity and cross-reactivity of antibodies by light chain shuffling, and highlights the potential of naïve antibody libraries to discover broadly neutralizing antibodies against snake venom toxins.

The research article has been published in Nature Communications:
Ledsgaard, L., Wade, J., Jenkins, T.P. *et al.* Discovery and optimization of a broadly-neutralizing human monoclonal antibody against long-chain α-neurotoxins from snakes.*Nat Commun* **14**, 682 (2023). https://doi.org/10.1038/s41467-023-36393-4

nature communications

Article

https://doi.org/10.1038/s41467-023-36393-4

Discovery and optimization of a broadly-neutralizing human monoclonal antibody against long-chain α-neurotoxins from snakes

Received: 24 June 2022

Accepted: 23 January 2023

Published online: 08 February 2023

Check for updates

Line Ledsgaard[1], Jack Wade[1], Timothy P. Jenkins[1], Kim Boddum[2], Irina Oganesyan[3], Julian A. Harrison[3], Pedro Villar[4], Rachael A. Leah[4], Renato Zenobi[3], Sanne Schoffelen[1], Bjørn Voldborg[1], Anne Ljungars[1], John McCafferty[4], Bruno Lomonte[5], José M. Gutiérrez[5] ✉, Andreas H. Laustsen[1] ✉ & Aneesh Karatt-Vellatt[4] ✉

Snakebite envenoming continues to claim many lives across the globe, necessitating the development of improved therapies. To this end, broadly-neutralizing human monoclonal antibodies may possess advantages over current plasma-derived antivenoms by offering superior safety and high neutralization capacity. Here, we report the establishment of a pipeline based on phage display technology for the discovery and optimization of high affinity broadly-neutralizing human monoclonal antibodies. This approach yielded a recombinant human antibody with superior broadly-neutralizing capacities in vitro and in vivo against different long-chain α-neurotoxins from elapid snakes. This antibody prevents lethality induced by *Naja kaouthia* whole venom at an unprecedented low molar ratio of one antibody per toxin and prolongs the survival of mice injected with *Dendroaspis polylepis* or *Ophiophagus hannah* whole venoms.

Each year, snakebite envenoming exacts a high death toll and leaves hundreds of thousands of other victims maimed for life[1]. Antivenoms based on polyclonal antibodies isolated from the plasma of immunized animals are currently the only specific treatment option against severe envenomings[2,3]. While these medicines are essential and life-saving and will remain a cornerstone in snakebite therapy for years to come, an opportunity now exists to modernize treatment by exploiting the benefits of recombinant DNA and antibody technology[4]. Indeed, recombinant antibodies and antibody fragments have already been generated against a variety of snake venom toxins[5–8], as well as multiple studies involving monoclonal antibodies derived using hybridoma technology have been reported[9–12] (see Laustsen et al.[13] for a comprehensive overview and Pucca et al.[2] for an overview of the historical context). Within this area of research, it has also been demonstrated that monoclonal antibodies targeting snake venom toxins can be developed using various platforms, such as phage display technology[6], an in vitro methodology that can be used to actively select for antibodies with high-affinity and cross-reactivity[14,15]. In addition, the use of human antibody libraries in combination with phage display technology allows for the discovery of fully human

[1]Department of Biotechnology and Biomedicine, Technical University of Denmark, DK-2800 Kongens Lyngby, Denmark. [2]Sophion Bioscience, DK-2750 Ballerup, Denmark. [3]Department of Chemistry and Applied Biosciences, ETH Zurich, CH-8093 Zurich, Switzerland. [4]IONTAS Ltd., Cambridgeshire CB22 3FT, UK. [5]Instituto Clodomiro Picado, Facultad de Microbiología, Universidad de Costa Rica, San José 11501-2060, Costa Rica. ✉e-mail: jose.gutierrez@ucr.ac.cr; ahola@bio.dtu.dk; akv@maxion.co.uk

antibodies that are likely to have high treatment tolerability in patients[16].

It has been speculated that monoclonal antibodies developed by these means could be used to formulate recombinant antivenoms that elicit fewer adverse reactions, are cost-competitive to existing therapy, and can be fine-tuned to have superior efficacy[16–20]. Phage display technology could be particularly valuable for discovering monoclonal antibodies against highly potent toxins with low immunogenicity that fail to elicit a strong antibody response in animals used for immunization[21,22]. This is the case for low molecular mass neurotoxins and cytotoxins of the three-finger toxin (3FTx) family, which are abundant in Elapidae venoms, such as cobra and mamba venoms[23–26]. These elapid venoms, unlike Viperidae venoms, typically consist of neurotoxic and cytoxic components that elicit tissue damage as well as paralysis in bite victims[1]. However, antibodies derived directly from naïve libraries often lack sufficiently high affinity to enable toxin neutralization[15]. Affinity can be improved by further site-directed or random mutagenesis of the antibody paratopes, which can also lead to broadening of the neutralizing capacity of naïve antibodies[27]. However, in addition to mutation of the antibody binding regions, retaining the heavy chains and exploring alternative light chains, a technique known as light chain-shuffling, has shown significant promise as well[21,28]. Here, a phage display library is generated by pairing a heavy or light chain from a specific antibody with a naïve repertoire of the partner chain and performing a new selection campaign[15]. Nevertheless, until now it remained unknown whether this technology could be used to generate antibodies that possess high affinity while simultaneously having a broad neutralization capacity, i.e., are able to neutralize several related toxins from the venoms of different snake species.

Previously, using a naïve human scFv-based phage display library[15], we described the discovery and characterization of the human monoclonal antibody, 368_01_C05, against α-cobratoxin (P01391), a potent neurotoxin from the monocled cobra, *Naja kaouthia*. Notably, this antibody could prolong the survival of mice injected with lethal doses of α-cobratoxin, although it failed to prevent lethality[15]. As a follow-up development, in the present study we constructed light-chain-shuffled antibody libraries based on this clone with the aim of using a phage display-based cross-panning campaign to simultaneously improve the affinity and expand the neutralizing capacity of the antibody against α-neurotoxins from the venoms of several snake species. Cross-panning was carried out between α-cobratoxin[29] and α-elapitoxin[30], a neurotoxin from the venom of the black mamba, *Dendroaspis polylepis*[25]. These two α-neurotoxins share 70% sequence identity and both cause neuromuscular blockade by binding to the nicotinic acetylcholine receptor (nAChR) in muscle cells[29,30].

In this work, we "cross-panned" the chain-shuffled scFv library on these two toxins under stringent conditions to discover antibodies with improved affinity and cross-reactivity in comparison to the parent antibody. Using this strategy, we were able to generate an antibody that not only has improved affinity to α-cobratoxin, but also significantly broadened cross-neutralization capacity against other α-neurotoxins from the venoms of elapid snakes from the genera *Dendroaspis, Ophiophagus, Bungarus*, and *Naja*.

Results

Affinity maturation, cross-panning, and scFv characterization

Human light-chain-shuffled scFv-based phage display libraries were created by pairing the heavy chain of antibody 368_01_C05 with a naïve repertoire of human light chains. Then, phage display cross-pannings using two toxins with 70% sequence identity, α-cobratoxin from *N. kaouthia* and α-elapitoxin from *D. polylepis*, were conducted according to the overview provided in Fig. 1a. Phage display selection outputs from the third round were subcloned into the pSANG10-3F expression vector, and 736 monoclonal scFvs were tested for their ability to bind

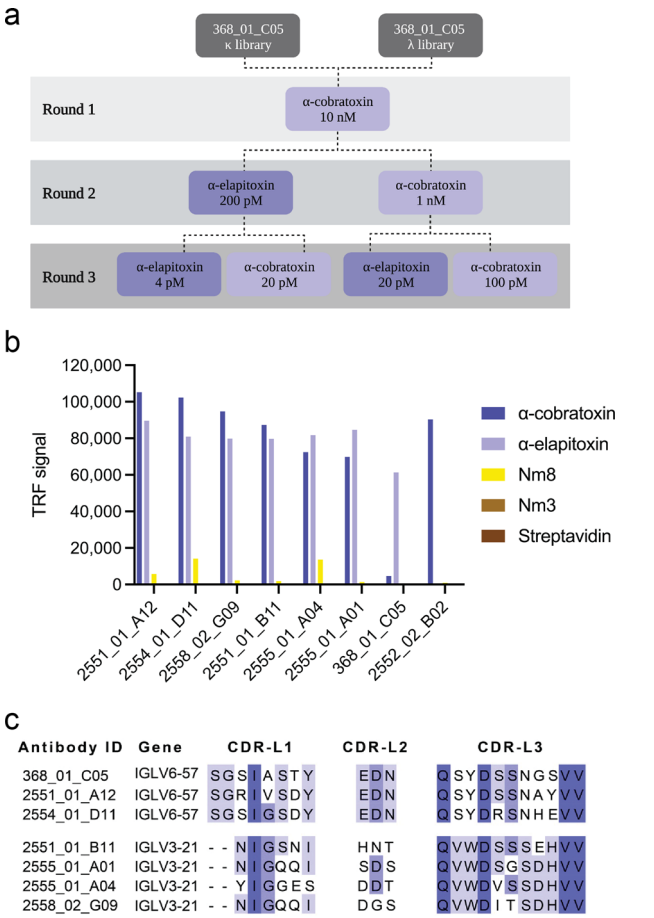

Fig. 1 | Cross-panning selection strategy as well as assay and sequence data for selected IgGs. a Selection strategy illustrating how cross-panning was performed, including antigen concentrations. **b** ENC DELFIA showing cross-reactivity of the top six-affinity matured IgGs (2551_01_A12, 2554_01_D11, 2558_02_G09, 2551_01_B11, 2555_01_A04, and 2555_01_A01) in comparison with parental IgG (368_01_C05) and clone 2552_02_B02 from a previously published study[15]. **c** Comparison of CDR-L1, CDR-L2, and CDR-L3 sequences for the top six chain-shuffled antibodies and the parental antibody.

to α-cobratoxin, α-elapitoxin, and streptavidin in both direct dissociation-enhanced lanthanide fluorescence immunoassays (DELFIAs) and expression-normalized capture (ENC) DELFIAs. From here, 203 scFvs (all displaying binding to at least one of the two toxins with negligible binding to streptavidin) were randomly selected for sequencing. Of these, 67 scFvs were unique according to the sequence of their light chain CDR3 region, 2 of them having kappa light chains and the remaining 65 having lambda light chains. The top 62 clones, based on sequence diversity and binding behavior, were reformatted to the fully human IgG1 format. Following expression in HEK293 cells, ENC DELFIAs were run using the crude expression supernatant to rank the IgG binding to α-cobratoxin, α-elapitoxin, a venom fraction from *N. melanoleuca* (Nm8) containing a long neurotoxin homologous to OH-55 (Q53B58) and long neurotoxin 2 (P01388)[31]. In addition, streptavidin was included as negative control. This revealed that more than half of the clones were cross-reactive against all three toxins/venom fractions, demonstrating significant improvement in both binding and cross-reactivity when compared to the parental antibody.

To help guide the selection of lead candidates, the suitability of the 62 clones for future antibody development was investigated by characterizing biophysical properties that are indicative of their "developability" profiles. To this end, we analyzed the purity and nonspecific column interaction pattern of all IgGs using size-exclusion

Table 1 | AC-SINS shift, SEC analysis results (% monomer content and relative elution volume), and transient expression yields for the top six light chain-shuffled IgGs (2551_01_A12, 2554_01_D11, 2558_02_G09, 2551_01_B11, 2555_01_A04, and 2555_01_A01) in comparison with the parental IgG (368_01_C05)

	AC-SINS	SEC analysis		Production
Antibody ID	Shift (nm)	Monomer (%)	Elution (mL)	Yield (mg/L)
2551_01_A12	3	100.0	1.48	18.1
2554_01_D11	1	94.8	1.48	47.1
2558_02_G09	1	95.6	1.48	38.5
2551_01_B11	1	96.2	1.50	30.4
2555_01_A04	1	100.0	1.47	25.8
2555_01_A01	1	96.7	1.47	45.4
368_01_C05	0	97.5	1.45	30.0
2552_02_B02*	32	100.0	1.82	22.6

*IgG 2552_02_B02 from a previous study was also included.

chromatography (SEC). In addition, the propensity for self-aggregation was evaluated in an AC-SINS assay, in which IgGs are concentrated around gold nanoparticles pre-coated with anti-Fc antibodies, where a reduced inter-particle distance (measured by increased plasmon wavelengths) indicates that the immobilized IgGs interact unspecifically[32]. For this analysis, we also included an IgG from a previous study (2552_02_B02)[15], that has been reported to neutralize lethality induced by *N. kaouthia* whole venom in vivo, but had never been characterized for cross-reactivity to other long-chain α-neurotoxins nor been analyzed for its "developability" properties. The SEC data (% monomeric content and relative elution volumes—a metric for assessing nonspecific interaction with the SEC column), AC-SINS shifts, binding data, expression yields (full dataset see Table S1), and light chain germline diversity were used to select the top six antibody candidates for further characterization. These antibodies were named 2551_01_A12, 2554_01_D11, 2558_02_G09, 2551_01_B11, 2555_01_A04, and 2555_01_A01 (Fig. 1b and Table 1). Additionally, the data showed that the previously published IgG 2552_02_B02 had a poor developability score, both judged by its late elution in the SEC analysis and its high shift in the AC-SINS assay. In fact, this antibody performed at a similarly poor level as the 'poor developability' control (bococizumab, AC-SINC shift of 33 nm) that was used for comparison, whereas all antibodies derived from the 368_01_C05 parental clone possessed developability profiles similar to the 'good developability' control antibody (Alirocumab, AC-SINS shift of 3 nm). In addition, 2552_02_B02 showed no cross-reactivity to any of the long-chain α-neurotoxins it was tested against, clearly distinguishing its binding profile from the antibodies derived from the 368_01_C05 parent (Fig. 1b).

Analysis of the antibody sequences revealed that the six affinity matured antibodies had light chains belonging to two different germlines, germline IGLV3-21 for 2551_01_B11, 2555_01_A01, 2555_01_A04, and 2558_02_G09 and germline IGLV6-57 for 2551_01_A12 and 2554_01_D11. The parental antibody had germline IGLV6-57, meaning that two of the six affinity matured antibodies had light chains belonging to the same germline as the parental antibody. From the comparison of the three light chain CDR regions of the antibodies presented in Fig. 1c, it could also be seen that for the two antibodies maintaining the parental germline, the CDR-L2 was identical to the parental, whereas the CDR-L1 and CDR-L3 had 2–3 amino acid differences. For the remaining four antibodies with different light chain germline, all V_L CDR sequences were significantly different from the parent antibody sequence.

To evaluate whether the light-chain-shuffling campaign generated antibodies with improved affinity, surface plasmon resonance (SPR) was used to determine the affinity of the top six antibodies as well as the parental antibody. To this end, all antibodies were reformatted to the monovalent Fab format to measure the 1:1 binding kinetics of each antibody against both α-cobratoxin and α-elapitoxin (for SPR sensorgrams see Fig. S1). The data showed that all six antibodies displayed higher affinity for both toxins than the parental antibody (Table 2). The largest improvement was observed for 2551_01_A12 and 2554_01_D11 (32 and 50-fold improvement of binding to α-cobratoxin and 13 and 8-fold improvement of binding to α-elapitoxin, respectively), providing both antibodies with low single-digit nanomolar affinities to both toxins. Thus, a significant improvement in both affinity and cross-reactivity was observed. Antibodies 2551_01_A12 and 2554_01_D11 were selected for further characterization based on affinity, cross-reactivity, expression yield, and developability data.

Because the binding profiles of the cross-reactive antibodies derived from antibody 368_01_C05 were significantly different from antibody 2552_02_B02, SPR was used to determine if the antibodies bound the same or overlapping epitopes on α-cobratoxin (see Fig. S2). Using 2554_01_D11 as a representative of the cross-reactive antibodies, this study revealed that neither of the two antibodies 2552_02_B02 or 2554_01_D11 could bind α-cobratoxin if the other antibody was already bound to the toxin, suggesting that the antibodies recognized the same or overlapping epitopes.

Native mass spectrometry reveals cross-reactivity to several toxins from elapid snakes of three different genera

To further explore the cross-reactivity of the discovered antibodies, IgG 2554_01_D11 was tested for its binding to toxins in five whole venoms, including *N. kaouthia*, *N. melanoleuca*, *N. naja*, *Ophiophagus hannah*, and *D. polylepsis*. These venoms from African (*D. polylepsis* and *N. melanoleuca)* and Asian (*N. kaouthia*, *N. naja* and *O. hannah)* snakes all possess a relatively high content of long-chain α-neurotoxins, ranging from 13.2% for *D. polylepsis*[25] to 55% for *N. kaouthia*[24], except *N. naja*, which has been reported to have a long-chain α-neurotoxin content of approximately 2–5%[33]. For this purpose, native mass spectrometry (MS), was used to investigate the interactions between the antibody and toxins from the four snake venoms.

Prior to native mass spectrometry analysis, the venoms and IgG were fractionated using SEC (Fig. S3). IgG was mixed with each of the SEC-generated toxin fractions before analysis using native MS to determine binding (Fig. S3). This analysis revealed that 2554_01_D11 only bound toxins of masses in the range expected for the group of three-finger toxins (3FTx) to which all α-neurotoxins belong. To identify the toxins, the toxin:antibody complexes were isolated using MS/MS and subjected to collisional dissociation to eject the toxins from the antibody, allowing their intact mass to be determined. The primary dissociation products from these experiments were proteins of masses between 7800 and 8200 Da, corresponding to typical masses of long-chain α-neurotoxins (Fig. 2).

The sequences of the toxins bound by 2554_01_D11 were investigated via top-down proteomics to confirm the identities of these toxins. For these experiments, the toxin:antibody complexes were purified using SEC. Toxins were dissociated from the antibody by applying a high cone voltage. This is a focusing voltage applied to the cone, which is located in the source region of the instrument. Increasing this voltage leads to harsh conditions that can dissociate noncovalent complexes. Since this dissociation occurs before the quadrupole, the most prominent charge state of each ejected toxin could then be isolated using MS/MS for top-down sequencing. This isolation is important, as it ensures that the peptide fragmentation peaks only correspond to the toxin of interest. For the toxins with masses between 7800 and 8200 Da, only one readily discernible peptide fragment series was detected for each precursor ion. The limited amount of sequence data obtained from these experiments is attributed to the presence of disulfide bonds present in snake venom

Table 2 | Affinity measurements between antibodies and toxins using Surface Plasmon Resonance (SPR)

	α-cobratoxin			α-elapitoxin		
Antibody ID	**K_D (nM)**	**k_{on} (M·s)**	**k_{off} (s^{-1})**	**K_D (nM)**	**k_{on} (M·s)**	**k_{off} (s^{-1})**
2551_01_A12	2.79	1.80×10^5	5.02×10^{-4}	1.12	1.25×10^5	1.40×10^{-4}
2554_01_D11	1.78	1.28×10^5	2.29×10^{-4}	1.69	1.05×10^5	1.77×10^{-4}
2558_02_G09	2.77	2.14×10^5	5.94×10^{-4}	3.04	1.39×10^5	4.22×10^{-4}
2551_01_B11	4.27	1.17×10^5	5.00×10^{-4}	2.87	6.37×10^5	1.83×10^{-4}
2555_01_A04	7.46	2.22×10^5	1.65×10^{-3}	2.21	9.26×10^5	2.05×10^{-4}
2555_01_A01	8.41	2.02×10^5	1.70×10^{-3}	1.81	1.00×10^5	1.81×10^{-4}
368_01_C05	89.6	1.83×10^4	1.64×10^{-2}	14.3	6.47×10^4	9.25×10^{-4}

SPR was used to measure the affinity of the top six chain-shuffled antibodies (2551_01_A12, 2554_01_D11, 2558_02_G09, 2551_01_B11, 2555_01_A04, and 2555_01_A01) and the parental antibody (368_01_C05) in the Fab format to both α-cobratoxin and α-elapitoxin. The dissociation constants, on-rates, and off-rates are provided. For sensorgrams, see Fig. S1.

toxins, which cannot be broken using this fragmentation technique[34–36].

A BLAST search against all available elapid protein sequences revealed that the peptide sequences obtained by top-down analysis were unique to long-chain α-neurotoxins and that each peptide only had one complete match to long-chain α-neurotoxin homologs from the investigated venom. Sequence data combined with the detected masses of the toxins revealed that 2554_01_D11 was capable of binding to long-chain α-neurotoxin-containing SEC fractions across all tested venoms. This suggested that this antibody is cross-reactive against long-chain α-neurotoxins present in all five tested venoms, further highlighting the broadly cross-reactive behavior of 2554_01_D11.

The toxin homologs specifically identified to be bound by 2554_01_D11 were long neurotoxin 2 (A8N285) from *O. hannah*, α-cobratoxin (P01391) from *N. kaouthia*, long neurotoxin 2 (P01388) and long neurotoxin (P0DQQ2) from *N. melanoleuca*, long neurotoxin 4 (P25672) from *N. naja*, and α-elapitoxin (P01396) from *D. polylepis*. In addition, the antibody was shown to bind α-bungarotoxin (P60615) from *B. multicinctus* using SPR (Fig. S4). The average sequence similarity of the seven toxins was 62% (stdev: 9.9%), with an identity of 38% across all toxins; a total of 28 amino acid positions (primarily located at the active site) were identical across all toxins (Fig. 3a). The highest identity was observed between α-cobratoxin and long neurotoxin 2 from *N. melanoleuca* (83%), and the lowest identity was observed between long neurotoxin 2 from *N. melanoleuca* and α-bungarotoxin (51%). Additionally, a structural comparison was performed via root-mean-square deviation (RMSD) and revealed a mean pruned/total similarity of 0.81 Å/3.1 Å (stdev: 0.26 Å/1.23 Å), respectively; the best match appeared to be between long neurotoxin and long neurotoxin 2 from *N. melanoleuca* (0.23 Å/0.23 Å) and the poorest match appeared to be between long neurotoxin 2 from *O. hannah* and α-cobratoxin (pruned: 1.18 Å) and α-elapitoxin and α-bungarotoxin (total: 4.5 Å; Fig. 3b). For α-cobratoxin, the amino acid residues involved in binding to the nicotinic acetylcholine receptor have been highlighted both in the sequence (Fig. 3a) and in the structure on the toxin (Fig. 3c). Additionally, the residues that, through a high-density peptide microarray-based study[37], have been identified to be involved in the binding between antivenom-derived antibodies and α-elapitoxin and long neurotoxin 2 from *N. melanoleuca*, have been highlighted in the toxin sequence in Fig. 3a and in the toxin structure in Figs. 3d, e.

Increased in vitro neutralization potency and broadening of cross-neutralization

After having established the broadly cross-reactive nature of one of the top two chain-shuffled antibodies (2554_01_D11), automated patch-clamp technology was applied to assess whether binding translated into functional neutralization in vitro for 2551_01_A12 and 2554_01_D11, as well as for the parental clone, 368_01_C05. Here, a human derived cell line endogenously expressing nAChR was used to measure the acetylcholine-dependent current. α-cobratoxin inhibited this current in a concentration-dependent manner, and the IC_{80} value for the toxin was determined. Thereafter, the concentration-dependent neutralization of the current-inhibiting effect of α-cobratoxin by the three antibodies was determined. The results demonstrated that all three antibodies were able to fully neutralize the effects of α-cobratoxin, whereas an irrelevant isotype control antibody (recognizing a dendrotoxin) had no effect (Fig. 4a). The parental antibody, 368_01_C05 neutralized α-cobratoxin-mediated inhibition of acetylcholine-dependent currents with an EC_{50} value of 4.9 nM and a relatively shallow concentration-response curve slope. In contrast, the optimized antibodies, 2551_01_A12 and 2554_01_D11 exhibited improved EC_{50} values of 2.6 and 1.7 nM, respectively, with steeper slopes for the concentration-response curves. These EC_{50} values translate into toxin:antibody molar ratios of 1:1.23 for 368_01_C05, 1:0.65 for 2551_01_A12, and 1:0.43 for 2554_01_D11. Since each IgG has two binding sites, the theoretically lowest amount of IgG needed to neutralize the effect of one toxin would be 0.5 IgGs.

To determine if the increased cross-reactivity to other α-neurotoxins translated into cross-neutralization, a single concentration antibody screen was set up using the Qube 384 system. Here, the three antibodies (368_01_C05, 2551_01_A12, and 2554_01_D11) were tested against α-cobratoxin from *N. kaouthia*, α-elapitoxin from *D. polylepis*, and Nm8 from *N. melanoleuca*, which all were toxins that 2554_01_D11 had been shown to bind through native MS. In addition, α-bungarotoxin was included, as it has 58% sequence identity to α-cobratoxin, is commercially available, and is an important toxin to neutralize in the venom of *B. multicinctus*. As a control, Nm3, a venom fraction from *N. melanoleuca* containing a short-chain α-neurotoxin that also binds to the nAChR but is not bound by any of the three antibodies, was included. This automated patch-clamp screening revealed that α-cobratoxin and α-elapitoxin could be neutralized by all three antibodies in this assay (Fig. 4b). Additionally, the chain-shuffled clones were able to neutralize α-bungarotoxin and partially neutralize the α-neurotoxins present Nm8, none of which was achieved by the parental clone. Collectively, the results of the in vitro neutralization assays using automated patch-clamp demonstrated that the chain-shuffled antibodies were both more potent in their neutralization of α-cobratoxin, as well as more broadly neutralizing than the parental antibody, inhibiting the effect of α-neurotoxins from snakes of three different genera inhabiting both Asia and Africa. Based on binding, developability, affinity, expression, and in vitro neutralization data, 2554_01_D11 was selected as the top candidate for in vivo testing.

In vitro neutralization data translate to complete or partial in vivo neutralization of snake venoms from different genera and continents

To verify that the in vitro cross-neutralization potential of 2554_01_D11 translated into in vivo cross-neutralization, animal experiments were set up to evaluate the ability of the antibody to prevent or delay venom-induced lethality. First, we evaluated the neutralization of α-

https://doi.org/10.1038/s41467-023-36393-4

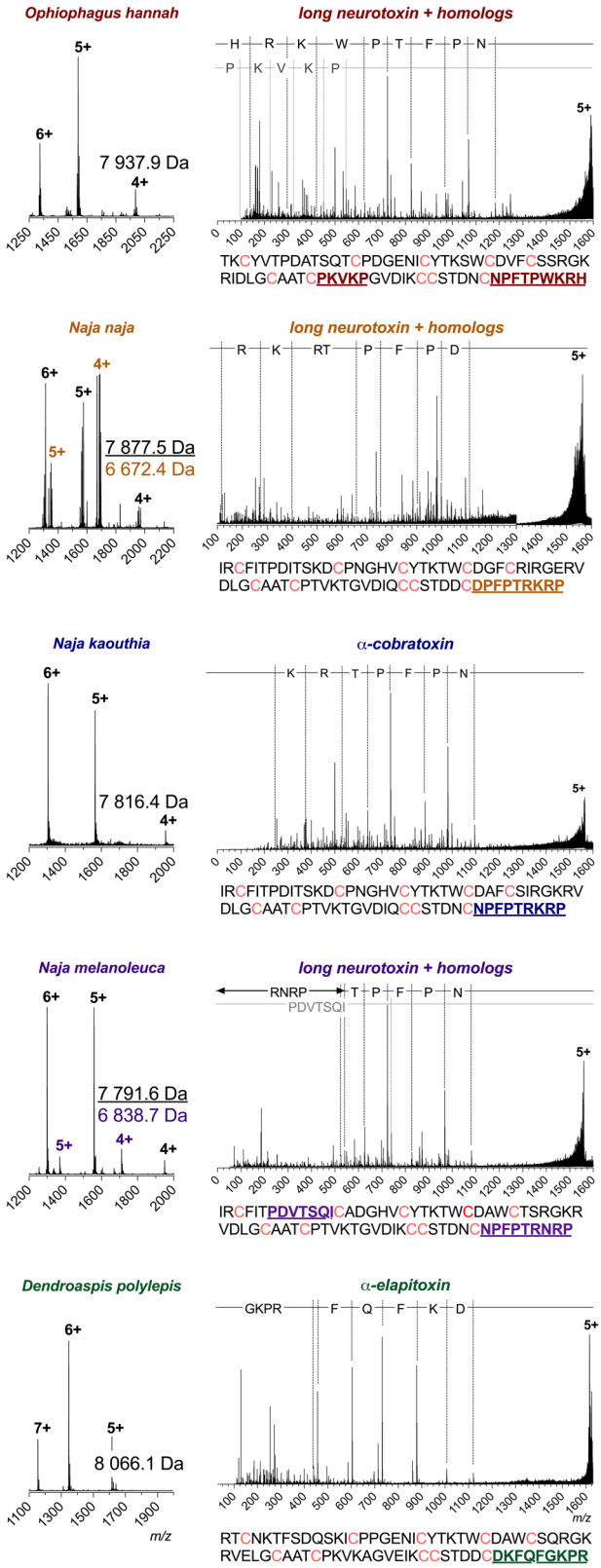

Fig. 2 | Intact masses and top-down sequence analysis of toxins bound by 2554_01_D11. Names above the mass spectra have been color-coded for each species as follows: *O. hannah* (red), *N. naja* (orange), *N. kaouthia* (blue), *N. melanoleuca* (purple) and *D. polylepis* (green). The spectra on the left-hand side show the charge state distribution for the toxins ejected from the antibody complex by applying a high cone voltage, where the masses of the identified toxins are given in Daltons. The top-down sequence spectra for the most prominent charge state of each toxin are shown on the right-hand side. The difference in *m/z* is outlined via dotted lines on top and matches the specific amino acid or peptide. The full amino acid sequence for the proposed identity of the toxins is given below each spectrum, with the matching peptides found during the top-down analysis colored and underlined. Cysteines in the sequence are colored pink.

cobratoxin. Two LD_{50}s of this neurotoxin were incubated with 2554_01_D11 in a 1:1 or 1:2 toxin:antibody molar ratio, and the toxicity was tested i.v. in mice. Animals receiving the toxin alone died within 30 min of injection with evident signs of neurotoxic paralysis, whereas all mice receiving the toxin incubated with the antibody, at the two molar ratios tested, survived without showing signs of intoxication (Fig. 5).

Then, snake venoms from three different species belonging to three genera, one from Africa, i.e., *D. polylepis*, and two from Asia, *i.e., N. kaouthia* and *O. hannah*, were included. Notably, each of these venoms contains a substantial amount of long-chain α-neurotoxins (a relative abundance of 13.2%[25], 55%[24], and ~20%[38], respectively). Two LD_{50}s of each venom were preincubated with 2554_01_D11 in a 1:1 and 1:2 toxin:antibody molar ratio for *N. kaouthia* (Fig. 6a) and O. *hannah* (Fig. 6b) or a 1:3 toxin:antibody molar ratio for *D. polylepis* (Fig. 6c) before being administered i.v. to the mice. As controls, mice were injected with venom alone, venom preincubated with commercial antivenoms of known efficacy against the venoms (except in the case of *O. hannah*, where no antivenom was available), or venom preincubated with an antibody isotype control.

The results of the studies demonstrated that all mice in the venom-only control group, as well as the mice receiving venom preincubated with the isotype control antibody, died within the first hour after the challenge, with evident signs of limb paralysis and respiratory difficulty. As expected, mice receiving *N. kaouthia* or *D. polylepis* venoms preincubated with commercially available antivenoms survived for the entire observation period, and no signs of neurotoxicity were observed. In experiments where mice were injected with venoms incubated with 2554_01_D11, results varied depending on the venom. In the case of *N. kaouthia* venom, complete neutralization was observed at both toxin:antibody molar ratios, since mice survived during the 48-hour observation time. Moreover, the mice showed no signs of neurotoxicity, i.e., limb paralysis or respiratory difficulty during the whole period. In the case of *O. hannah*, there was a dose-dependent delay in the time of death compared to controls receiving venom alone (Fig. 6b). Likewise, a delay in the time of death was observed in the case of *D. polylepis* venom (Fig. 6c).

Next, the ability of the antibody to abrogate the lethality of *N. kaouthia* venom in rescue-type experiments was assessed. For this, the subcutaneous (s.c.) route of venom injection was used to more closely reproduce the actual circumstances of envenoming. The LD_{50} estimated by the s.c. route was 10.3 μg (95% confidence interval: 5.0–16.8 μg). Mice were challenged by the s.c. route with a dose of venom corresponding to 2 LD_{50}s, i.e., 20.6 μg, followed by the i.v. administration of the 2554_01_D11 antibody in a volume of 100 μL at a molar ratio of 1:2.5 or 1:2.0 (toxin:antibody). Control mice injected with venom-only died within 40–60 min, with evident signs of limb and respiratory paralysis. When the antibody was administered immediately after venom injection, all mice survived the 24 h observation period and showed no evidence of limb or respiratory paralysis. When the antibody was provided 10 min after venom injection, two out of four mice died, but there was a delay in the time of death (150 and 180 min). The other two mice survived the 24 h observation time and did not show signs of paralysis (Fig. 6d).

Discussion

Here, we demonstrate that an antibody discovered from a naïve human library with limited cross-reactivity to other α-neurotoxins and without the ability to prevent lethality induced by α-cobratoxin in mice can be

https://doi.org/10.1038/s41467-023-36393-4

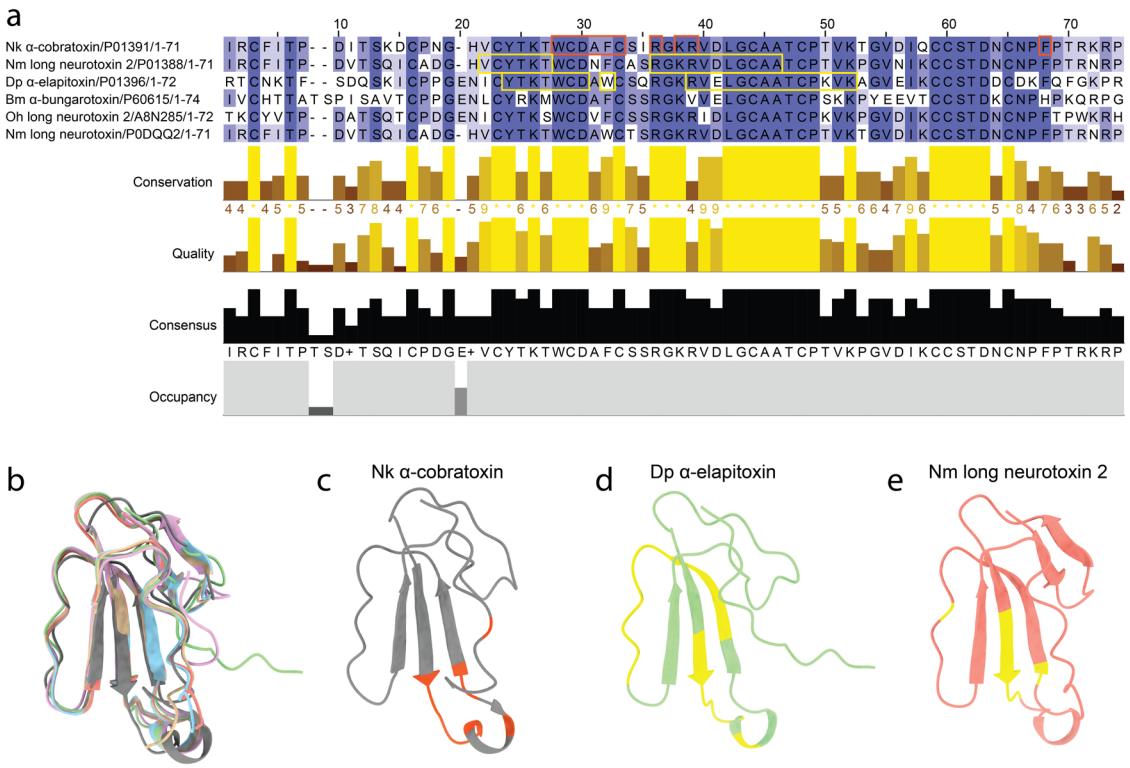

Fig. 3 | Alignment and epitope identification of all investigated long-chain α-neurotoxins, i.e., α-cobratoxin (P01391/1CTX) from *N. kaouthia*, α-elapitoxin (P01396/AF-P01396) from *D. polylepis*, α-bungarotoxin (P60615/1HC9) from *B. multicinctus*, long neurotoxin 2 (A8N285/AF-A8N285) from *O. hannah*, and long neurotoxin (P0DQQ2), long neurotoxin 4 from *N. naja* (P25672/AF-P25672), and long neurotoxin 2 (P01388/AF-P01388) from *N. melanoleuca*. **a** Sequence alignment using Clustal Omega with boxes indicating residues involved in binding to the nicotinic acetylcholine receptor (orange) or bound by antivenom antibodies (yellow). **b** Structural alignment in ChimeraX with the following colors representing each toxin: orange (long neurotoxin 2 from *N. melanoleuca*), beige (long neurotoxin 2 from *O. hannah*), purple (α-bungarotoxin), green (α-elapitoxin from *D. polylepis*), blue (long neurotoxin 4 from *N. naja*), and gray (α-cobratoxin from *N. kaouthia*). **c** Amino acid residues on α-cobratoxin known to be involved in binding to its native target, *i.e.*, the nicotinic acetylcholine receptor[39] (orange). **d** Amino acid residues in α-elapitoxin suggested to be bound by antivenom antibodies based on high-density peptide microarray analysis[37] (yellow). **e** Amino acid residues in long neurotoxin 2 from *N. melanoleuca* suggested to be bound by antivenom antibodies based on high-density peptide microarray analysis[37] (yellow).

improved by light chain-shuffling, resulting in enhanced affinity, potency, and cross-neutralization capacity.

The most promising antibody we discovered, 2554_01_D11, bound seven long-chain α-neurotoxins deriving from five snakes of four genera distributed across both Asia and Africa. Notably, cross-reactive binding was detected despite sequence alignment of the seven α-neurotoxins revealing substantial differences in sequence identity, with an overall identity of only 31%. This is likely because, despite the low overall identity, a total of 29 positions in the toxin sequences contain identical amino acid residues across all seven α-neurotoxins, including most of the residues previously identified as playing a significant role in the binding between α-cobratoxin/α-bungarotoxin and the nAChR[39]. Specifically, these amino acid residues include Trp25, Cys26, Asp27, Ala28, Phe29, Cys30, Arg33, Lys35, and Arg36/Val39 (α-cobratoxin/α-bungarotoxin) on loop II and Phe65/Val39 (α-cobratoxin/α-bungarotoxin) on the C-terminus, where a single mutation of one of these residues has been shown to cause a more than five-fold decrease in affinity to the nAChR[40]. Furthermore, high-density peptide microarray analysis previously suggested that positions 22–27 and 36–46 represent linear B-cell epitopes for antibodies to long neurotoxin 2 from *N. melanoleuca*, recognized by one of the most effective antivenoms available (SAIMR, produced by SAVP), like positions 24–30, 32, and 39–50 do for α-elapitoxin[37]. This emphasizes the potential importance of Trp25, Cys26, Asp27, Ala28, Phe29, Cys30, and Arg36 for the ability of antibodies to recognize this toxin. Together, these findings present a plausible explanation for the broad cross-reactivity we observed for 2554_01_D11 and indicates the importance of epitope similarity (as opposed to overall sequence identity) in the pursuit of cross-reactive antibodies[4]. However, the boundaries of the cross-reactivity of 2554_01_D11 have not been established in this study, as all long-chain α-neurotoxins investigated were recognized by the antibody. Future work aiming to investigate the boundaries of cross-reactivity could include testing the antibody for binding to long-chain α-neurotoxins from other snakes, such as *B. candidus*[41], *B. fasciatus*[41], or *N. haje legionis*[42]. Such studies could potentially provide general cues to how antibody cross-reactivity can be optimized for antibodies targeting toxins and similar antigens.

In addition to cross-reactive binding, we also demonstrated the broad neutralizing potential of 2554_01_D11. In vivo studies showed that lethality induced by three snake venoms of different genera distributed across both Asia and Africa was either prevented or delayed by the antibody, 2554_01_D11. For *N. kaouthia* venom, the antibody was able to completely prevent lethality in envenomed mice with no signs of neurotoxicity even at the lowest tested toxin:antibody molar ratio of 1:1. Moreover, this antibody was able to neutralize lethality induced by the venom of *N. kaouthia* in rescue-type experiments, which more closely resemble the actual circumstances of envenoming[43]. Complete neutralization was achieved when the antibody was administered immediately after the venom challenge, and even after a delay of 10 min between venom and antibody administration, 2 out of 4 mice survived and death was delayed in the other two.

Despite the antibody 2554_01_D11 possessing very similar in vitro affinities to α-cobratoxin and α-elapitoxin from *D. polylepis*, the antibody was unable to prevent in vivo lethality induced by *D. polylepis*

https://doi.org/10.1038/s41467-023-36393-4

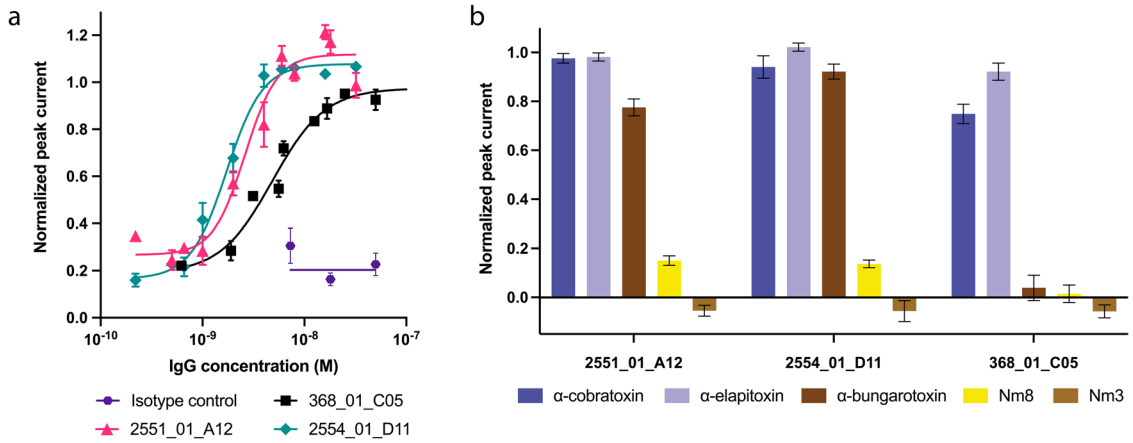

Fig. 4 | Electrophysiological determination of the in vitro cross-neutralizing potential of 2551_01_A12, 2554_01_D11, and 368_01_C05. Automated patch-clamp experiments were performed to determine the ability of the antibodies to prevent the current-inhibiting effect that α-neurotoxins exert on the nAChR. **a** Concentration-response curves illustrating how increasing concentrations of the three antibodies prevent nAChR blocking by α-cobratoxin (SD shown, each data-point based on at least $n = 4$ independent experiments, one experiment equals 10 cells). **b** Single concentration plot outlining the cross-neutralizing potential of the antibodies against α-cobratoxin from *N. kaouthia*, α-elapitoxin from *D. polylepis*, α-bungarotoxin from *B. multicinctus*, and Nm8 from *N. melanoleuca* (SD shown, $n = 6$ independent experiments, of which each equals 10 cells). In addition, a negative control Nm3, a fraction from *N. melanoleuca* venom containing a short α-neurotoxin, was included. The toxin to antibody molar ratios used were 1:22 for α-cobratoxin, 1:40 for α-elapitoxin, 1:5 for α-bungarotoxin, 1:2.3 for Nm8, and 1:3.2 for Nm3.

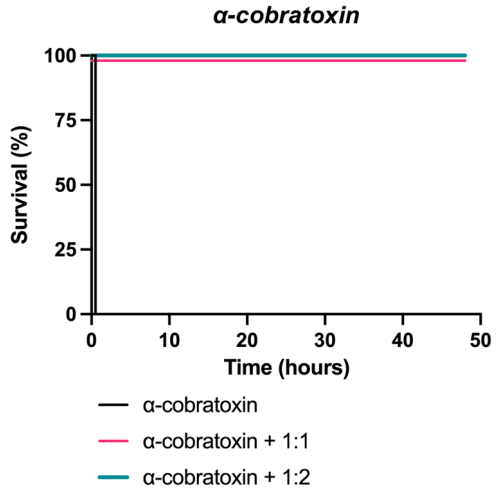

Fig. 5 | Kaplan–Meier survival curves for mice challenged with α-cobratoxin preincubated with or without the antibody 2554_01_D11. Two LD50s of α-cobratoxin (*N. kaouthia*) were preincubated with the antibody, 2554_01_D11, at various neurotoxin:antibody ratios and then administered i.v. into groups of four mice. Controls included mice receiving α-cobratoxin alone (see Materials and Methods for details). Signs of toxicity were observed, and deaths were recorded for a maximum period of 48 h.

venom, even at the tested toxin:antibody molar ratio of 1:3. Survival was, however, prolonged by several hours, suggesting that the antibody provided partial neutralization of the venom. These results are perhaps not surprising, as the venom of *D. polylepis* is more complex than that of *N. kaouthia*, and it is well-established that toxins other than long-chain α-neurotoxins (i.e., short-chain α-neurotoxins and dendrotoxins) play important roles in the toxicity of *D. polylepis* venom[25]. Where lethality of *N. kaouthia* venom is mainly attributed to the high content of long-chain α-neurotoxins, the short-chain α-neurotoxins present in *D. polylepis* venom have been estimated to contribute approximately one-third of the toxicity of the venom[25]. Thus, even if all long-chain α-neurotoxins were neutralized in the venom, neutralization of short-chain α-neurotoxins and possibly even dendrotoxins could still be necessary to prevent venom-induced lethality. As the affinity of the antibody to α-elapitoxin was almost identical to that of α-cobratoxin, we speculate that the antibody, 2554_01_D11, might be able to neutralize the effects of the long-chain α-neurotoxins from *D. polylepis* but that the mice eventually die due to lethality induced by short-chain α-neurotoxins and possibly dendrotoxins. Similarly, the lethal effects of the venom of *O. hannah* were only delayed, probably since this venom also consists of a mixture of both long and short-chain α-neurotoxins.

In this study, monoclonal IgG antibodies with broad cross-reactivity to different long-chain α-neurotoxins were discovered, and an epitope binning study revealed that the cross-reactive antibody 2554_01_D11 bound the same or an overlapping epitope to the previously reported antibody 2552_02_B02, which only recognizes α-cobratoxin[15]. In the future, determination of the structure of the two antibodies in complex with α-cobratoxin might provide further insight into how two antibodies binding to the same or overlapping epitope with similar affinity can display such different levels of cross-reactivity.

When comparing the neutralizing capacities of the two antibodies, 2554_01_D11 and 2552_02_B02, another noteworthy observation emerges. Antibody 2554_01_D11 possessed significantly higher efficacy in neutralizing *N. kaouthia* venom in vivo than what was reported for 2552_02_B02[15]. Whereas 2554_01_D11 neutralized all signs of neurotoxicity at the lowest tested dose of 1:1 toxin to antibody molar ratio, 2552_02_B02 only prevented lethality induced by *N. kaouthia* venom in 3 out of 4 mice at a 1:4 molar ratio, with mice showing clear signs of neurotoxicity. These results were especially remarkable, as the two antibodies performed similarly both in electrophysiological in vitro neutralization assays and had similar affinities to α-cobratoxin (490 pM for 2552_02_B02 and 1.78 nM for 2554_01_D11). Except for the difference in cross-reactivity profiles, the only significant difference between the two antibodies was in their developability profiles. In these developability assessment assays, 2554_01_D11 performed similarly to Aliricumab (control for good developability), whereas 2552_02_B02 performed comparably to Bococizumab (control for poor developability)[44]. It is thus possible that this difference in self-association and interaction with the SEC column seen in these assays may correlate with different pharmacokinetic or pharmacodynamic properties of the two antibodies, which could explain their contrasting performance in vivo. This suggests that detailed developability characterization should be included as part of early discovery to maximize

https://doi.org/10.1038/s41467-023-36393-4

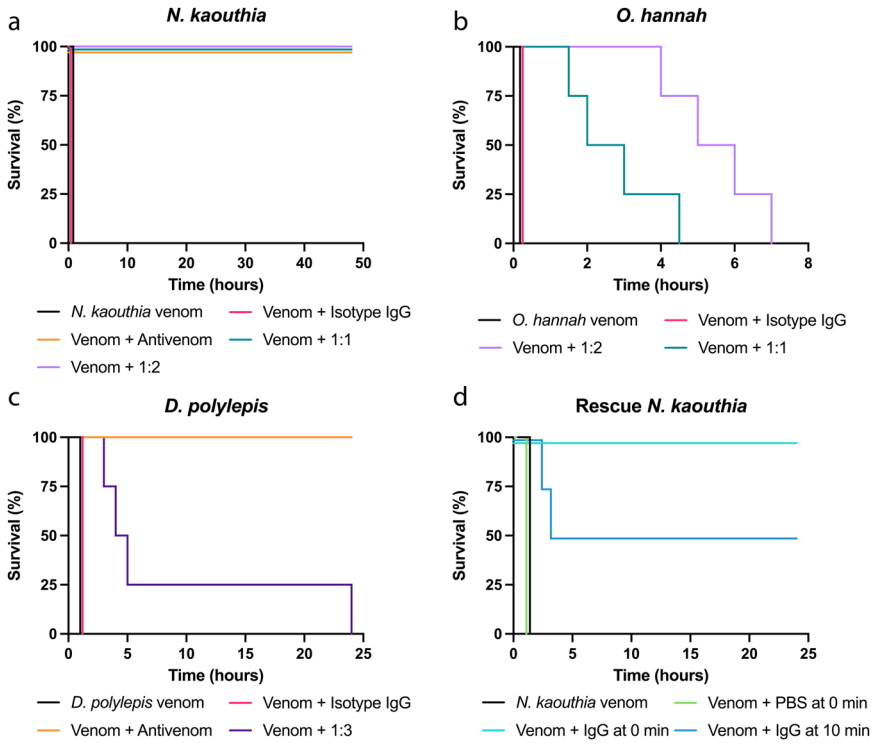

Fig. 6 | Kaplan–Meier survival curves for envenomed mice treated with the antibody 2554_01_D11. a–c Mixtures containing 2 LD_{50}s of venom of either *N. kaouthia*, *O. hannah*, or *D. polylepis* were preincubated with the antibody, 2554_01_D11, at various neurotoxin:antibody ratios and then administered i.v. into groups of four mice. Controls included mice receiving venom alone, or venom incubated with either an irrelevant isotype antibody control or commercial horse-derived antivenoms (see Materials and Methods for details). Signs of toxicity were observed, and deaths were recorded for a maximum period of 48 h. **d** *N. kaouthia* venom at 2 LD_{50}s was administered s.c. following by i.v. administration of IgG 2554_01_D11 either immediately or 10 min following venom injection. As controls, mice received either venom s.c. or venom s.c. followed by PBS i.v. immediately after envenoming. Signs of toxicity were observed, and deaths were recorded for 24 h. Mice receiving antibody immediately following venom administration had a dose of 1:2.5 toxin to antibody molar ratio, while mice receiving antibody 10 min post venom administration had an antibody dose of 1:2 toxin to antibody molar ratio.

the in vivo efficacy and clinical success of recombinant antivenoms. Furthermore, whilst this study focuses on α-neurotoxins, we hypothesize that similar in vitro strategies for affinity maturation and increased cross-reactivity could find utility for other classes of toxins comprising clusters of similar isoforms (e.g., phospholipase A_2s).

In conclusion, this study demonstrates the utility of combining cross-panning strategies in phage display with affinity maturation using chain-shuffling for the development of high-affinity human monoclonal IgG antibodies that show broadly-neutralizing effects against neurotoxic elapid snake venoms in vitro and in vivo. Such antibodies might be useful for designing future envenoming therapies, but more importantly, the pipeline presented here could also be exploited for the development of broadly-neutralizing antibodies against other targets of medical importance. These targets could include toxins from venomous animals other than snakes, but also hypervariable and mutating antigens from infectious bacteria, viruses, and parasites, or even neoepitopes in noninfectious diseases.

Methods

Protocols for in vivo experiments were approved by the Institutional Committee for the Use and Care of Animals (CICUA), University of Costa Rica (approval number CICUA 82–08).

Toxin preparation

α-cobratoxin (L8114), α-bungarotoxin (L8115), and whole venoms from *N. kaouthia* (L1323), *N. melanoleuca* (L1318), *D. polylepis* (L1309), and *O. hannah* (L1357) were obtained from Latoxan SAS, France. Venom fractions containing long α-neurotoxins (Dp7 from *D. polylepis* and Nm8 from *N. melanoleuca*) were isolated from crude venom by fractionation using RP-HPLC (Agilent 1200). Venoms were fractionated using a C18 column (250 × 4.6 mm, 5 µm particle; Teknokroma), and elution was carried out at 1 mL/min using Solution A (water supplemented with 0.1% TFA) and a gradient towards solution B (acetonitrile supplemented with 0.1% TFA): 0% B for 5 min, 0–15% B over 10 min, 15–45% B over 60 min, 45–70% B over 10 min, and 70% B over 9 min[25,31]. Fractions were collected manually and evaporated using a vacuum centrifuge. Toxins were dissolved in phosphate buffered saline (PBS: 137 mM NaCl, 3 mM KCl, 8 mM $Na_2HPO_4.2H_2O$, 1.4 mM KH_2PO_4, pH 7.4) and biotinylated by amine coupling using a 1:1 molar ratio of α-cobratoxin:EZ-Link™ NHS-PEG_4-Biotin reagent (Thermo Scientific, A39259). For the remaining toxins, a 1:1.5 toxin:biotin molar ratio was used. Free biotin was removed using 4 K MWCO ultracentrifugation membranes (Amicon Ultra-4, UFC8000324) in accordance with the desalting protocol in the manufacturers guidelines. Following purification, the degree of biotinylation was determined using MALDI-TOF in an Ultraflex II TOF/TOF spectrometer (Bruker Daltonics).

Library generation using chain-shuffling

Light chain-shuffled libraries containing the heavy chain variable domain of the 368_01_C05, diversified with a naïve repertoire of light variable domains, were created by subcloning the 368_01_C05 heavy chain variable domain into pSANG4 phage display vectors containing naïve kappa and lambda light chain germlines. The heavy chain was prepared by PCR amplification from the pSANG10-3F expression vector using the Platinum SuperFi Green polymerase (Thermo Fisher Scientific, 12359010), and sub-cloned into the phagemid vectors using *XhoI* (NEB, R0146S) and *NcoI* (NEB, R3193L) restriction enzymes. Ligations were performed overnight at 16 °C using 500 ng of light

chain vector and a 4-fold excess of heavy chain. Each library was purified using a MiniElute purification kit (Qiagen, 28006), eluted in 10 μL nuclease free water (Thermo Scientific, 10977035), and transformed into one aliquot electrocompetent TG1 cells (Lucigen, 605022) using a 0.2 cm Gene Pulser Cuvette (BioRad, 1652086). The library was immediately transferred into pre-warmed recovery medium (Corning, 354253) and incubated for 1 h at 37 °C, 220 rpm. Cells were pelleted, re-suspended in 500 μL of recovery media, plated on 2TYGA (2TY, 2% glucose, 50 μg/mL ampicillin), and incubated overnight at 30 °C. The library size was estimated based on counting the number of individual colonies from a dilution series of the library. The kappa library size was estimated to 1.67×10^8 and the lambda library to 1.01×10^8 individual transformats respectively. Colony PCR revealed that 96% of the transformants had successful insert of the heavy chain. The library was re-suspended in 2TYGA media containing 25% glycerol and left to homogenize for one hour with end over end rotation at room temperature before being stored at −80 °C.

Library rescue, solution-based phage display selection, and polyclonal DELFIA

Phages were rescued from the light chain-shuffled libraries by first diluting the cells to an OD_{600} of 0.1 in 50 mL of pre-warmed 2TYGA and incubating at 37 °C, 280 rpm. This equated to enough cells to obtain a 10-fold coverage of the library size. Once the cells had reached $OD_{600} = 0.5$, a 10-fold excess of proteolytic sensitive helper phage[45] was added for 1 h at 37 °C, 150 rpm to allow for infection. Cultures were centrifuged at 3,200 rpm for 2 min, the supernatant discarded, and cells were re-suspended in 2TYKA (2TY, 50 μg/mL kanamycin, 100 μg/mL ampicillin) media and the phages propagated overnight at 25 °C, 280 rpm. A TG1 colony was picked from a pre-prepared plate and used to inoculate 5 mL of 2TY media and incubated overnight at 30 °C, 280 rpm. The next day, the supernatant was obtained by centrifuging the overnight culture for 10 min, 10,500 × *g* at 4 °C, and a 1 mL volume of supernatant, sufficient for both the selection with antigen and a no-antigen reference, was spun under the same conditions to remove any residual cells and used for selection. At this point, 125 μL of each kappa and lambda library was combined into a 250 μL volume and blocked in a final concentration of 3% MPBS (PBS + 3% w/v milk: VWR, A0830.1000), in parallel with 80 μL streptavidin-coated Dynabeads (Fisher Scientific, M-280), for one hour with end over end rotation. Streptavidin-specific phages were de-selected by adding 80 μL of the blocked streptavidin beads to the blocked library for one hour with end over end rotation. The library with streptavidin beads was placed on a magnetic rack, and the supernatant containing non-streptavidin specific phages was transferred to a clean Eppendorf tube. Biotinylated long neurotoxin, diluted in 3% MPBS, was added to the de-selected library at a final concentration of 10 nM and incubated as described for previous steps followed by addition of streptavidin beads. Therafter, a KingFisher Flex (Thermo Scientific, 711-82573) system was used to wash the beads with biotinylated toxin and bound phages 3 times with PBST (PBS + 0.1% tween) and PBS before elution using 200 μL, 1 mg/mL trypsin (Sigma-Aldrich, T9201-500MG) prepared in 50 mM Tris, 1 mM $CaCl_2$, pH 8.0 buffer. 200 μL of the eluted phages was used to infect 5 mL of TG1 cells grown to an OD_{600} of 0.5, for 1 h at 37 °C, 150 rpm. Cells were subsequently spun for 10 min at 2000 g and re-suspended in 200 μL of media before plating. In addition, dilution plates ranging from 5–500,000-fold dilution of the supernatant were plated to determine the background and enrichment of antigen specific phages. The next day, colonies on the output plate were scraped and resuspended in 2TYGA supplemented with 25 % glycerol and the cells were homogenized with end-over end rotation for several hours. OD_{600} was measured, and the cells were stored at −80 °C until subsequent rescue and further rounds of selection. Two consecutive rounds to enrich for cross-reactivity were performed by cross-panning between α-cobratoxin and α-elapitoxin. The lead 2554_01_D11 clone originated from a selection strategy using 1 nM and 100 pM of antigen in the second and third round respectively.

To assess the polyclonal output of the individual selections, the binding was measured to biotinylated α-cobratoxin and biotinylated α-elapitoxin (both 60 μL, 5 μg/mL) captured on coated streptavidin (60 μL, 10 μg/mL). MPBS and streptavidin were included as negative controls. Black MaxiSorp plates (Nunc) were used and coating was performed overnight at 4 °C. The generation of phages from each selection round was performed as previously described for phage display. The prepared phage supernatants were diluted 100-fold in 3% MPBS and blocked alongside the immobilized antigen for 1 h at room temperature. With three washes in PBST and PBS between each incubation step, 60 μL of phages were first incubated for 1 h to allow for binding. Thereafter, bound phages were detected by the addition of 60 μL, 1 μg/mL, of anti-M13 mouse antibody (GE Healthcare) prepared in 3% MPBS. Finally, anti-M13 was detected using 0.5 μg/mL of an anti-mouse antibody conjugated to europium (Perkin Elmer) diluted in 3% MPBS), incubated for 30 min, followed by 100 μL of DELFIA enhancement solution (Perkin Elmer). The signal readout was performed by time resolved fluorescence (TRF) with 320 nm excitation and 615 nm emission wavelengths.

Subcloning, screening, and sequencing of scFvs

The genes encoding the scFvs from five of the obtained selection outputs (representing different cross-panning strategies) were PCR amplified using M13leadseq (AAATTATTATTCGCAATTCCTTTGGTTG TTCCT) and Notmycseq (GGCCCCATTCAGATCCTCTTCTGAGATGAG) primers and subcloned into the pSANG10-3F expression vector using the *Nco*I and *Not*I restriction enzymes. Following transformation into the *E. coli* strain BL21 (DE3) (New England Biolabs), 184 individual colonies were picked from each selection and used for expression of soluble scFv. Cells were first grown at 30 °C, 200 rpm, overnight in 150 μL of 2TYKA media containing 2% glucose. Expression was then induced in 96 well polypropylene microtiter plates (Greiner Bio-One) containing 150 μL of autoinduction media and incubated overnight at 30 °C, 800 rpm with 80% humidity. Binding of the scFv was assessed in both a direct and an expression-normalized DELFIA. For direct binding, MaxiSorp plates were coated overnight with streptavidin (60 μL, 10 μg/mL). The next day, following washing, biotinylated α-cobratoxin and α-elapitoxin (60 μL, 5 μg/mL) diluted in 3% MPBS were added and incubated for one hour. To assess scFv binding, 25 μL supernatant from the harvested overnight cultures was transferred to each well containing an equal volume of 6% MPBS for one hour to permit binding. Bound scFv was detected with an anti-FLAG M2 antibody (Sigma-Aldrich) conjugated with europium (PerkinElmer), produced in house according to the manufacturers guidelines, in the steps described above for the polyclonal DELFIA. In addition, an expression-normalized DELFIA was run. Here, black MaxiSorp plates were coated overnight with anti-FLAG (Sigma) (60 μL, 2.5 μg/mL). The next day, following washing, 25 μL supernatant mixed with 25 μL 6% MPBS was incubated for one hour at room temperature. After washing, 60 μL of 10 nM biotinylated α-cobratoxin and α-elapitoxin diluted in 3% MPBS was left to bind for one hour. Bound antigen was finally detected using 0.2 ng/μL of europium-conjugated streptavidin diluted in DELFIA assay buffer (Perkin Elmer), followed by enhancement solution and recording of emission as described above. Based on the signal intensity, the top 203 clones were cherry-picked and sequenced (Eurofins Genomics sequencing service) using the S10b primer (GGCTTTGTTAGCAGCCGG ATCTCA). The antibody frameworks and the CDR regions of the light chains were annotated using Geneious Biologics (Biomatters), and 67 clones were identified as unique based on light chain CDR3 regions.

Reformatting and screening of IgG and Fab formats

A total of 62 clones were selected for reformatting into human IgG1 and Fab format. The V_H and V_L domains were subcloned into a pINT12

vector for Fab expression and pINT3 vector for IgG expression. Each vector had the respective heavy chain constant domains and light chain constant domain pre-cloned for each format. The individual variable domains were PCR amplified from the pSANG10-3F expression vector using pSang10_pelB (CGCTGCCCAGCCGGCCATGG) and HLINK3_R (CTGAACCGCCTCCACCACTCGA) for the V_H and LLINK2_F (CTCTGGCGGTGGCGCTAGC) and 2097_R (GATGGTGATGATG ATGTGCGGATGCG) for the V_L. The PCR amplicons were prepared by digestion with *Nco*I and *Xho*I (V_H digestion) and *Nhe*I and *Not*I (V_L digestion) endonucleases. A four-part ligation including both variable domains, either the pINT3 or pINT12 vector containing the respective heavy chain constant domains, and a stuffer region containing the C_L and CMV promoter cut with *Nco*I and *Not*I, was performed with T4 DNA ligase (Roche, 10481220001). Each of the respective Fab and IgG formats were produced for screening at a 700 μL scale by transient mammalian expression using Expi293™ cells (Thermo). After transfection using a ratio of 1 μg DNA/mL of Expi293™ cells with ExpiFectamine™ 293 (ThermoFisher, A14525) as per the manufacturers guidelines, transfected cells were incubated for 4 days in an orbital shaker at 37 °C, 5% CO_2, 70% humidity with 1000 rpm shaking. Cells were harvested, and supernatants containing IgGs were purified with protein A using MabSelect SuRe (Neo Biotech, NB-45-00036-100), and Fabs using anti-C_H1 resin (Thermo Scientific, 194320010). A volume of 10 × PBS sufficient to give a 1 × PBS final concentration was added to each well of supernatant. For IgG containing supernatants, 100 μL of protein A diluted 4-fold in PBS was added to each well and incubated overnight at 4 °C. Likewise, Fab supernatant was incubated overnight with 100 μL of anti-C_H1 resin diluted 5-fold in PBS. Supernatants were transferred to a Unifilter membrane (GE Healthcare, 7700-2804) and loaded onto a 96 deep well microplate. In centrifugation intervals of 1 min, 1000 × *g*, the flow through was removed, then the resin was washed twice with 500 μL PBS, and antibody was eluted with 75 μL, 0.2 M Glycine, pH 2.6 into a new plate containing 25 μL of 2 M Tris pH 8.0 neutralization buffer. Antibodies were desalted using Zeba Spin Desalting plates (Thermo Scientific, 89808) into PBS.

Produced clones were selected for further developability characterization by assessing their binding strength as full length IgGs and Fabs to a one-spot concentration of α-cobratoxin, α-elapitoxin, and Nm8, by a capture DELFIA assay. Black Maxisorp plates (Nunc) were coated with 50 μL, 2.5 μg/mL anti-C_H1 antibody (Hybridoma Reagent Laboratory, HP6046P) or anti-hIgG (Jackson ImmunoResearch, 109-005-098) and incubated overnight at 4 °C. The next day, after washing the plates three times in PBS and blocking for an hour in 3% MPBS, 50 μL of supernatants diluted 4-fold in 4% MPBS was added to each well and incubated for 1 h at room temperature. After three washes in PBS and PBST, antigen (50 μL, 1 nM) prepared in 3% MPBS was added to test wells. As a control, a 1:500 dilution of streptavidin conjugated with europium in DELFIA assay buffer was added. After 1 hour, the test wells were washed, and streptavidin conjugated europium was added as for the control wells for 30 min. After a final wash, 50 μL of DELFIA enhancement solution was added, plates were placed on a shaker for 5 min, and binding was detected by time resolved fluorescence measured on a PHERAstar FSX (BMG, Labtech) system using excitation and emission wavelengths of 320 and 615 nm.

Six antibodies (2551_01_A12, 2554_01_D11, 2558_02_G09, 2551_01_B11, 2555_01_A04, and 2555_01_A01) and nivolumab were selected for further in vitro characterization and produced as IgGs at either a 300 mL or 500 mL scale. The production conditions and sample preparation for purification were the same as for the small-scale production, with the exception that the supernatants were first filtered using a 0.45 μm filter and purified using an Äkta Pure system (Cytiva) with a HiTrap™ 5 mL MabSelect™ Prism A column (Cytiva, GE17549854). Antibodies were eluted with 1.6 mL, 0.1 M citrate buffer, pH 3.0 into 300 μL, 2 M Tris pH 8.0 neutralizing solution. The eluate was buffer exchanged into 222 mM sucrose, 6.44 mM L-Histidine, 4.77 mM L-Histidine HCl, 0.0003% polysorbate 80 using P50 gel filtration columns (CentriPure, CP-0113-Z010.0-001). Antibodies were concentrated to 4–8 mg/mL using pre-rinsed Amicon® Ultra-4 Centrifugal Filter Units with a 50 KDa cutoff (Millipore, UFC8050) and flash frozen in liquid nitrogen for long term storage at −80 °C.

Developability characterization

To aid in the selection of the top antibody candidates for further characterization, the biophysical behavior of the 62 reformatted clones in the IgG format was characterized using HPLC-SEC and AC-SINS. For HPLC-SEC, the purified antibodies were loaded onto a Superdex 200 Increase 5/150 column at a flow rate of 0.25 mL/min using an Agilent 1100 HPLC instrument. AC-SINS was performed to measure the self-propensity of antibodies. Gold nanoparticles were coated with a 0.4 mg/mL, 20 mM NaAc, pH 4.3 solution containing a 4:1 ratio of anti-human IgG Fc capture:non-capture antibodies. The antibody coating solution was mixed with the gold nanoparticles in a 1:9 volume ratio at room temperature for 1 h and the remaining sites blocked with a 0.1 μM final concentration of thiolated PEG. After filtering through a 0.22 μm PVDF membrane (Millex-GV, 13 nm, Millipore), the gold nanoparticles were present in the retentate, and were eluted in 1/10th the volume of PBS. The prepared gold nanoparticles (10 μL) were mixed with test antibody (100 μL, >50 ug/ml in PBS) at room temperature for 2 h in a polypropylene plate, after which they were transferred to a polystyrene UV transparent plate, centrifuged briefly, and data collected by measuring the absorbance from 510 to 570 nm in increments of 2 nm. The self-association propensity was calculated by importing and processing the raw absorbance as described perviously[32].

Surface plasmon resonance

The binding affinity of the corresponding Fab versions of the top six affinity matured antibodies as well as the parental clone to α-cobratoxin and α-elapitoxin was determined using surface plasmon resonance (SPR; BIAcore T100, GE Healthcare). α-elapitoxin and α-cobratoxin were immobilized to a target level of 20 response units (RU) by amine coupling to carboxymethylated dextran on a CM5 biosensor chip (Cytiva, BR100530). The biosensor surface was activated using 1-Ethyl-3-(3-dimethylaminopropyl) carbodiimide (EDC)/N-hydroxysuccinimide followed by an injection of 5 μg/mL of α-neurotoxin prepared in 10 mM NaOAc pH 4. A no antigen flow cell was allocated as a reference. After immobilization the surface was washed and de-activated using ethanolamine. Antibody Fab fragments were prepared in running buffer: 10 mM HEPES, 150 mM NaCl, and 3 mM EDTA, 0.05% P20 (HEPES), adjusted to pH 7.4, in a 3-fold dilution series from 81 to 390 pM. A flow rate of 40 μL/min was used throughout the experiment with an association time of 120 s and a dissociation time of 450 s for each Fab. The biosensor surface was regenerated using two consecutive 30 s injections of 10 mM Glycine, 4 M sodium chloride pH 2.0. Measurements were conducted using 5–7 analyte concentrations for each antibody and included a no antibody blank. The blank and reference flow cell backgrounds were subtracted in the BIAcore T100 Evaluation Software, a 1:1 Langmuir binding model and a global model was used for fitting of the data and calculations of kinetic parameters.

Epitope binning experiments were performed using a sandwich setup, whereby one antibody was immobilized on a CM5 sensor chip using amine coupling, prior to flowing α-cobratoxin with a competing antibody. The 2554_01_D11 Fab (10 μg/mL, 10 mM sodium acetate pH 5.0) was immobilized to a level of 450 RU, and 20 nM α-cobratoxin prepared in HEPES buffer (10 mM, HEPES, 150 mM NaCl, 50 mM MES, 0.05% P20, pH 7.4) was incubated with 200 nM of either test 2552_02_B02 Fab or control Fab. Dual binding was then measured by injecting the α-cobratoxin and Fab solution over the immobilized 2554_01_D11 flow cell for 120 s. The immobilized 2554_01_D11 Fab flow

cell was used to measure the affinity to α-bungaratoxin, prepared in a 3-fold titration series from (2.1 μM to 9 nM) in HEPES buffer and regenerated as decribed above. The background subtraction and data processing was performed as described for α-elapitoxin and α-cobratoxin.

Determining cross-reactivity using native mass spectrometry

Sample preparation. Venoms and antibody samples were fractionated and exchanged into 200 mM ammonium acetate by size exclusion chromatography (SEC). Briefly, 2–5 mg of whole venom was dissolved in 200 mM ammonium acetate[46,47]. Size exclusion was then performed on this whole venom solution using a Superdex Increase 200 10/300 GL column (Cytiva, Massachusetts, United States) pre-equilibrated with 200 mM ammonium acetate. Samples were collected and stored at 4 °C until use. Prior to analysis, aliquots of the venom and IgG 2554_01_D11 SEC fractions were mixed in a 1:1 ratio (*v*/*v*). The final concentration of the antibody was approximately 3 μM after mixing. The concentration of toxins in the SEC fractions was not adjusted prior to mixing with the antibody.

Native mass spectrometry. All mass spectrometry (MS) experiments were performed on a SELECT SERIES cyclic IMS mass spectrometer (Waters, Manchester, U.K.) which was fitted with a 32,000 *m/z* quadrupole, as well as an electron capture dissociation (ECD) cell (MSvision, Almere, Netherlands), the latter of which was situated in the transfer region of this mass spectrometer. Approximately 4 μL of sample was nanosprayed from borosilicate capillaries (prepared in-house) fitted with a platinum wire. Spectra were acquired in positive mode, with the *m/z* range set to 50–8,000. Acquisitions were performed for five minutes at a rate of 1 scan per second. The operating parameters for the MS experiments were as follows, unless otherwise stated: capillary voltage, 1.2–1.5 kV; sampling cone, 20 V; source offset, 30 V; source temperature, 28 °C; trap collision energy, 5 V; transfer collision energy, 5 V; and ion guide RF, 700 V. This instrument was calibrated with a 50:50 acetonitrile:water solution containing 20 μM cesium iodide (99.999%, analytical standard for HR-MS, Fluka, Buchs, Switzerland) each day prior to measurements.

Top-down proteomics of toxins bound by 2554_01_D11. The toxin:antibody complexes were purified using SEC using the methods described above. Toxins were ejected from the protein complex during the MS experiments by setting the cone voltage to 160 V. The 5^+ ions (most abundant charge state) of the ejected toxins were selected by tandem MS (MS/MS) and subjected to fragmentation by applying a trap voltage between 80 and 100 V as well as a transfer voltage between 20 and 50 V. Peptide sequence assignment was performed for 1^+ fragmentation ions using the BioLynx package, which is a part of the MassLynx v4.1 software.

Sequence alignment

Sequence alignment was performed in Clustal Omega[48] and visualized in Jalview[49] using α-cobratoxin (P01391) from *N. kaouthia*, α-elapitoxin (P01396) from *D. polylepis*, α-bungarotoxin (P60615) from *B. multicinctus*, long neurotoxin 2 (A8N285) from *O. hannah*, and long neurotoxin (P0DQQ2) and long neurotoxin 2 (P01388) from *N. melanoleuca*. Structures for each toxin were retrieved prioritizing high-resolution X-ray resolved structures and included the following: P01391 = 1CTX (2.8 Å, X-ray), P01388 = AF-P01388-F1 (AlphaFold2 predicted), P01396 = AF-P01396-F1 (AlphaFold2 predicted), P60615 = 1HC9 (1.8 Å, X-ray), A8N285 = AF-A8N285-F1 (AlphaFold2 predicted), and P0DQQ2 = AF-P0DQQ2-F1 (AlphaFold2 predicted). Structural alignment and root-mean-square deviation (RMSD) analysis were performed in ChimeraX[50]. Epitopes of P01388 and P01396 were identified using the STAB Profiles tool[37] (https://venom.shinyapps.io/stab_profiles/).

In vitro neutralization using electrophysiology (QPatch)

To determine the ability and potency with which the affinity matured clones 2551_01_A12 and 2554_01_D11, as well as the parental antibody 368_01_C05, were able to neutralize the effects of α-cobratoxin, whole-cell patch-clamp experiments were conducted using rhabdomyosarcoma cells (CCL-136, ATCC):

Planar whole-cell patch-clamp experiments were carried out on a QPatch II automated electrophysiology platform (Sophion Bioscience), where 48-channel patch chips with 10 parallel patch holes per channel (patch hole diameter ~1 μm, resistance 2.00 ± 0.02 MΩ) were used.

The human derived Rhabdomyosarcoma RD cell line endogenously expresses the muscle-type nicotinic acetylcholine receptors (nAChR), composed of the α1, β1, δ, γ and ε subunits. The cells were cultured according to the manufacturer's guideline and on the day of the experiment, enzymatically detached from the culture flask and brought into suspension.

For patching, the extracellular solution contained (in mM): 145 NaCl, 10 HEPES, 4 KCl, 1 $MgCl_2$, 2 $CaCl_2$, and 10 glucose, pH adjusted to 7.4 and osmolality adjusted to 296 mOsm and the intracellular solution contained (in mM): 140 CsF, 10 HEPES, 10 NaCl, 10 EGTA, pH adjusted to 7.3 and osmolality adjusted to 290 mOsm.

In the experiments, a nAChR mediated current was elicited by 70 μM acetylcholine (ACh, Sigma-Aldrich), approximately the EC_{80} value, and after compound wash-out, 2 U acetylcholinesterase (Sigma-Aldrich) was added to ensure complete ACh removal. The ACh response was allowed to stabilize over 3 ACh additions, before the 4th addition was used to evaluate the effect of α-cobratoxin (4 nM α-cobratoxin, reducing the ACh response by 80%), in combination with varying concentrations of IgG. α-cobratoxin and IgGs were co-incubated at least 30 min before application, and the patched cells were preincubated with α-cobratoxin and IgG for 5 min prior to the 4th ACh addition.

The inhibitory effect of α-cobratoxin was normalized to the full ACh response (4th response normalized to 3rd response), plotted in a non-cumulative concentration-response plot and a Hill fit was used to obtain EC50 values for each IgG. The data analysis was performed in Sophion Analyzer (Sophion Bioscience) and GraphPad Prism (GraphPad Software).

In vitro cross-neutralization using electrophysiology (Qube 384)

To determine the broader cross-neutralizing potential of the top two affinity matured antibodies and the parent antibody, automated patch-clamp experiments using the Qube 384 electrophysiology platform (Sophion Bioscience) were conducted:

Planar whole-cell patch-clamp experiments were carried out on a Qube 384 automated electrophysiology platform (Sophion Bioscience), where 384-channel patch chips with 10 parallel patch holes per channel (patch hole diameter ~1 μm, resistance 2.00 ± 0.02 MΩ) were used.

Both the RD cell line, the extracellular solution and the intracellular solution were similar to what was used in the QPatch experiments. Again, a nAChR mediated current was elicit by 70 μM ACh, and after compound wash-out, 2 U acetylcholinesterase was added to ensure complete ACh removal.

In the Qube 384 experiments, a 2nd ACh addition was used to evaluate the toxin effect (in nM: α-cobratoxin 1.47 nM, α-elapitoxin 0.81, nM 8 14, nM3 10.30) in combination of varying concentrations of IgG. α-cobratoxin and IgGs were co-incubated at least 30 min before application, and the patched cells were preincubated with α-cobratoxin and IgG for 5 min prior to the 2nd ACh addition.

The inhibitory effect of the toxins was normalized to the full ACh response and averaged in the group. The data analysis was performed in Sophion Analyzer (Sophion Bioscience) and Excel (Microsoft).

Production of IgG for in vivo experiments

The variable chains (V_L and V_H) were PCR-amplified from the pSANG10-3F vector and cloned into a single expression vector using the NEBuilder® cloning technique. The expression vector contained the constant domain sequences of the respective human IgG heavy chain (with LALA[51] and YTE[52] mutation) and human lambda light chain. After cloning and sequence verification the plasmid was purified using NucleoBond Xtra Midi EF (Macherey-Nagel) according to the manufacturer's instructions.

A CHO-S cell line with pre-established landing pad (isoCHO-EP[53]) was cultivated in CD CHO medium, supplemented with 8 mM L-Glutamine and 2 µL/mL anticlumping agent at 37 °C, 5% CO_2 at 120 rpm (shaking diameter 25 mm). The cell line was transfected with IgG expression vector and Cre-recombinase vector in 3:1 ratio (w:w) at a concentration of 10^6 cells/mL using FreeStyle MAX transfection reagent (Thermo Fischer Scientific) according to the manufacturer's recommendation. Stable cell pools were generated by adding 5 µg/mL blasticidin five days post-transfection, and after recovery (>95% viability), cells were single cell sorted using a fluorescence activated cell sorter. After expansion, the IgG producing cell line was seeded at 10^6 cells/mL in 2 L complete culture medium and cultured for 144 h. Thereafter, cell cultures were harvested by centrifugation. The clear supernatant was loaded on a 25 mL MabSelect PrismA column (Cytiva) equilibrated with 20 mM sodium phosphate and 150 mM NaCl (pH 7.2). Elution was performed with 0.1 M sodium citrate (pH 3). Elution fractions were neutralized with 1 M Tris (pH 9), using 2 mL per 10 mL of elution fraction followed a buffer exchange to Dulbecco's PBS using a HiPrep 26/10 desalting column. IgG was concentrated using an Amicon® Ultra-15 centrifugal filter unit (30 kDa NMWL), sterile filtered.

Animals

Animal experiments were conducted in CD-1 mice of both sexes weighing 18–20 g (corresponding to 4–5 weeks old). Mice were supplied by Instituto Clodomiro Picado and experiments were conducted following protocols approved by the Institutional Committee for the Use and Care of Animals (CICUA), University of Costa Rica (approval number CICUA 82-08). Mice were provided food and water *ad libitum* and housed in Tecniplast Eurostandard Type II 1264C cages (L25.0 cm × W40.0 cm × H14.0 cm) in groups of 4 mice per cage. Animals were maintained at 18–24 °C, 60–65% relative humidity and 12:12 light-dark cycle.

In vivo preincubation neutralization experiments

The in vivo neutralizing potential of 2554_01_D11 against α-cobratoxin and whole venoms of *N. kaouthia*, *D. polylepis*, and *O. hannah* was assessed by i.v. injection of IgG preincubated with toxin or venoms using groups of four mice per treatment. Mixtures of a constant amount of toxin or venom and various amounts of antibody were prepared and incubated for 30 min at 37 °C. Then, aliquots of the mixtures containing 2 LD_{50}s of toxin or venoms (for α-cobratoxin 4.0 µg; for *N. kaouthia*, 9.12 µg; for *D. polylepis*, 25.8 µg; and for *O. hannah*, 40 µg) were injected into the caudal vein of mice using an injection volume of 150–200 µL. Control mice were injected with either toxin alone, venom alone, venom preincubated with an isotype control IgG or, in the cases of *N. kaouthia* and *D. polylepis* venoms, they were also preincubated with commercial horse-derived antivenoms known to be effective against these venoms. For *N. kaouthia* Snake Venom Antiserum from VINS Bioproducts Limited (batch number: 01AS13100), at a proportion of 0.2 mg venom per mL antivenom was used. For *D. polylepis*, Premium Serum and Vaccines antivenom (batch number: 062003), at a proportion of 0.12 mg venom per mL antivenom was used. These proportions were selected based on information on neutralization provided in the prospects of these products. In the case of *O. hannah* venom, no effective commercial antivenom was available and, therefore, this control group was not included.

IgG was injected using 1:1 and 1:2 α-neurotoxin:IgG molar ratios for α-cobratoxin, *N. kaouthia* venom and *O. hannah* venom and a 1:3 α-neurotoxin:IgG molar ratio for *D. polylepis* venom. In the case of venoms, for calculating molar ratios, based on toxicovenomic studies, it was estimated that 55% of *N. kaouthia* venom[24], 13.2% of *D. polylepis* venom[25], and 40% of *O. hannah* venom consisted of α-neurotoxins[54]. Following injection, animals were observed for signs of neurotoxicity, and survival was monitored for 48 h. The results are presented in Kaplan–Meier plots, generated with Prism v.9.4.1.

In vivo rescue neutralization experiments

To assess whether the antibody was capable of neutralizing the venom of *N. kaouthia* in an experimental setting that more closely resembles the actual circumstances of envenoming, a rescue-type experiment was designed. For this, the s.c. route was used for injection of venom, while the antibody was administered i.v. First, the s.c., LD_{50} of *N. kaouthia* venom was estimated by injecting various doses of venom, diluted in 100 µL of PBS, into groups of four mice. Animals were observed for 24 h, deaths were recorded, and the LD_{50} was estimated by probits[55]. For neutralization experiments, groups of four mice first received a challenge dose of 20.6 µg of venom by the s.c. route, dissolved in 100 µL of PBS, corresponding to 2 LD_{50}s. Then, antibody 2554_01_D11 was administered i.v. in the caudal vein, in a volume of 100 µL, either immediately or 10 min following venom administration. The amount of antibody administered was 535 µg (immediately) and 412 µg (10 min), corresponding to neurotoxin: antibody molar ratios of 1:2.5 and 1:2.0, respectively. Mice were observed for 24 h for the onset of neurotoxic manifestations, and times of death were recorded and presented in Kaplan-Meier plots, generated with Prism v.9.4.1.

Statistics and reproducibility

No statistical method was used to predetermine the sample size. The experiments were not randomized. The investigators were not blinded to allocation during experiments and outcome assessment. All in vitro *data* was performed at least 4 times independently. Data were excluded for analysis based on the following quality filters (per site, each site records from 10 cells): Current minimum 500 pA and seal resistance minimum 50 XX.

Reporting summary

Further information on research design is available in the Nature Portfolio Reporting Summary linked to this article.

Data availability

The data that supports the findings of this study are available from the corresponding authors upon reasonable request.

References

1. Gutiérrez, J. M. et al. Snakebite envenoming. *Nat. Rev. Dis. Prim.* **3**, 1–21 (2017).
2. Pucca, M. B. et al. History of envenoming therapy and current perspectives. *Front. Immunol.* **10**, 1598 (2019).
3. Hamza, M. et al. Clinical management of snakebite envenoming: future perspectives. *Toxicon X* **11**, 100079 (2021).
4. Laustsen, A. H. *Handbook of Venoms and Toxins of Reptiles* (CRC Press, 2021).
5. Richard, G. et al. In vivo neutralization of α-Cobratoxin with high-affinity Llama single-domain antibodies (V_HHs) and a V_HH-Fc antibody. *PLoS One* **8**, e69495 (2013).
6. Laustsen, A. H. et al. In vivo neutralization of dendrotoxin-mediated neurotoxicity of black mamba venom by oligoclonal human IgG antibodies. *Nat. Commun.* **9**, 3928 (2018).
7. Roncolato, E. C. et al. Human antibody fragments specific for Bothrops jararacussu venom reduce the toxicity of other Bothrops sp. venoms. *J. Immunotoxicol.* **10**, 160–168 (2013).

8. Cardoso, D. F. et al. Neutralizing human anti crotoxin scFv isolated from a nonimmunized phage library. *Scand. J. Immunol.* **51**, 337–344 (2000).
9. Lomonte, B. & Kahan, L. Production and partial characterization of monoclonal antibodies to *Bothrops asper* (terciopelo) myotoxin. *Toxicon* **26**, 675–689 (1988).
10. Lomonte, B., Gutiérrez, J., Ramírez, M. & Díaz, C. Neutralization of myotoxic phospholipases A_2 from the venom of the snake *Bothrops asper* by monoclonal antibodies. *Toxicon* **30**, 239–245 (1992).
11. Masathien, C., Billings, P. & Ratanabanangkoon, K. Production and characterization of monoclonal antibodies neutralizing the post-synaptic neurotoxin 3 from *Naja kaouthia*venom. *Toxicon* **3**, 290 (1995).
12. Boulain, J. C. et al. Neutralizing monoclonal antibody specific for *Naja nigricollis* toxin alpha: preparation, characterization and localization of the antigenic binding site. *Biochemistry* **21**, 2910–2915 (1982).
13. Laustsen, A. H. et al. From fangs to pharmacology: the future of snakebite envenoming therapy. *Curr. Pharm. Des.* **22**, 5270–5293 (2016).
14. Ahmadi, S. et al. An in vitro methodology for discovering broadly-neutralizing monoclonal antibodies. *Sci. Rep.* **10**, 10765 (2020).
15. Ledsgaard, L. et al. In vitro discovery of a human monoclonal antibody that neutralizes lethality of cobra snake venom. *mAbs* **14**, 2085536 (2022).
16. Kini, R. M., Sidhu, S. S. & Laustsen, A. H. Biosynthetic Oligoclonal Antivenom (BOA) for snakebite and next-generation treatments for snakebite victims. *Toxins* **10**, 534 (2018).
17. Casewell, N. R., Jackson, T. N. W., Laustsen, A. H. & Sunagar, K. Causes and consequences of snake venom variation. *Trends Pharmacol. Sci.* **41**, 570–581 (2020).
18. Jenkins, T. P. & Laustsen, A. H. Cost of manufacturing for recombinant snakebite antivenoms. *Front. Bioeng. Biotechnol.* **8**, 703 (2020).
19. Ledsgaard, L. et al. Antibody cross-reactivity in antivenom research. *Toxins* **10**, E393 (2018).
20. Laustsen, A. H., Johansen, K. H., Engmark, M. & Andersen, M. R. Recombinant snakebite antivenoms: a cost-competitive solution to a neglected tropical disease? *PLoS Negl. Trop. Dis.* **11**, e0005361 (2017).
21. Laustsen, A. H., Greiff, V., Karatt-Vellatt, A., Muyldermans, S. & Jenkins, T. P. Animal immunization, in vitro display technologies, and machine learning for antibody discovery. *Trends Biotechnol.* **39**, 1263–1273 (2021).
22. Roncolato, E. C. et al. Phage display as a novel promising antivenom therapy: a review. *Toxicon* **93**, 79–84 (2015).
23. Tan, K. Y., Tan, C. H., Fung, S. Y. & Tan, N. H. Venomics, lethality and neutralization of *Naja kaouthia*(monocled cobra) venoms from three different geographical regions of Southeast Asia. *J. Proteom.* **120**, 105–125 (2015).
24. Laustsen, A. H. et al. Snake venomics of monocled cobra (*Naja kaouthia*) and investigation of human IgG response against venom toxins. *Toxicon. J. Int. Soc. Toxinol.* **99**, 23–35 (2015).
25. Laustsen, A. H., Lomonte, B., Lohse, B., Fernandez, J. & Gutierrez, J. M. Unveiling the nature of black mamba (*Dendroaspis polylepis*) venom through venomics and antivenom immunoprofiling: Identification of key toxin targets for antivenom development. *J. Proteom.* **119**, 126–142 (2015).
26. Ainsworth, S. et al. The medical threat of mamba envenoming in sub-Saharan Africa revealed by genus-wide analysis of venom composition, toxicity and antivenomics profiling of available antivenoms. *J. Proteom.* **172**, 173–189 (2018).
27. Rodríguez-Rodríguez, E. R. et al. Broadening the neutralizing capacity of a family of antibody fragments against different toxins from Mexican scorpions. *Toxicon* **119**, 52–63 (2016).
28. Marks, J. D. et al. By–passing immunization: building high affinity human antibodies by chain shuffling. *Bio/Technol.* **10**, 779–783 (1992).
29. Alkondon, M. & Albuquerque, E. X. α-Cobratoxin blocks the nicotinic acetylcholine receptor in rat hippocampal neurons. *Eur. J. Pharmacol.* **191**, 505–506 (1990).
30. Wang, C.-I. A. et al. Isolation and structural and pharmacological characterization of α-elapitoxin-Dpp2d, an amidated three finger toxin from black mamba venom. *Biochemistry* **53**, 3758–3766 (2014).
31. Lauridsen, L. P., Laustsen, A. H., Lomonte, B. & Gutiérrez, J. M. Exploring the venom of the forest cobra snake: toxicovenomics and antivenom profiling of *Naja melanoleuca*. *J. Proteom.* **150**, 98–108 (2017).
32. Liu, Y. et al. High-throughput screening for developability during early-stage antibody discovery using self-interaction nanoparticle spectroscopy. *mAbs* **6**, 483–492 (2014).
33. Sintiprungrat, K. et al. A comparative study of venomics of *Naja naja* from India and Sri Lanka, clinical manifestations and antivenomics of an Indian polyspecific antivenom. *J. Proteom.* **132**, 131–143 (2016).
34. Lermyte, F., Tsybin, Y. O., O'Connor, P. B. & Loo, J. A. Top or middle? up or down? Toward a standard lexicon for protein top-down and allied mass spectrometry approaches. *J. Am. Soc. Mass Spectrom.* **30**, 1149–1157 (2019).
35. Mitchell Wells, J. & McLuckey, S. A. Collision-induced dissociation (CID) of peptides and proteins. *Methods in Enzymology* Vol. 402 148–185 (Academic Press, 2005).
36. Lingdong Quan, M. L. CID, ETD, and HCD fragmentation to study protein post-translational modifications. *Mod. Chem. Appl.* **1**, e103 (2013).
37. Krause, K. E. et al. An interactive database for the investigation of high-density peptide microarray guided interaction patterns and antivenom cross-reactivity. *PLoS Negl. Trop. Dis.* **14**, e0008366 (2020).
38. Tan, C. H., Tan, K. Y., Fung, S. Y. & Tan, N. H. Venom-gland transcriptome and venom proteome of the Malaysian king cobra (*Ophiophagus hannah*). *BMC Genom.* **16**, 687 (2015).
39. Bourne, Y., Talley, T. T., Hansen, S. B., Taylor, P. & Marchot, P. Crystal structure of a Cbtx–AChBP complex reveals essential interactions between snake α-neurotoxins and nicotinic receptors. *EMBO J.* **24**, 1512–1522 (2005).
40. Fruchart-Gaillard, C. et al. Experimentally based model of a complex between a snake toxin and the α7 nicotinic receptor. *Proc. Natl Acad. Sci. USA* **99**, 3216–3221 (2002).
41. Rusmili, M. R. A., Yee, T. T., Mustafa, M. R., Hodgson, W. C. & Othman, I. Proteomic characterization and comparison of Malaysian *Bungarus candidus*and *Bungarus fasciatus* venoms. *J. Proteom.* **110**, 129–144 (2014).
42. Malih, I. et al. Proteomic analysis of Moroccan cobra *Naja haje legionis*venom using tandem mass spectrometry. *J. Proteom.* **96**, 240–252 (2014).
43. Knudsen, C. et al. Novel snakebite therapeutics must be tested in appropriate rescue models to robustly assess their preclinical efficacy. *Toxins* **12**, 528 (2020).
44. Dyson, M. R. et al. Beyond affinity: selection of antibody variants with optimal biophysical properties and reduced immunogenicity from mammalian display libraries. *mAbs* **12**, 1829335 (2020).
45. Kristensen, P. & Winter, G. Proteolytic selection for protein folding using filamentous bacteriophages. *Fold. Des.* **3**, 321–328 (1998).
46. Wang, C. R., Bubner, E. R., Jovcevski, B., Mittal, P. & Pukala, T. L. Interrogating the higher order structures of snake venom proteins using an integrated mass spectrometric approach. *J. Proteom.* **216**, 103680 (2020).

47. Harrison, J. A. & Aquilina, J. A. Insights into the subunit arrangement and diversity of paradoxin and taipoxin. *Toxicon . J. Int. Soc. Toxinol.* **112**, 45–50 (2016).
48. Madeira, F. et al. The EMBL-EBI search and sequence analysis tools APIs in 2019. *Nucleic Acids Res.* **47**, W636–W641 (2019).
49. Waterhouse, A. M., Procter, J. B., Martin, D. M. A., Clamp, M. & Barton, G. J. Jalview Version 2—a multiple sequence alignment editor and analysis workbench. *Bioinformatics* **25**, 1189–1191 (2009).
50. Pettersen, E. F. et al. UCSF ChimeraX: structure visualization for researchers, educators, and developers. *Protein Sci. Publ. Protein Soc.* **30**, 70–82 (2021).
51. Xu, D. et al. In vitro characterization of five humanized OKT3 effector function variant antibodies. *Cell. Immunol.* **200**, 16–26 (2000).
52. Dall'Acqua, W. F. Increasing the affinity of a human IgG1 for the neonatal Fc receptor: biological consequences. *J. Immunol.* **169**, 5171–5180 (2002).
53. Grav, L. M. Minimizing clonal variation during mammalian cell line engineering for improved systems biology data generation. *ACS Synth. Biol.* **7**, 2148–2159 (2022).
54. Petras, D., Heiss, P., Süssmuth, R. D. & Calvete, J. J. Venom proteomics of Indonesian King Cobra, *Ophiophagus hannah*: integrating top-down and bottom-up approaches. *J. Proteome Res.* **14**, 2539–2556 (2015).
55. Finney, D. *Probits Analysis* (Cambridge University Press, 1971).

Acknowledgements

A.H.L. is supported by a grant from the European Research Council (ERC) under the European Union's Horizon 2020 research and innovation program [850974], by a grant from the Villum Foundation [00025302], and a grant from Wellcome [221702/Z/20/Z]. T.P.J. has received funding from the European Union's Horizon 2020 research and innovation program under the Marie Sklodowska-Curie grant agreement no. 713683 (COFUNDfellowsDTU). I.O. and J.A.H. are supported by the Swiss National Foundation, grants #202220_178765 and 200020_207354 and a R'EQUIP grant, which supported the purchase of the SELECT SERIES Cyclic IMS mass spectrometer with additional ECD and SID cells (grant #206021_198122). B.G.V. and S.S. are supported by a grant from the Novo Nordisk Foundation NNF20SA0066621.

Author contributions

J.M.C., B.L., J.M.G., A.H.L., and A.K.V. conceived and initiated the project; J.M.C., J.M.G., A.H.L., and A.K.V. supervised the project; L.L., J.W., T.P.J., K.B., I.O., J.A.H., P.V., R.A.L., S.S., B.L., J.M.G., A.H.L., and A.K.V. performed laboratory experiments and data analysis; J.W., T.P.J., K.B., I.O., J.A.H., R.Z., B.V., A.L., B.L., and A.K.V. contributed to the writing of the manuscript; L.L., J.M.G., and A.H.L. wrote the manuscript.

Competing interests

The Authors declare the following competing interests: L.L., J.M.C., B.L., J.M.G., A.H.L., and A.K.V., are inventors on a patent (EP 22170880.3), jointly owned by the Technical University of Denmark, IONTAS Ltd., and the University of Costa Rica, covering the use of the antibodies described in this article. The remaining authors declare no competing interests.

Additional information

Supplementary information The online version contains supplementary material available at https://doi.org/10.1038/s41467-023-36393-4.

Correspondence and requests for materials should be addressed to José M. Gutiérrez, Andreas H. Laustsen or Aneesh Karatt-Vellatt.

Peer review information *Nature Communications* thanks the anonymous reviewer(s) for their contribution to the peer review of this work.

5. Structural characterization of cross-reactive pH-dependent antibodies

This scientific manuscript delves into the mechanisms underlying cross-reactivity and pH-dependent binding of the antibodies developed in Chapter 4. Given the significant effect that light chain shuffling had on antibody cross-reactivity and neutralization, we wondered whether the optimized light chains for these antibodies could also introduce pH-dependent antigen binding. The pool of antibodies in Chapter 4 was first screened for pH-dependent binding properties to different long-chain α-neurotoxins using biolayer interferometry, which identified one antibody able to bind pH-dependently to all long-chain α-neurotoxins tested. To investigate the mechanism for the pH-dependent binding properties of this antibody, X-ray crystallography was chosen to determine whether pH-dependent binding was facilitated by the antibody paratope or epitope.

Determining the structure of the antibody bound to α-cobratoxin revealed the molecular basis for the cross-reactivity of this lineage of antibodies, by which the antibody mimics the receptor residues targeted by conserved residues in long-chain α-neurotoxins. However, the antibody paratope and epitope were shared with other antibodies that were non-pH-dependent, indicating that the pH-dependent binding mechanism for this antibody resided outside the paratope and epitope, and pre-empted further structural studies. Determining structures of the antibody bound at high resolution at different pH identified a network of residues located in the heavy-light chain interface region that responded to low pH, indicating that the chain interface environment was the stage for the broad pH-dependent binding behaviour for this antibody.

We conclude by describing a mechanism for the light chain-driven introduction of pH-dependent binding for this antibody. We have not yet been able to perform a proof of concept experiment to confirm this mechanism, and so the manuscript is in preparation and presented in the form of a draft.

Structure of a neurotoxin-neutralizing antibody reveals determinants for broad reactivity and a pH-responsive allosteric switch

Jack Wade[1], Nina Strancar[1], Charlotte Rimbault[1], Line Ledsgaard[1], Giang Thi Tuyet Nguyen[1], Anne Ljungars[1], Tulika[1], Markus-Frederik Bohn[1], Jens Preben Morth[1], Andreas H. Laustsen[1]*

[1]Department of Biotechnology and Biomedicine, Technical University of Denmark, DK-2800 Kongens Lyngby, Denmark
[2]Department of General, Inorganic and Theoretical Chemistry, and Center for Molecular

Corresponding author:
Andreas Hougaard Laustsen
ahola@bio.dtu.dk

Keywords: pH-dependent antibody binding; allostery, cross-reactivity, broadly-neutralizing antibody; snake toxins; antivenom; toxin-antibody complex; crystal structure

Abstract

Antibodies can recognize distinct epitopes and protein folds on pathogens, making them a valuable resource for therapeutic antibody discovery across different indications. One of the intrinsic functions of antibodies is to bind with high affinity to specific epitopes on pathogens through their variable domain, thereby neutralizing their targets. By introducing histidine mutations to the CDRs of antibodies, the antibody affinity can be engineered to be pH-dependent, resulting in the development of antibodies capable of neutralizing multiple antigens. This allows antibodies to release antigens during their recycling pathway to the lysosome degradation system, improving the pharmacology of the antibody by allowing for multiple antigen-binding cycles. However, the mechanisms behind how antibodies can accommodate pH-dependent antigen binding are not well understood and could inform antibody engineering and design. In this study, we analysed how cross-reactive antibodies against long-chain α-neurotoxins can accommodate both antibody function and pH-dependent binding properties. We show that specificity was primarily determined by the paratope which interacted with the neurotoxin in a manner that mimicked the acetylcholine receptor- neurotoxin interface. This led to broad reactivity against multiple-antigens via binding trough the CDRH3 loop of the antiboody. In contrast, determinants of pH-dependent binding are located away from the toxin interface. The pH-dependent antibodies are functional, and can neutralize long-chain alpha-neurotoxin *in vivo*. Notably, the fold difference in pH-dependent binding allows for the release of long-chain α-neurotoxins within the duration of the antibody recycling pathway.

Introduction

Monoclonal antibodies are typically characterized by their specific binding to a target antigen. However, in many cases, cross-reactivity can be an important feature of therapeutic monoclonal antibodies. For example, defined cross-reactivity between shared antigens from different species can facilitate the evaluation of antibody safety and efficacy as therapeutic candidates in relevant animal models[1]. Another example is in the treatment of rapidly evolving pathogens, where cross-reactive antibodies are crucial for enforcing therapeutic robustness[2]. Cross-reactive antibodies are also required for the treatment of snakebite envenoming, where the use of antibodies that neutralize homologous toxins found across different snake species may be sufficient to allow broad-spectrum usage[3]. Traditionally, polyvalent antivenoms derived from immunized animals are used for treatment. Although these antivenoms have saved many lives, their usage can lead to severe immunogenicity-related side effects, and they have a low content of neutralizing antibodies with high production costs. Therefore, the discovery of human antibodies of known sequence to enable recombinant production has gained increased focus.[4–7]

One toxin class that has been identified as paramount to developing broadly neutralizing antibodies is the long-chain α-neurotoxins. Long-chain α-neurotoxins contribute to the neurotoxicity of snake venoms by targeting the cholinergic system, specifically by inhibiting two types of nicotinic acetylcholine receptors (nAChR), the muscle and the neuronal α7 homopentameric nAChR.[8] Two long-chain α-neurotoxins, α-Bungaratoxin (α-bgtx) from the banded krait *B. multicinctus* and α-Cobratoxin (α-cbtx), from the *N. siamensis* cobra, have been the subject of extensive studies and have been used to define the molecular mechanism by which long-chain α-neurotoxins exert their inhibitory effects on the nervous system.[9–11] Structural characterization of these long-chain α-neurotoxins bound to different AChR homologs by crystallography and cryo-EM has revealed the molecular determinants of their interaction with the nAChR, and how the structure of long-chain α-neurotoxins relates to their function.[9,9,10]As part of the three-finger protein family, long-chain α-neurotoxins are small, 8 kDa proteins that have three fingers stabilized by 4 intramolecular disulfide bridges. Their structure is ridged and has a high level of structural complementarity to the nAChR, causing them to bind with an exceptionally high affinity (sub nM KD values) and inhibit the nAChR with high potency. All three fingers are implicated in the interaction with the nAChR, but central to their nAChR receptor inhibition is the finger II, which protrudes into the acetylcholine ligand binding pocket situated at the α-γ and α-δ nAChR receptor subunit interfaces. Highly conserved arginine residues located at the apex of finger II insert the acetylcholine binding pocket, forming cation-π interactions with the aromatic residues in the nAChR interface responsible for coordinating acetylcholine, therefore inhibiting acetylcholine binding and nAChR signalling.

The finger II region of long-chain α-neurotoxins has been identified as a potential epitope for cross-reactive, neutralizing antibodies in polyvalent antivenom by searching for linear antibody epitopes using high-density peptide microarrays.[12] Even with sufficient affinity and cross-reactivity, however, one antibody molecule can conventionally only neutralize one antigen molecule, presenting a limitation to how low an antibody can be dosed. Therefore, in addition to cross-reactivity, monoclonal antibodies have been engineered to possess the ability to be reused and neutralize multiple antigens. This has been achieved by engineering the antibodies' antigen binding affinity to be pH-dependent, allowing the antibody, but not the antigen, to be recycled through the neonatal Fc receptor (FcRn)[10]. Once an antibody is internalized into a cell, either by pinocytosis or mediated by Fc receptors,[11] it enters into acidified endosomes where it binds to the neonatal Fc receptor (FcRn) in a pH-dependent manner. Binding to FcRn rescues the antibody

from lysosomal degradation and subsequently releases it back into circulation.[10] By carefully fine-tuning the antibody affinity to have weaker antigen binding at acidic pH, the antibody will release its cargo in the endosome, sending the antigen to the lysosome for degradation, whilst the antibody itself is recycled back into circulation, ready to target more antigens. The engineering of pH-sensitive binding in the antibody variable domains is typically achieved by either introducing histidine mutations sequentially into CDR loops (histidine walking) or combinatorial histidine-scanning approaches using *in vitro* display technologies.[10,12–14] Understanding how antibody binding can be affected by changes in pH could expand the possibilities for engineering pH-dependent antibodies, in particular for pH-determinants located outside the epitope, which may be beneficial in cases where the number of epitope residues is restricted, such as conserved epitopes bound by cross-reactive antibodies; or when pH-dependent interactions are not able to be accommodated in the antibody paratope without a significant loss of antibody function.

We have recently shown that cross-reactive human antibodies, discovered using phage display, were able to neutralize diverse long-chain α-neurotoxins *in vitro*.[6] These antibodies were discovered using phage display from a naïve antibody phage display library against a long-chain α-neurotoxin from the monocled cobra (*Naja kaouthia*).[7] By using an affinity maturation technique known as light chain shuffling, and cross-panning between *N. kaouthia* and *D. polylepis* long-chain α-neurotoxins during phage display selections, we succeeded in expanding the neutralization capacity of antibodies *in vitro*. One light chain shuffled antibody, 2554_01_D11, demonstrated broad neutralization of long-chain α-neurotoxins *in vivo*, prolonging the survival of mice challenged with whole venom from *N. kaouthia*, *O. hannah*, and *D. polylepis* elapids.[6] However, we did not define the molecular basis for cross-reactivity, as well as explore any pH-dependent antigen binding. In this study, we investigated the molecular basis for antibody neutralization and the relationship between the antibody paratope, epitope, and paratope independent factors on pH-dependent antigen binding in a panel of light chain shuffled cross-reactive antibodies specific to long-chain α-neurotoxins. Structural studies revealed that cross-reactivity was achieved by exploiting a conserved functional constraint in long-chain α-neurotoxins required for their inhibition of the nAChR, determined by the antibody heavy chain paratope. In addition to being cross-reactive, one light chain shuffled antibody, 2555_01_A01, was able to bind pH-dependently to all long-chain α-neurotoxins tested. Structural characterization of 2555_01_A01 bound to α-cbtx at different pH suggest that broad pH-dependent binding was conferred away from the paratope-epitope interface, in the light-heavy chain interface.

Results

Profiling cross-reactivity and pH-dependent binding for light chain shuffled antibodies

To determine whether cross-reactivity and pH-sensitivity could be coupled, a panel of antibodies were screened for pH-sensitive binding to three long-chain α -neurotoxins: *N. kaouthia* (α-cbtx), *D. polylepis* (α-eptx) and *B. multicinctus* (α-bgtx) using biolayer interferometry (BLI). The parent antibody was discovered from a naïve antibody phage display library against α-cbtx, and had been affinity matured by light chain shuffling using α-cbtx and α-eptx antigens to improve cross-reactivity.[1] In total, 7 affinity matured, light chain shuffled clones were chosen for further characterization based on their binding signals to α-cbtx and α-eptx (Table. S2) and their light chain CDR sequence diversity. Clones were grouped into two light chain germlines, IGVL3-23: 2558_02_G09, 2555_01_A01, 2555_01_A04, 2551_01_B11 and IGLV6-57: 2554_01_D11, 2554_01_E01, 2551_01_A12 and the parent antibody. Clones from the same germline had similar CDR sequences, and all clones had the same CDRL3 and CDRL2 loop length. The LCDR1 loop varied most both in terms of length and sequence diversity between the germlines (Fig. 1A).

The affinities of antibodies to α-cbtx and α-eptx were in agreement with the previously reported SPR values. Values ranged between 33.8 - 2.9 nM for α-cbtx, and clones displayed slightly higher affinities to a-eptx ranging from 0.89 – 0.44 nM (Table. S1&2). To assess whether light chain shuffling yielded improvements in cross-reactivity, α-bgtx was included due to not being used in the discovery process and having a low sequence identity to α-cbtx (58%). All clones bound with substantially lower affinity to α-bgtx, with KD values ranging from 3μM – 122 nM (Fig. 1C, Table. S3&S4). The effect of the light chain on cross-reactivity was most pronounced for the light chain shuffled clones from the IGLV6-57 germline, which exhibited an order of magnitude higher binding affinity to α-bgtx in comparison to both the parent antibody and clones from the IGVL3-23 germline (Fig. 1B). This suggests that affinity-matured clones bearing light chains from the IGLV6-57 germline had improved interactions with conserved regions of long-chain α-neurotoxins, possibly to the conserved finger II region, which is central in their inhibition of the nAChR.

Antibodies classified as being pH-dependent typically have a minimum of 4-fold difference in affinity or dissociation rate between pH 7.4 and pH < 6.0.[13,14] Based on this, one antibody originating from the IGVL3-23 germline, 2555_01_A01, exhibited pH-dependent binding against all three long-chain α-neurotoxins (Fig. 1C-E). 2555_01_A01 was most pH-sensitive to α-cbtx, having an average of 19-fold difference in dissociation rate between pH 7.4 and pH 5.5, followed by α-bgtx (11.7-fold) and α-eptx (7.90). By contrast, the parent antibody and the remaining affinity matured clones were only moderately pH-sensitive to each of the long-chain alpha neurotoxins, ranging in pH-sensitivity from 1.82 – 4.94 fold. The least pH-dependent antibodies originated from the IGVL6-57 germline, but were also the more cross-reactive, highlighted most clearly for the broadly neutralizing 2554_01_D11 antibody which had a pH-dependent binding fold-difference of 1.82 - 3.35 between pH 5.5 and pH 7.4, but had the highest affinity to α-bgtx. To verify that the most pH-sensitive antibody, 2555_01_A01, was able to neutralize long-chain α-neurotoxins, a pre-incubation *in vivo* experiment was conducted with 2555_01_A01 and α-cbtx. 2555_01_A01 provided protection to α-cbtx up to the traditional 24 hour observation window (Fig. 1F), however, mice were observed dead at 48 hours. To investigate the basis for the broad cross-reactivity of this lineage of antibodies, and the role of the light chain in facilitating pH-dependent binding, the 2555_01_A01 was chosen for structural characterization by X-ray crystallography.

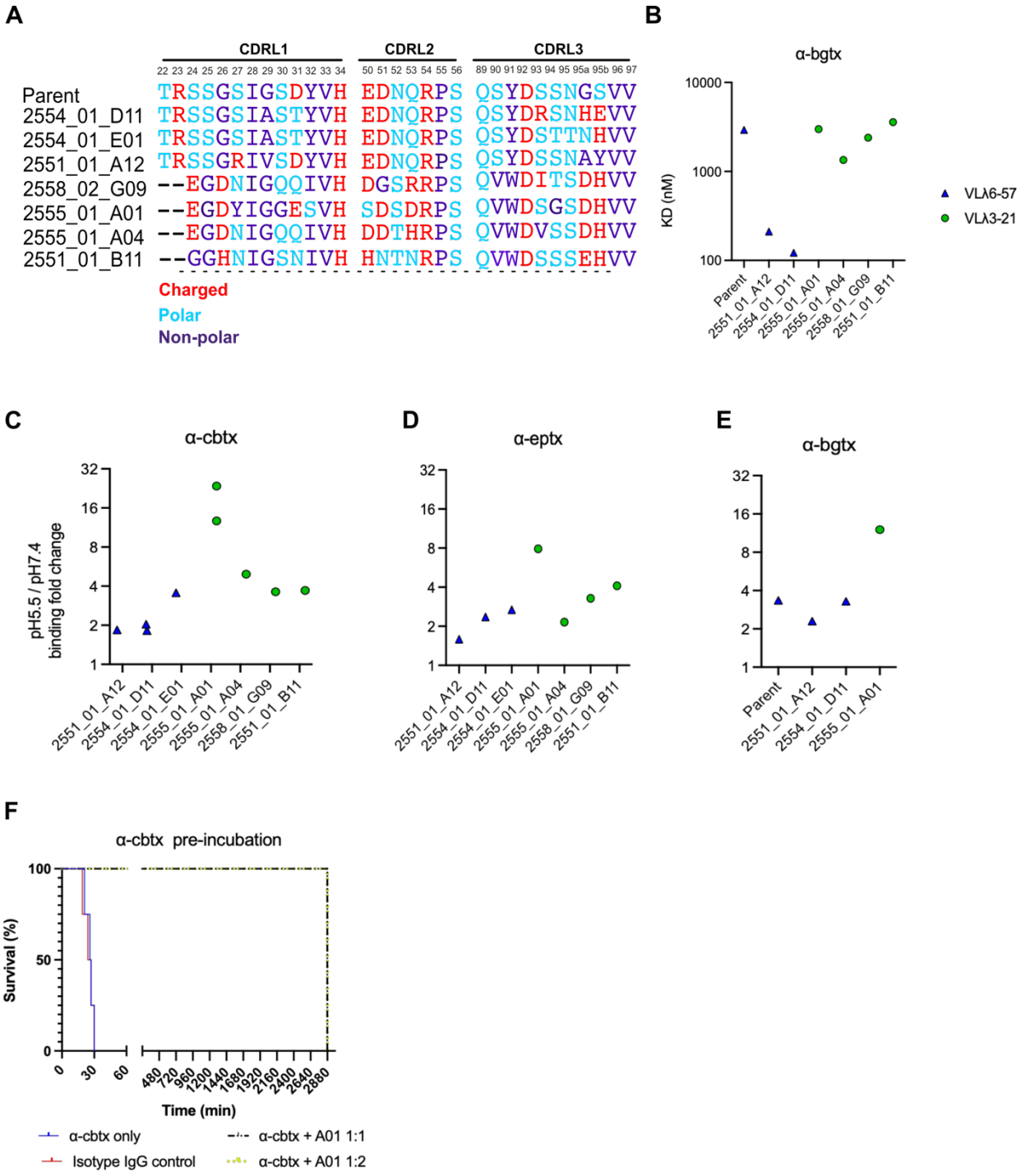

Figure 1 Binding characterization and *in vivo* neutralization of long-chain α-neurotoxins.
(A) Light chain complementary determining region loop sequences for the antibodies used in the study, numbered according to the Kabat scheme. The properties of amino acid residues are coloured and described beneath the sequences. (B) Affinity of anti-long chain neurotoxin clones to α-bgtx at pH 7.4, data points are coloured according to the antibody light chain germline. (C-E) pH-sensitive binding fold differences of anti-long chain neurotoxin clones to α-cbtx, α-eptx and α-bgtx. The fold difference for the IGVLλ and parent clones binding to to α-bgtx was measured as a product of their affinity difference under steady-state conditions at pH 5.5 and pH 7.4, all other fold differences were measured as the change

in dissociate rate between pH 5.5 and 7.4. (F) Kaplan-Meier survival curves for the 2555_01_A01 antibody pre-incubated with α-cbtx.

Overall structure

To first understand the structural basis for the broad recognition of long chain α-neurotoxins by 2555_01_A01 and related clones, we determined the crystal structure of the 2555_01_A01 antibody in scFv format bound to α-cbtx at 1.6 Å resolution (Fig. 2A, Table 1). Two scFv molecules and two α-cbtx molecules were present in the asymmetric unit and exhibited $P2_12_12_1$ space group symmetry. Each α-cbtx molecule was bound by two scFv molecules, forming an interface with the heavy chain from one scFv and the light chain from the other in a 1:2 (α-cbtx:scFv) stoichiometry. We observed a clear preference for a 1:1 stoichiometry during the preparation of the complex by gel filtration (Fig. 2B), indicating that one of these interfaces was a crystallographic-driven interface. To assess whether either the heavy chain or light chain interfaces were crystallographic-driven interfaces, the Complexation Significance Scores (CSS) for the heavy chain and light chain- α-cbtx interfaces were compared in PISA. The light chain α-cbtx CSS score was 0, which meant that this interface was not significant in forming the complex, and 0.41 for the heavy chain interface. Accordingly, the α-cbtx molecule forming an interface with the heavy chain was treated as the principal molecule involved in the interaction for that scFv, and was chosen to characterize the interaction.

We were able to observe paratope-epitope interactions between the 2555_01_A01 scFv and α-cbtx at high resolution, which revealed the recognition of a highly conserved epitope by the antibody CDRH3 loop. At 24 residues long, the CDRH3 was stabilized by an intramolecular disulfide bridge and extended between finger I and II of α-cbtx, recognizing a conformational epitope in the three-finger neurotoxin fold. The complex revealed a tight interface, resulting in a total buried surface area of 952.4 $Å^2$, 864 $Å^2$ contributed by the CDRH3, and 87.8 $Å^2$ by the CDRL3 loop.

Table 1: Data collection and refinement statistics for 2555_01_A01 bound to α-cbtx

	pH 6.0	pH 5.5	pH 4.5
Wavelength (Å)	0.95	0.95	0.98
Resolution range (Å)	60.57 - 1.90 (1.96 - 1.9)	41.58 - 1.60 (1.66 - 1.6)	42.52 - 1.55 (1.61 - 1.55)
Space group	P 21 21 21	P 21 21 21	P 21 21 21
Unit cell (Å) (°)	76.95 82.65 98.19 90 90 90	76.87 83.15 98.34 90 90 90	76.86 83.86 98.65 90 90 90
Total reflections	99496 (9810)	419481 (28766)	486522 (47473)
Unique reflections	49774 (4905)	83281 (8097)	92830 (9113)
Multiplicity	2.0 (2.0)	5.0 (3.6)	5.2 (5.2)
Completeness (%)	99.25 (99.15)	99.36 (98.42)	99.65 (98.86)
Mean I/sigma(I)	12.62 (2.75)	10.90 (1.38)	10.86 (1.20)
R-work	0.19 (0.30)	0.18 (0.38)	0.20 (0.42)
R-free	0.25 (0.36)	0.23 (0.40)	0.22 (0.45)
ligands	64	131	65
solvent	502	554	519
Protein residues	634	634	634

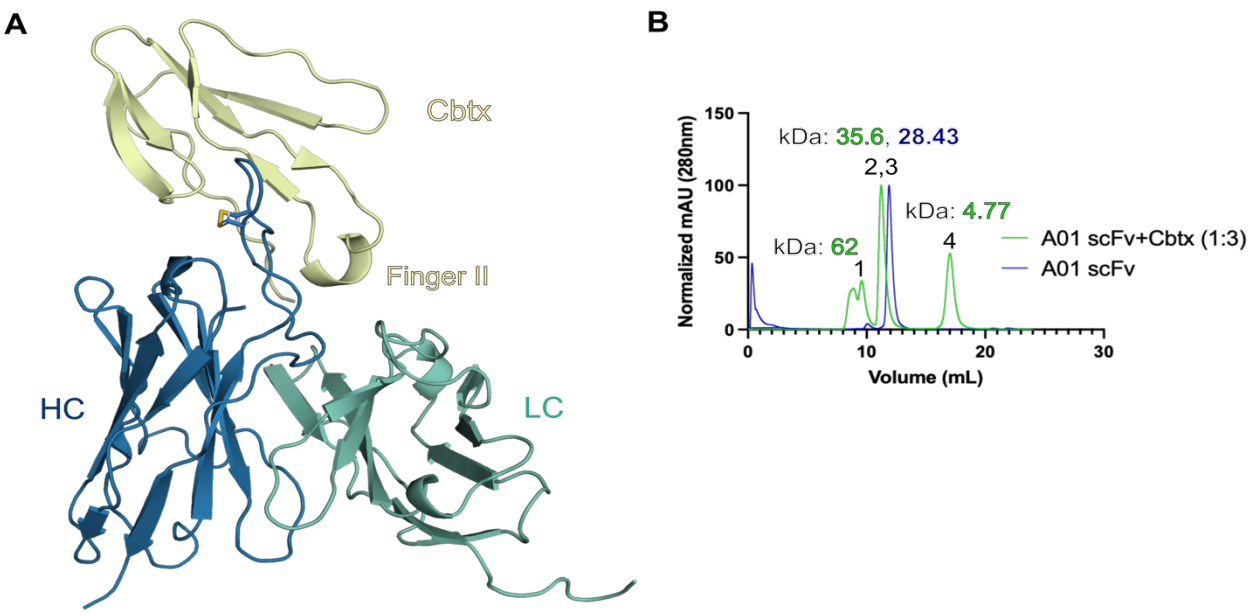

Figure 2. 2555_01_A01 antibody bound to α-cobratoxin . (A) 2555_01_A01 scFv bound to α-cbtx. The antibody heavy chain (blue) recognizes the Finger II of α-cbtx (pale yellow) through the CDRH3, conformationally stabilized by an intramolecular disulfide bridge (yellow). The antibody light chain is colored in green. (B) SEC chromatogram overlay of 2555_01_A01 unbound and in complex with α-cbtx.

Heavy chain CDR3 contains determinants for cross-reactivity.

Long chain α-neurotoxins induce paralysis by inhibiting nicotinic acetylcholine receptor (nAChR)-acetylcholine interaction. A loop in the nAChR, loop C, is a key responsive element required for neurotransmitter binding and is targeted by R33 and R36 residues on the tip of finger II on long chain α-neurotoxins. Both arginine residues engage aromatic residues on loop C, which coordinate with the acetylcholine molecule. A structural alignment of the Torpedo AChR[15] and bound 2555_01_A01 structures revealed that aromatic $Y190_{nAChR}$ and $Y198_{nAChR}$ residues on loop C were superimposable with $Y99_{HC}$ and $Y100e_{HC}$ on the CDRH3 of 2555_01_A01, engaging $R33_{cbtx}$ and $R36_{cbtx}$ on α-cbtx (Fig. 3A). The CDRH3 loop registers 11 hydrogen bonds and a salt bridge to $R33_{cbtx}$, $R36_{cbtx}$, and $D26_{cbtx}$ residues, in addition to forming numerous hydrophobic interactions and hydrogen bonds to the backbone of α-cbtx (Fig. 3B). The hydroxyl group of $Y100e_{HC}$ on CDHR3 forms a hydrogen bond to $D26_{cbtx}$ and is oriented between $R36_{cbtx}$ and $R33_{cbtx}$ residues, forming cation-π interactions to both $R33_{cbtx}$ and $R36_{cbtx}$. The guanidinium group of $R33_{cbtx}$ is engaged in further cation-π interactions with $Y99_{HC}$, and a salt-bridge to $D95_{HC}$ on CDRH3, forming the core of the interaction. The interaction with $R36_{cbtx}$ is supported by 2 hydrogen bonds from $S100c_{HC}$ residue on CDRH3. As R36 is a valine in α-bgtx, the reduced capacity of α-bgtx to form hydrogen bonds and cation-π interactions with $Y100e_{HC}$ and $S100c_{HC}$ may explain the lower affinity of all antibodies to α-bgtx.

Facing the C-terminal side of α-cbtx (Fig. 3C) reveals the contribution of the light chain to the interaction. $D95a_{LC}$ on CDRL3 forms a salt bridge to $R70_{cbtx}$ and a hydrogen bond with $Y100f_{HC}$, buttressing the cation-π interaction between $Y100f_{HC}$ and $R70_{cbtx}$. Position $95a_{LC}$ on CDRL3 was variant in all the affinity matured light chains and may explain the increase in affinity of 2555_01_A01 and related antibodies to α-cbtx compared to the parent antibody,

which has glycine at this position. Overall, the CDRH3 loop in 2555_01_A01 and related clones engages long-chain α-neurotoxins through receptor mimicry to achieve cross-reactivity, and as a result, neutralize long-chain α-neurotoxins by inhibiting key residues important for their inhibition of nAChRs. Although these results rationalise the cross-reactivity of 2555_01_A01 and related clones through the CDRH3 interaction, it does not explain the broad pH-dependent binding of 2555_01_A01, as the paratope of 2555_01_A01 is shared with clones that bind pH-independently. Therefore, the pH sensitivity of 2555_01_A01 must lie outside the paratope-epitope interface.

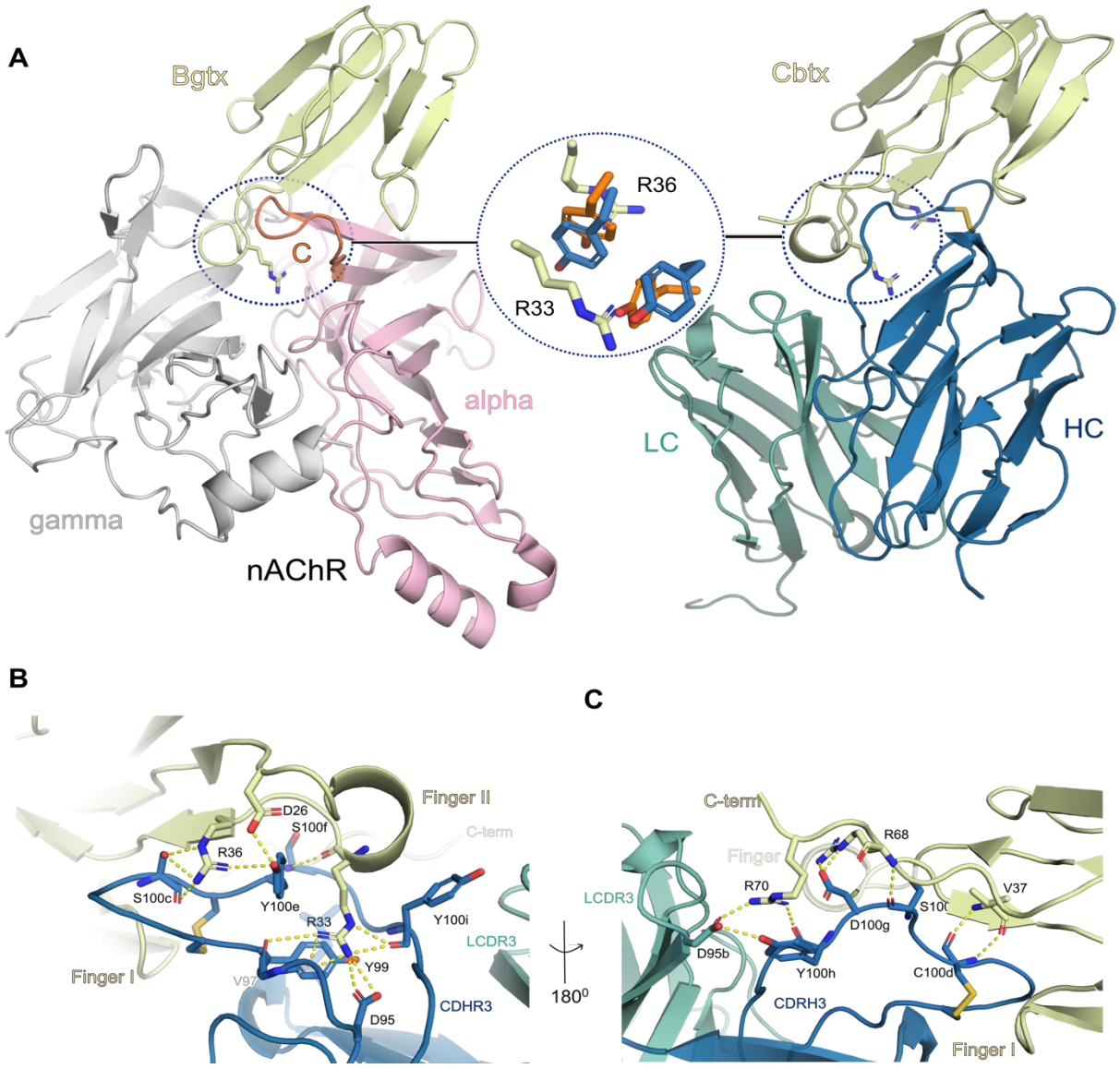

Figure 3. Neutralization of α-cobratoxin by 2555_01_A01 antibody. (A) From left to right: Structure of the *Torpedo* nAChR bound to α-bgtx (6uwz). Finger II of α-bgtx (pale yellow) is bound at the interface between the beta (grey) and alpha (pink) domains of nAChR, R33 on finger II is shown in stick format. The key response element loop C (orange) is depicted on the alpha domain of the nAChR. An overlay of tyrosine residues on loop C and CDRH3 (blue) coordinating to R33 and R36 on long-chain α-neurotoxins, illustrating mimicry of interactions between nAChR and 2555_01_A01. Right: 2555_01_A01 bound to α-cbtx. (B) Core interactions between the CDRH3 and Finger II of α-cbtx, targeting conserved residues in long-chain α-neurotoxins (R33, R36, D26). (C) Opposing view of interactions to the backbone and C-Terminal of α-cbtx by CDRH3 and CDRL3 loops.

Broad pH-sensitivity determinants located at the light chain interface

As the light chain was the variable component between each antibody, we investigated the role of the light chain in the observed pH-dependent binding of 2555_01_A01. A crystallography optimization screen enabled us to generate crystals and determine structures of 2555_01_A01 bound to α-cbtx at different pH levels (Table 1). The space group and asymmetric unit were the same across all three structures, with no apparent differences in crystal packing, allowing us to identify potential determinants for pH-dependent binding. We initially focused on charged residues in the 2555_01_A01 light chain and identified two charged residues, $G95a_{LC}D$ and $S95b_{LC}H$, that had been introduced into the CDRL3 loop following light chain shuffling. Analyzing their role in binding, we observed that $H95b_{LC}$ forms a hydrogen bond to $S95_{LC}$, located near the apex of the β-hairpin loop in CDRL3, which positions $D95a_{LC}$ to interact with $R70_{cbtx}$ on α-cbtx (Fig. 4A). Comparing the conformation of $H95b_{LC}$ in structures determined at pH 6.0 and pH 4.5 showed that $H95b_{LC}$ was pH-responsive, exhibiting a change in rotamer position and hydrogen bond network at pH 4.5 (Fig. 4B). At pH 4.5 the $H95b_{LC}$ indole ring hydrogen bond was also remodelled, switching from the $S95_{LC}$ main chain to the $D95a_{LC}$ main chain, destabilizing the interaction between $D95a_{LC}$ and $R70_{cbtx}$, lowering the affinity to α-cbtx. The effect of $H95b_{LC}$ and $D95a_{LC}$ (which may also be protonated) on the interaction to α-cbtx was tested by the double mutation, $D95a_{LC}H$ and $H95b_{LC}E$ (2555_01_A01-HE), as these were the residues observed in the equivalent positions of the non-pH-dependent 2554_01_D11 antibody. This resulted in a 2-3 fold reduction in pH-dependent binding to α-cbtx (Fig. 4C) and explained the elevated level of pH-dependent binding that 2555_01_A01 has to α-cbtx in comparison to α-bgtx and α-eptx long-chain α -neurotoxins. The α-bgtx and α-eptx long-chain α-neurotoxins feature a P70 as opposed to an R70 seen in α-cbtx, and would not be able to form a salt bridge with $D95a_{LC}$ to lower the affinity of the 2555_01_A01 antibody to these long-chain α-neurotoxins through the CDRL3 loop. However, this did not fully account for the pH-dependent binding of 2555_01_A01, as 2555_01_A01-HE was still 10-fold more pH-sensitive than the non-pH-dependent 2554_01_D11 antibody (Fig. 4C). 2555_01_A01 was also more pH-sensitive than antibodies that had both the $D95A_{LC}$ and $H95b_{LC}$ residues (Fig. 1A). Therefore, $H95b_{LC}$ and $D95a_{LC}$ residues alone do not explain the broad pH-dependent binding behavior of 2555_01_A01.

The 2555_01_A01 antibody contains another histidine residue, $H34_{LC}$, which is located in the CDRL1 loop and conserved between all antibodies (Fig. 1A). We speculated that despite being conserved, the surrounding amino acid residue environment of this histidine may be unique to 2555_01_A01 and contribute to its broad pH-dependent binding. To investigate this, we compared the structures of 2555_01_A01 bound to α-cbtx at pH 5.5 and pH 4.5, which were nearly identical in resolution limits and statistics, to identify any differences in the environment of $H34_{LC}$. Analysis of the structure of 2555_01_A01 bound to α-cbtx at pH 5.5 revealed that $H34_{LC}$ is solvent-exposed and forms side chain-mediated hydrogen bonds to a water molecule and the main chain of $S50_{LC}$ on CDRL2. $H34_{LC}$ is located at the interface between the heavy chain and light chain, packed beneath $Y100l_{HC}$ in CDRH3, where it forms π-π interactions (Fig. 4D). At pH 5.5, $Y100l_{HC}$ occupies a pocket at the interface above $H34_{LC}$, with the phenol ring of $Y100l_{HC}$ positioned towards the LCDR2 loop and the $Y100l_{HC}$ main chain towards the CDRH3 loop. The $Y100l_{HC}$ main chain forms a hydrogen bond with the side chain carboxyl group of $D95_{HC}$ in CDRH3, stabilizing the interaction between $D95_{HC}$ and $R33_{cbtx}$ on α-cbtx (Fig. 4D). At pH 4.5, the $Y100^{L}{}_{HC}$ side chain forms a new hydrogen bond to $S50_{LC}$, and $S50_{LC}$ forms weaker intramolecular and intermolecular hydrogen bonds to itself and $H34_{LC}$ to accommodate the new hydrogen bond to $Y100l_{HC,}$ (Fig. 4E). The error associated with these hydrogen bonds was checked in the web server

(http://cluster.physics.iisc.ernet.in/dpi/), which confirmed the hydrogen bond differences between pH 5.5 and pH 4.5 were greater than the associated error, and the lengths had changed between the two pH. Next, we compared differences in electron density in these residues by subtracting the X-ray crystal diffraction patterns between the pH 5.5 and pH 4.5 data sets, which is more sensitive to detecting changes in the co-ordinate position of atoms than when using the refined models and removes model bias. This revealed positive electron density above the plane of the phenol ring of $Y100l_{HC}$, meaning that the phenol ring had moved downwards towards $H34_{LC}$ at pH 4.5 due to a more favourable cation-π interaction with the positively charged $H34_{LC}$ (Fig. 4F). Positive electron density was also observed along the main chain of $Y100l_{HC}$ and above the side chain carboxyl group of $D95_{HC}$, indicating that the change in position of $Y100l_{HC}$ had translated through to the interaction between $D95_{HC}$ and $R33_{cbtx}$. The electron density of S50 had also changed, as expected due to the change in the hydrogen bond network already observed for this residue. Other electron density map differences were mainly observed in cysteine bridges, possibly due to radiation damage during data collection. Collectively, these findings indicate that S50, $Y100l_{HC}$ and $D95_{HC}$ all responded to the change in pH between pH 5.5 and pH 4.5, possibly as a consequence of H34 protonation. This may affect the interaction between $D95_{HC}$ and $R33_{cbtx}$ by shifting the $Y100l_{HC}$ residue position and weakening the hydrogen bond $Y100l_{HC}$ makes with $D95_{HC}$, destabilizing the interaction between $D95_{HC}$ and $R33_{cbtx}$. Because $R33_{cbtx}$ is highly conserved, this explains why pH-dependent binding is observed to all long-chain α-neurotoxins. Notably, although all the non-pH-dependent antibodies have $D95_{HC}$, $Y100l_{HC}$ and $H34_{LC}$ residues, they differ at position $S50_{LC}$, containing either a D, E or H (Fig. 1A) residue at this site. $S50_{LC}$ does not form a hydrogen bond to $Y100l_{HC}$ at pH 5.5 (or pH 6.0, data not shown), but does form a new hydrogen bond to $Y100l_{HC}$ at pH 4.5. This may indicate a more flexible interface between $Y100l_{HC}$ and $S50_{LC}$. In contrast, the D, E and H residues have hydrogen bonding capability and have a longer side chain than $S50_{LC}$, which may stabilize $Y100^{L}{}_{HC}$ at the chain interface by forming a stable hydrogen bond to $Y100l_{HC}$ at both neutral and acidic pH, thus preventing any effects of $H34_{LC}$ protonation. Hence, we describe a model where the hydrogen bonding network around $H34_{LC}$, as opposed to the protonation of $H34_{LC}$ itself, allows $H34_{LC}$ to affect binding by modulating the position of residues on the CDRH3 important for the interactions with conserved residues on long-chain α-neurotoxins.

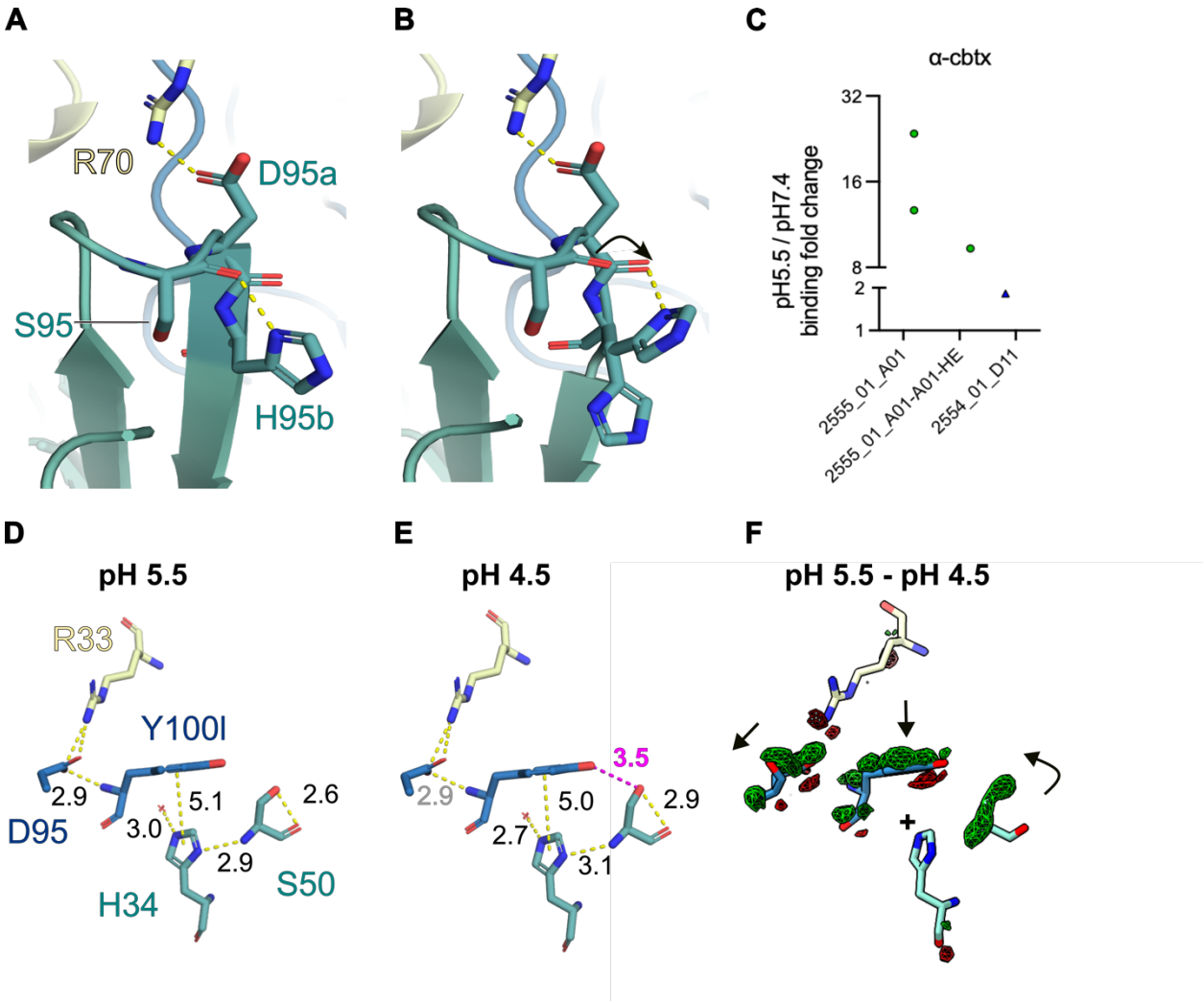

Figure 4. Light chain effects on pH-sensitive binding for 2555_01_A01 antibody. (A) Rear view of the CDRL3 (green) interface with α-cbtx (pale yellow) at pH 6.0. Hydrogen bonds shown in yellow. (B) Remodeled H95b hydrogen bond following rotamer change at pH 4.5 indicated by the black arrow. (C) Effect of D95a and H95b on pH-dependent binding by a double mutation into a non-pH dependent HE motif seen in the non-pH-dependent 2554_01_D11 antibody. (D) Proposed residue network involved in pH-dependent binding for 2555_01_A01 as seen in the pH 4.5 model. (E) *Fo-Fo* subtraction of proposed residues using refined pH 5.5 and pH 4.5 data sets. The pH 4.5 model is shown and highlights the electron density above the phenyl ring at pH 5.5. Heavy chain and associated residues are shown in blue, light chain green and α-cbtx pale yellow, respectively. Fourier maps contoured at 3 σ.

Discussion

Here, we report on the neutralization mechanism of a lineage of cross-reactive, light chain-shuffled human monoclonal antibodies discovered through phage display technology, targeting long-chain α-neurotoxins. We also provide insights into the pH-dependent binding mechanism of one neutralizing antibody, 2555_01_A01, which displayed both pH-dependent binding and cross-reactivity, thus showcasing that these two therapeutically relevant properties are not mutually exclusive.

By determining the bound structure of 2555_01_A01 to α-cbtx, we found that the antibody utilized conserved functional constraints in long-chain α-neurotoxins that are required for their inhibition of the nAChR, by mimicking the conserved interactions that long-chain α-neurotoxins make with the nAChR through receptor mimicry. This mechanism of neutralization may be useful in optimizing this and other antibodies for improved cross-reactivity, *e.g.*, through structure-guided engineering to present residues in the antibody paratope to further mimic the nAChR and form interactions with other conserved residues on long-chain α-neurotoxins important for function.

When testing the *in vivo* neutralization capacity of 2555_01_A01 against α-cbtx using a pre-incubation model, whereby mice were injected with antibody pre-incubated with α-cbtx, 2555_01_A01 was able to prevent lethality in mice during the traditional 24-hour assay period. However, 2555_01_A01 was unable to provide complete protection, as mice were observed to be dead at 48 hours. These findings are surprising, as we previously demonstrated that a related antibody, 2554_01_D11, which shares the same heavy chain, biophysical properties, and neutralizing epitope as 2555_01_A01, was able to confer full protection[6]. We also previously observed this delayed lethality in mice that were challenged with a preincubated mixture of α-cbtx and a recombinant monospecific anti-α-cbtx IgG, 2552_02_B02[7]. We attributed the delayed lethality observed for the 2552_02_B02 antibody to its sub-optimal biophysical properties, as 2552_02_B02 binds with higher affinity than 2554_01_D11 and competes with the same neutralizing epitope, and we would therefore expect to have a similar level of functionality. In addition to developability aspects, we here propose another parameter that might influence the ability of these antibodies to neutralize long-chain α-neurotoxins, namely the dissociation rate of the antibody as opposed to the overall affinity. This hypothesis is supported by a comparison of the dissociation rates of the three antibodies to α-cbtx. In contrast to the slow dissociation rate of 2554_01_D11 (2.18×10^{-4}/s) from α-cbtx, both the 2555_01_A01 and 2552_02_B02 antibodies have faster dissociation rates of 4.86×10^{-4}/s, 6.26×10^{-4}/s (2555_01_A01, duplicate measurements) and 5.5×10^{-4}/s (2552_02_B02, single measurement), respectively. These faster dissociation rates may allow α-cbtx to be released from the α-cbtx-antibody complex over time and accumulate in the neuromuscular junction, even when the affinity is higher as determined for 2552_02_B02. It is conceivable that once α-cbtx accumulates in the neuromuscular junctions, it will bind strongly to nAChRs, from which it does not dissociate, causing complete neuromuscular blockage, leading to the observed delayed lethality. These observations and this hypothesis highlight the relevance of extending the observation period of monoclonal IgGs during *in vivo* assessment to discriminate between antibody candidates.

In relation to the origin of the pH-dependent antigen binding properties observed for 2555_01_A01, we found that the light chain is responsible for equipping the antibody with these properties, independently of the antibody paratope. Fully elucidating the basis of the paratope-independent, pH-dependent antigen binding mechanisms would be useful for engineering purposes, which currently rely heavily on the single use of histidine residues[16,17]. Moreover, in antibodies, many more amino acid residues are present outside the paratope (*i.e.*, in the framework

region and any CDRs not interacting with the antigen), and these constitute a larger sequence space for engineering pH-dependent binding properties than that of the paratope. Engineering pH-dependent antigen binding properties outside the antibody paratope may thus be advantageous for some antibody-antigen interfaces, where engineering the paratope might be detrimental to the specificity and function of the antibody.

In this work, we discovered that a paratope-independent mechanism was robust in facilitating pH-dependent binding to a range of long-chain α-neurotoxins, consistently delivering nearly an order of magnitude difference in affinity between pH of pH 5.5 and pH 7.4. We propose that the chain interface environment is the stage for this paratope-independent, pH-dependent binding mechanism for the 2555_01_A01 antibody, specifically conferred by the histidine residue in the CDRL1 loop of the antibody. In a similar setting, Kolmar et al. also identified histidine residues in the CDRL1 and CDRL3 loops that were important in conferring paratope-independent, pH-dependent antigen binding properties to the carcinoembryonic antigen-related cell adhesion 5 molecule[18]. The light chain in their approach was chosen because it was precluded from the binding interaction to enable pairing with two different heavy chains in a bispecific antibody format, without affecting their binding, called "common light chain technology." The identified histidine mutations that conferred pH-dependent antigen binding properties by the common light chain accumulated in the anchoring position of the CDR1 and CDR3 loops, in comparable sites to the histidine residues located in the 2555_01_A01 light chain. As the light chain employed in the bispecific antibody developed by Kolmar et al. was not involved in the interaction with the antigen, the introduction of pH-dependent antigen binding properties by the common light chain was, like 2555_01_A01, also independent of the paratope. This observation suggests that a similar pH-dependent binding mechanism was introduced to the antibody paratope by both sets of antibody light chains, which was conferred to heavy chains that had very different target specificities.

However, in their study, Kolmar et al. did not elucidate the mechanism of the light chain in conferring pH-dependent binding. In this study, we observed structural changes in residues located at the chain interface, surrounding the histidine residue located in the 2555_01_A01 CDRL1 loop between structures determined at pH 5.5 and pH 4.5. We hypothesize that these residues are important in facilitating the pH-dependent antigen binding properties of 2555_01_A01 by affecting the CDRH3 loop structure and paratope. However, this histidine residue was conserved among all the antibodies in this study, suggesting that either the local environment around this histidine residue may be unique to the 2555_01_A01 antibody, allowing histidine to confer pH-dependent binding, or that there is a histidine-independent pH-sensitive determinant in the 2555_01_A01 light chain. We hypothesize that the hydrogen bond network in the 2555_01_A01 enables this antibody to bind pH-dependently by allowing histidine to affect the antibody CDRH3 loop structure and binding. In the future, point mutations or determining the structure of a non-pH-dependent antibody, such as the 2554_01_D11 antibody, could guide the investigation into whether the histidine residue conserved in the LCDR1 loop of 2555_01_A01 was crucial for the pH-dependent antigen binding.

We have not yet established the limits of a paratope-independent approach in conferring pH-dependent antigen binding properties. Antibodies that can release antigens for lysosomal degradation during antibody recycling *in vivo* have dissociation rates between 10^{-2}-10^{-3}/s at pH ≤ 6.0 and are characterized by slow dissociation rates at neutral pH, typically ≤ 10^{-4}/s [1,2]. We have verified that 2555_01_A01 was able to release α-cbtx in a human FcRn cellular antibody recycling assay within the duration of the recycling pathway, as no bound 2555_01_A01 antibody was detected following recycling (Tulika Ph.D thesis, chapter 5). This was in contrast to the non-pH-

dependent 2554_01_D11 antibody, which remained complexed to α-cbtx upon recycling, indicating that 2555_01_A01 may have kinetics amenable to facilitating the antibody-mediated lysosomal degradation of α-cbtx. Although the fold-difference in dissociation rate between pH 7.4 and pH 5.5 was sufficient for 2555_01_A01 to release α-cbtx in this assay, a greater fold difference would be required for antibodies that have slower dissociation rates than 2555_01_A01, and may necessitate the introduction of pH-dependent determinants in the paratope-epitope interface. Nevertheless, we show that a pH-dependent antigen binding mechanism driven independently of the antibody paratope was accommodated in a cross-neutralizing antibody against long-chain α-neurotoxins. pH-dependent antigen binding via this mechanism did not negatively affect any parameters important for the antibody function and could thus be a useful approach to engineer this property into antibodies without detriment to antibody specificity.

Conclusion

The structure we present here outlines the mechanism for the broad cross-reactivity and neutralization of antibodies discovered using phage display from a naïve antibody repertoire, which will guide engineering for improved neutralization potency. For instance, the antibody could be engineered to further mimic conserved interactions between nAChR and long-chain α-neurotoxins important for function. Lastly, we provide evidence for an allosteric pH-sensitive binding mechanism for the broad pH-dependent binding of 2555_01_A01, conferred by the antibody light chain, and enabled pH-sensitivity to be coupled with cross-reactivity.

Materials and methods

SuperTEV expression

SuperTEV endoprotease was expressed using the pET39-mCherry-superTEV expression vector in BL21(DE3) cells (New England Biolabs, NEB-C2527H) as described previously (Rimbault et al, submitted).

Expression of antibody formats

Full-length human IgGs were produced using mammalian expression as described previously[20]. Fabs were produced in two batches, the first by Human Embryonic Kidney cells, the second by Chinese Hamster Ovary cells[6].

To produce scFv for crystallography, C-term TEV-His-tagged scFv was produced in BL21(DE3) cells (New England Biolabs, NEB-C2527H) and purified by Nickel affinity purification as described previously,[18] with the exception that Tunair™ shake flasks were used to increase expression. Following Nickel affinity purification, the scFv was buffer-exchanged into 20 mM Tris, 50 mM NaCl, 5 mM EDTA, pH 8.0 buffer using PD-10 columns (Merck, GE17-0851-01), and up-concentrated to 10 mg/mL using 10 kDa MWCO membranes (Fisher Scientific, 10781543). The C-terminal tag was removed by incubation with the superTEV endoprotease overnight at 4 °C using a 1:20 molar ratio of superTEV:scFv.

Once the C-terminal tag was removed, monomeric scFv was purified by size exclusion chromatography using an NGC Quest™ 10 Plus Chromatography system and a Superdex 75 10/60 HiLoad column (Cytiva, 28989333), which was run using 5 mM Tris, 20 mM NaCl, pH 8.0 buffer at 4 °C as eluent. The concentration of scFv was estimated based on the predicted A280 absorbance of 1 mg/mL of protein using the Expasy ProtParam tool.

Octet screening of pH-sensitive antibodies

An Octet RED96 system (ForteBio) was used to characterise the affinities and pH-sensitivity of antibody Fab fragments. All reagents were transferred into black 96-well plates (Greiner Bio-One, 655209) before starting the assay, which was run at 24 °C using a 1000 rpm shake speed. Streptavidin biosensor tips (Sartorius, 18-5136) were equilibrated in kinetics buffer (Sartorius, 18-1105), prepared in PBS (137 mM NaCl, 3 mM KCl, 8 mM $Na_2HPO_4.2H_2O$, 1.4 mM KH_2PO_4, pH 7.4) for 10 min in the dark before the start of the assay. The long chain α-neurotoxin was biotinylated as described previously[6] and diluted in kinetics buffer to a concentration of 0.4 μg/mL. Equilibrated biosensors were dipped into biotinylated long chain α-neurotoxin wells for 120 s to allow for sufficient loading, and a no-toxin coated biosensor was used as a reference. Biosensors were then transferred into HEPES-MES (10 mM HEPES 50 mM MES-NaCl 0.05% P20, pH 7.4) running buffer and equilibrated for 30 s before being primed in 10 mM glycine, 2 M NaCl, pH 2.0 regeneration buffer for 3 cycles. Each cycle consisted of 10 s of regeneration and 10 s of neutralization in kinetics buffer. Primed biosensors were transferred into running buffer for 60 s to obtain a stable baseline before being transferred into Fab-containing wells for 120 s. The antibody Fab fragments were prepared in running buffer in a 3-fold titration series in a concentration range spanning from 10-fold lower to 10-fold higher than the expected K_D. Dissociation of bound Fab in running buffer was given 1000 s for sufficient dissociation for high-affinity interactions. In the case of affinities and dissociation rates measured at acidic pH, the

running buffer was adjusted to pH 5.5. Data was processed in the Octet evaluation software (version 12.2.2.4). The reference was subtracted from the binding curves, and a 1:1 binding model with a global fit was used to fit all curves. The K_D values were determined either by a product of the kinetic rates (k_d/k_a) or by steady-state analysis. Flow cells were regenerated by 5 × 10 s cycles of regeneration solution followed by neutralization.

Crystallography: Sample preparation, data collection, and model building

Lyophilized long chain α-neurotoxin α-cbtx (Latoxan) was re-suspended in Tris-NaCl (5 mM Tris, 20 mM NaCl, pH 8.0) buffer at a concentration between 5-10 mg/mL. Freshly prepared scFv was added in a 1:3 molar ratio of scFv:α-cbtx and incubated overnight at 4 °C to allow binding. The complex was purified using an NGC Quest™ 10 Plus Chromatography system and a Superdex 75 10/300GL column (Cytiva), which was run at 4 °C using Tris-NaCl (5 mM Tris, 20 mM NaCl, pH 8.0) buffer as the eluent. The scFv-α-cbtx complex was up-concentrated to 14 mg/mL using 3.0 kDa MWCO ultracentrifugation units (Fisher Scientific) prior to plating.

Crystallization was performed using the sitting drop vapor diffusion method at 21 °C. Drops were set up either at a 1:1 or 1:2 molar ratio of reservoir to protein in a total volume of 0.3 µL in a 96-well drop format on SWISSCI MRC 2 Well Crystallization Plates (JENA). The wells were sealed with crystal clear tape and equilibrated against 50 µL of reservoir solution at 21 °C. Small crystals appeared in the 1:2 condition (0.1 M Bis-Tris, 0.2 M ammonium sulfate, 25% PEG3350, pH 6.5) in under a week. An optimization screen was performed around this condition in 1.2 µL drops and 100 µL reservoir. Crystals developed after two weeks and were harvested using mounted CryoLoops (Hampton Research) with cryoprotection performed by adding glycerol to a neighbour drop with no crystals to a final concentration of 20%. A 300 µm loop was used to fish several crystals. The loop edge was kept in contact with the cryosolution for approx. 5 s to equilibrate before flash freezing the crystal in liquid nitrogen and shipping these to the beamline for remote data collection.

Diffraction data collection was carried out at the P13 beamline (PETRAIII, EMBL, Germany) (PMID: 28009574). The beamline features a 6M PILATUS detector. Data were collected at 100 K for a full sweep of 360° with an oscillation degree of 0.1°, with 0.050 s exposure time, at 12700 eV. The complete data set was processed from 360° (3600 images) with the x-ray beam reduced to 50% intensity.

The structure of 2555_01_A01 bound to α-cbtx was determined by molecular replacement with Phaser-MR (PMID: 17164524) using an AlphaFold2 (PMID: 34265844) model of the expected scFv structure and the toxin PDB ID 4AEA as a search model. Model building and refinement were performed with phenix.refine (PMID: 20124702) and Coot (PMID: 20383002). Data collection and refinement statistics are summarized in Table 1. Molecular graphics were presented with PyMOL Molecular Graphics System (Version 2.2r7pre, Schrödinger, LLC).

Animals

In vivo assays were conducted in CD-1 mice of both sexes of 18–20 g body weight, supplied by Instituto Clodomiro Picado, following protocols approved by the Institutional Committee for the Use and Care of Animals (CICUA), University of Costa Rica (approval number CICUA 82–08). Mice were housed in cages in groups of 4 and were provided food and water *ad libitum*.

In vivo preincubation experiments

The *in vivo* neutralizing potential of antibody 2555_01_A01 against α-cbtx from the venom of *N. kaouthia* was assessed. The antibody was incubated with α-cbtx at toxin:antibody molar ratios of 1:1 and 1:2. Controls included α-cbtx incubated with either 0.12 M NaCl, 0.04 M phosphates, pH 7.2 (PBS) or with an isotype control IgG. After incubation, aliquots of 100 µL, containing 4 µg α-cbtx, corresponding to 2 Median Lethal Doses (LD_{50}), were injected intravenously, in the caudal vein, to groups of four mice. Following injection, animals were observed for signs of neurotoxicity, and survival was monitored for 48 hours. Deaths were recorded, and Kaplan–Meier curves were used to represent mouse survival along time.

Acknowledgments
The authors are supported by a grant from the European Research Council (ERC) under the European Union's Horizon 2020 research and innovation program [850974], by a grant from the Villum Foundation [00025302], and a grant from Wellcome [221702/Z/20/Z]. The synchrotron data was collected at the beamline operated by EMBL Hamburg at the PETRA III storage ring (DESY, Hamburg, Germany). We would like to thank Isabel Bento and Gleb Bourenkov for the assistance in using the beamline.

Conflict of interest
The authors declare no conflict of interest.

Bibliography

1. Li, F. *et al.* CS1003, a novel human and mouse cross-reactive PD-1 monoclonal antibody for cancer therapy. *Acta Pharmacol. Sin.* **42**, 142–148 (2021).
2. Ledsgaard, L. *et al.* Advances in antibody phage display technology. *Drug Discov. Today* **27**, 2151–2169 (2022).
3. Laustsen, A. H., Bohn, M.-F. & Ljungars, A. The challenges with developing therapeutic monoclonal antibodies for pandemic application. *Expert Opin. Drug Discov.* **17**, 5–8 (2022).
4. Pucca, M. B. *et al.* History of Envenoming Therapy and Current Perspectives. *Front. Immunol.* **10**, 1598 (2019).
5. Rivera-de-Torre, E. *et al.* Strategies for Heterologous Expression, Synthesis, and Purification of Animal Venom Toxins. *Front. Bioeng. Biotechnol.* **9**, 811905 (2022).
6. Ledsgaard, L. *et al. Discovery of a broadly-neutralizing human antibody that can rescue mice challenged with neurotoxin-rich snake venoms*. http://biorxiv.org/lookup/doi/10.1101/2022.06.17.496531 (2022) doi:10.1101/2022.06.17.496531.
7. Glanville, J. *et al. Venom protection by antibody from a snakebite hyperimmune subject*. http://biorxiv.org/lookup/doi/10.1101/2022.09.26.507364 (2022) doi:10.1101/2022.09.26.507364.
8. CHANG, C. C. & LEE, C. Y. ISOLATION OF NEUROTOXINS FROM THE VENOM OF BUNGARUS MULTICINCTUS AND THEIR MODES OF NEUROMUSCULAR BLOCKING ACTION. *Arch Int Pharmacodyn* **144**, 241–57 (1963).
9. Jenkins, T. P. & Laustsen, A. H. Cost of Manufacturing for Recombinant Snakebite Antivenoms. *Front. Bioeng. Biotechnol.* **8**, 703 (2020).
10. Igawa, T. *et al.* Antibody recycling by engineered pH-dependent antigen binding improves the duration of antigen neutralization. *Nat. Biotechnol.* **28**, 1203–1207 (2010).
11. Iwayanagi, Y. *et al.* Inhibitory FcγRIIb-Mediated Soluble Antigen Clearance from Plasma by a pH-Dependent Antigen-Binding Antibody and Its Enhancement by Fc Engineering. *J. Immunol.* **195**, 3198–3205 (2015).
12. Murtaugh, M. L., Fanning, S. W., Sharma, T. M., Terry, A. M. & Horn, J. R. A combinatorial histidine scanning library approach to engineer highly pH-dependent protein switches: Engineering pH-Sensitive Protein Switches. *Protein Sci.* **20**, 1619–1631 (2011).
13. Bogen, J. P. *et al.* Dual Function pH Responsive Bispecific Antibodies for Tumor Targeting and Antigen Depletion in Plasma. *Front. Immunol.* **10**, 1892 (2019).
14. Schröter, C. *et al.* A generic approach to engineer antibody pH-switches using combinatorial histidine scanning libraries and yeast display. *mAbs* **7**, 138–151 (2015).
15. Seifert, S. A. & Boyer, L. V. Recurrence phenomena after immunoglobulin therapy for snake envenomations: part 1. Pharmacokinetics and pharmacodynamics of immunoglobulin antivenoms and related antibodies. *Ann. Emerg. Med.* **37**, 189–195 (2001).
16. Yap, M. K. K., Tan, N. H., Sim, S. M., Fung, S. Y. & Tan, C. H. Pharmacokinetics of Naja sumatrana (Equatorial Spitting Cobra) Venom and Its Major Toxins in Experimentally Envenomed Rabbits. *PLoS Negl. Trop. Dis.* **8**, e2890 (2014).
17. Igawa, T. *et al.* Engineered Monoclonal Antibody with Novel Antigen-Sweeping Activity In Vivo. *PLoS ONE* **8**, e63236 (2013).
18. Ledsgaard, L. *et al. In vitro* discovery of a human monoclonal antibody that neutralizes lethality of cobra snake venom. *mAbs* **14**, 2085536 (2022).

19. Sampei, Z. *et al.* Antibody engineering to generate SKY59, a long-acting anti-C5 recycling antibody. *PLOS ONE* **13**, e0209509 (2018).
20. Ledsgaard, L. *et al. In vitro* discovery of a human monoclonal antibody that neutralizes lethality of cobra snake venom. *mAbs* **14**, 2085536 (2022).

Supporting information

Table S1: Affinity kinetics of antibodies binding to α-cobratoxin

Antibody	*KD pH7.4 (M)*	*k_a pH7.4 (1/Ms)*	*k_{dis} pH7.4 (1/s)*	*k_{dis} pH 5.5 (1/s)*	***k_{dis} (5.5/7.4)***
Parent	8.96E-08	1.83E+04	1.64E-02	N/D	**N/D**
2551_01_A12	4.19E-09	9.19E+04	3.85E-04	7.07E-04	**1.84**
2554_01_D11	2.91E-09	7.48E+04	2.18E-04	3.96E-04	**1.82**
2554_01_E01	7.75E-09	3.50E+04	2.71E-04	9.65E-04	**3.56**
2555_01_A04	3.19E-08	1.55E+04	4.92E-04	2.43E-03	**4.94**
2555_01_A01	3.38E-08	1.44E+04	4.86E-04	6.18E-03	**12.70**
2551_01_B11	6.85E-09	6.76E+04	4.62E-04	1.71E-03	**3.71**
2558_02_G09	3.41E-09	1.10E+05	3.73E-04	1.35E-03	**3.62**
A01-HE	5.40E-08		2.36E-03	2.20E-02	**9.32**
2555_01_A01 (n=2)	1.46E-08	4.27E+04	6.26E-04	1.68E-02	**26.83**
2554_01_D11 (n=2)	2.90E-09		1.6E-04	3.27E-04	**2.04**

Table S2: Affinity kinetics of antibodies binding to α-elapitoxin

Antibody	*KD pH 7.4 (M)*	*ka pH 7.4 (1/Ms)*	*kdis pH 7.4 (1/s)*	*kdis pH 5.5 (1/s)*	***k_{dis} (5.5/7.4)***
Parent	1.43E-08	6.47E+04	9.25E-04		
2551_01_A12	5.58E-10	2.15E+05	1.20E-04	1.91E-04	**1.59**
2554_01_D11	7.83E-10	1.81E+05	1.42E-04	3.37E-04	**2.37**
2554_01_E01	8.90E-10	1.75E+05	1.56E-04	4.18E-04	**2.68**
2555_01_A04	4.38E-10	2.64E+05	1.15E-04	2.48E-04	**2.15**
2555_01_A01	8.94E-10	2.35E+05	2.10E-04	1.66E-03	**7.90**
2551_01_B11			1.95E-04	8.00E-04	**4.10**
2558_02_G09	6.20E-10	2.34E+05	1.45E-04	4.76E-04	**3.28**

Table S3: Affinity kinetics of antibodies binding to α-bungaratoxin

Antibody	*KD pH 7.4 (M)*	*Ka 7.4 (1/Ms)*	*Kdis pH 7.4 (1/s)*	Kdis ph 5.5 (1/s)	**K_{dis} (5.5/7.4)**
2551_01_A12	2.108E-07	1.504E04	3.171E-03	7.333E-03	**2.31**
2554_01_D11	1.22401E-07	9.46E+03	1.16E-03	3.88E-03	**3.35**

Table S4: Steady state kinetics of antibodies binding to α-bungaratoxin

Antibody	*KD pH 7.4 (M)*	*KD pH 5.5 (M)*	***KD (5.5/7.4)***
Parent	2.93E-06	9.65E-06	**3.29**
2555_01_A04	1.35E-06	N/D	**N/D**
2555_01_A01	2.99E-06	3.50E-05	**11.69**
2551_01_B11	3.585E+09	N/D	**N/D**
2558_02_G09	2.39E-06	N/D	**N/D**

6. Antibody framework engineering for modular discovery of pH-dependent antibodies

In this Chapter, we build on the findings in Chapter 5 to create a phage display library designed to confer broad pH-dependent antigen binding properties to antibodies, to improve the discovery of pH-dependent antibodies against different targets using *in vitro* display technology. We conceptualize an approach to introduce a generic pH-switch into the antibody variable domain by conferring pH-dependent binding properties through the antibody framework region. Specifically, through the heavy-light chain framework interface region. In the first step towards this aim, a phage display library diversifying select positions within the framework chain interface has been created and validated.

The results are presented in the form of a manuscript draft as further data is needed to conclude this study.

An antibody framework module that confers modular pH-dependent antigen binding properties

Jack Wade[1], Charlotte Rimbault[1], Line Ledsgaard[1], Thomas Fryer[2], Markus-Frederik Bohn[1], Andreas H. Laustsen[1]*

[1]Department of Biotechnology and Biomedicine, Technical University of Denmark, DK-2800 Kongens Lyngby, Denmark
[2]Diversity and Prototyping, Novozymes, Kongens Lyngby, Denmark

Corresponding author:
Andreas Hougaard Laustsen
ahola@bio.dtu.dk

Keywords: Phage display, Antibody engineering, pH-dependent antigen binding

Abstract

Antibody-mediated target degradation is an attractive strategy to neutralize antigens due to the possibilities of achieving therapeutic efficacy at very low doses and modulating the function of a target without binding to an inhibitory epitope. A classical, antibody-based approach to degrade extracellular proteins using non-stoichiometric drug:target ratios is via the antibody recycling neonatal Fc receptor, FcRn. This requires pH-dependent target engagement to selectively release the target for lysosomal degradation during the FcRn-mediated antibody recycling pathway. Recycled in its unbound state back into circulation, the antibody is thus available to bind other target antigens. However, the discovery of antibodies with pH-dependent antigen binding properties is laborious and typically requires further optimization of pH-sensitive interactions in a low-throughput manner. Here, we describe an approach to engineer pH-dependent antigen binding properties directly into antibodies by targeting the antibody framework region.

Introduction

Antibodies are an attractive class of therapeutics due to their typically high specificity and affinity for their target, together with the ability to engage effector functions.[1] Multiple mechanisms exist for therapeutic antibodies to exert their efficacy, one of them being to neutralize their target antigen by binding to an inhibitory epitope. However, when targets require multi-epitope coverage to be fully neutralized, or evolve rapidly to resist inhibition, the use of specific antibodies may be challenged.

An alternative route to neutralizing targets is to remove them entirely by promoting their degradation by cellular pathways.[2] This was first achieved by developing small, heterobifunctional molecules named ProTACs (proteolysis targeting chimers) that bridge intracellular targets with an E3 ubiquitin ligase to form ternary complexes. The induced proximity between the enzyme and its target within the complex leads to target-ubiquitinylation and degradation by the 26S proteosome.[3] Antibodies naturally use cytosolic E3 ubiquitin ligase TRIM21[4,5] for proteosomal degradation of extracellular targets, such as viruses, that have entered the cell through host cell receptors and escaped the lysosome degradation system.

To facilitate the degradation of extracellular targets prior to cellular entry, modular technologies have been developed to target bound antibodies to different endogenous cell surface lysosome trafficking receptors. These receptors constitutively internalize their ligands at the cell surface and release them into pre-lysosomal compartments for transfer and degradation in the lysosomes.[6–8] Antibodies engineered either chemically with glycans or genetically with cytokines have been successful in co-opting glycan-sensing receptors[9,10] and cytokine decoy receptors[11] to degrade a range of cell surface and extracellular proteins.[9–11]

Alternatively, the antibody recycling neonatal Fc receptor (FcRn), which binds pH-dependently to the antibody Fc domain, has been employed for degrading plasma antigens.[12] FcRn naturally has a high affinity for the Fc domain at acidic pH and low affinity at neutral pH. This allows the antibody to bind FcRn in the acidic endosome and be rescued from lysosomal transfer and degradation. Upon being returned to the cell surface, lower affinity at neutral pH subsequently causes the antibody to be released from FcRn into the plasma. Antibodies that have low affinity for their target at endosomal acidic pH selectively release the target for lysosomal degradation during recycling, whereas the antibody itself is returned back to the plasma unbound.[13] This allows the antibody to neutralize multiple target molecules (non-stoichiometric neutralization) and theoretically be administered at a lower dose than a conventional antibody.[12–14] By engineering the antibody Fc domain to interact with a higher affinity to FcRn at neutral pH, the internalization rate, and therefore the antigen degradation rate of recycling antibodies, is increased.[15] As the effect of the affinity between antibody and FcRn at either endosomal acidic or plasma neutral pH on antibody half-life has been characterized, this provides an opportunity for finetuning the degradation rate of the antigen and the antibody half-life to the biology of the target.[14,16]

Although Fc variants with differential pH dependencies to FcRn have been developed, the engineering of pH-dependent antigen binding properties is extensive and typically performed on a case-by-case basis. As histidine residues exhibit a change in charge within the physiological pH range of the antibody recycling pathway, these have successfully been introduced into the complementarity-determining regions (CDRs) of antibodies to engineer pH-switches into non-pH-dependent antibodies based on computational design or by using *in vitro* display technologies.[13,17–20] In an effort to discover antibodies with pH-dependent antigen binding properties *a priori* using phage display, histidine-doped libraries have been created in which the CDRs of the

antibodies have been enriched with histidine residues. However, the discovered antibodies typically require further tuning of pH-dependent affinities.[21,22]

Here, we investigate the hypothesis that reducing the sequence space required for encoding pH-dependent antigen binding properties, by using a minimal set of mutations unaffected by antigen binding within the antibody framework, could provide a consistent means of discovering pH-dependent antibodies in a single discovery campaign. A framework library was produced and validated, on route to this aim.

Results

Framework region library design and validation

In order to engineer a conserved pH-dependent determinant into the antibody, we hypothesized that a structural change located at the centre of the antibody variable region, within the light-heavy chain framework interface, could provide a robust means of lowering binding affinity at acidic pH independent of the antigen identity. To identify framework mutations that could confer such pH-sensitive antigen binding properties, we chose a light chain shuffled, anti-long chain α-neurotoxin IgG, 2554_01_D11, previously discovered using phage display selection[23]. The affinity of 2554_01_D11 to α-cobratoxin was high at both pH 7.4 and pH 5.1, with dissociation constant (K_D) values of 2.3 nM and 10.4 nM, respectively (Fig.1 A and B). The dissociation rate was two orders of magnitude lower than previously reported pH-sensitive clones discovered using *in vitro* display technologies,[24,25] and were therefore chosen for framework engineering.

For the creation of a binding framework interface library based on the single-chain variable fragment (scFv) format, we chose residues located at homologous positions in the heavy and light chains, as residues in this region have led to structural changes important for neutralization for antibodies generated using *in vivo* discovery approaches (Fig. 1C&D).[26] We also took precedence to avoid residues located in the framework interface region that remove light chain pairing, such as those found in single-domain antibodies.[27] In total, 8 residues were selected for randomization with the NNK codon, 4 heavy chain: Q39, G44, V89, Q105, and 4 light chain: Q38, A43, D85, and G100 . The library size was estimated to have a diversity of 4.5×10^{10} unique clones based on the number of individual transformants and approached the theoretical size of the library. Colony PCR screening showed that 56/57 inserts (98%) were full-length (Fig. S2). Sequencing 27 colonies revealed that 19 (70%) had an open reading frame, were unique, and possessed mutations observed at each position. A parsimonious approach was used to maintain wild-type residues in each clone during the creation of the library using Golden Gate assembly. This was approached by spiking competing wild-type assembly fragments to lower the mutational level of each clone. In accordance with this approach, there were no clones that contained mutations in all 8 positions chosen in the library design, with the number of mutations ranging from 2 and 7 for each clone.

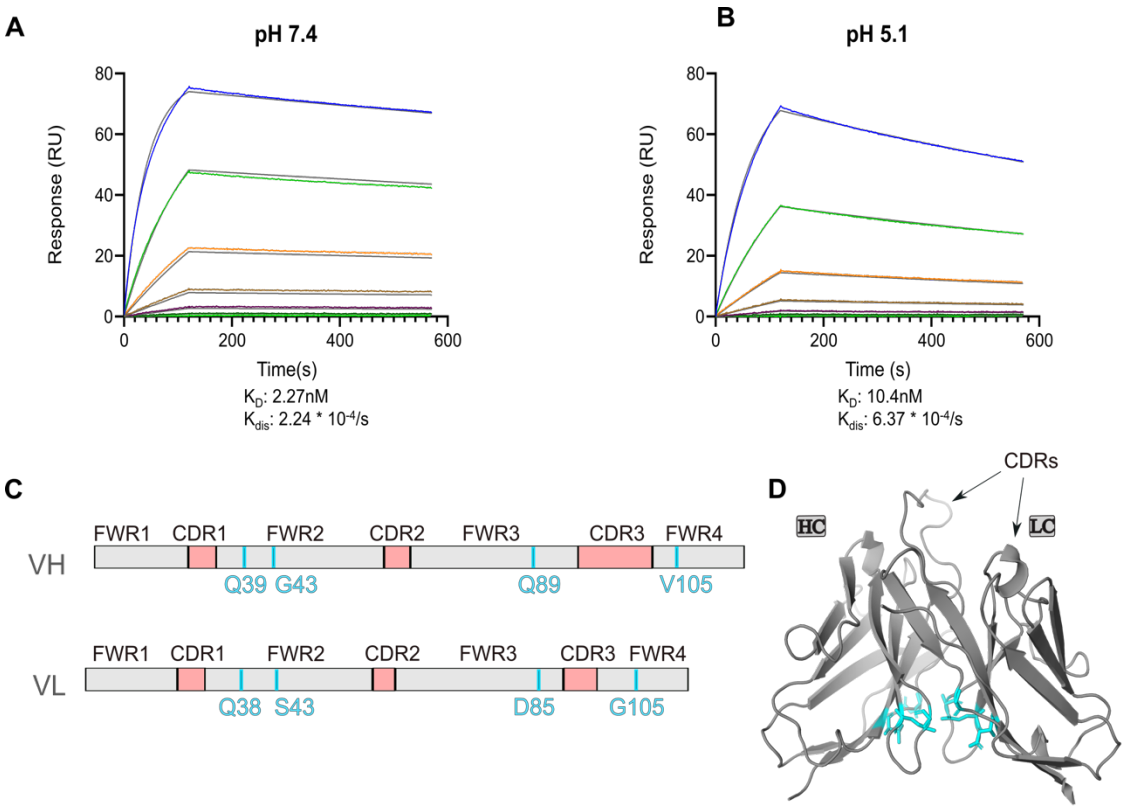

Fig 1. Binding characterization of the 2554_01_D11 antibody by SPR and framework library design. (A) Sensorgrams for the monovalent 2554_01_D11 Fab binding to immobilized α-cobratoxin measured at pH 7.4 and (B) pH 5.1. (C) Library design highlighting sites selected for library creation (cyan), numbered using the Kabat scheme. (D) The location of the residues is shown on the variable domain of the 2555_01_A01 antibody (grey), which is a light chain variant of 2554_01_D11 (2555_01_A01) clone.

Selection of framework mutations providing universal pH-sensitive antigen binding properties to scFvs using phage display

To validate the utility of the library, two rounds of phage display selection were performed using 50 nM of α-cobratoxin for both rounds, upon which selected clones were sent for DNA sequencing. The concentration of α-cobratoxin was kept the same for both rounds to minimize selection bias for the parent antibody, which has a K_D of 2 nM (Fig. 1A), which could have been favoured if stringent selection conditions (lowering of the concentration of α-cobratoxin) had been employed.

Enrichment of phages was observed between both rounds (Fig. 2). Sequencing 10 clones confirmed that these clones were a full-length variable domain and unique, and that full coverage of each position in the library had been achieved (Table. S2). There were no wild-type sequences, and most clones had 2-3 mutations. Off-site mutations were also observed, and the binding capability of these individual clones has not yet been verified.

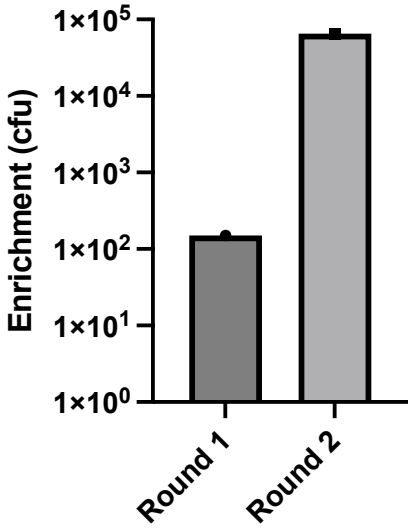

Fig 2. Enrichment of phages from two rounds of selection using the binding framework interface library. Enrichment was calculated by fold-difference between test and no-antigen control selections.

Discussion

Recycling IgG antibodies bind their cognate antigen with high affinity at neutral pH (7.4) and low affinity at acidic pH (< 6.0), allowing for the release of the antigen in the endosome, and subsequent lysosomal degradation of the antigen, whilst the antibody is rescued by FcRn-mediated pathways.[12] The process of engineering antibodies with pH-dependent antigen binding properties typically requires multiple rounds of discovery and cumbersome design and analysis of individual mutants to selectively lower affinity at pH < 6.0. Many of these approaches have focused on the use of histidine residues due to the change in the charge state of this amino acid at endosomal acidic pH. Histidine residues can either be introduced into the CDRs of antibodies in a low-throughput fashion by creating rationally designed panels of antibody mutants that can be tested on-by-one,[12] or they can be introduced semi-randomly at scale into the CDRs of synthetic antibody libraries allowing for higher throughput discovery[18,19,21,28], *e.g.*, via phage display selection.[29]

As an alternative strategy, we hypothesised that pH-dependent binding conferred by the antibody framework itself, specifically mediated by amino acid residues located in the light-heavy chain interface, could serve as a modular antibody scaffold for discovering pH-dependent antibodies. An important benefit of this approach is speculated to be that pH-dependent antigen binding could, in theory, be less dependent of the CDRs, thereby dramatically expanding the range of compatible paratopes for recycling antibodies. In turn, this strategy could improve the rapidity and precision of discovery campaigns seeking to find pH-dependent antibodies against different targets. The underlying rationale for this hypothesis is that the framework interface facilitates antibody-antigen binding by modulating the orientation of the heavy and light chains.[30–33] If the heavy-light chain orientation can be engineered to conformationally change dependent on the pH, then this could serve as a generic mechanism to lower binding affinity at a given pH and enable the design of *in vitro* display libraries consisting of pH-dependent antibodies bearing this synthetic framework module.

In this work, we generated a framework chain-interface library from a non-pH-dependent antibody to test this concept. If pH-dependent antibodies can subsequently be discovered from this library, we envisage that these antibodies can be used as generic scaffolds to generate new synthetic libraries of antibodies with pH-dependent binding pre-determined by their framework region. The benefit of pH-dependent antigen binding being 'pre-determined' in each clone would alleviate the need for histidine doping or other low-throughput engineering approaches for the discovery of recycling antibodies. Recycling antibodies possessing such a universal module for pH-dependent antigen binding could potentially be useful for a range of indications needing continuous neutralization of endogenous antigens, such as proteinases,[13] cytokines[14], tumor-associated antigens,[19] and C5 complement factor[34,35] to lower the treatment frequency. In addition, such antibodies might also find utility in the neutralization of exogenous antigens, such as toxins, where recyclability might enable lowering of the therapeutic dose.[14,36]

For therapy, antibodies need to be stable at high concentrations to be administered at a dose required for efficacy. Additionally, biophysical parameters, such as exhibiting a low propensity to aggregate, are important to limit their potential immunogenicity and systemic clearance following administration.[37,38] These are also important properties for recycling antibodies, as these antibodies require good pharmacokinetics to remain in circulation to continually bind and degrade their antigens.[12] To meet the demands for future therapeutic applications, we deliberately designed our specialized libraries based on an antibody that has previously been determined to possess good biophysical properties, including low aggregation propensity and hydrophobicity, and has been functionally validated to be efficacious *in vivo*.[23] Nevertheless, the effect of framework mutations

in the heavy-light chain interface on the developability of prospective antibodies discovered from our library remains unknown. It has, however, already been established that antibodies that acquire mutations in the framework interface region during *in vivo* somatic hypermutation can have a lower melting temperature as an effect of an increased flexibility in the antibody variable domain.[39] The effect of framework mutations on the stability of antibodies isolated from our library may, thus, need to be evaluated. Such evaluation will both be important for choosing specific antibodies to be taken further into development, as well as for selecting a specific antibody framework for the design of further synthetic libraries that contain our module that may confer broad pH-dependent antigen binding properties. If successful, we anticipate the application of such specialized libraries could be of broad interest in the field of antibody discovery and standardize the discovery effort for obtaining recycling antibodies for therapeutic applications.

Materials and methods

Expression of Fab and IgG

Both antibody formats were produced using mammalian expression as described previously.[23] In brief, the V_H and V_L domains were subcloned from the scFv-pSANG10-3F vector into a pINT12 vector for Fab expression and pINT3 vector for IgG expression. Individual V_H and V_L domains were PCR amplified using pSang10_pelB (CGCTGCCCAGCCGGCCATGG) and HLINK3_R (CTGAACCGCCTCCACCACTCGA) primers for the V_H domain and LLINK2_F (CTCTGGCGGTGGCGCTAGC) and 2097_R (GATGGTGATGATGATGTGCGGATGCG) primers for the V_L domain. The V_H was subsequently cut using *Nco*I and *Xho*I endonucleases and the V_L with *Nhe*I and *Not*I. The respective domains were assembled into either the pINT3 or pINT12 vector in a four-component ligation using T4 DNA ligase (Roche, 10481220001). The vector contained the respective heavy chain constant domains for the Fab and IgG in addition to a stuffer region containing the C_L and CMV promoter, also cut with *Nco*I and *Not*I. The resulting Fab and IgG formats were produced using transient mammalian expression using Expi293™ cells with ExpiFectamine™ 293 (ThermoFisher, A14525) as per the manufacturers guidelines. The cells were harvested and the resulting supernatants containing the IgGs purified using protein A resin (Neo Biotech, NB-45-00036-100) and the Fabs with anti-C_H1 resin (Thermo Scientific, 194320010). The purified antibodies were then desalted into PBS and snap frozen for long term storage.

SPR

The measurement of the antibody affinity at variable pH was performed by immobilizing long neurotoxin to a CM5 dextran chip by amine coupling, and flowing antibody Fab fragments in HEPES-MES (10 mM HEPES 50 mM MES-NaCl 0.05% P20, pH7.4) buffered at either pH 7.4 or pH 5.1 as described previously.[40] A double background subtraction was performed using a no-protein reference flow cell and a buffer only injection. The affinity was determined as a product of the k_{off} / k_{on} rates using a 1:1 model and a global fit.

Creation of phage display library by Golden Gate assembly

The framework library was derived from the 2554_01_D11 scFv sequence, purchased codon optimized from Eurofins in a pEX-K168 vector. A pSANG4 phagemid was sequence verified and used to obtain the phagemid backbone. Individual inserts containing the framework and CDR regions of 2554_01_D11 were PCR amplified using either mutagenic or wild-type oligonucleotides (included to lower the average number of mutations per clone). The phagemid backbone was amplified using pSANG4Myc_BbsI_For and pSANG4M13_BbsI_Rev primers. All primers (Table S1) were ordered from TAG Copenhagen, and contained BpiI type-IIS restriction sites for golden gate assembly. The overhang fidelity was checked in the NEB fidelity tool and in the case of mutagenic oligonucleotides, one framework position was diversified per oligo using the NNK codon.

All PCR's were performed using the Q5 Hot Start HF polymerase (NEB, M0494S) in a 2-step PCR program, using the following template unless otherwise stated: Reagents were prepared in a volume of 25 µL, consisting of 0.5 µM of each primer, 1 × diluted Q5 High-Fidelity Master Mix, 40 pg of DNA and made up to 25 µL with nuclease-free water (Thermo Scientific, 10977035). DNA was amplified using the following program: Initial denaturation, 98 °C, 30 s; amplification for 30 cycles, 98 °C, 10 s, and 72 °C, 15 s; final extension, 72 °C, 5 min. Four PCRs were

performed for each insert and cleaned using a Genejet PCR Purification Kit (Thermo Scientific, K0702). For the preparation of the phagemid backbone, twenty PCRs were performed with an extended amplification time of 98 °C, 10 s, and 72 °C, 110 s, with 1 ng of pSANG4 phagemid used as the template. The pSANG4 backbone amplicon had the DNA template removed by adding 0.5 µL of FastDigest DpnI (Thermo Scientific, FD1704) to each PCR and was incubated for 15 min at 37 °C. Lastly, the phagemid amplicon was gel purified using a GeneJET Gel Extraction Kit (Thermo Scientific, K0692). The purity of all amplicons was confirmed by agarose gel electrophoresis and quantified by Nanodrop (Thermo Scientific, NanodropOne).

Sequential golden gate assembly reactions were used to construct the library. Firstly, individual V_H and V_L domains were assembled from 2.4 µg of inserts, this equated to 2700 fmoles (roughly 300 ng) of each of the three mutagenic inserts and their competing wild-type counterparts, added at an equal molar ratio to lower the average mutational frequency of each clone. To improve scalability, the amount of enzyme for each assembly was lowered below the manufacturers' guidelines to 0.6 µL of BpiI (Fisher Scientific, FD1014), 90 U of T4 DNA Ligase and 2.8 µL of 10 × T4 Ligase buffer (NEB, M0202T) per 1000 fmoles of DNA and made up to a final volume of 600 µL with nuclease-free water. The reaction was left overnight at 37 °C in a water bath, without an obvious detriment to the assembly efficiency (Fig S1). After extraction from a 1.2 % agarose gel, 4 ng (more than 100 fold higher than the theoretical diversity) of each assembled domain was divided between four separate PCRs, amplified, and cleaned using the GeneJET PCR Purification Kit (Thermo Scientific, K0702) before assembling the scFv. This was done to scale up each domain whilst maintaining diversity. The scFv was assembled using equal molar ratios of each V_H and V_L domain using the same enzyme and incubation conditions as described for the V_H and V_L sub-assemblies, and extracted from a 1.2 % agarose gel, yielding 21 ng (2×10^{10}) scFv molecules. Lastly, twenty-one PCRs were performed with the extracted scFv to obtain a sufficient amount of DNA to make a large library. An input of 1 ng extracted scFv and 0.1 µM of Insert_1_For and pSANG4_Myc_M13_Rev primers (Fig 1S) were used in each PCR. The number of cycles was reduced to fifteen to lower the prospect of off-site mutations and the amplicon was cleaned using the GeneJET PCR Purification Kit, yielding 2.6 µg of DNA.

Lastly, golden gate incorporation of library DNA into the phagemid backbone was performed using 4.4 µg of phagemid backbone and 2.2 µg of scFv DNA in a 1 : 3 molar ratio of phagemid : scFv. To drive an efficient assembly, the amount of enzyme was increased to 1400 U of T4 DNA Ligase, 12.5 µL Ligase buffer, and 2.8 µL BpiI per 1000 fmoles of DNA, made up to a final volume of 800 µL with nuclease-free water and incubated overnight at 37 °C. The library was cleaned using the MiniElute PCR Purification Kit (Qiagen, 28006) and eluted using 40 µL of nuclease-free water pre-heated to 60 °C to give a total of 3.2 µg of DNA. In total twenty electroporations were performed using 2 µL of library for each aliquot of electrocompetent TG1 cells (Lucigen, 60000-PQ763-F) as described previously[40].

To confirm the presence of inserts and correct assembly, individual transformants were picked for colony PCR screening using phagemid backbone-specific primers (pSANG_5th_For and pSANG_seq_Rev) and submitted for sequencing using the gpII_Rev primer.

Phage display

Phage display selections were performed in solution using a 50 nM concentration of biotinylated α-cobratoxin. Phages were rescued from the library by seeding 200 mL of cells to an OD_{600} = 0.1 in 2TY Glucose Ampicillin (100 μg / mL) media (2TYGA), this number of cells equated to the theoretical size of the library. Cells were incubated at 37 °C, 280 rpm until OD_{600} = 0.5, then a 10-fold excess of proteolytic sensitive helper phage was added for 1 hr at 37 °C, 150 rpm to allow for infection. The cultures were spun at 3,200 rpm for 2 minutes, the supernatant was discarded, and the cells were resuspended in 2TYKA media (2TYGA + 50 μg / mL Kanamycin). The phages were then propagated overnight at 25°C and 280 rpm. A TG1 colony was selected from a pre-prepared plate and used to inoculate 5 mL of 2TY media and incubated overnight at 30°C, 280 rpm. The next day, the supernatant was obtained by centrifuging the overnight culture for 10 minutes at 10,500 x g and 4°C. Phages were precipitated by adding 1/10 volume of PEG/NaCl (20 % PEG 6000/2.5 M NaCl) and incubated on ice for 1 hr before centrifugation at 4,500 rpm for 10 minutes at 4°C to pellet the phages. The phage pellet was re-suspended in 1 mL of PBS, transferred to an Eppendorf tube, and centrifuged at 14,000 rpm for 10 min at 4°C to remove any residual cells. The supernatant was transferred to an Eppendorf tube containing 250 μL PEG/NaCl and spun at 14,000 rpm for 10 min at 4°C. The supernatant was discarded, and the phage pellet was re-suspended in 1 mL PBS. The solution was spun down at 14,000 rpm for 10 min at 4 °C until no cell pellet was observed. Phages were immediately used for the phage display selections, for long-term storage, phages were stored in 20 % (w/v) glycerol at -80 °C.

Two selections were performed in parallel with and without α-cobratoxin using 2^{12} phages. Phages, biotinylated α-cobratoxin (100 nM) and 2 × 80 μL streptavidin-coated Dynabeads (Fisher Scientific, M-280) were blocked in 3% MPBS (PBS + 3% milk: VWR, A0830.100) with end-over-end rotation for 1 hr at room temperature. Equal volumes of blocked α-cobratoxin and phages were mixed and phages were permitted to bind for 1 hr with end-over-end rotation. Blocked streptavidin beads were then added to the phage - α-cobratoxin solution for 5 min with end-over-end rotation to capture phages bound to the biotinylated α-cobratoxin. The captured streptavidin Dynabeads were washed 3 times with PBST (PBS + Tween20) and 3 times with PBS before phages were eluted by adding 100 μL trypsin (1 mg/mL, Sigma-Aldrich, T9201-500MG) and incubating for 15 min with end-over-end rotation. The phage eluent was used to infect TG1 cells grown to an OD_{600} = 0.5 and incubated for 1 hr at 37 °C, 150 rpm. Cells were prepared for plating by spinning at 2000 g, for 10 min at room temperature. Dilution plates were prepared ranging from 5 to 500,000-fold dilution of the supernatant on 2TYGA plates to determine the background and enrichment of antigen-specific phages. The following day, colonies on the output plate were scraped and resuspended in 2TYGA media with 25% glycerol, then homogenized for several hours with end-over-end rotation. The OD_{600} was measured, and the cells were stored at -80°C for subsequent rescue and the next selection round. The enrichment was determined by dividing the number of colony-forming units on the test plate by the number of colony-forming units from the no-antigen selection.

Acknowledgments

This research was founded by the Villum Foundation (00025302) and the European Research Council (ERC) under the European Union's Horizon 2020 research and innovation programme (850974).

Competing interests
All authors declare no conflict of interest.

Supporting information

Table S1: Primers used for golden gate assembly, cloning and sequencing

Primer name	Sequence BpiI recognition sites are underlined
Insert 1_For	ggctacgaagacacccccagccggccatggctc
H2_39Rev	ggctacgaagactaccatccactccaaaccttggcccggtgcknnacgaacccagctaatcg
H2_42Rev	ggctacgaagactaccatccactccaaacckngcccggtgcctgacgaacccagctaatcg
H2_43Rev	ggctacgaagactaccatccactccaaknnttggcccggtgcctgacgaacccagctaatcg
H2_WTRev	ggctacgaagactaccatccactccaaaccttggcccggtgcctgacgaacccagctaatcg
H2_45Rev	ggctacgaagactaccatccactcknnaccttggcccggtgcctgacgaacccagctaatcg
H2_For	ggctacgaagactaatgggtggtattatcccgatttttggtactgctaattatgcgc
H3_89Rev	ggctacgaagactatcacgggcgcagtaataknnagcggtatcatcgctacg
H3_WTRev	ggctacgaagactatcacgggcgcagtaatacacagcggtatcatcgctacg
H3_For	ggctacgaagactagtgataatctgggttattgcagcggcggctcc
H4_105Rev	ggctacgaagactaagacggtgactaaggtacckknnaccccaaacatcc
H4_WTRev	ggctacgaagactaagacggtgactaaggtaccttgaccccaaacatcc
H4_For	ggctacgaagactagtctcgagcggtggtggcggctccgg
L2_37Rev	ggctacgaagactagacggtcgtcggtgacgagcccgggcgknnctgataccaatgcac
L2_43Rev	ggctacgaagactagacggtcgtcggknncgagcccgggcgctgctgatacc
L2_WTRev	ggctacgaagactagacggtcgtcggtgacgagcccgggcgctgctgataccaatgcac
L2_For	ggctacgaagactacgtcatctatgaggacaaccagcgtccgagcggggtgc
L3_85Rev	ggctacgaagactagcttggcagtagtaknncgcctcgtcctcg
L3_WTRev	ggctacgaagactagcttggcagtagtagtccgcctcgtcctcg
L4_100For	ggctacgaagactaaagctacgaccgctctaaccacgaagttgtttttggcnnkggtacgaagctgac
pSANG4_Myc_M13_Rev v2	ggctacgaagactacaacttttcaacagtttctgcggccccattcagatcctcttc
pSANG4Myc_BbsI_For	ggctacgaagactagttgtttagcaaaacctcatacagaaaattcatttactaacgtctgg
pSANG4_Vector_Rev	ggctacgaagaccatgggccgcatagaaaggaacaac
pSANG5th_For	tggaaaaacgccagcaacgc
-96gIII	ccctcatagtt gcgtaacg

Generation of scFv library and cloning into pSANG4 phagemid vector

Golden gate assembly of the scFv library was performed in two separate assemblies as described in the Methods. First, by assembling the individual light and heavy chains, and second, by assembling the full-length scFv. Between each assembly step the amount of DNA was scaled-up by PCR in order to maintain diversity and generate a large library. Amplification of the assembled heavy and light chains by PCR gave clear dominant bands of the expected size around 400 bp for the HC and 500 bp for the LC (Fig S1A). An initial scaling of the subsequently assembled scFv showed some non-specific products, which was reduced when lowering the primer and gel extracted scFv DNA amounts (Fig S1B).

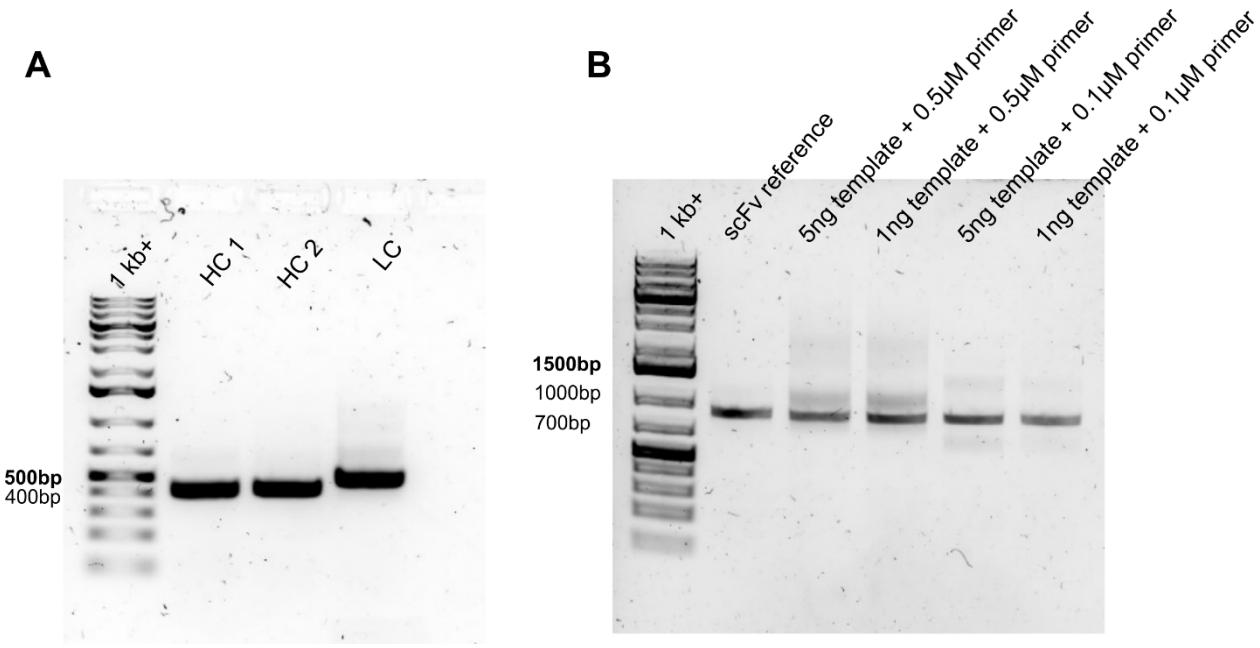

Fig S1. Up-scaling of inserts following golden gate assembly. (A) Up-scaling of individual heavy (HC) and light chains (LC). Two PCRs were carried out with the heavy chain as the reverse primer contained a mutation site. (B) PCR optimization of assembled scFv library following gel extraction. Different input amounts of extracted scFv and concentrations of each primer were tested. The scFv reference was generated from the purchased scFv vector used to build the library. The 1ng scFv + 0.1µM primer concentration showed the purest product and was taken forward to electroporation.

After scaling up the assembled scFv and electroporating into TG1 cells, colony PCRs were carried out on randomly selected transformants using pSANG4 backbone specific primers to assess the percentage of clones that had an scFv insert. The expected 2 kb amplicon size was present in 56/57 clones (Fig S2A). To check that the inserts originated from the golden gate assembly, and not from the phagemid template DNA used to generate the phagemid backbone, five colony PCR products were treated with BpiI enzyme. None of the transformants were cut, confirming that the scFv insert was assembled DNA. The template phagemid scFv amplicon containined two BpiI restriction sites, which led to multiple bands after incubation with BpiI (Fig S2B).

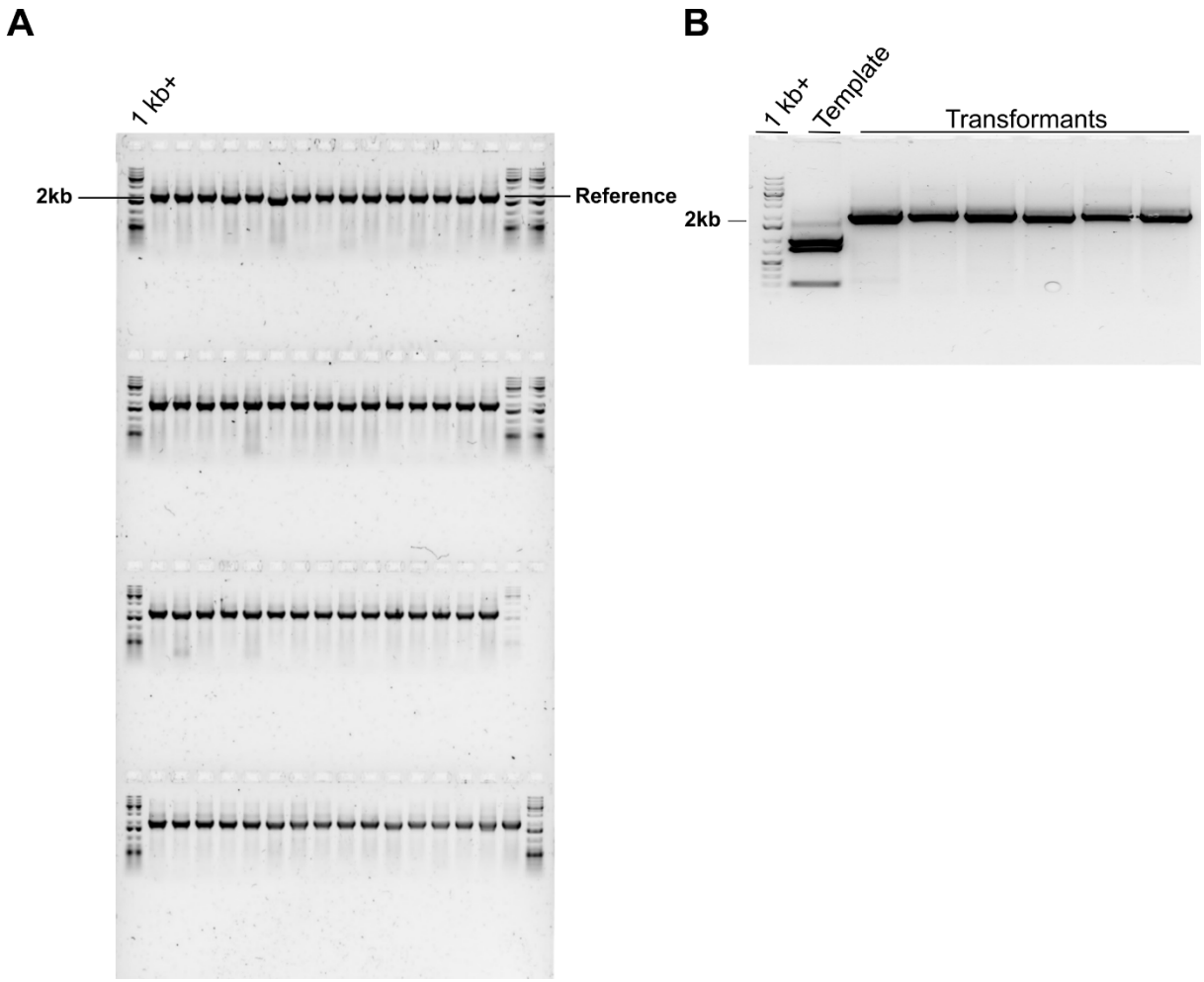

Fig S2. Cloning efficiency of the scFv library into pSANG4 phagemid. (A) Agarose gel analysis of colony PCR amplicons from individual transformants using the pSANG5th_For and gpiIII primers. A reference amplicon was generated from the template pSANG4 phagemid used in the library creation. (B) Restriction digestion of amplicons derived from 6 library transformants and the reference using BpiI endonuclease. The reference scFv had BpiI restriction sites and was included as control.

Table S2: Sequences of random clones picked after round 2 of phage display selection from the framework chain interface library.

VH:

WT:	QVQLVQSGAEVKKPGSSVKVSCKASGGTFSSYAISWVRQAPGQGLEWMGGIIPIFGTANYAQKFQGRVTITADESTSTAYMELRSLRSDDTAVYYCARDNLGYCSGGSCYSDYYYYYMDVWGQGTLVTV
C1:	HVQLVQSGAEVKKPGSSVKVSCKASGGTFSSYAISWVRQAPGQTLEWMGGIIPIFGTANYAQKFQGRVTITADESTSTAYMELRSLRSDDTAVYYCARDNLGYCSGGSCYSDYYYYYMDVWGQGTLVTV
C2:	QVQLVQSGAEVKKPGSSVKVSCKASGGTFSSYAISWVRSAPGQGLEWMGGIIPIFGTANYAQKFQGRVTITADESTSTAYMELRSLRSDDTAVYYCARDNLGYCSGGSCYSDYYYYYMDVWGVGTLVTV
C3:	QVQLVQSGAEVKKPGSSVKVSCKASGGTFSSYAISWVRQAPGQGLEWMGGIIPIFGTANYAQKFKGRVTITADESTSTAYMELRSLRSDDTADYYCARDNLGYCSGGSCYSDYYYYYMDVWGQGTLVTV
C4:	QVQLVQSGAEVKKPGSSVKVSCKASGGTFSSYAISWVRQAPGQRLEWMGGIIPIFGTANYAQKFQGRVTITADESTSTAYMELRSLRSDDTAQYYCARDNLGYCSGGSCYSDYYYYYMDVWGQGTLVTV
C5:	QVQLVQSGAEVKKPGSSVKVSCKASGGTFSSYAISWVRRAPGQGLEWMGGIIPIFGTANYAQKFQGRVTITADESTSTAYMELRSLRSDDTAQYYCARDNLGYCSGGSCYSDYYYYYMDVWGQGTLVTV
C6:	QVQLVQSGAEVKKPGSSVKVSCKASGGTFSSYAISWVRQAPGQNLEWMGGIIPIFGTANYAQKFQGRVTITADESTSTAYMELRSLRSDDTAVYYCARDNLGYCSGGSCYSDYYYYYMDVWGQGTLVTV
C7:	QVQLVQSGAEVKKPGSSVKVSCKASGGTFSSYAISWVRTAPGQGLEWMGGIIPIFGTANYAQKFQGRVTITADESTSTAYMELRSLRSDDTATYYCARDNLGYCSGGSCYSDYYYYYMDVWGQGTLVTV
C8:	QVQLVQSGAEVKKPGSSVKVSCKASGGTFSSYAISWVRQAPGQYLEWMGGIIPIFGTANYAQKFQGRVTITADESTSTAYMELRSLRSDDTAVYYCARDNLGYCSGGSCYSDYYYYYMDVWGQGTLVTV
C9:	QFQLVQSGAEVKKPGSSVKVSCKASGGTFSSYAISWVRQAPGQGLEWMGGIIPIFGTANYAQKFQGRVTITADESTSTAYMELRSLRSDDTATYYCARDNLGYCSGGSCYSDYYYYYMDVWGQGTLVTV
C10:	QVQLVQSGAEVKKPGSSVKVSCKASGGTFSSYAISWVREAPGQGLEWMGGIIPIFGTANYAQKFQGRVTITADESTSTAYMELRSLRSDDTAIYYCARDNLGYCSGGSCYSDYYYYYMDVWGQGTLVTV

VL:

WT:	NFMLTQPRSVSESPGKTVTISCTRSSGSIGSDYVHWYQQRPGSSPTTVIYEDNQRPSGVPDRFSGSIDSSSNSASLTISGLKTEDEADYYCQSYDRSNHEVVFGGGTKLTVL
C1:	NFMLTQPRSVSESPGKTVTISCTRSSGSIGSDYVHWYQQRPGSSPTTVIYEDNQRPSGVPDRFSGSIDSSSNSASLTISGLKTEDEADYYCQSYDRSNHEVVFGGGTKLTVL
C2:	NFMLTQPRSVSESPGKTVTISCTRSSGSIGSDYVHWYQQRPGSSPTTVIYEDNQRPSGVPDRFSGSIDSSSNSASLTISGLKTEDEADYYCQSYDRSNHEVVFGGGTKLTVL
C3:	NFMLTQPRSVSESPGKTVTISCTRSSGSIGSDYVHWYQQRPGSRPTTVIYEDNQRPSGVPDRFSGSIDSSSNSASLTISGLKTEDEADYYCQSYDRSNHEVVFGGGTKLTVL
C4:	NFMLTQPRSVSESPGKTVTISCTRSSGSIGSDYVHWYQQRPGSQPTTVIYEDNQRPSGVPDRFSGSIDSSSNSASLTISGLKTEDEATYYCQSYDRSNHEVVFGVGTKLTVL
C5:	NFMLTQPRSVSESPGKTVTISCTRSSGSIGSDYVHWYQQRPGSKPTTVIYEDNQRPSGVPDRFSGSIDSSSNSASLTISGLKTEDEADYYCQSYDRSNHEVVFGGGTKLTVL
C6:	NFMLTQPRSVSESPGKTVTISCTRSSGSIGSDYVHWYQQRPGSSPTTVIYEDNQRPSGVPDRFSGSIDSSSNSASLTISGLKTEDEADYYCQSYDRSNHEVVFGWGTKLTVL
C7:	NFMLTQPRSVSESPGKTVTISCTRSSGSIGSDYVHWYQFRPGSSPTTVIYEDNQRPSGVPDRFSGSIDSSSNSASLTISGLKTEDEADYYCQSYDRSNHEVVFGGGTKLTVL
C8:	NFMLTQPRSVSESPGKTVTISCTRSSGSIGSDYVHWYQQRPGSSPTTVIYEDNQRPSGVPDRFSGSIDSSSNSASLTISGLKTEDEAAYYCQSYDRSNHEVVFGGGTKLTVL
C9:	NFMLTQPRSVSESPGKTVTISCTRSSGSIGSDYVHWYQQRPGSSPTTVIYEDNQRPSGVPDRFSGSIDSSSNSASLTISGLKTEDEADYYCQSYDRSNHEVVFGGGTKLTVL
C10:	NFMLTQPRSVSESPGKTVTISCTRYSGSIGSDYVHWYQVRPGSSPTTVIYEDNQRPSGVPDRFSGSIDSSSNSASLTISGLKTEDEAHYYCQSYDRSNHEVVFGHGTKLTVL

VH: Variable heavy chain, VL: Variable light chain, Magenta: Sites chosen for library creation, Cyan: Observed mutations

Bibliography

1. Pantaleo, G., Correia, B., Fenwick, C., Joo, V. S. & Perez, L. Antibodies to combat viral infections: development strategies and progress. *Nat. Rev. Drug Discov.* **21**, 676–696 (2022).
2. Ahn, G., Banik, S. M. & Bertozzi, C. R. Degradation from the outside in: Targeting extracellular and membrane proteins for degradation through the endolysosomal pathway. *Cell Chem. Biol.* **28**, 1072–1080 (2021).
3. Zou, Y., Ma, D. & Wang, Y. The PROTAC technology in drug development: The PROTAC technology in drug development. *Cell Biochem. Funct.* **37**, 21–30 (2019).
4. Foss, S. *et al.* Potent TRIM21 and complement-dependent intracellular antiviral immunity requires the IgG3 hinge. *Sci. Immunol.* **7**, eabj1640 (2022).
5. Mallery, D. L. *et al.* Antibodies mediate intracellular immunity through tripartite motif-containing 21 (TRIM21). *Proc. Natl. Acad. Sci.* **107**, 19985–19990 (2010).
6. Ghosh, P., Dahms, N. M. & Kornfeld, S. Mannose 6-phosphate receptors: new twists in the tale. *Nat. Rev. Mol. Cell Biol.* **4**, 202–213 (2003).
7. Janssens, R., Struyf, S. & Proost, P. The unique structural and functional features of CXCL12. *Cell. Mol. Immunol.* **15**, 299–311 (2018).
8. York, S. J., Arneson, L. S., Gregory, W. T., Dahms, N. M. & Kornfeld, S. The Rate of Internalization of the Mannose 6-Phosphate/Insulin-like Growth Factor II Receptor Is Enhanced by Multivalent Ligand Binding. *J. Biol. Chem.* **274**, 1164–1171 (1999).
9. Ahn, G. *et al.* LYTACs that engage the asialoglycoprotein receptor for targeted protein degradation. *Nat. Chem. Biol.* **17**, 937–946 (2021).
10. Banik, S. M. *et al.* Lysosome-targeting chimaeras for degradation of extracellular proteins. *Nature* **584**, 291–297 (2020).
11. Pance, K. *et al.* Modular cytokine receptor-targeting chimeras for targeted degradation of cell surface and extracellular proteins. *Nat. Biotechnol.* (2022) doi:10.1038/s41587-022-01456-2.
12. Igawa, T. *et al.* Antibody recycling by engineered pH-dependent antigen binding improves the duration of antigen neutralization. *Nat. Biotechnol.* **28**, 1203–1207 (2010).
13. Chaparro-Riggers, J. *et al.* Increasing Serum Half-life and Extending Cholesterol Lowering in Vivo by Engineering Antibody with pH-sensitive Binding to PCSK9. *J. Biol. Chem.* **287**, 11090–11097 (2012).
14. Igawa, T. *et al.* Engineered Monoclonal Antibody with Novel Antigen-Sweeping Activity In Vivo. *PLoS ONE* **8**, e63236 (2013).
15. Grevys, A. *et al.* A human endothelial cell-based recycling assay for screening of FcRn targeted molecules. *Nat. Commun.* **9**, 621 (2018).
16. Yang, D. *et al.* Maximizing *in vivo* target clearance by design of pH-dependent target binding antibodies with altered affinity to FcRn. *mAbs* **9**, 1105–1117 (2017).
17. Hong, S.-T., Su, Y.-C., Wang, Y.-J., Cheng, T.-L. & Wang, Y.-T. Anti-TNF Alpha Antibody Humira with pH-dependent Binding Characteristics: A constant-pH Molecular Dynamics, Gaussian Accelerated Molecular Dynamics, and In Vitro Study. *Biomolecules* **11**, 334 (2021).
18. Schröter, C. *et al.* A generic approach to engineer antibody pH-switches using combinatorial histidine scanning libraries and yeast display. *mAbs* **7**, 138–151 (2015).
19. Bogen, J. P. *et al.* Dual Function pH Responsive Bispecific Antibodies for Tumor Targeting and Antigen Depletion in Plasma. *Front. Immunol.* **10**, 1892 (2019).
20. Sulea, T. *et al.* Structure-based engineering of pH-dependent antibody binding for selective targeting of solid-tumor microenvironment. *mAbs* **12**, 1682866 (2020).

21. Bonvin, P. *et al.* *De novo* isolation of antibodies with pH-dependent binding properties. *mAbs* **7**, 294–302 (2015).
22. Könning, D. *et al.* Construction of Histidine-Enriched Shark IgNAR Variable Domain Antibody Libraries for the Isolation of pH-Sensitive vNAR Fragments. in *Antibody Engineering* (eds. Nevoltris, D. & Chames, P.) vol. 1827 109–127 (Springer New York, 2018).
23. Ledsgaard, L. *et al.* Discovery and optimization of a broadly-neutralizing human monoclonal antibody against long-chain α-neurotoxins from snakes. *Nat. Commun.* **14**, 682 (2023).
24. Bogen, J. P. *et al.* Dual Function pH Responsive Bispecific Antibodies for Tumor Targeting and Antigen Depletion in Plasma. *Front. Immunol.* **10**, 1892 (2019).
25. Schröter, C. *et al.* A generic approach to engineer antibody pH-switches using combinatorial histidine scanning libraries and yeast display. *mAbs* **7**, 138–151 (2015).
26. Zhou, J. O., Zaidi, H. A., Ton, T. & Fera, D. The Effects of Framework Mutations at the Variable Domain Interface on Antibody Affinity Maturation in an HIV-1 Broadly Neutralizing Antibody Lineage. *Front. Immunol.* **11**, 1529 (2020).
27. Vincke, C. *et al.* General Strategy to Humanize a Camelid Single-domain Antibody and Identification of a Universal Humanized Nanobody Scaffold. *J. Biol. Chem.* **284**, 3273–3284 (2009).
28. Klaus, T. & Deshmukh, S. pH-responsive antibodies for therapeutic applications. *J. Biomed. Sci.* **28**, 11 (2021).
29. Ledsgaard, L. *et al.* Advances in antibody phage display technology. *Drug Discov. Today* **27**, 2151–2169 (2022).
30. Xu, K. *et al.* Epitope-based vaccine design yields fusion peptide-directed antibodies that neutralize diverse strains of HIV-1. *Nat. Med.* **24**, 857–867 (2018).
31. Ovchinnikov, V., Louveau, J. E., Barton, J. P., Karplus, M. & Chakraborty, A. K. Role of framework mutations and antibody flexibility in the evolution of broadly neutralizing antibodies. *eLife* **7**, e33038 (2018).
32. Klein, F. *et al.* Somatic Mutations of the Immunoglobulin Framework Are Generally Required for Broad and Potent HIV-1 Neutralization. *Cell* **153**, 126–138 (2013).
33. Kwong, P. D. & Mascola, J. R. Human Antibodies that Neutralize HIV-1: Identification, Structures, and B Cell Ontogenies. *Immunity* **37**, 412–425 (2012).
34. Lee, J. W. *et al.* Ravulizumab (ALXN1210) vs eculizumab in adult patients with PNH naive to complement inhibitors: the 301 study. *Blood* **133**, 530–539 (2019).
35. Sampei, Z. *et al.* Antibody engineering to generate SKY59, a long-acting anti-C5 recycling antibody. *PLOS ONE* **13**, e0209509 (2018).
36. Kroetsch, A. *et al.* Engineered pH-dependent recycling antibodies enhance elimination of Staphylococcal enterotoxin B superantigen in mice. *mAbs* **11**, 411–421 (2019).
37. Ausserwöger, H. *et al.* Non-specificity as the sticky problem in therapeutic antibody development. *Nat. Rev. Chem.* **6**, 844–861 (2022).
38. Dyson, M. R. *et al.* Beyond affinity: selection of antibody variants with optimal biophysical properties and reduced immunogenicity from mammalian display libraries. *mAbs* **12**, 1829335 (2020).
39. Madan, B. *et al.* Mutational fitness landscapes reveal genetic and structural improvement pathways for a vaccine-elicited HIV-1 broadly neutralizing antibody. *Proc. Natl. Acad. Sci.* **118**, e2011653118 (2021).
40. Ledsgaard, L. *et al.* *In vitro* discovery of a human monoclonal antibody that neutralizes lethality of cobra snake venom. *mAbs* **14**, 2085536 (2022).

7. Nanobody valence engineering using the p53 self-assembly protein

In Chapter 7, we test an engineering approach to enhance the valence and half-life properties of nanobodies, which are a monovalent antibody format that is unable to interact with FcRn, therefore limiting their use in certain applications due to their inherently short half-life.

Here, we employ the p53 protein to increase the valence of nanobodies and functionalize them with IgG-Fc to enable cellular recycling. The p53 protein self-assembles into a tetramer, here we use this property to assemble nanobodies into multivalent proteins by genetically fusing nanobodies into the p53 protein. The nanobody used in this study was specific to α-cobratoxin, a long-chain α-neurotoxin from the *N. kaouthia* elapid. We designed nanobody formats to contain up to 16 nanobodies and verified different parameters important for their application. These included characterizing their molecular size and correct assembly, neutralization potency, and recycling capabilities. We show that multivalent nanobodies assembled as stable multimeric proteins (Quads), and this translated into enhanced neutralization capacity against α-cobratoxin. We also found that the nanobody was cross-reactive to long-chain α-neurotoxin from the forest cobra, *N. melanoleuca*. Finally, when measuring the ability of Quads to be recycled in cells in a cellular recycling assay indicative of serum half-life, we show that Quads functionalized with IgG-Fc were rescued from cellular degradation and recycled from the cell into the extracellular environment. Collectively, these results show the versatility of using the self-assembly p53 protein to tune the valence of nanobodies and improve their half-life, opening the possibility of re-purposing nanobodies for different applications. Such possibilities include avidity-driven mechanisms of action, such as enhancing the neutralization potency of nanobodies that have a reduced binding affinity to viral escape mutants.

The manuscript has been published in Bioconjugate Chemistry.
Jack Wade, Charlotte Rimbault, Hanif Ali, Line Ledsgaard, Esperanza Rivera-de-Torre, Maher Abou Hachem, Kim Boddum, Nadia Mirza, Markus-Frederik Bohn, Siri A. Sakya, Fulgencio Ruso-Julve, Jan Terje Andersen, and Andreas H. Laustsen, *Bioconjugate Chemistry* **2022** *33* (8), 1494-1504, DOI: 10.1021/acs.bioconjchem.2c00220

Bioconjugate Chemistry

pubs.acs.org/bc

Article

Generation of Multivalent Nanobody-Based Proteins with Improved Neutralization of Long α-Neurotoxins from Elapid Snakes

Jack Wade,[▽] Charlotte Rimbault,[▽] Hanif Ali, Line Ledsgaard, Esperanza Rivera-de-Torre, Maher Abou Hachem, Kim Boddum, Nadia Mirza, Markus-Frederik Bohn, Siri A. Sakya, Fulgencio Ruso-Julve,* Jan Terje Andersen, and Andreas H. Laustsen*

Cite This: *Bioconjugate Chem.* 2022, 33, 1494−1504

Read Online

ACCESS | Metrics & More | Article Recommendations | Supporting Information

ABSTRACT: Recombinantly produced biotherapeutics hold promise for improving the current standard of care for snakebite envenoming over conventional serotherapy. Nanobodies have performed well in the clinic, and in the context of antivenom, they have shown the ability to neutralize long α-neurotoxins *in vivo*. Here, we showcase a protein engineering approach to increase the valence and hydrodynamic size of neutralizing nanobodies raised against a long α-neurotoxin (α-cobratoxin) from the venom of the monocled cobra*Naja kaouthia*. Based on the p53 tetramerization domain, a panel of anti-α-cobratoxin nanobody-p53 fusion proteins, termed Quads, were produced with different valences, inclusion or exclusion of Fc regions for endosomal recycling purposes, hydrodynamic sizes, and spatial arrangements, comprising up to 16 binding sites. Measurements of binding affinity and stoichiometry showed that the nanobody binding affinity was retained when incorporated into the Quad scaffold, and all nanobody domains were accessible for toxin binding, subsequently displaying increased blocking potency *in vitro* compared to the monomeric format. Moreover, functional assessment using automated patch-clamp assays demonstrated that the nanobody and Quads displayed neutralizing effects against long α-neurotoxins from both *N. kaouthia* and the forest cobra *N. melanoleuca*. This engineering approach offers a means of altering the valence, endosomal recyclability, and hydrodynamic size of existing nanobody-based therapeutics in a simple plug-and-play fashion and can thus serve as a technology for researchers tailoring therapeutic properties for improved neutralization of soluble targets such as snake toxins.

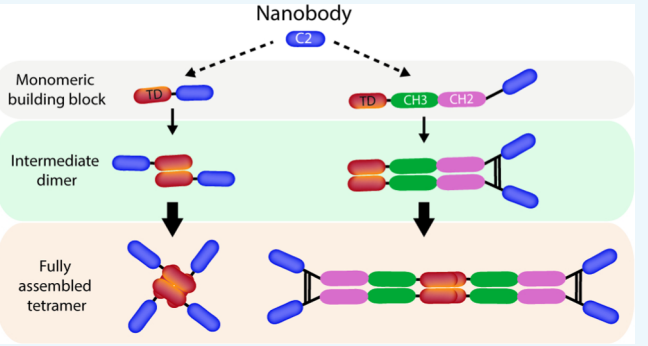

INTRODUCTION

Snakebite envenoming is a neglected tropical disease with over 2 million victims envenomed each year on a global level. These cases result in more than 100,000 fatalities and 300,000 permanent disabilities,[1] leaving behind both a large health and socioeconomic burden.[2] The current standard of care, in the form of antivenom derived from hyperimmunized animals, contains a heterologous polyclonal mixture of both neutralizing and non-neutralizing antibodies.[3] This form of immunotherapy saves lives and verifies the use of antibodies as a therapeutic approach against envenoming. However, administration of heterologous polyclonal antibodies carries risks of adverse reactions due to the high immunogenicity of the recovered animal-derived antibodies and poor batch-to-batch reproducibility as well as a low therapeutic content of neutralizing antibodies.[1,4]

Recombinantly produced antivenom based on human or humanized antibody sequences could alleviate some of these drawbacks. Further, they can be engineered to have improved therapeutic properties, such as enhanced binding and neutralization potency and optimized pharmacokinetics (PK), depending on what antibody format is employed.[5,6] As such, different antibody formats have been investigated, of which some have demonstrated good efficacy *in vivo*, including *in vitro* discovered fully human immunoglobulin Gs (IgGs) and nanobodies (V_HHs).[7−9] While nanobodies possess traits desirable for therapeutic development, such as their low immunogenicity[10] and high thermal stability and production titers in microbial expression systems,[11,12] they are a monovalent format that experiences rapid clearance, a potential limitation toward their use in certain diseases, including neutralization of toxins with delayed release from the bite site in cases of snakebite envenoming.

Existing approaches to increase the serum half-life of nanobodies involve fusion to proteins, such as IgG Fc or

Received: May 6, 2022
Revised: July 1, 2022
Published: July 23, 2022

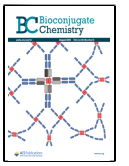

https://doi.org/10.1021/acs.bioconjchem.2c00220
Bioconjugate Chem. 2022, 33, 1494−1504

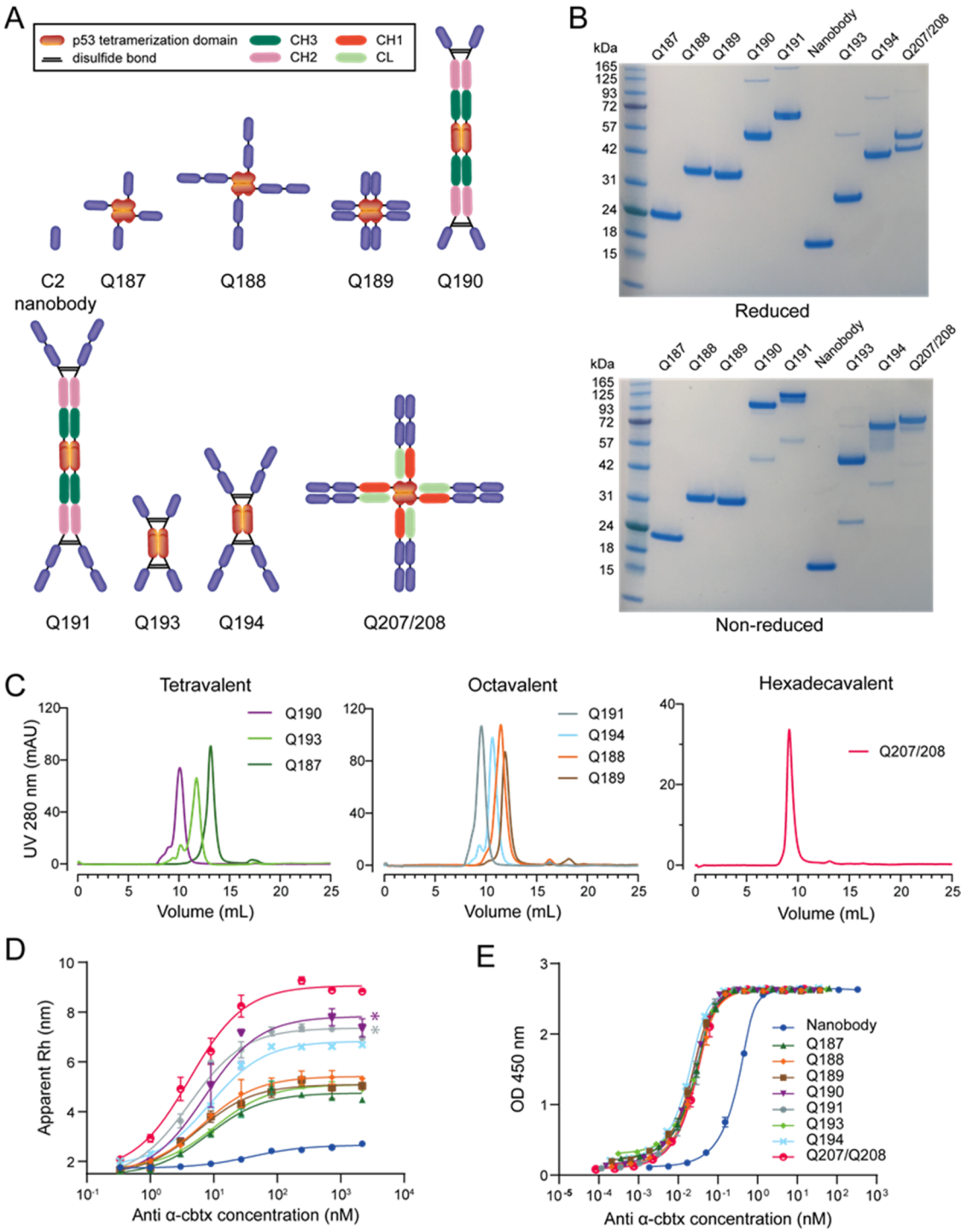

Figure 1. Engineering of Quad molecules. (A) Schematic structural overview of the different Quad formats generated using the p53 tetramerization domain. (B) Nonreducing and reducing colloidal blue-stained SDS-PAGE analysis of the eight Quad constructs and the nanobody. (C) Assessment of purity and monomeric assembly of the Quads via size-exclusion chromatography analysis displayed according to their binding domain valency. The chromatograms were obtained on a HiLoad Superdex200 Increase 10/300 GL column with PBS as an eluent. (D) Binding curve established with FIDA showing the apparent hydrodynamic radius of the indicator α-cbtx-Alexa488 (100 nM) as a function of anti-α-cbtx (0−2.1 μM) in PBST buffer. The K_D values were calculated from the binding isotherm and are available in Table S2. Represented results are from a single experiment with technical repeats performed in duplicate. *Denotes Quad formats that had increased interaction with the FIDA capillary. (E) ELISA binding assay of Quads to immobilized α-cbtx. Each data point represents the mean of two independent experiments ± SD. The K_D values were calculated from the binding curves and are available in Table S4.

human serum albumin (HSA) that are able to interact with the neonatal Fc receptor (FcRn).[13,14] FcRn mediates the rescue of IgG from lysosomal degradation through pH-dependent interactions, namely, a higher affinity interaction at acidic relative to neutral pH. Binding with a high affinity within the acidified environment of the endosome prevents trafficking into the lysosome, and a drop in affinity at neutral pH facilitates release back into the serum. Engineering IgG Fc and

https://doi.org/10.1021/acs.bioconjchem.2c00220
Bioconjugate Chem. 2022, 33, 1494−1504

HSA to have a greater affinity differential between these two pH values has led to the discovery of antibodies and alternative formats with prolonged half-life.[15,16]

The use of self-assembly domains could concomitantly lead to enhanced potency and half-life of nanobodies by increasing valence, accommodating additional nanobody binding and IgG Fc-effector domains that engage both the antigen and FcRn in a single molecule. Larger formats with increased valence could potentially be administered at a lower therapeutic dose, have increased half-life due to a slower rate of glomerular clearance enabling a lowering of the frequency of administration, and have greater exposure to toxins in circulation. The effects of PK on the neutralization of systemically acting toxins for larger, multivalent formats could mechanistically be a benefit in intercepting toxins before they reach their target during the early course of envenoming as well as neutralization of toxins that re-enter circulation in later stages. Investigating the effect of antibody PK on the neutralization of systemically acting toxins has so far received limited attention. However, technologies that allow for the precise tailoring of drug pharmacokinetics without complicating or further adding cost to the manufacturing process might find utility in the development of novel types of recombinant antivenoms with improved therapeutic properties.[17]

In this study, we apply a protein tetramerization technology based on the p53 tetramerization domain (TD) [18] to produce a panel of nanobody-based antibody formats with varied hydrodynamic radius, valence, and inclusion or exclusion of IgG Fc domains, termed Quads. Quads rely on intermolecular self-assembly from simple monomeric building blocks to form stable tetramers. As such, we demonstrate successful engineering of Quads with up to 16 binding domains targeting α-cobratoxin (α-cbtx) from *Naja kaouthia*. These novel multivalent molecules were assessed for their long-term structural integrity and binding affinity as well as their neutralization potency and half-life potential. The findings show a functional benefit of increasing valence on blocking and neutralization of α-cbtx, a trait maintained against long α-neurotoxins (Lα Ntxs) from *N. melanoleuca*, in addition to improved FcRn-mediated recycling and rescue from cellular degradation of Quads designed to contain IgG Fc domains. In combination, the results presented here demonstrate that the Quad multimerization technology could serve as a versatile platform for fine-tuning the molecular parameters of nanobodies, which might find therapeutic utility, for example, in targeting snake toxins like α-cobratoxin with improved efficacy.

RESULTS AND DISCUSSION

Engineering of Quad Molecules. The low-molecular-weight C2 anti-α-cbtx nanobody was used to engineer novel multivalent antibody formats (Quads) using a flexible multimerization technology described previously.[18] This yielded a total of eight different multivalent Quads, with or without intact Fc regions, of varying size, shape, and flexibility, possessing valences ranging from tetravalent to hexadecavalent (Figure 1A and Table S1). An important first step in the analysis of these novel multivalent antibody molecules was to show that they could be produced in adequate yields as soluble secreted proteins with high purity and structural integrity. Following transient expression in HEK293 cells and affinity purification of the proteins directly from the culture supernatant, yields of the Quad proteins were calculated (Table 1) using the molar extinction coefficient and protein absorbance at 280 nm. Many of the titers of the Quad proteins with a larger molecular weight were found to be higher than the native nanobody, suggesting that multimerization did not hamper Quad production. Quad titers were also competitive with other tetravalent antibody formats produced in a similar expression system based on a clinically validated IgG scaffold.[19] The ease of production of Quads from simple monomeric (single polypeptide chain) building blocks that self-assemble into tetramers inside the cell might also indicate that these molecules could potentially be produced microbially, which would provide an opportunity for low-cost manufacture.[20] If this speculation were to hold true, it would have important implications for the economic feasibility of bringing Quads to the market against neglected tropical diseases, such as snakebite envenoming, where low cost of treatment is essential.[21]

Table 1. Blocking Potency, Size-Exclusion Chromatography, and Production Analysis of the Different Quad Formats

	blocking		SEC analysis		production
molecule (valency)	IC_{50} (nM)	V_HH/Quad	main peak (%)	elution (mL)	yield (mg/L)
V_HH (1)	0.80	1	100.0	17.56	83
Q187 (4)	0.18	4.7	97.0	13.15	83
Q188 (8)	0.11	7.7	97.0	11.48	75
Q189 (8)	0.10	8.7	95.0	11.90	108
Q190 (4)	0.21	3.9	88.5	10.09	125
Q191 (8)	0.13	6.3	98.0	9.56	65
Q193 (4)	0.19	4.5	81.0	11.75	67
Q194 (8)	0.11	7.4	86.0	10.65	37
Q207/208 (16)	0.05	15.4	98.6	9.17	100

Structural Analysis of Quad Proteins. To analyze whether the Quads had assembled as multimeric proteins, their size was analyzed under denaturing (SDS-PAGE) and native conditions (size-exclusion chromatography, SEC) (Figure 1B,C). The molecular sizes of the monomeric subunits and fully assembled tetrameric Quads are supplied in Table S1. Single prominent bands on SDS-PAGE separated according to the molecular weight of different Quad proteins. Quads containing disulfide bridges (Q190-Q194 and Q207/208) dissembled into their monomeric subunits when ran under reducing conditions, and there was no obvious proteolytic degradation or aggregation (Figure 1). SEC showed all Quads eluted as single-dominant peaks, except for Q190, Q193, and Q194 that also had a minor percentage of higher molecular weight species, and were >95% tetrameric after being stored for a year at 4 °C (Figure 1C and Table 1 and S6). Quads Q193 and Q194, designed to have a more compact, linear structure, consistently had lower elution volumes and a larger hydrodynamic radius than their Quad counterparts Q187-Q189 that had similar molecular weights but a more globular architecture (Tables 1 and S2). The hydrodynamic radii of the Quads bound to α-cbtx, as determined by flow-induced dispersion analysis (FIDA), ranged from 4.58 to 9.06 nm (Figure 1D and Table S2). A comparison of select unbound Quads Q189, Q193, and Q194 using DLS showed that the population mean sizes ranked in accordance with that seen for the FIDA, and the samples were over 90% monodisperse with no peaks corresponding to partially assembled intermediates (Table S3). The relevance of the increased hydrodynamic size and valence of Quads in comparison to the nanobody could potentially lead to a lower renal clearance[22] and a more

https://doi.org/10.1021/acs.bioconjchem.2c00220
Bioconjugate Chem. 2022, 33, 1494−1504

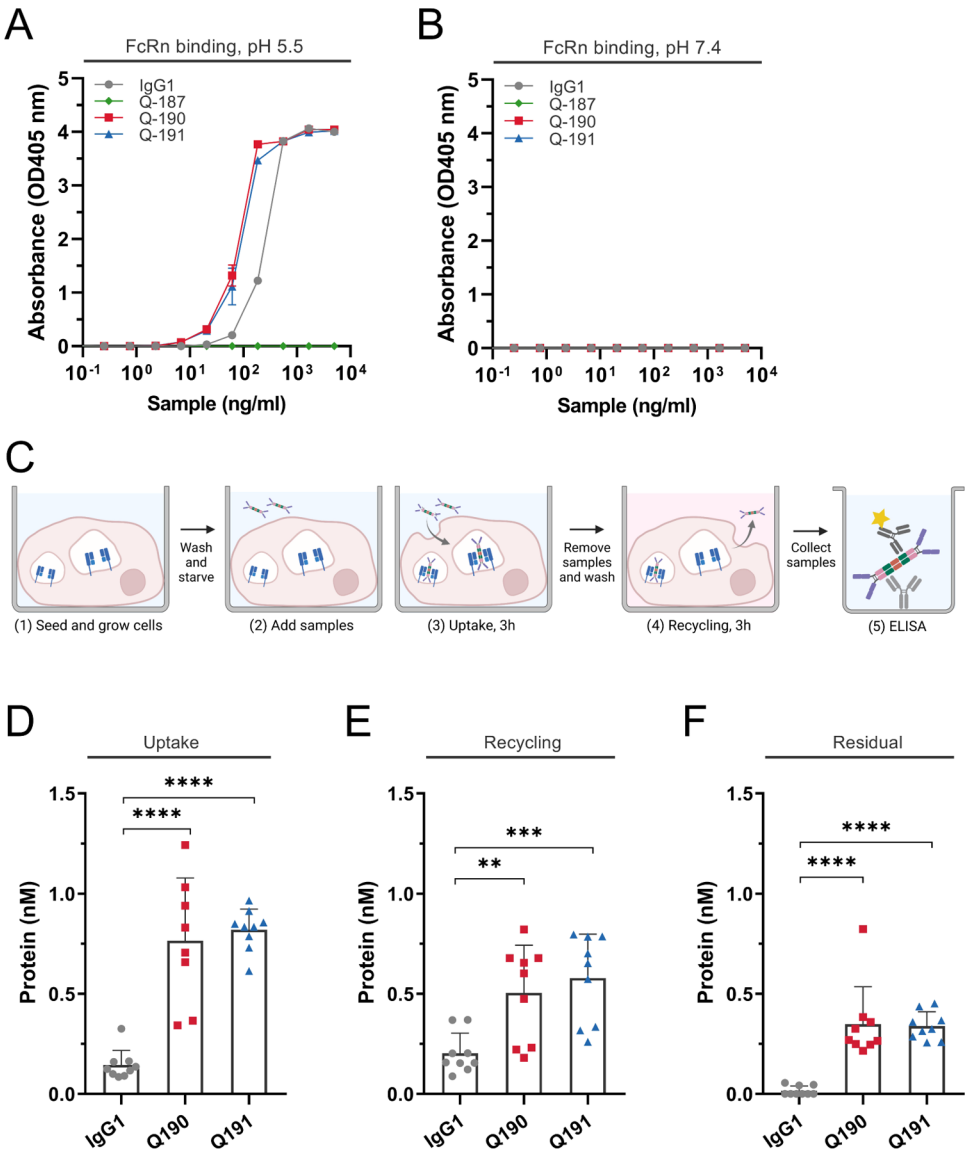

Figure 2. FcRn binding and transport properties of the Quad molecules. (A, B) FcRn-ELISA binding assays were obtained for NIP-IgG1-WT, Q187, Q190, and Q191 at acidic pH (pH 5.5) and neutral pH (pH 7.4). (C) Schematic overview of the HERA protocol. Quads and anti-NIP-IgG1 were added to starved HMEC1-hFcRn cells (1−2) and incubated for 3 h to allow for uptake (3), followed by lysis. Samples were removed, followed by a new 3 h incubation period with fresh medium to allow recycling and release into the medium, or retention inside the cells measured after lysis of the cells (4). Proteins present in the lysates and recycling medium were quantified by two-way anti-Fc ELISA (5). The figure was created with Biorender.com. (D−F) ELISA quantification of the amounts taken up, recycled, or accumulated. Data represents three independent experiments; mean ± SD, unpaired Student's *t*-test: *$p > 0.05$, **$p > 0.01$, ***$p > 0.001$, **** $p > 0.0001$.

favorable biodistribution profile for toxin neutralization. Furthermore, Quads engineered to contain Fc domains, such as Q190 and Q191, might potentially have an even more prolonged serum half-life, as these Quads contain double the amount of Fc domains compared to a standard IgG antibody. A feature that could potentially be useful when targeting toxins that enter circulation late after the envenoming episode due to venom depot effects.[17]

Drug pharmacokinetics and pharmacodynamics can be influenced by antidrug immune responses. The p53 tetramerization domain is a protein of human origin and was used to drive the assembly of Quads that were either comparable in size to an IgG or smaller than an IgM antibody.[23] Due to the natural compatibility with the human immune system, it is anticipated that the p53-TD would be less immunogenic than nonhuman tetramerization domains, such as streptavidin and the viral capsid protein VP1. Prediction of immunogenicity is a challenge, and even with fully human antibodies, such as adalimumab, antidrug antibodies have been shown to arise upon administration of the antibody.[24] The effect of an immune response against human multimerization domains potentially leads to an interference in the biology of the native protein in a patient. In this relation, it could be speculated that because the p53 resides intracellularly, it might cause less of a detriment than tetramerization domains that function within the plasma, such as transthyretin, might do. On the other hand, it cannot be excluded that intracellular domains have more immunogenic properties when entering the extracellular environment, though a comprehensive study conducted by Katchman et al. (2016) mapping p53 immunogenicity did not indicate that the TD domain of p53 is particularly immunogenic.[25] The structural integrity of the different

https://doi.org/10.1021/acs.bioconjchem.2c00220
Bioconjugate Chem. 2022, 33, 1494−1504

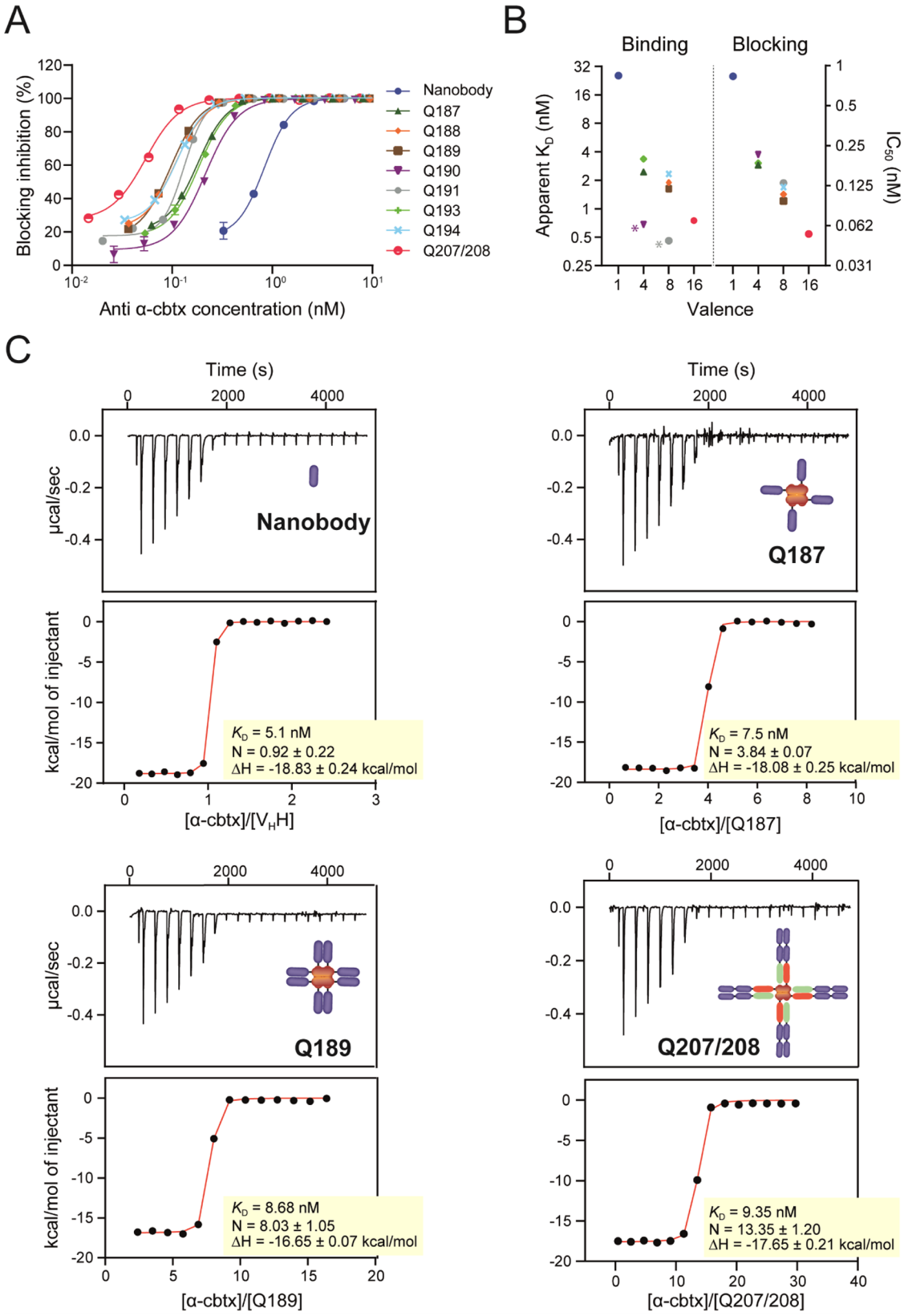

Figure 3. Apparent affinity and blocking characterization of Quad molecules to α-cbtx. (A) Blocking of the α-cbtx/AChR interaction with Quad molecules in an ELISA-based assay. Each data point represents the mean of two independent experiments ± SD. (B) Comparison between apparent K_D and IC_{50} blocking potency. * Denotes Quad formats that had increased interaction with the FIDA capillary. (C) Representative isothermal titration calorimetry thermograms and curve fits for titrations of V_HH, Q187, Q189, and Q207/208 into α-cbtx. Binding affinity (K_D) and stoichiometry (N) are the average of two independent titrations.

https://doi.org/10.1021/acs.bioconjchem.2c00220
Bioconjugate Chem. 2022, 33, 1494−1504

Quads was further verified in two separate binding assays, either by indirect ELISA or FIDA. Both assays showed that the multivalent Quads were able to bind α-cbtx in a dose-dependent manner. For the ELISA, all Quads exhibited higher binding capacity and lower K_D values for immobilized α-cbtx compared to the nanobody (Figure 1E and Table S4). Binding to α-cbtx immobilized on a surface promotes avid binding. In the timeframe of this assay, there were, however, no clear differences in binding strength seen between the respective multivalent Quads, likely due to the very low dissociation constants of multiple binding domains simultaneously engaged with the toxins on the surface. Taken together, this confirmed that the Quads were assembled correctly and were functional as tetrameric proteins.

Quad Molecules Bind Human FcRn in a pH-Dependent Manner and are Rescued from Intracellular Degradation. Repurposing FcRn for efficient recycling of Quads requires tight binding at pH <6.0 and low affinity at neutral pH.[26,27] To verify that the Quads exhibited pH-dependent binding to human FcRn (hFcRn) similar to that of IgG, ELISA was performed. Titrated amounts of the Quads were coated in wells followed by adding a site-specific biotinylated recombinant hFcRn, preincubated with streptavidin conjugated with alkaline phosphatase. The experiment was performed at both pH 5.5 and 7.4, and a full-length human IgG1 with specificity for the hapten NIP was included as a positive control (Figure 2A,B). The results revealed that the Fc-containing Q190 and Q191 bound the receptor at acidic pH, where the binding responses measured were stronger than for the IgG1 control, while none of the formats bound at neutral pH. As expected, Q187 lacking an Fc domain did not bind under either pH conditions.

To address if pH-dependent FcRn binding of the Quads translated into rescue from intracellular degradation, a human endothelial cell-based recycling assay (HERA) based on the adherent human endothelial cell line stably overexpressing human hFcRn (HMEC1-hFcRn) was employed.[13] Equimolar amounts of Q190 and Q191 were added to the cells in parallel with full-length IgG1. After 3 h of incubation, cells were either lysed to assess the amounts taken up or washed and placed in the IgG-depleted growth medium to allow for cell-internalized molecules to be recycled and released into the medium. After an additional 3 h incubation period, the medium was collected, and the cells were lysed. To quantify the levels of cellular uptake, recycling, and accumulation, samples were analyzed in a two-way Fc-specific ELISA. Data showed that more than fivefold of Q190 and Q191 was detected inside the cells after the uptake step compared to full-length IgG1 (Figure 2D). About 2.5-fold more of the Quads were recycled back to the medium (Figure 2E), while about 7.0-fold more were detected inside the cells at the termination of the assay compared with IgG1 (Figure 2F). Thus, the Quads were found to be exocytosed and released into the medium and, as such, rescued from intracellular degradation, which is in line with pH-dependent hFcRn binding in ELISA. The increased avidity for receptor binding gained through the presence of additional Fc in Quad antibodies may explain the increased uptake, recycling, and accumulation inside cells compared with that of IgG1. To this end, we would expect the Quads to be rescued by hFcRn *in vivo* with a plasma half-life comparable to that of conventional IgG, but further investigation would be required in an *in vivo* setting, such as an hFcRn transgenic mouse model, to define the precise pharmacokinetic parameters of Quad-based antibodies.

In contrast to other self-assembly domains, such as those based on human apoferritin,[28] the spatial arrangement of the p53 tetramerization product enables the Fc regions to dimerize in the scaffold in a stoichiometry of one Fc to two self-assembly proteins. Although restricted to iterations of two, antigen-binding domains fused to Fc regions affords a clear 1:2 and 1:4 stoichiometry of Fc:antigen-binding domain in a configuration that is accessible to FcRn-mediated recycling, without adding further engineering steps and complexity to the production method.

Multivalent Quads Show Enhanced Blocking Potency. The C2-nanobody-binding domain used to engineer the different Quad formats has previously been shown to neutralize α-cbtx *in vivo*.[9] In an ELISA-based blocking assay, the nanobody and the different Quad formats were analyzed for their ability to block the interaction between α-cbtx and the acetylcholine receptor (AChR). To assess the effect of increased binding domain valency on the neutralization potency, Quad proteins were directly compared to the monovalent nanobody in the blocking assay. As expected, an increase in neutralization potency was observed for the multivalent Quad proteins compared to the monovalent nanobody (Figure 3A and Table 1), and the IC_{50} and apparent K_D values measured using FIDA correlated with the increasing binding domain valency (Figure 3B).

Estimating the binding stoichiometry of a representative tetravalent (Q187, N = 3.84), octavalent (Q189, N = 8.03), and hexadecavalent (Q207/208, N = 13.4) Quad by isothermal titration calorimetry indicated that the nanobody domains present in the scaffolds, whether fused adjacently or in tandem to one another, were all accessible to α-cbtx (Figure 2C). Further analysis of thermodynamic parameters verified that binding of the nanobody domains to α-cbtx was only modestly dependent of neighboring nanobody binding domains in the scaffold, with binding enthalpies (16.7−18.1 kcal/mol) and affinities (K_D = 7−10 nM) for Quads being comparable to the monovalent nanobody (18.8 kcal/mol, 5.1 nM) (Figure 3C and Table S5). The modular design of the nanobody domains within the Quad scaffold opens up the possibility to engineer bispecific or multispecific Quad formats that can neutralize multiple different toxins simultaneously. The use of such multispecific molecules could, thus, reduce the number of components required in a prospective recombinant antivenom product, thereby likely simplifying production and formulation, which could lead to a lower cost of manufacture.

Collectively, these data provide the first proof of concept for the retained nanobody binding affinity and blocking efficacy in multivalent Quad proteins, which offers a strategy for tailoring multispecificities, size, and recycling properties.

Cross-Neutralization of Structurally Similar Long Neurotoxins Using a Whole-Cell Patch Clamp Assay. The ability of the C2 nanobody and the Quads to functionally neutralize the effects of α-cbtx and three similar LαNtxs was tested *in vitro* using an automated whole-cell patch-clamp assay. Here, a human-derived rhabdomyosarcoma RD cell line, endogenously expressing the muscle-type nicotinic AChR (nAChR), was used to determine the neutralization capacity of the Quads on the current-inhibiting effect elicited by the toxins. The EC_{80} of acetylcholine as well as the IC_{80}s of four LαNtxs (α-cbtx from *N. kaouthia*, α-elapitoxin (α-eptx) from *Dendroaspis polylepis*, α-bungarotoxin (α-bgtx) from *Bungarus*

https://doi.org/10.1021/acs.bioconjchem.2c00220
Bioconjugate Chem. 2022, 33, 1494−1504

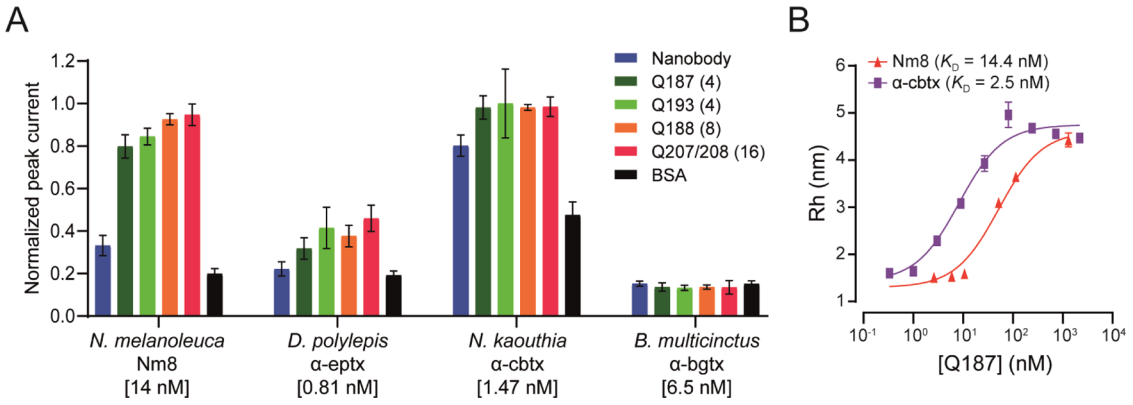

Figure 4. Cross-neutralization of long α-neurotoxins using the C2 nanobody and Quad proteins. (A) Neutralization assessment against α-cbtx from *N. kaouthia,* LαNtxs present in venom fraction Nm8 from *N. melanoleuca*, α-eptx from *D. polylepis,* and α-bgtx from *B. multicinctus*. Error bars represent the ±SD of four replicates. (B) Binding affinity against neutralized LαNtxs characterized using FIDA. Binding profiles were measured as a change in the apparent hydrodynamic radius of the indicators (LαNtxs from *N. kaouthia* and *N. melanoleuca*) following addition of increased concentrations of Q187. The K_D values were calculated from the binding isotherm. Represented results are from a single experiment with technical repeats performed in duplicate.

multicinctus, and a fraction (Nm8) from *N. melanoleuca* containing an isoform of LαNtx OH55 and long α-neurotoxin 2), were determined. IC_{80} values were 1.47 nM for α-cbtx, 0.81 nM for α-eptx, 6.5 nM for α-bgtx, and 14 nM for Nm8. Neutralization was observed for two out of the four toxins tested, with Nm8 from *N. melanoleuca* venom being neutralized alongside the cognate α-cbtx (Figure 4A). The benefit of increased binding domain valency of Quads, resulting in increased functional affinity, corresponding to low nM apparent K_D values as determined by FIDA (Figure 4B), can be seen from their ability to fully neutralize both α-cbtx and the LαNtxs present in venom fraction Nm8. Although there was evidence of binding to α-eptx, Quads were unable to achieve full neutralization at the concentrations tested, indicating that the affinity between the Quads and this toxin was possibly too low for neutralization at the tested Quad to toxin ratio. In this relation, it is possible that better neutralization could be achieved using higher Quad concentrations. For α-bgtx, no inhibitory effects were observed, which was not unexpected, as this toxin shares the lowest level of sequence identity relative to α-cbtx (58%), compared to the isoform of LαNtx OH55 (72%) and long α-neurotoxin 2 (83%) from *N. melanoleuca* and α-eptx (79%) from *D. polylepis*. In summary, presenting the neutralizing nanobody in the different Quad formats improves neutralization potency across closely related toxins, suggesting that key interfacial determinants responsible for broad reactivity are maintained within the Quad scaffold.

CONCLUSIONS

In this work, we employed a protein engineering approach to construct tetrameric proteins, termed Quads, comprising a nanobody binding domain and a p53 tetramerization domain, with or without additional Fc domains. These Quad proteins could be engineered to have increased valency of up to 16 binding domains and hydrodynamic radii ranging between 4.58 and 9.06 nm. Importantly, the Quads displayed improved blocking and neutralization *in vitro* and were also able to cross-neutralize LαNtxs from *N. melanoleuca* and, to a lesser degree, neutralize α-eptx from *D. polylepis*. Therefore, this multivalent binding protein concept presents a tunable and versatile technology platform for enhancing the potency of existing nanobodies simply by multimerization, allowing for the assembly of a large number of binding domains in a single molecule. Apart from increasing the molecular size and functional affinity, we proved that the Quads retained pH-dependent binding to hFcRn, which translated into cellular recycling, predictive for half-life extension *in vivo*.[29] These parameters could potentially be used to further improve the efficacy and pharmacokinetic properties of nanobodies targeting snake toxins. In this relation, one possibility could be to develop Quad molecules with multiple different nanobodies targeting different toxins in a multispecific and multivalent format, enabling that a single molecule could be used to target complex toxin mixtures, i.e., snake venoms. Moreover, the application of Quads outside the context of recombinant antivenom could also find utility in disease settings that rely on avidity for increased safety and potency, such as receptor superclustering, engagement of receptors involved in viral escape and immune regulation, and general multiprotein targeting.

METHODS

Cloning, Protein Expression, and Purification of Multivalent Anti-α-cobratoxin Quads and Chimeric α7-AChR. The sequence of a high-affinity llama-derived nanobody (C2 V_HH) against α-cbtx[9] was used as the binding domain to generate Quads, as previously described.[18,30] Quad expression plasmids were designed to contain the C2 anti-α-cbtx nanobody sequence linked to either the human p53 tetramerization domain via a flexible linker $(G_4S)_2$ in some configurations or linked to the human IgG1 Fc via the hinge region in other configurations. For those formats containing Fc, the p53-TD domain was linked directly onto the C-terminus of the CH3 domain without any linkers. In configurations where V_HHs were linked in tandem, a short linker (G_4S) was used. A gene encoding a chimeric version of the extracellular domain of α7-acetylcholine receptor (α7-AChR) was also introduced into the pTT5 expression vector.[31] Genes were all constructed through DNA synthesis (Twist Bioscience), and all constructs contained a C-terminal polyhistidine tag to facilitate purification. Recombinant proteins were generated through transient transfection in HEK293 cells using Expifectamine 293 reagent according to

https://doi.org/10.1021/acs.bioconjchem.2c00220
Bioconjugate Chem. 2022, 33, 1494−1504

the manufacturer's recommendations (Thermo Fisher Scientific). Multimerized C2 Quad proteins and recombinant chimeric α7-AChR were purified directly from the culture supernatant using His60 Ni Superflow gravity columns (Clonetech). All proteins were buffer exchanged and concentrated into PBS (137 mM NaCl, 3 mM KCl, 8 mM $Na_2HPO_4{\cdot}2H_2O$, 1.4 mM KH_2PO_4, pH 7.4) using Amicon columns (Millipore), and aliquots were stored at 4 or −80 °C for long-term storage.

Size-Exclusion Chromatography. Quad proteins were analyzed at a concentration of 1 mg/mL using an NGC Quest 10 plus chromatography system with a HiLoad Superdex200 increase 10/300 GL with PBS as an eluent. The flow rate used was 0.5 mL/min. The observed size of the proteins was determined for the elution volumes of the main peak after calibration of the column with high-molecular-weight protein standards (protein standard mix 15−600 kDa, 69385, Sigma-Aldrich).

Toxin Labeling and Biotinylation. Lyophilized α-cbtx (Latoxan, L8114) was labeled with Alexa-Fluor 488 TFP ester as per the manufacturer's guidelines (Thermo Fisher, 208121). Briefly, the toxin solution (50 μg, 1 mg/mL in PBS) was pH adjusted by adding a tenth volume of 1 M sodium hydroxide. Labeling was performed by adding a twofold molar excess of the dye and incubating at room temperature for 15 min. Free dye was subsequently removed using a dye removal column (Pierce Dye removal column) following the kit instructions, and the presence of free dye was checked using a FIDA One instrument (FIDA Biosystems). Protein concentration was measured using a NanoDrop (Thermo Scientific), and the dye contribution to the absorbance at 280 nm reading was accounted for using equations described in the referenced protocol.

Biotinylation of α-cbtx was performed using EZ-Link NHS-PEG_4-Biotin at a 1:1.5 (toxin/biotinylation reagent) molar ratio and was purified using Amicon Ultra-4 Centrifugal Filter Units with a 3 kDa MWCO membrane, as previously described.[8] The degree of biotinylation was analyzed using MALDI-TOF in an Ultraflex II TOF/TOF spectrometer (Bruker Daltonics).

α-cbtx Binding Analysis by Indirect ELISA. High-binding 96-well plates (Corning) were coated overnight at 4 °C with 50 ng/well of α-cbtx resuspended in PBS. With three washes in between each subsequent step using PBST (137 mM NaCl, 3 mM KCl, 8 mM $Na_2HPO_4{\cdot}2H_2O$, 1.4 mM KH_2PO_4, 0.1% (v/v) Tween 20) and incubation at room temperature for 1 h, the coated ELISA plates were blocked with PBST + 1% (w/v) BSA (NEB, B9000S), followed by the addition of serially diluted 1 in 3-fold of anti-α-cbtx Quads, starting with a top concentration of 5 μg/mL performed in duplicate. Specific binding of anti-α-cbtx Quads to α-cbtx was detected with the addition of HRP-conjugated anti-His (Abcam, diluted 1:10,000 in PBST), followed by the addition of 100 μL/well of 3,3′,5,5′-tetramethylbenzidine (TMB) to generate the assay signal. The colorimetric reaction was stopped with the addition of 1 M sulfuric acid, and the absorbance was measured at 450 nm using a CLARIOstar microplate reader (BMG Labtech). The dissociation constants were calculated from the curves as described previously,[32] and presented data points are displayed as mean ± SD values of duplicate measurements.

FIDA Binding Analysis Instrument Setup. Affinity measurements were conducted on a FIDA One instrument, using light-emitting diode (LED)-induced fluorescence detection (FIDA Biosystems ApS, Copenhagen, Denmark) with an excitation wavelength of 480 nm and a high-pass emission filter (515 nm cut-off). A standard fused-silica capillary (inner diameter: 75 μm, outer diameter: 375 μm, length total: 100 cm, length to detection window: 84 cm, Fida Biosystems ApS) was coated with HS reagent (Fida Biosystems ApS). The capillary was prepared by rinsing with 1 M NaOH for 600 s at 3500 mbar and washed with MilliQ water for 300 s at 3500 mbar. The HS reagent was applied for 600 s at 3500 mbar, followed by a final MilliQ wash, and the baseline was allowed to normalize overnight in water.

FIDA Binding Characterization of Quad Molecules. Labeled α-cbtx, termed indicator, was diluted to a fixed concentration of 100 nM, and binding was measured as a product of average complex size change over a threefold dilution series (0.11−2,187 nM) of Quad, termed analyte, in PBST (PBS supplemented with 0.05% Tween) buffer. The indicator and analyte were held in separate vials and mixed within the capillary. The template for each assay cycle commenced by equilibrating the capillary with running buffer at 3500 mbar, followed by the sequential injection of analyte and indicator for 20 s at 3500 mbar and 10 s at 50 mbar, respectively. Mobilization of indicator and analyte toward the detector was initiated with a final injection of analyte for 180 s at 400 mbar. To improve diffusivity of larger Quads, a mobilization time of 430 s at 167 mbar was applied, and for Quads that interacted more strongly with the capillary, a wash step consisting of 300 s at 3500 mbar using 1 M NaCl and 1% Tween was used. Each signal (Taylorgram) was processed in the FIDA One data analysis software (V2.04), whereby the change in diffusivity following binding was converted into the hydrodynamic radius using equations described previously.[33] The Taylorgram fraction was adjusted manually to ensure that there was a sufficient baseline to ensure accurate fitting, and a minimal fitting fraction was employed. A mean data point of duplicate measurements of the hydrodynamic radius for each analyte concentration was plotted on a log10 scale in FIDA analysis software, and a 1:1 toxin/Quad binding stoichiometry and an excess indicator model were used to fit the measurements. The K_D values were calculated directly from the binding isotherm fits.[33] Proteins and running buffer were kept in separate compartment chambers at 4 °C and room temperature, respectively. Technical repeats for each Quad were performed at least to the duplicate level at a capillary temperature of 25 °C.

Dynamic Light Scattering (DLS). The Dh of the Quads was determined by dynamic light scattering using a ZETASIZER NANO (Malvern) instrument. Quad protein (1 mg/mL, PBS) was spun at a maximum speed for 10 min at 4 °C and added to a 1 mL cuvette (LabX, DTS0012) and measured at a fixed temperature of 20 °C with a duration of 10 s per read. Particle size determinations were obtained from an accumulation of three reads using the instrument software.

Isothermal Titration Calorimetry (ITC). The binding affinities between α-cbtx and the C2 nanobody and selected Quad molecules were analyzed by ITC, using a MicroCal ITC_{200} instrument (Malvern Panalytical) at 25 °C. Proteins were dialyzed (Thermo Scientific Slide-A-Lyzer Dialysis Cassettes, 3.5 K MWCO, 0.5 mL: 11859410) against 250 volumes of sterile PBS, followed by centrifugation at max speed at 4 °C for 20 min. Thereafter, protein concentrations were determined using the theoretical molar extinction coefficients calculated based on the amino acid content using the Expasy

https://doi.org/10.1021/acs.bioconjchem.2c00220
Bioconjugate Chem. 2022, 33, 1494−1504

ProtParam tool. The C2 nanobody and the Quads were loaded in the cell and titrated with the toxin, and the nanobody was diluted to 30 μM in the cell and the toxin to 300 μM in the syringe. For the Quads with 4, 8, and 16 binding sites, the toxin concentration was fixed to 220 μM and Quads diluted to 4, 2, and 1 μM, respectively. The titrations were carried out in two independent duplicates using different toxin batches at 25 °C, starting with an injection of 0.4 μL followed by 19 injections of 2.0 μL (subsequently spaced by 240 s between the injections). After correction with the heat of dilution, as determined by blank injections of toxins into a buffer using the same injection regiment as for the toxin-protein titrations, the thermograms were integrated. A single set of equivalent and independent binding site model was fit to the resulting binding isotherms, which allowed for the determination of the equilibrium association constant (K_A), the binding stoichiometry (N), and the molar binding enthalpy (ΔH). The data are reported as the mean ± SD of duplicate measurements, and data processing and model fits were performed using the Origin plug-in provided with the instrument.

FcRn Binding ELISA. ELISA was performed to quantify the FcRn binding of the Quad molecules in a pH-dependent manner. Quads (Q187, Q190, and Q191) and control (full-length IgG1 WT) were designed, produced, and purified as described previously.[13,34−36] Molecules were diluted in PBS at a final dilution ranging from 0.488 to 1,000 ng/mL and coated by adding 100 μL to ELISA wells and incubated at 4 °C overnight. Plates were blocked by adding 250 μL of PBS supplemented with 4% (w/v) skimmed milk (M; VWR, A0830), followed by incubation on a shaker for 1 h at room temperature. Plates were washed four times with 200 μL of PBST between all subsequent steps. Next, biotinylated truncated monomeric hFcRn (hFcRn-bio) (Immunitrack, ITF01) was incubated with streptavidin conjugated with alkaline phosphatase (Roche, 11089161001) at a 1:1 molar ratio for 20 min and added to the plate at final concentrations of 0.25 μg/mL FcRn and 3.36 μg/mL streptavidin-AP diluted in PBST-M (pH 5.5 and 7.4, respectively). After 1 h, the ELISA signal was developed by adding 100 μL of 10 μg/mL *p*-nitrophenyl-phosphate substrate (Sigma-Aldrich, S0942-200TAB) dissolved in diethanolamine solution to all wells. A Sunrise spectrophotometer (Tecan) was used to measure absorbance at 405 nm.

Human Endothelial Cell Line Stably Overexpressing hFcRn. HMEC-1 cells stably expressing HA-FcRn-EGFP (HMEC-1-FcRn)[37] were cultured at 37 °C and 8% CO_2 in MCDB131 medium (Gibco, 10372019) supplemented with 2 mM L-glutamine (Sigma, G4251), 25 μg/mL streptomycin/25 U/mL penicillin (Sigma-Aldrich, P4458), 10% FCS (Sigma-Aldrich, F7524), 10 ng/mL mouse epidermal growth factor (Gibco, PMG8043), 1 μg/mL hydrocortisone (Sigma-Aldrich H0888), 100 μg/mL G418 (Gibco, 11558616), and 50 μg/mL blasticidine (Gibco, A1113903) to maintain FcRn expression.

HERA. HERA experiments were performed as described in Grevys et al., 2018.[13] Briefly, 1.5 × 10^5 HMEC-1-FcRn cells were seeded in 250 μL of culturing medium per well in two 48-well plates (Costar) (uptake and recycling plate). The medium was removed from all wells 20−24 h after seeding, and the cells were washed twice in 250 μL of prewarmed Hank's balanced salt solution (HBSS; Thermo Fisher, 14025100). Cells were starved at 37 °C for 1 h in the prewarmed HBSS. Next, anti-NIP-IgG1 and Quad molecules (Q190 and Q191) were prepared at a final concentration of 800 nM in the prewarmed HBSS and added to cells at a final volume of 125 μL in technical triplicates in both plates. After a 3 h incubation period, the samples were removed, and the cells were washed four times in 250 μL ice-cold HBSS. Uptake plates were frozen at −80 °C following aspiration of washing medium, while 220 μL of prewarmed serum-free growth medium supplemented with 1X MEM nonessential amino acids (Gibco, 11140-050) was added to the recycling plates. After another 3 h incubation period, recycling samples were harvested and frozen at −20 °C. Residual plates were washed four times with ice-cold HBSS and frozen at −80 °C to the day of analysis.

For HERA analysis, frozen cells were lysed by adding 220 μL of RIPA buffer (Thermo Fisher, 89901) supplemented with 1X complete protease inhibitor cocktail (Roche, 11836145001) and incubated on a shaker for 10 min on ice. Cellular debris were removed by 5 min centrifugation at 10,000*g*. Proteins present in the lysates and recycling medium were quantified by two-way anti-Fc ELISA. Ninety-six well plates (Costar) were coated with anti-hIgG Fc (Sigma, I2136) diluted 1:1,000 in PBS and incubated overnight at 4 °C. The next day, plates were blocked by adding 250 μL of PBST-M and washed four times with PBST. Next, cell lysates (containing uptake and residual) and medium (containing recycled proteins) were added to the plates, in addition to serial dilutions from 0.122 to 250 ng/mL of the proteins tested diluted in PBST-M, which were used as standards to quantify protein levels. Following a 2 h incubation period at room temperature, a goat anti-human Fc polyclonal antibody conjugated to alkaline phosphatase (Sigma-Aldrich, A9544) diluted 1:5,000 in PBST-M was added and incubated for 1 h at room temperature. The ELISA was developed, and absorbance was measured as indicated above.

HERA experiments were independent and numerical data were summarized as the mean ± SD using GraphPad Prism9 software (San Diego, CA). Each global mean was compared using an unpaired Student's *t*-test. Two-tailed *p*-values ≤ 0.05 were considered statistically significant.

In Vitro Blocking ELISA. *In vitro* neutralization of the α-cbtx interaction with α7-AChR by Quads was performed using a similar ELISA protocol to that described above but with some modifications. Briefly, high-binding 96-well plates (Corning) were coated overnight at 4 °C with 100 ng of α7-AChR/well. With three washes in between each subsequent step, using PBST (PBS + 0.1% Tween 20), and incubation at room temperature for 1 h, the coated ELISA plates were blocked with 1% BSA. Next, mixtures of serially diluted anti-α-cbtx Quads starting at 5 μg/mL and a fixed amount of biotinylated α-cbtx (0.0175 μg/mL) were preincubated at room temperature for 30 min prior to being added to the coated plates. Wells containing only the biotinylated α-cbtx with no added anti-α-cbtx Quad or wells containing blocking buffer only (0.1% BSA in PBST) were used as controls to determine the percentage α-cbtx α7-AChR binding inhibition. Free α-cbtx bound to α7-AChR was detected using HRP-conjugated streptavidin (Abcam, 1 in 15,000 dilution in PBST). The ELISA signal was measured as described above in the indirect ELISA. Each concentration was run in duplicate and presented as mean ± SD values.

***In Vitro* Cross-Neutralization of Long α-Neurotoxins Using an Automated Patch Clamp.** Planar whole-cell patch-clamp experiments were carried out on a Qube 384 automated electrophysiology platform (Sophion Bioscience), where 384-channel patch chips with 10 parallel patch holes per

https://doi.org/10.1021/acs.bioconjchem.2c00220
Bioconjugate Chem. 2022, 33, 1494−1504

channel (patch hole diameter ~1 μm, resistance 2.00 ± 0.02 MΩ) were used.

A human-derived rhabdomyosarcoma RD cell line (CCL-136, from ATCC) endogenously expressing the muscle-type nicotinic acetylcholine receptors (nAChR) composed of the α1, β1, δ, γ, and ε subunits was used. The cells were cultured according to the manufacturer's guidelines. On the day of the experiment, cells were enzymatically detached from the culture flask and brought into suspension. For patching, the extracellular solution contained 145 mM NaCl, 10 mM HEPES, 4 mM KCl, 1 mM $MgCl_2$, 2 mM $CaCl_2$, and 10 mM glucose, pH adjusted to 7.4, and osmolality adjusted to 296 mOsm, while the intracellular solution contained 140 mM CsF, 10 mM HEPES, 10 mM NaCl, 10 mM EGTA, pH adjusted to 7.3, and osmolality adjusted to 290 mOsm.

In the experiments, an nAChR-mediated current was elicited by 70 μM acetylcholine (ACh, Sigma-Aldrich), approximately the EC_{80} value, and after compound wash-out, 2 U acetylcholinesterase (Sigma-Aldrich) was added to ensure complete ACh removal. A second ACh addition was used to evaluate the effect of the toxin (app. IC_{80} value; α-cbtx 1.5 nM; α-eptx 0.81 nM; α-bgtx 6.4 nM; Nm8 14.0 nM) in combination with 3 nM of Quad. Toxins and Quads were prepared in extracellular solution supplemented with 0.1% BSA and co-incubated for at least 30 min before application, and the patched cells were preincubated with the toxin and Quad mixture for 5 min prior to the second ACh addition. Measurements were performed in quadruplicate, and the error is reported as the mean ± SD. The inhibitory effect of the toxins was normalized to the full ACh response and averaged in the group. The data analysis was performed in a Sophion analyzer (Sophion Bioscience).

■ ASSOCIATED CONTENT

Supporting Information

The Supporting Information is available free of charge at https://pubs.acs.org/doi/10.1021/acs.bioconjchem.2c00220.

FIDA complex sizes and affinities; ITC thermodynamic parameters; ELISA binding; SEC retention volumes; percentage areas; and calculated molecular weights and DLS (Tables S1−S6) (PDF)

■ AUTHOR INFORMATION

Corresponding Authors

Andreas H. Laustsen − *Department of Biotechnology and Biomedicine, Technical University of Denmark, DK-2800 Kongens, Lyngby, Denmark;* orcid.org/0000-0001-6918-5574; Email: ahola@bio.dtu.dk

Fulgencio Ruso-Julve − *Department of Immunology, Oslo University Hospital Rikshospitalet, N-0372 Oslo, Norway; Department of Pharmacology, Institute of Clinical Medicine, University of Oslo, N-0372 Oslo, Norway;* orcid.org/0000-0001-6500-6807; Email: fulgencr@medisin.uio.no

Authors

Jack Wade − *Department of Biotechnology and Biomedicine, Technical University of Denmark, DK-2800 Kongens, Lyngby, Denmark;* orcid.org/0000-0001-5465-7399

Charlotte Rimbault − *Department of Biotechnology and Biomedicine, Technical University of Denmark, DK-2800 Kongens, Lyngby, Denmark;* orcid.org/0000-0002-4760-8430

Hanif Ali − *Quadrucept Bio Ltd., London EC1V 2NX, United Kingdom*

Line Ledsgaard − *Department of Biotechnology and Biomedicine, Technical University of Denmark, DK-2800 Kongens, Lyngby, Denmark*

Esperanza Rivera-de-Torre − *Department of Biotechnology and Biomedicine, Technical University of Denmark, DK-2800 Kongens, Lyngby, Denmark*

Maher Abou Hachem − *Department of Biotechnology and Biomedicine, Technical University of Denmark, DK-2800 Kongens, Lyngby, Denmark;* orcid.org/0000-0001-8250-1842

Kim Boddum − *Sophion Bioscience, DK-2750 Ballerup, Denmark*

Nadia Mirza − *Fida Biosystems ApS, DK-2860 Søborg, Copenhagen, Denmark*

Markus-Frederik Bohn − *Department of Biotechnology and Biomedicine, Technical University of Denmark, DK-2800 Kongens, Lyngby, Denmark*

Siri A. Sakya − *Department of Immunology, Oslo University Hospital Rikshospitalet, N-0372 Oslo, Norway; Department of Pharmacology, Institute of Clinical Medicine, University of Oslo, N-0372 Oslo, Norway*

Jan Terje Andersen − *Department of Immunology, Oslo University Hospital Rikshospitalet, N-0372 Oslo, Norway; Department of Pharmacology, Institute of Clinical Medicine, University of Oslo, N-0372 Oslo, Norway;* orcid.org/0000-0003-1710-1628

Complete contact information is available at: https://pubs.acs.org/10.1021/acs.bioconjchem.2c00220

Author Contributions

▽J.W. and C.R. contributed equally to this work.

Notes

The authors declare the following competing financial interest(s): Hanif Ali is a shareholder in Quadrucept Bio Ltd and is a named inventor on patent applications covering Quad multimerization technology and related features.

■ ACKNOWLEDGMENTS

The authors are supported by a grant from the European Research Council (ERC) under the European Union's Horizon 2020 research and innovation programme (grant no. 850974) and by a grant from the Villum Foundation (grant no. 00025302). The authors would also like to thank Fidabio for technical assistance, data analysis, and instrument handling. The Carlsberg Foundation is acknowledged for Research Infrastructure grant (grant no. 2011-01-0598) for the ITC instrument and for Research Infrastructure grant (grant no. CF19-0055) for the FIDA One instrument. J.T.A., F.R.-J., and S.A.S. were funded by the Research Council of Norway (grant nos. 287927 and 314909).

■ REFERENCES

(1) Bolon, I.; Durso, A. M.; Botero Mesa, S.; Ray, N.; Alcoba, G.; Chappuis, F.; Ruiz de Castañeda, R. Identifying the Snake: First Scoping Review on Practices of Communities and Healthcare Providers Confronted with Snakebite across the World. *PLoS One* **2020**, *15*, No. e0229989.

(2) Gutiérrez, J. M.; Calvete, J. J.; Habib, A. G.; Harrison, R. A.; Williams, D. J.; Warrell, D. A. Snakebite Envenoming. *Nat. Rev. Dis. Primers* **2017**, *3*, No. 17063.

(3) Laustsen, A.; Engmark, M.; Milbo, C.; Johannesen, J.; Lomonte, B.; Gutiérrez, J.; Lohse, B. From Fangs to Pharmacology: The Future of Snakebite Envenoming Therapy. *Curr. Pharm. Des.* **2016**, *22*, 5270−5293.
(4) Gutiérrez, J. M.; Williams, D.; Fan, H. W.; Warrell, D. A. Snakebite Envenoming from a Global Perspective: Towards an Integrated Approach. *Toxicon* **2010**, *56*, 1223−1235.
(5) Laustsen, A. H.; María Gutiérrez, J.; Knudsen, C.; Johansen, K. H.; Bermúdez-Méndez, E.; Cerni, F. A.; Jürgensen, J. A.; Ledsgaard, L.; Martos-Esteban, A.; Øhlenschlæger, M.; et al. Pros and Cons of Different Therapeutic Antibody Formats for Recombinant Antivenom Development. *Toxicon* **2018**, *146*, 151−175.
(6) Hong, H.; Li, C.; Gong, L.; Wang, J.; Li, D.; Shi, J.; Zhou, Z.; Huang, Z.; Wu, Z. Universal Endogenous Antibody Recruiting Nanobodies Capable of Triggering Immune Effectors for Targeted Cancer Immunotherapy. *Chem. Sci.* **2021**, *12*, 4623−4630.
(7) Laustsen, A. H.; Karatt-Vellatt, A.; Masters, E. W.; Arias, A. S.; Pus, U.; Knudsen, C.; Oscoz, S.; Slavny, P.; Griffiths, D. T.; Luther, A. M.; et al. In Vivo Neutralization of Dendrotoxin-Mediated Neurotoxicity of Black Mamba Venom by Oligoclonal Human IgG Antibodies. *Nat. Commun.* **2018**, *9*, No. 3928.
(8) Ledsgaard, L.; Laustsen, A. H.; Pus, U.; Wade, J.; Villar, P.; Boddum, K.; Slavny, P.; Masters, E. W.; Arias, A. S.; Oscoz, S.; et al. *In vitro* discovery of a human monoclonal antibody that neutralizes lethality of cobra snake venom. *mAbs* **2022**, *14*, No. 2085536.
(9) Richard, G.; Meyers, A. J.; McLean, M. D.; Arbabi-Ghahroudi, M.; MacKenzie, R.; Hall, J. C. In Vivo Neutralization of α-Cobratoxin with High-Affinity Llama Single-Domain Antibodies (VHHs) and a VHH-Fc Antibody. *PLoS One* **2013**, *8*, No. e69495.
(10) Rossotti, M. A.; Bélanger, K.; Henry, K. A.; Tanha, J. Immunogenicity and Humanization of Single-domain Antibodies. *FEBS J.* **2021**, No. febs.15809.
(11) Yang, M.; Zhu, G.; Korza, G.; Sun, X.; Setlow, P.; Li, J. Engineering Bacillus Subtilis as a Versatile and Stable Platform for Production of Nanobodies. *Appl. Environ. Microbiol.* **2020**, *86*, No. e02938-19.
(12) Salema, V.; Fernández, L. Á. High Yield Purification of Nanobodies from the Periplasm of E. Coli as Fusions with the Maltose Binding Protein. *Protein Expression Purif.* **2013**, *91*, 42−48.
(13) Grevys, A.; Nilsen, J.; Sand, K. M. K.; Daba, M. B.; Øynebråten, I.; Bern, M.; McAdam, M. B.; Foss, S.; Schlothauer, T.; Michaelsen, T. E.; et al. A Human Endothelial Cell-Based Recycling Assay for Screening of FcRn Targeted Molecules. *Nat. Commun.* **2018**, *9*, No. 621.
(14) Ward, E. S.; Ober, R. J. Targeting FcRn to Generate Antibody-Based Therapeutics. *Trends Pharmacol. Sci.* **2018**, *39*, 892−904.
(15) Dall'Acqua, W. F.; Kiener, P. A.; Wu, H. Properties of Human IgG1s Engineered for Enhanced Binding to the Neonatal Fc Receptor (FcRn). *J. Biol. Chem.* **2006**, *281*, 23514−23524.
(16) Bern, M.; Nilsen, J.; Ferrarese, M.; Sand, K. M. K.; Gjølberg, T. T.; Lode, H. E.; Davidson, R. J.; Camire, R. M.; Bækkevold, E. S.; Foss, S.; et al. An Engineered Human Albumin Enhances Half-Life and Transmucosal Delivery When Fused to Protein-Based Biologics. *Sci. Transl. Med.* **2020**, *12*, No. abb0580.
(17) Knudsen, C.; Ledsgaard, L.; Dehli, R. I.; Ahmadi, S.; Sørensen, C. V.; Laustsen, A. H. Engineering and Design Considerations for Next-Generation Snakebite Antivenoms. *Toxicon* **2019**, *167*, 67−75.
(18) Miller, A.; Carr, S.; Rabbitts, T.; Ali, H. Multimeric Antibodies with Increased Valency Surpassing Functional Affinity and Potency Thresholds Using Novel Formats. *mAbs* **2020**, *12*, No. 1752529.
(19) Miersch, S.; Li, Z.; Saberianfar, R.; Ustav, M.; Brett Case, J.; Blazer, L.; Chen, C.; Ye, W.; Pavlenco, A.; Gorelik, M.; et al. Tetravalent SARS-CoV-2 Neutralizing Antibodies Show Enhanced Potency and Resistance to Escape Mutations. *J. Mol. Biol.* **2021**, *433*, No. 167177.
(20) Lee, Y. J.; Jeong, K. J. Challenges to Production of Antibodies in Bacteria and Yeast. *J. Biosci. Bioeng.* **2015**, *120*, 483−490.
(21) Cao, J.; Perez-Pinera, P.; Lowenhaupt, K.; Wu, M.-R.; Purcell, O.; de la Fuente-Nunez, C.; Lu, T. K. Versatile and On-Demand Biologics Co-Production in Yeast. *Nat. Commun.* **2018**, *9*, No. 77.
(22) Du, B.; Jiang, X.; Das, A.; Zhou, Q.; Yu, M.; Jin, R.; Zheng, J. Glomerular Barrier Behaves as an Atomically Precise Bandpass Filter in a Sub-Nanometre Regime. *Nat. Nanotechnol.* **2017**, *12*, 1096−1102.
(23) Radomsky, M. Macromolecules Released from Polymers: Diffusion into Unstirred Fluids. *Biomaterials* **1990**, *11*, 619−624.
(24) Pedersen, M. E.; Østergaard, J.; Glintborg, B.; Hetland, M. L.; Jensen, H. Assessment of Immunogenicity and Drug Activity in Patient Sera by Flow-Induced Dispersion Analysis. *Sci. Rep.* **2022**, *12*, No. 4670.
(25) Katchman, B. A.; Barderas, R.; Alam, R.; Chowell, D.; Field, M. S.; Esserman, L. J.; Wallstrom, G.; LaBaer, J.; Cramer, D. W.; Hollingsworth, M. A.; Anderson, K. S. Proteomic Mapping of P53 Immunogenicity in Pancreatic, Ovarian, and Breast Cancers. *Proteomics: Clin. Appl.* **2016**, *10*, 720−731.
(26) Ward, E. S.; Devanaboyina, S. C.; Ober, R. J. Targeting FcRn for the Modulation of Antibody Dynamics. *Mol. Immunol.* **2015**, *67*, 131−141.
(27) Pyzik, M.; Sand, K. M. K.; Hubbard, J. J.; Andersen, J. T.; Sandlie, I.; Blumberg, R. S. The Neonatal Fc Receptor (FcRn): A Misnomer? *Front. Immunol.* **2019**, *10*, No. 1540.
(28) Rujas, E.; Kucharska, I.; Tan, Y. Z.; Benlekbir, S.; Cui, H.; Zhao, T.; Wasney, G. A.; Budylowski, P.; Guvenc, F.; Newton, J. C.; et al. Multivalency Transforms SARS-CoV-2 Antibodies into Ultrapotent Neutralizers. *Nat. Commun.* **2021**, *12*, No. 3661.
(29) Grevys, A.; Frick, R.; Mester, S.; Flem-Karlsen, K.; Nilsen, J.; Foss, S.; Sand, K. M. K.; Emrich, T.; Fischer, J. A. A.; Greiff, V.; et al. Antibody Variable Sequences Have a Pronounced Effect on Cellular Transport and Plasma Half-Life. *iScience* **2022**, *25*, No. 103746.
(30) Miller, A.; Leach, A.; Thomas, J.; McAndrew, C.; Bentley, E.; Mattiuzzo, G.; John, L.; Mirazimi, A.; Harris, G.; Gamage, N.; et al. A Super-Potent Tetramerized ACE2 Protein Displays Enhanced Neutralization of SARS-CoV-2 Virus Infection. *Sci. Rep.* **2021**, *11*, No. 10617.
(31) Li, S.-X.; Huang, S.; Bren, N.; Noridomi, K.; Dellisanti, C. D.; Sine, S. M.; Chen, L. Ligand-Binding Domain of an A7-Nicotinic Receptor Chimera and Its Complex with Agonist. *Nat. Neurosci.* **2011**, *14*, 1253−1259.
(32) Eble, J. A. Titration ELISA as a Method to Determine the Dissociation Constant of Receptor Ligand Interaction. *J. Vis. Exp.* **2018**, No. e57334.
(33) Pedersen, M. E.; Gad, S. I.; Østergaard, J.; Jensen, H. Protein Characterization in 3D: Size, Folding, and Functional Assessment in a Unified Approach. *Anal. Chem.* **2019**, *91*, 4975−4979.
(34) Grevys, A.; Bern, M.; Foss, S.; Bratlie, D. B.; Moen, A.; Gunnarsen, K. S.; Aase, A.; Michaelsen, T. E.; Sandlie, I.; Andersen, J. T. Fc Engineering of Human IgG1 for Altered Binding to the Neonatal Fc Receptor Affects Fc Effector Functions. *J. Immunol.* **2015**, *194*, 5497−5508.
(35) Norderhaug, L.; Olafsen, T.; Michaelsen, T. E.; Sandlie, I. Versatile Vectors for Transient and Stable Expression of Recombinant Antibody Molecules in Mammalian Cells. *J. Immunol. Methods* **1997**, *204*, 77−87.
(36) Foss, S.; Watkinson, R. E.; Grevys, A.; McAdam, M. B.; Bern, M.; Høydahl, L. S.; Dalhus, B.; Michaelsen, T. E.; Sandlie, I.; James, L. C.; Andersen, J. T. TRIM21 Immune Signaling Is More Sensitive to Antibody Affinity Than Its Neutralization Activity. *J. Immunol.* **2016**, *196*, 3452−3459.
(37) Weflen, A. W.; Baier, N.; Tang, Q.-J.; Van den Hof, M.; Blumberg, R. S.; Lencer, W. I.; Massol, R. H. Multivalent Immune Complexes Divert FcRn to Lysosomes by Exclusion from Recycling Sorting Tubules. *Mol. Biol. Cell* **2013**, *24*, 2398−2405.

https://doi.org/10.1021/acs.bioconjchem.2c00220
Bioconjugate Chem. 2022, 33, 1494−1504

8. Conclusion and Future perspectives

8.1. **Development of pH-dependent antibodies**

Snakebite envenoming has a crippling effect on the lives of many in developing countries, and there is a need to improve the quality and accessibility of snakebite treatments for these people. This project began by developing the key components for such a treatment in the form of human monoclonal antibodies discovered from a naïve antibody repertoire using phage display technology.[1] The potency of these antibodies, as well as their cross-reactivity, was improved by optimizing the antibody light chain through light chain shuffling. This was followed by the structural characterization of one of these antibodies to understand its unique binding properties, which included both neutralization and pH-dependent antigen binding. These properties may be important in improving the quality and accessibility of snakebite treatment, as they can lead to enhanced potency and lowering of the therapeutic dose.

Understanding how neutralizing antibodies can acquire pH-dependent binding would be informative for the future engineering and discovery of pH-dependent antibodies and was the main aim of this thesis. pH-dependent target binding enables antibodies to have a longer duration of action, such as prolonged neutralization of soluble targets, and may therefore enable such antibodies to potentially be administered at a lower dose.[65] This is due to the release of antigens in acidic endosomes during antibody recycling, which allows an antibody to re-bind another target molecule when recycled back into the bloodstream by FcRn (recycling antibodies). Thus enabling an antibody to neutralize more than one target molecule. Mechanistically understanding how recycling antibodies can bind pH-dependently is usually overlooked during antibody development, and therefore there is limited information available to guide the engineering of this property. The introduction of histidine residues is often employed and has been successfully used to introduce pH-dependent binding into antibodies specific for a range of antigens.[42] However, the number of histidine mutations required can be extensive[1] and potentially lead to sequence liabilities and/or the introduction of non-natural or non-human motifs.

This thesis aimed to increase the understanding of how antibodies can bind pH-dependently to their antigen by using a panel of fully human neutralizing antibodies specific to long-chain α-neurotoxins. Having measured the pronounced effect that affinity maturation via light chain shuffling had on cross-reactivity, improving affinity to different neurotoxins by an order of magnitude, the question was asked whether the antibody light chain could also improve pH-dependent antigen binding. The panel of light chain shuffled antibody clones developed in Chapter 4 were screened for pH-dependent antigen binding, which led to the identification of one antibody clone that consistently showed a near order of magnitude fold difference in antigen binding affinity between pH 7.4 and pH 5.5. Inspecting the sequence of this clone revealed that it had the same histidine profile as antibodies that were non-pH-dependent, and it was hypothesized that pH-dependency could either be encoded independently of histidine residues, or that there was a specific mechanism that allowed the histidine residues to confer pH-dependent binding properties to this antibody. In both scenarios, this could be informative in the future design of pH-dependent antibodies, beyond the single use of histidine residues.

Insights into pH-dependent antibody binding mechanisms have been revealed through X-ray crystallography. In one case, structural analysis of pH-dependent antibodies bound to their antigen has associated pH-dependent binding with the presence of histidine residues in the antibody epitope.[2] In the case of a neutralizing HIV-1 antibody targeting the HIV envelope,

pH-dependent binding was identified inadvertently as a result of a conformational change in the CDRH3 antibody loop.[3] This conformational change was pH-dependent, and translated to pH-dependent binding, with two clear conformational states observed during the characterization of the antibody. Although pH-dependent binding was not a design feature for this antibody, it does progress the current understanding of how antibodies can exhibit pH-dependent binding independently of the antibody paratope and epitope. Structures of the neutralizing HIV-1 antibody have been determined at pH 8.5 and pH 6.1, and the authors showed that the two conformational changes for this antibody were mediated by residues in the interface region between the heavy and light chains. The mechanism for the pH-dependent conformational switching was speculated to be due to changes in the protonation state of a histidine residue on the light chain located in the chain interface, leading to a possible electrostatic repulsion with a lysine residue, and a change in the hydrogen bonding network that opened the conformation of the CDRH3 loop (affecting the CDRH3 loop conformation and introducing pH-dependent binding). However, this mechanism was not confirmed, possibly due to not having sufficiently high-resolution datasets. But also possibly because their interpretations were based on the endpoint, after the pH-determinants within the antibody had taken effect on the antibody structure, and they could only observe the consequence, as opposed to the cause, of pH-dependent binding.

In this study, we identified residues that were responsive to pH in the chain interface region by characterizing the antibody bound at different pH. As with the anti-HIV antibody, our model for pH-dependent binding is reliant on a histidine residue located on the antibody light chain, in the antibody chain interface, which indirectly affects the antibody interaction through the CDRH3 loop. However, in contrast to describing an electrostatic repelling mechanism between protonated histidine and lysine, we describe how a relaxed interface between the heavy chain and light chain allows a histidine residue in this region to affect the CDRH3 loop structure and the interaction with the antigen. Crystallizing the antibody bound at different acidic pH has given us insight into the potential origin of the pH-dependent binding mechanism of this antibody, which was unclear in other crystallography approaches. This could be supported by molecular dynamic simulations to specifically link the identified network changes in the antibody structure to a broader structural change in the paratope to affect binding at pH < 6.0.

The presence of histidine residues in the light chain responsible for conferring pH-dependent binding independently of the antibody paratope has been observed for other antibodies, as has been discussed above for an antibody specific to HIV 1, and has also been discussed in Chapter 5 for an antibody specific to the carcinoembryonic antigen (CEACAM5) antigen.[50] This suggests that a light chain-driven, paratope-independent approach to introducing pH-dependent antigen binding could be a broadly applicable approach to introduce pH-dependent binding into antibodies targeting different target classes. Additionally, these findings indicate the potential need for a paratope-independent approach to introduce pH-dependent antigen-binding properties. As demonstrated in this research, the interactions that were most favourable for antibody function, *i.e.,* the neutralization of long-chain α-neurotoxins, mimicked the conserved interactions that long-chain α-neurotoxins make with the acetylcholine receptor, and were not favourable for pH-dependent antigen binding.

There appears to be a limit to the level of pH-dependent binding that can be engineered with this approach. In this study, we found that the antibody light chain introduced close to an order of magnitude difference in binding strength between pH 7.4 and pH 5.5 for an antibody targeting different long-chain α-neurotoxins. Additionally, the pH-responsive light chain of the anti-CEACAM5 antibody also reported similar fold differences in binding strength in the same pH range.[2] While the affinity of the anti-HIV 1 antibody at acidic and neutral pH was not measured, the study by Prades et al. did find that the conformer associated with acidic pH had

an order of magnitude lower affinity than the dominant conformer at pH 7.4. Collectively, this points to roughly one order of magnitude pH-dependent binding that can be introduced through the light chain independently of the paratope. When engineering antibodies with pH-dependent antigen binding properties, dissociation rates of 10^{-2} s^{-1} to 10^{-3} s^{-1} at pH < 6.0 are desirable for efficient antigen release within the recycling pathway. However, for antibodies with dissociation rates $<10^{-5}$ s^{-1}, exclusively engineering pH-sensitivity through the light chain in a paratope-independent fashion may not reduce the dissociation rate enough at acidic pH to enable sufficient release of antigen. To identify antibodies with other pH-dependent binding mechanisms, immune libraries enriched for higher affinity antibodies can be screened for pH-dependency. Additionally, antibody formats devoid of a light chain, such as nanobodies, could be screened for pH-dependent antibodies to identify exclusive pH-dependent mechanisms.

This project discovered a potent, pH-dependent neutralizing human monoclonal antibody cross-reactive to long-chain α-neurotoxins from a naïve antibody library without applying pH-elution during selections. This highlights that naïve libraries can be a source of antibodies with pH-dependent antigen binding properties, which can be discovered even when phage display selections are designed mostly to improve antibody function, such as cross-panning and affinity stringent selections. In the context of snakebite envenoming therapy, pH-dependent, recycling antibodies may potentially help lower the dose and thereby improve the cost of recombinant antivenoms for people in developing countries. Long-chain α-neurotoxins may be one group of toxins that is particularly relevant to target with a recycling antibody, as they are injected at high doses by many elapid snakes. However, the rate of antibody recycling may need to be increased to match the fast-acting pharmacokinetics of long-chain α-neurotoxins *in vivo* and enable multiple neutralization cycles. If the recycling rate were to be insufficient, then engineering the Fc with mutations to increase the affinity to FcRn at neutral pH has a demonstrated effect on enhancing the rate of recycling and the amount of antigen neutralized by each recycling antibody molecule.[40]

Currently, pH-dependent antibodies are predominantly engineered by employing histidine residues due to the change in charge state that this residue experiences during antibody recycling. Our hypothesis suggests that the change in the charge state of a histidine residue is not the deciding factor in conferring pH-dependent binding, and that the hydrogen bonding network of residues surrounding the histidine within the heavy-light chain interface is equally important in enabling histidine to exert an effect on structure and binding. Proving this hypothesis would facilitate the engineering of pH-dependent antibodies, *e.g.,* by focusing engineering efforts on the heavy-light chain interface region, specifically on hydrogen bonding networks to residues surrounding existing histidine residues in the interface region. This approach could reduce the number of mutations required for introducing pH-dependent antigen binding into monoclonal antibodies, and potentially be less detrimental to the antibody specificity, binding affinity, and function at neutral pH. As observed in our study, pH-dependent antigen binding conferred away from the antibody paratope was not detrimental to any of these parameters.

Lastly, this knowledge could also be utilized to improve the discovery of antibodies with pH-dependent antigen binding properties to many target classes using *in vitro* display technologies. As an example, this could be achieved by engineering a pH-sensitive interface between the antibody heavy and light chains as a pre-determined feature in antibodies within a synthetic *in vitro* display library. Although an antibody with pH-dependent antigen binding properties was discovered in the work behind this thesis when using a validated naïve library, pH-dependent binders were rare. This highlights how advantageous a specialized library for discovering pH-dependent antibodies could potentially be. To this aim, a library has been designed from a non-pH-dependent monoclonal antibody to determine whether pH-dependent binding can be introduced away from the CDR loops in the heavy-light framework chain

interface. Engineering the antibody framework could be advantageous for discovering pH-dependent antibodies, as the framework is less likely to be affected by binding due to having an increased distance to the epitope-paratope interaction. On the other hand, the effect that framework mutations may have on the antibody structure at neutral pH, and therefore how functional a prospective library would be, is an important consideration. This project demonstrated how conformationally specific the antibody paratope had to be to interact with a highly conserved epitope on long-chain α-neurotoxins, which required a highly functional, diverse naïve library to be developed. It is thus unknown whether this level of structural diversity and functionality needs to be maintained in libraries with mutations in the framework. If it is possible to introduce pH-dependent antigen binding properties through framework mutations, then an important consideration will be the potential effect this may have on the functionality of the library, and therefore the scope to which the library can be applied.

In conclusion, we have identified an antibody with pH-dependent antigen properties discovered from a naïve antibody library, highlighting the use of naïve antibody libraries as a source of antibodies with such properties. We determined the neutralization mechanism for this antibody and established the basis for cross-reactivity, through molecular mimicry of the acetylcholine receptor interaction with long-chain α-neurotoxins. In our approach to elucidate the pH-dependent binding mechanism for this antibody, we determined crystal structures of the antibody bound at different acidic pH. We highlight that the binding properties of the antibody were not a limitation in this approach *i.e.*, trying to crystalize an antibody at a pH that was very unfavourable for the antibody to bind. Evidently, the factors favourable for the crystal formation were most dominant, and this allowed us to gain a deeper molecular insight into pH-dependent binding mechanism than other approaches. We introduce a new paradigm for engineering pH-dependent antigen binding into monoclonal antibodies by releasing hydrogen bonding constraints on residues surrounding histidine residues located in the antibody chain interface. This provides a new direction for engineering pH-dependent binding into antibody variable domains and could be a broadly applicable approach to the engineering and discovery of antibodies with pH-dependent antigen binding properties, such as recycling antibodies. This information will improve the development of antibodies that need to have a long-acting duration of target inhibition and/or need to be administered at a low dose, which might be broadly applicable to the treatment of soluble proteins that drive autoimmune responses, cardiovascular diseases, envenomings, and other toxin-driven pathologies.

8.2. **Valence engineering using the self-assembly p53 protein**

The nanobody is a small, monovalent antibody format that has utility in imaging, diagnostics, and immunotherapy.[3] In this thesis, we applied the self-assembly p53 tetramerization protein to increase the valence of nanobodies. Multivalent nanobodies (Quads) were produced as stable proteins and led to an enhanced neutralization capacity of long-chain α-neurotoxins when tested functionally. Additionally, Quads functionalized with IgG-Fc domains were able to bind to the neonatal Fc receptor, FcRn, and were recycled in a cellular assay. Although the Quads did accumulate in cells compared to a conventional IgG, the ability of Quads to interact with FcRn indicates that they are likely to engage other Fc receptors and share the effector function properties of IgGs, possibly with improved potency due to having two IgG-Fc domains. As with all novel formats, Quads would need to be assessed for their developability, as well their pharmacokinetics *in vivo*.[94]

The use of the p53 protein affords a 'plug-and-play' approach to generate molecules with new functionalities. Here, we incorporated IgG-Fc domains that enabled multivalent nanobodies to be recycled. The plug-and-play approach could also be extended to generate bispecific or multi-specific proteins with new mechanisms of action. Nanobodies specific to different antigens could be genetically fused to individual p53 monomers to target multiple epitopes on viral proteins or toxins for enhanced potency. Alternatively, Quads could be used as a screening tool to investigate new target combinations by designing Quad molecules that bind to different cell receptors simultaneously, for example, to improve the activation of immune cells. Lastly, Quads can be produced with different flexibilities and proximities between binding domains and be arranged into a unique tetramer structure that may be better suited for cross-linking cells and applications involving receptor clustering. Finally, given their ability to self-assemble, it may be possible that Quad subunits can be produced microbially and be allowed to self-assemble downstream, which may potentially allow for lower cost of manufacture of these advanced molecules.[4]

In conclusion, we show that the p53 domain is an approach to tune the binding properties of nanobodies and concomitantly extend their half-life and neutralization potency. The versatility of both nanobodies and the p53 protein may open for new applications for nanobodies, such as the design of molecules for multi-targeting applications and avidity-driven mechanisms of action.

9. Bibliography

1. Schröter, C. *et al.* A generic approach to engineer antibody pH-switches using combinatorial histidine scanning libraries and yeast display. *mAbs* **7**, 138–151 (2015).
2. Liu, H. *et al.* Identification of a hotspot on PD-L1 for pH-dependent binding by monoclonal antibodies for tumor therapy. *Signal Transduct. Target. Ther.* **5**, 158 (2020).
3. Lan, W. *et al.* Investigation of anomalous charge variant profile reveals discrete pH-dependent conformations and conformation-dependent charge states within the CDR3 loop of a therapeutic mAb. *mAbs* **12**, 1763138 (2020).
4. GBD 2019 Snakebite Envenomation Collaborators *et al.* Global mortality of snakebite envenoming between 1990 and 2019. *Nat. Commun.* **13**, 6160 (2022).
5. Gutiérrez, J. M. *et al.* Snakebite envenoming. *Nat. Rev. Dis. Primer* **3**, 17063 (2017).
6. Chippaux, J.-P. Snakebite envenomation turns again into a neglected tropical disease! *J. Venom. Anim. Toxins Trop. Dis.* **23**, 38 (2017).
7. Rao, W. *et al.* The rise of genomics in snake venom research: recent advances and future perspectives. *GigaScience* **11**, giac024 (2022).
8. de Silva, H. A., Ryan, N. M. & de Silva, H. J. Adverse reactions to snake antivenom, and their prevention and treatment: Adverse reactions to snake antivenom, and their prevention and treatment. *Br. J. Clin. Pharmacol.* **81**, 446–452 (2016).
9. León, G. *et al.* Current technology for the industrial manufacture of snake antivenoms. *Toxicon* **151**, 63–73 (2018).
10. Attarde, S. *et al.* The Preclinical Evaluation of a Second-Generation Antivenom for Treating Snake Envenoming in India. *Toxins* **14**, 168 (2022).
11. Tan, C. H., Liew, J. L., Tan, K. Y. & Tan, N. H. Assessing SABU (Serum Anti Bisa Ular), the sole Indonesian antivenom: A proteomic analysis and neutralization efficacy study. *Sci. Rep.* **6**, 37299 (2016).
12. Laustsen, A. *et al.* From Fangs to Pharmacology: The Future of Snakebite Envenoming Therapy. *Curr. Pharm. Des.* **22**, 5270–5293 (2016).
13. Ryu, J. *et al.* Development of a CHO cell line for stable production of recombinant antibodies against human MMP9. *BMC Biotechnol.* **22**, 8 (2022).
14. Kini, R., Sidhu, S. & Laustsen, A. Biosynthetic Oligoclonal Antivenom (BOA) for Snakebite and Next-Generation Treatments for Snakebite Victims. *Toxins* **10**, 534 (2018).
15. Lakins, M. A. *et al.* FS222, a CD137/PD-L1 Tetravalent Bispecific Antibody, Exhibits Low Toxicity and Antitumor Activity in Colorectal Cancer Models. *Clin. Cancer Res.* **26**, 4154–4167 (2020).
16. Parren, P. W. H. I. & Burton, D. R. The antiviral activity of antibodies in vitro and in vivo. in *Advances in Immunology* vol. 77 195–262 (Elsevier, 2001).
17. Nowakowski, A. *et al.* Potent neutralization of botulinum neurotoxin by recombinant oligoclonal antibody. *Proc. Natl. Acad. Sci.* **99**, 11346–11350 (2002).
18. Sun, Y., Huang, T., Hammarström, L. & Zhao, Y. The Immunoglobulins: New Insights, Implications, and Applications. *Annu. Rev. Anim. Biosci.* **8**, 145–169 (2020).
19. Stanfield, R. L. & Wilson, I. A. Antibody Structure. *Microbiol. Spectr.* **2**, 2.2.06 (2014).
20. Zohar, T. & Alter, G. Dissecting antibody-mediated protection against SARS-CoV-2. *Nat. Rev. Immunol.* **20**, 392–394 (2020).
21. Bruhns, P. & Jönsson, F. Mouse and human FcR effector functions. *Immunol. Rev.* **268**, 25–51 (2015).

22. Oostindie, S. C., Lazar, G. A., Schuurman, J. & Parren, P. W. H. I. Avidity in antibody effector functions and biotherapeutic drug design. *Nat. Rev. Drug Discov.* **21**, 715–735 (2022).
23. Rudnick, S. I. & Adams, G. P. Affinity and Avidity in Antibody-Based Tumor Targeting. *Cancer Biother. Radiopharm.* **24**, 155–161 (2009).
24. Rujas, E. *et al.* Multivalency transforms SARS-CoV-2 antibodies into ultrapotent neutralizers. *Nat. Commun.* **12**, 3661 (2021).
25. Miller, A., Carr, S., Rabbitts, T. & Ali, H. Multimeric antibodies with increased valency surpassing functional affinity and potency thresholds using novel formats. *mAbs* **12**, 1752529 (2020).
26. Liu, K. *et al.* Structural basis of anti-PD-L1 monoclonal antibody avelumab for tumor therapy. *Cell Res.* **27**, 151–153 (2017).
27. Lee, J. Y. *et al.* Structural basis of checkpoint blockade by monoclonal antibodies in cancer immunotherapy. *Nat. Commun.* **7**, 13354 (2016).
28. Xiao, H. *et al.* Light chain modulates heavy chain conformation to change protection profile of monoclonal antibodies against influenza A viruses. *Cell Discov.* **5**, 21 (2019).
29. Amzel, L. M., Poljak, R. J., Saul, F., Varga, J. M. & Richards, F. F. The Three Dimensional Structure of a Combining Region-Ligand Complex of Immunoglobulin NEW at 3.5-Å Resolution. *Proc. Natl. Acad. Sci.* **71**, 1427–1430 (1974).
30. Klein, F. *et al.* Somatic Mutations of the Immunoglobulin Framework Are Generally Required for Broad and Potent HIV-1 Neutralization. *Cell* **153**, 126–138 (2013).
31. Ovchinnikov, V., Louveau, J. E., Barton, J. P., Karplus, M. & Chakraborty, A. K. Role of framework mutations and antibody flexibility in the evolution of broadly neutralizing antibodies. *eLife* **7**, e33038 (2018).
32. Fernández-Quintero, M. L. *et al.* Local and Global Rigidification Upon Antibody Affinity Maturation. *Front. Mol. Biosci.* **7**, 182 (2020).
33. Keizer, R. J., Huitema, A. D. R., Schellens, J. H. M. & Beijnen, J. H. Clinical Pharmacokinetics of Therapeutic Monoclonal Antibodies: *Clin. Pharmacokinet.* **49**, 493–507 (2010).
34. Akilesh, S., Christianson, G. J., Roopenian, D. C. & Shaw, A. S. Neonatal FcR Expression in Bone Marrow-Derived Cells Functions to Protect Serum IgG from Catabolism. *J. Immunol.* **179**, 4580–4588 (2007).
35. Challa, D. K. *et al.* Neonatal Fc receptor expression in macrophages is indispensable for IgG homeostasis. *mAbs* **11**, 848–860 (2019).
36. Zhang, Y. *et al.* Hijacking antibody-induced CTLA-4 lysosomal degradation for safer and more effective cancer immunotherapy. *Cell Res.* **29**, 609–627 (2019).
37. Chaparro-Riggers, J. *et al.* Increasing Serum Half-life and Extending Cholesterol Lowering in Vivo by Engineering Antibody with pH-sensitive Binding to PCSK9. *J. Biol. Chem.* **287**, 11090–11097 (2012).
38. Chan, J. C. Y. *et al.* A proprotein convertase subtilisin/kexin type 9 neutralizing antibody reduces serum cholesterol in mice and nonhuman primates. *Proc. Natl. Acad. Sci.* **106**, 9820–9825 (2009).
39. Altman, A. & Kong, K.-F. pH-sensitive anti-CTLA4 antibodies: yes to efficacy, no to toxicity. *Cell Res.* **29**, 601–602 (2019).
40. Igawa, T. *et al.* Engineered Monoclonal Antibody with Novel Antigen-Sweeping Activity In Vivo. *PLoS ONE* **8**, e63236 (2013).
41. Igawa, T. *et al.* Antibody recycling by engineered pH-dependent antigen binding improves the duration of antigen neutralization. *Nat. Biotechnol.* **28**, 1203–1207 (2010).
42. Sheridan, D. *et al.* Design and preclinical characterization of ALXN1210: A novel anti-C5 antibody with extended duration of action. *PLOS ONE* **13**, e0195909 (2018).

43. Ratanabanangkoon, K. *et al.* A pan-specific antiserum produced by a novel immunization strategy shows a high spectrum of neutralization against neurotoxic snake venoms. *Sci. Rep.* **10**, 11261 (2020).
44. Foss, S. *et al.* Potent TRIM21 and complement-dependent intracellular antiviral immunity requires the IgG3 hinge. *Sci. Immunol.* **7**, eabj1640 (2022).
45. Matthews-Palmer, T. R. S. *et al.* Structure of the cytoplasmic domain of SctV (SsaV) from the Salmonella SPI-2 injectisome and implications for a pH sensing mechanism. *J. Struct. Biol.* **213**, 107729 (2021).
46. Benton, D. J., Gamblin, S. J., Rosenthal, P. B. & Skehel, J. J. Structural transitions in influenza haemagglutinin at membrane fusion pH. *Nature* **583**, 150–153 (2020).
47. Pyzik, M. *et al.* The Neonatal Fc Receptor (FcRn): A Misnomer? *Front. Immunol.* **10**, 1540 (2019).
48. Vester, S. K. *et al.* SpySwitch enables pH- or heat-responsive capture and release for plug-and-display nanoassembly. *Nat. Commun.* **13**, 3714 (2022).
49. Tian, X. *et al.* An anti-CD98 antibody displaying pH-dependent Fc-mediated tumour-specific activity against multiple cancers in CD98-humanized mice. *Nat. Biomed. Eng.* **7**, 8–23 (2022).
50. Bogen, J. P. *et al.* Dual Function pH Responsive Bispecific Antibodies for Tumor Targeting and Antigen Depletion in Plasma. *Front. Immunol.* **10**, 1892 (2019).
51. Bonvin, P. *et al. De novo* isolation of antibodies with pH-dependent binding properties. *mAbs* **7**, 294–302 (2015).
52. Fu, Y. *et al.* Combination Foretinib and Anti-PD-1 Antibody Immunotherapy for Colorectal Carcinoma. *Front. Cell Dev. Biol.* **9**, 689727 (2021).
53. Baum, A. *et al.* Antibody cocktail to SARS-CoV-2 spike protein prevents rapid mutational escape seen with individual antibodies. *Science* **369**, 1014–1018 (2020).
54. Gray, A. *et al.* Animal-free alternatives and the antibody iceberg. *Nat. Biotechnol.* **38**, 1234–1239 (2020).
55. Engmark, M. *et al.* High-throughput immuno-profiling of mamba (Dendroaspis) venom toxin epitopes using high-density peptide microarrays. *Sci. Rep.* **6**, 36629 (2016).
56. Laustsen, A. H. *et al.* In vivo neutralization of dendrotoxin-mediated neurotoxicity of black mamba venom by oligoclonal human IgG antibodies. *Nat. Commun.* **9**, 3928 (2018).
57. Garcia-Moro, E. *et al.* Reversible structural changes in the influenza hemagglutinin precursor at membrane fusion pH. *Proc. Natl. Acad. Sci.* **119**, e2208011119 (2022).
58. Fiil, B. K. *et al.* Orally active bivalent VHH construct prevents proliferation of F4+ enterotoxigenic Escherichia coli in weaned piglets. *iScience* **25**, 104003 (2022).
59. Foote, J. & Winter, G. Antibody framework residues affecting the conformation of the hypervariable loops. *J. Mol. Biol.* **224**, 487–499 (1992).
60. Gaspar, M. *et al.* CD137/OX40 Bispecific Antibody Induces Potent Antitumor Activity that Is Dependent on Target Coengagement. *Cancer Immunol. Res.* **8**, 781–793 (2020).
61. Mimoto, F. *et al.* Engineered antibody Fc variant with selectively enhanced Fc RIIb binding over both Fc RIIaR131 and Fc RIIaH131. *Protein Eng. Des. Sel.* **26**, 589–598 (2013).
62. Johnston, R. J. *et al.* VISTA is an acidic pH-selective ligand for PSGL-1. *Nature* **574**, 565–570 (2019).
63. Viviani, V. R. *et al.* The proton and metal binding sites responsible for the pH-dependent green-red bioluminescence color tuning in firefly luciferases. *Sci. Rep.* **8**, 17594 (2018).
64. Maeda, A. *et al.* Identification of human IgG1 variant with enhanced FcRn binding and without increased binding to rheumatoid factor autoantibody. *mAbs* **9**, 844–853 (2017).

65. Nishimoto-Kakiuchi, A. *et al.* A long-acting anti–IL-8 antibody improves inflammation and fibrosis in endometriosis. *Sci. Transl. Med.* **15**, eabq5858 (2023).
66. Kroetsch, A. *et al.* Engineered pH-dependent recycling antibodies enhance elimination of Staphylococcal enterotoxin B superantigen in mice. *mAbs* **11**, 411–421 (2019).
67. Engler, F. A. *et al.* "Catch-and-Release" Anti-Carcinoembryonic Antigen Monoclonal Antibody Leads to Greater Plasma and Tumor Exposure in a Mouse Model of Colorectal Cancer. *J. Pharmacol. Exp. Ther.* **366**, 205–219 (2018).
68. Shen, Y. *et al.* Increased half-life and enhanced potency of Fc-modified human PCSK9 monoclonal antibodies in primates. *PLOS ONE* **12**, e0183326 (2017).
69. Henne, K. R. *et al.* Anti-PCSK9 Antibody Pharmacokinetics and Low-Density Lipoprotein-Cholesterol Pharmacodynamics in Nonhuman Primates Are Antigen Affinity–Dependent and Exhibit Limited Sensitivity to Neonatal Fc Receptor–Binding Enhancement. *J. Pharmacol. Exp. Ther.* **353**, 119–131 (2015).
70. Fukuzawa, T. *et al.* Long lasting neutralization of C5 by SKY59, a novel recycling antibody, is a potential therapy for complement-mediated diseases. *Sci. Rep.* **7**, 1080 (2017).
71. Morell, A., Terry, W. D. & Waldmann, T. A. Metabolic properties of IgG subclasses in man. *J. Clin. Invest.* **49**, 673–680 (1970).
72. Roopenian, D. C. & Akilesh, S. FcRn: the neonatal Fc receptor comes of age. *Nat. Rev. Immunol.* **7**, 715–725 (2007).
73. Karush, F. Multivalent Binding and Functional Affinity. in *Contemporary Topics in Molecular Immunology* (eds. Eisen, H. N. & Reisfeld, R. A.) 217–228 (Springer US, 1976). doi:10.1007/978-1-4684-8142-6_8.
74. Foote, J. & Eisen, H. N. Kinetic and affinity limits on antibodies produced during immune responses. *Proc. Natl. Acad. Sci.* **92**, 1254–1256 (1995).
75. Gilhus, N. E. & Verschuuren, J. J. Myasthenia gravis: subgroup classification and therapeutic strategies. *Lancet Neurol.* **14**, 1023–1036 (2015).
76. Hoffhines, A. J., Damoc, E., Bridges, K. G., Leary, J. A. & Moore, K. L. Detection and Purification of Tyrosine-sulfated Proteins Using a Novel Anti-sulfotyrosine Monoclonal Antibody. *J. Biol. Chem.* **281**, 37877–37887 (2006).
77. Landsteiner, K. *Die Spezifizität der Serologischen Reaktionen*. (Springer Berlin Heidelberg, 1933). doi:10.1007/978-3-662-33113-2.
78. Liu, L. *et al.* An antibody class with a common CDRH3 motif broadly neutralizes sarbecoviruses. *Sci. Transl. Med.* **14**, eabn6859 (2022).
79. Zhang, A. *et al.* Beyond neutralization: Fc-dependent antibody effector functions in SARS-CoV-2 infection. *Nat. Rev. Immunol.* (2022) doi:10.1038/s41577-022-00813-1.
80. Ng, K. W. *et al.* SARS-CoV-2 S2–targeted vaccination elicits broadly neutralizing antibodies. *Sci. Transl. Med.* **14**, eabn3715 (2022).
81. Fernández-Quintero, M. L., Heiss, M. C. & Liedl, K. R. Antibody humanization—the Influence of the antibody framework on the CDR-H3 loop ensemble in solution. *Protein Eng. Des. Sel.* **32**, 411–422 (2019).
82. Zhou, J. O., Zaidi, H. A., Ton, T. & Fera, D. The Effects of Framework Mutations at the Variable Domain Interface on Antibody Affinity Maturation in an HIV-1 Broadly Neutralizing Antibody Lineage. *Front. Immunol.* **11**, 1529 (2020).
83. Ledsgaard, L. *et al. In vitro* discovery of a human monoclonal antibody that neutralizes lethality of cobra snake venom. *mAbs* **14**, 2085536 (2022).
84. Vaccaro, C., Zhou, J., Ober, R. J. & Ward, E. S. Engineering the Fc region of immunoglobulin G to modulate in vivo antibody levels. *Nat. Biotechnol.* **23**, 1283–1288 (2005).

85. Goldstein, R., Sosabowski, J., Vigor, K., Chester, K. & Meyer, T. Developments in single photon emission computed tomography and PET-based HER2 molecular imaging for breast cancer. *Expert Rev. Anticancer Ther.* **13**, 359–373 (2013).
86. Singh Jaggi, J. *et al.* Improved tumor imaging and therapy via i.v. IgG–mediated time-sequential modulation of neonatal Fc receptor. *J. Clin. Invest.* **117**, 2422–2430 (2007).
87. Swiercz, R. *et al.* Use of Fc-Engineered Antibodies as Clearing Agents to Increase Contrast During PET. *J. Nucl. Med.* **55**, 1204–1207 (2014).
88. Ratanji, K. D., Derrick, J. P., Dearman, R. J. & Kimber, I. Immunogenicity of therapeutic proteins: Influence of aggregation. *J. Immunotoxicol.* **11**, 99–109 (2014).
89. Moussa, E. M. *et al.* Immunogenicity of Therapeutic Protein Aggregates. *J. Pharm. Sci.* **105**, 417–430 (2016).
90. Starr, C. G. & Tessier, P. M. Selecting and engineering monoclonal antibodies with drug-like specificity. *Curr. Opin. Biotechnol.* **60**, 119–127 (2019).
91. Grevys, A. *et al.* A human endothelial cell-based recycling assay for screening of FcRn targeted molecules. *Nat. Commun.* **9**, 621 (2018).
92. Gjølberg, T. T. *et al.* Biophysical differences in IgG1 Fc-based therapeutics relate to their cellular handling, interaction with FcRn and plasma half-life. *Commun. Biol.* **5**, 832 (2022).
93. Chung, S. *et al.* An *in vitro* FcRn- dependent transcytosis assay as a screening tool for predictive assessment of nonspecific clearance of antibody therapeutics in humans. *mAbs* **11**, 942–955 (2019).
94. Fernández-Quintero, M. L. *et al.* Assessing developability early in the discovery process for novel biologics. *mAbs* **15**, 2171248 (2023).

Appendices

A: Production of antibody for crystallography

Crystallography requires milligram quantities of pure protein for screening conditions that allow for crystals to form. This section describes the production, purification and preliminary crystallography results before the final dataset presented in Chapter 4.

Initial purification of antibody-neurotoxin complexes by gel filtration
Two cross-reactive anti-long chain α-neurotoxin antibodies, 2555_01_A01 and 2554_01_D11, were chosen for crystallography trials due to their marked difference in pH-dependent binding and cross-reactivity profiles. The variable region of both antibodies was produced in E.coli as an scFv, and underwent two rounds of purification, firstly by Nickel ion affinity chromatography followed by gel filtration (Chapter 5 Methods).
The 2554_01_D11 antibody was initially chosen for crystallography trials as it bound with the highest affinity to the two long-chain α-neurotoxins of interest, α-cobratoxin and α-bungarotoxin, which was speculated to help with the purification of the complex and crystallization. The antibody was left overnight to incubate with a slight molar excess of long-chain α-neurotoxin (1:1.5 molar ratio) prior to purification by size exclusion chromatography. Individual fractions were collected from the SEC purification run and analyzed by SDS-PAGE.

Size exclusion chromatography analysis revealed four peaks for both the overnight pre-incubations that had elution volumes in the range expected for a 2554_01_D11 scFv and long-chain α-neurotoxins (Fig. 1A and C). SDS-PAGE analysis of the first two peaks confirmed the presence of 2554_01_D11 scFv. Both contained long-chain α-neurotoxin as bands were observed near the 35 kDa and 10 kDa MW markers, which were consistent with previous observations for these proteins in the lab. The two higher volume peaks were similar in their MW as judged by SDS-PAGE, showing that these were two different forms of both long-chain α-neurotoxins, possibly monomer and dimer forms. As the difference in MW for the two 2554_01_D11 scFv SEC peaks equated to the MW of the larger form of each long-chain α-neurotoxin, this indicated that the 2554_01_D11 was selective for the larger form of these toxins.

Noted for subsequent purifications was evidence of scFv degradation, which was more pronounced in the α-cobratoxin purification prep having been prepared a week earlier. Additionally, the molar ratio would clearly need to be increased to saturate the binding of 2554_01_D11 scFv for both long-chain α-neurotoxins. For a first trial, however, all antibody peaks were pooled and taken forward for crystallography screening."

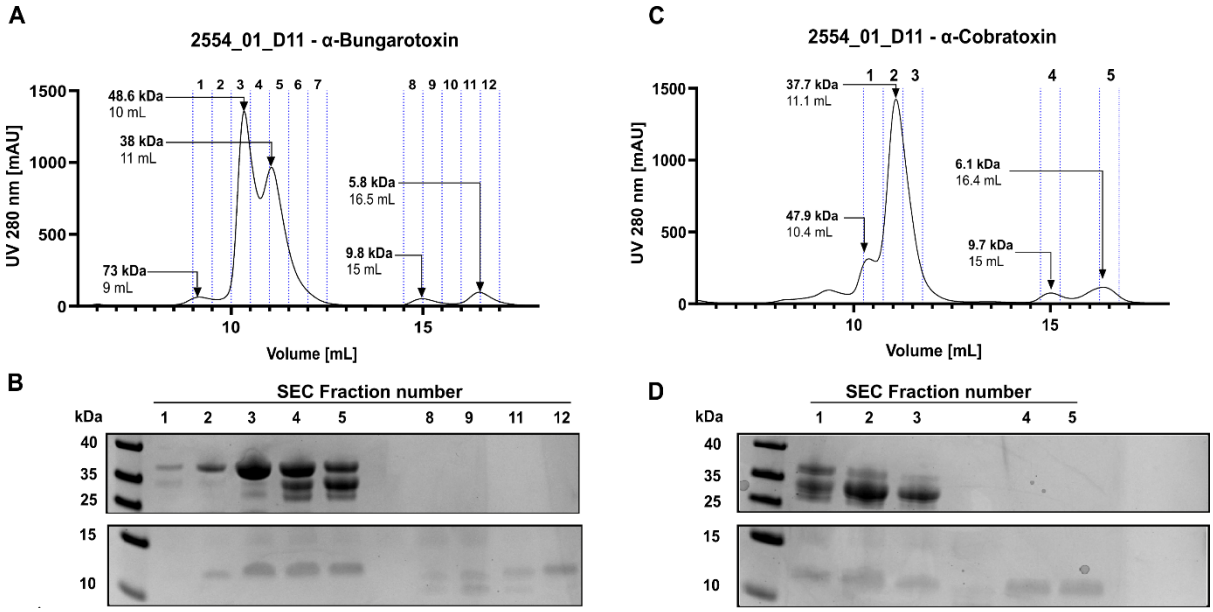

Fig 1. Size exclusion chromatography and SDS-PAGE gel analysis of pre-incubated long-chain α-neurotoxins with 2554_01_D11 scFv. SEC purification of 2554_01_D11 pre-incubated with α-bungarotoxin (A & B) and α-cobratoxin (C & D). All SEC chromatogram peaks are labelled with the elution volume and calculated MW. Determined MW were derived from a calibration curve from a commercial protein standard set.

First Crystal

Crystallography screens were set up separately for the 2554_01_D11 scFv purified with α-cobratoxin or α-bungarotoxin using a sitting drop method. After 20 days, a crystal appeared in the 2554_01_D11-α-cobratoxin plate, in a drop containing an equal volume of protein (9.15 mg/mL) and 0.15M D-L Malic acid pH 7.0 buffer with 20% w/v PEG3350 precipitant (Fig. 2). The crystal was stored in 20% glycerol for cryo-protection. However, due to the low level of purity resulting from scFv degradation and the complex not being exclusively purified (Fig. 1A&C), it was decided to improve scFv production and repeat the screen with a more homogeneous sample.

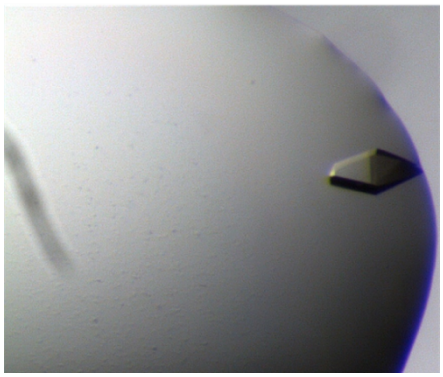

Fig 2. First crystal obtained from 2554_01_D11 and α-cobratoxin containing fractions. Subsequent data were highly anisotropic and there was no clear indication of toxin present.

scFv degradation

The scFv degradation was suspected to be caused by the C-terminal 6×His-FLAG tag. To test whether the tag was the source of degradation a time course degradation experiment was conducted using SEC purified 2555_01_A01 scFv and the C-terminal tag was detected by western blot with and without proteinase inhibitor. The results showed that the degraded product was the C-terminal tag, as the lower band near the 35 kDa marker, corresponding to the degraded product, was not detected by the anti-FLAG detection antibody (Fig. 4). The addition of protease inhibitor cocktail did not alter the antibody degradation. To address this issue, a C-terminal TEV cleavage site was introduced to remove the tag and preliminary cleavage efficiency tests were performed with SuperTev enzyme using a 1:20 molar ratio of scFv:enzyme with and without reducing agents (Fig 5). The tag was efficiently cleaved without the need for a reducing agent after overnight incubation at 4°C.

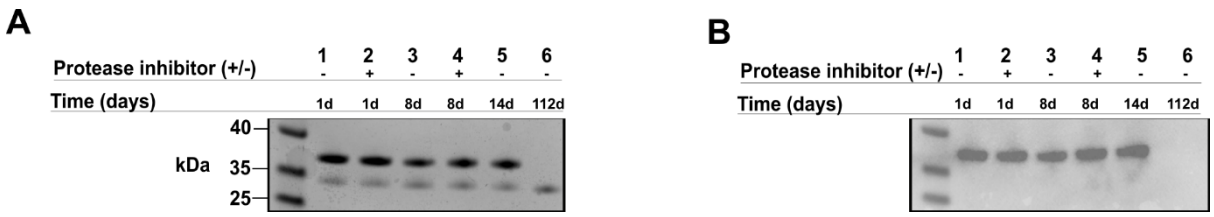

Fig 4. Time course degradation profile of 2555_01_A01 scFv antibody. (A) Coomassie-stained non-reduced SDS-PAGE gel analysis of 700 ng of antibody taken at varying time intervals, showing intact scFv between 35-40 kDa and a lower degraded band between 25-35 kDa. (B) Anti-FLAG tag detection of 50ng of each sample. To check whether degradation was a result of proteases, 1mM of protease inhibitor cocktail was added in parallel. The upper band between the 35 – 40 kDa markers corresponding to the intact scFv was detected.

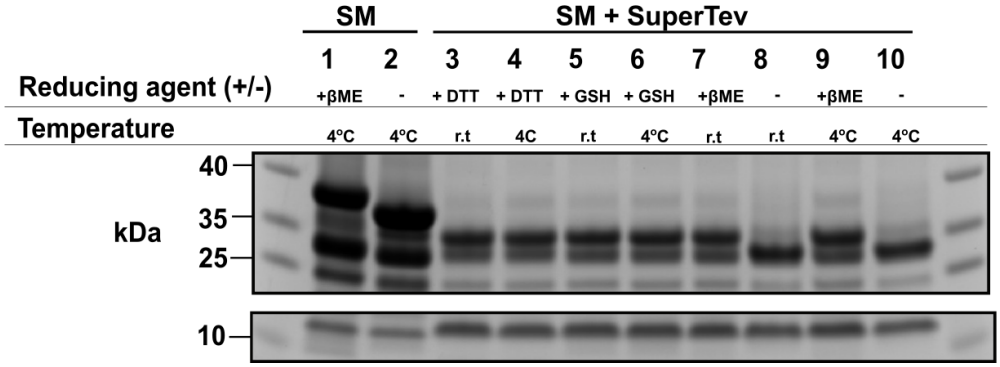

Fig 5. C-term tag cleavage tests with SuperTev protease. (A) Coomassie-stained SDS-PAGE gel analysis of 2µg of 2555_01_A01 scFv antibody incubated overnight with a 1:30 molar ratio of SuperTev: antibody. The reducing agent and temperature were varied. β-Mercaptoethanol was present in the loading dye as a reference for antibody reduction and not used in the overnight cleavage reaction. (B) SEC chromatogram overlay of SuperTev treated and non-treated antibody showing emergence of a cleaved peak of low molecular weight.

scFv antibody production

Lastly, the expression level of both scFv's was low (1-2 mg/L), and required 10 L productions to obtain sufficient protein to guarantee a single plate for crystallography screening. To try and improve the production yield, the culture flask was changed from an Erlenmyer to a Tunair™ shake flask. Tunair™ shake flasks yielded 4-8 mg/L of scFv post-SuperTEV tag removal and SEC purification, which was a sufficient quantity to set multiple plates for crystallography screening (Table 1). The final purification process for both 2554_01_D11 and 2555_01_A01 scFv molecules is shown in Figure 6.

Table 1: Production yield for 2555_01_scFv produced in Tunair™ flasks.

Production	*Culture volume (L)*	*Post Ni-resin (mg)*	*Post tag removal (mg)*
17/04/2022	2	67.05	13
21/06/2022	1		4.3
24/07/2022	1	42.0	7.6

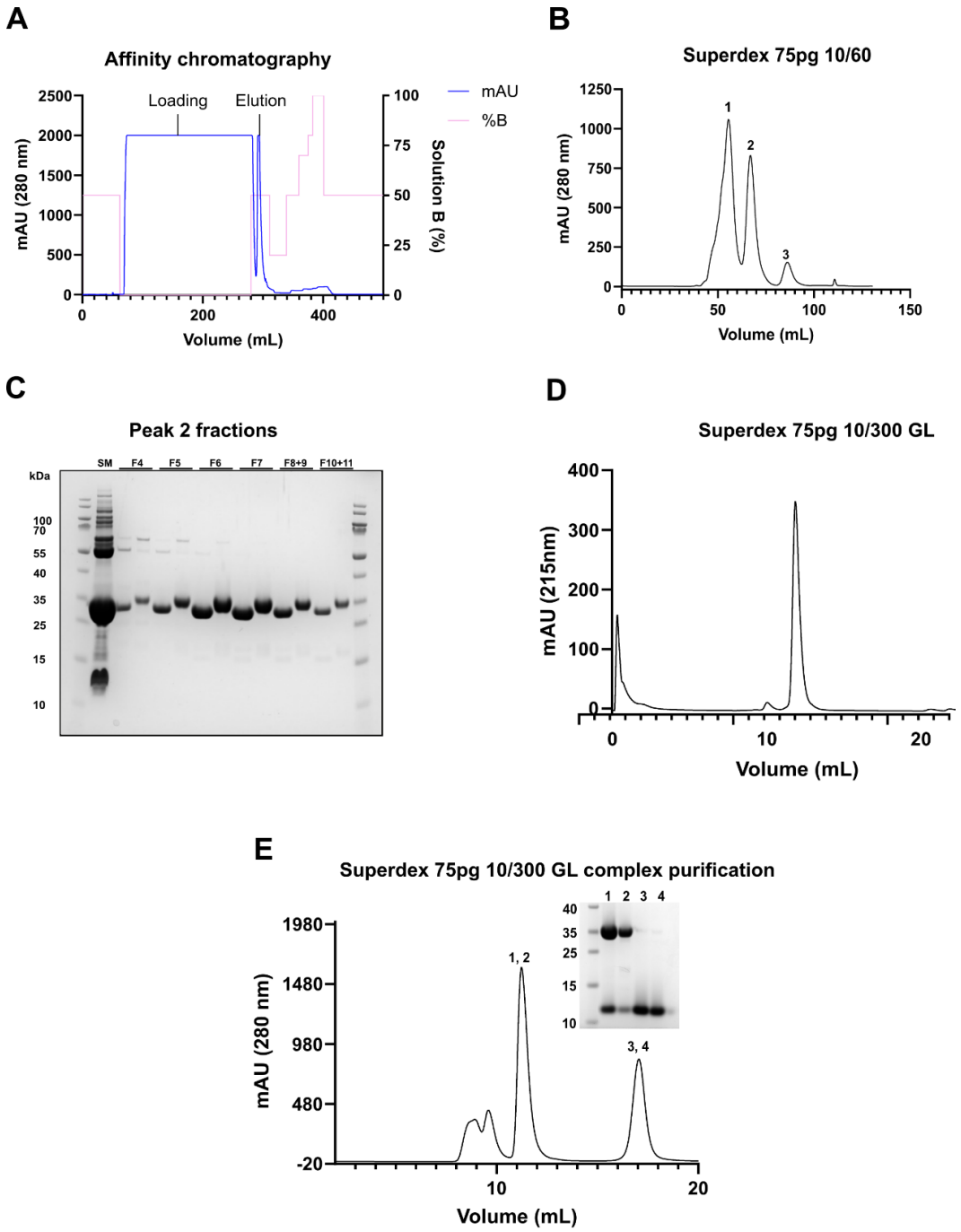

Fig 6. scFv purification process for crystallography. (A) scFv produced in E.coli BL21(DE3) is extracted from the periplasm and purified by Nickel affinity chromatography. (B) C-Terminal tag cleaved scFv is SEC purified using a Hi-Load 75pg Superdev 10/60 column. (C) Fractions from the main peak were analysed by SDS-PAGE. (D) Fractions 5-9 were pooled and analysed on a Superdex 75pg 10/300 GL column. (E) Monomeric scFv was incubated with α-cobratoxin overnight and the complex was purified by SEC. The corresponding SDS-PAGE gel of each of the fractions is shown, fractions 1 and 2 contain scFv bound to α-cobratoxin. A slight tail was seen for this peak, so only fraction 1 was taken forward for crystallography screening.

B: Biolayer interferometry curves and data tables.

Anti-long-chain α-neurotoxin antibodies binding to α-cobratoxin.
Data processing is described in Chapter 5 methods.

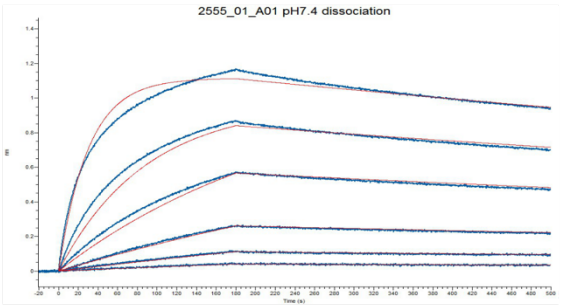

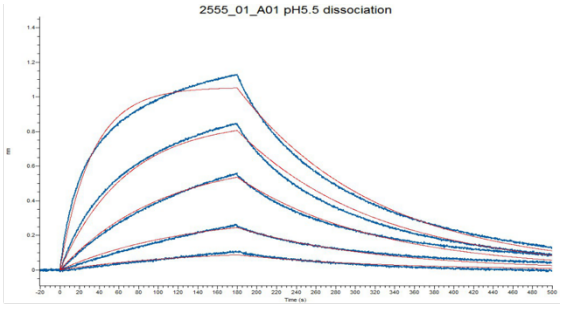

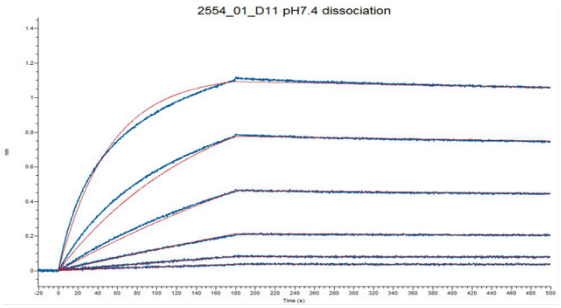

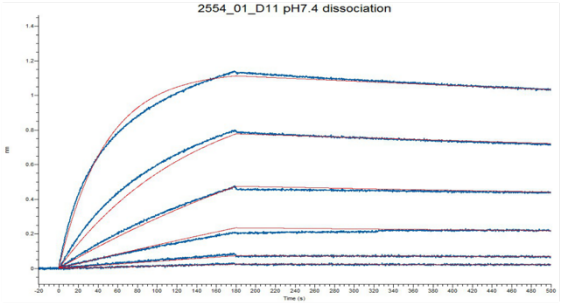

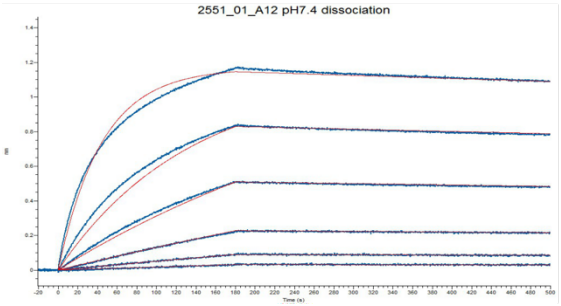

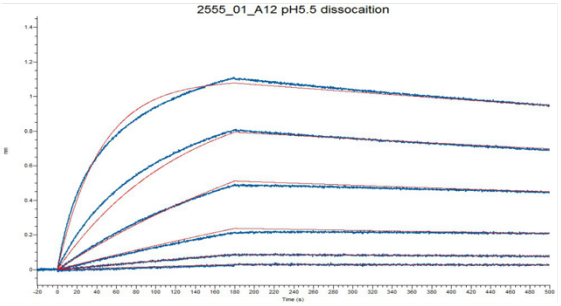

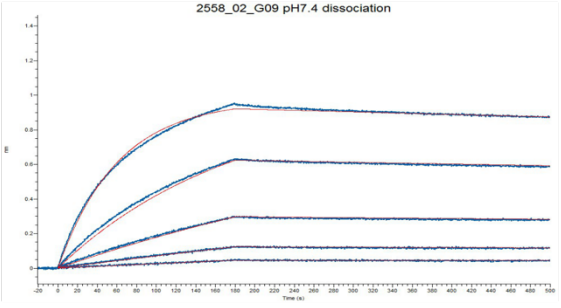

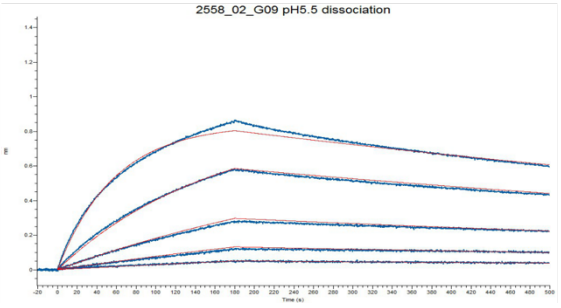

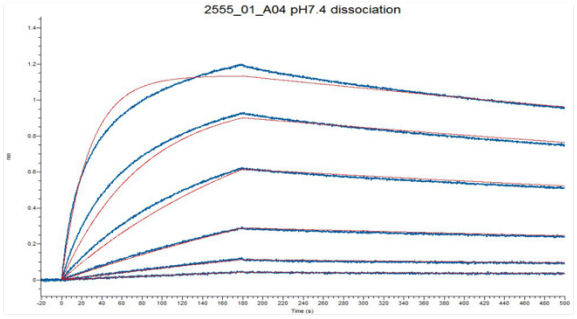
2555_01_A04 pH7.4 dissociation
nm
Time (s)

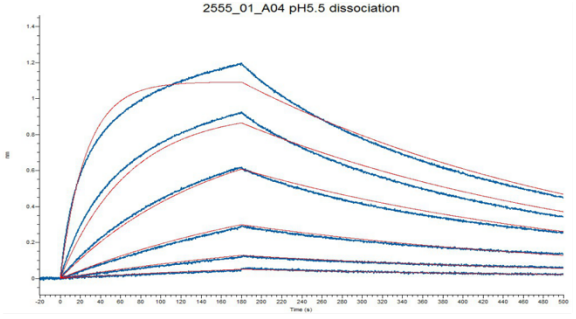
2555_01_A04 pH5.5 dissociation
nm
Time (s)

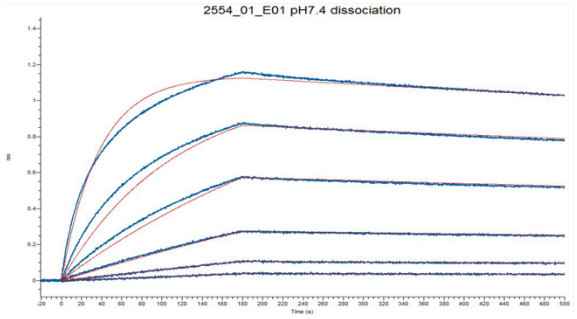
2554_01_E01 pH7.4 dissociation
nm
Time (s)

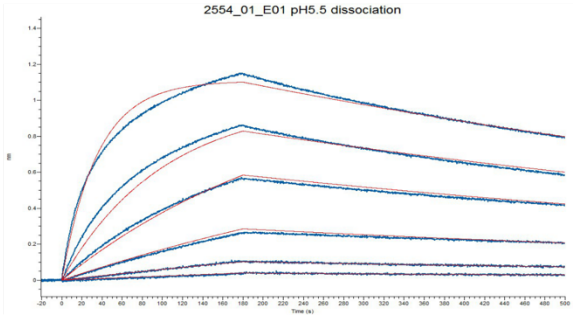
2554_01_E01 pH5.5 dissociation
nm
Time (s)

Anti-long-chain α-neurotoxin antibodies binding to α-elapitoxin.
Data processing is described in Chapter 5 methods

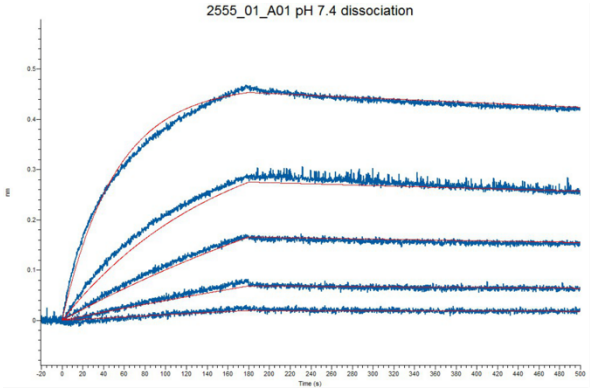

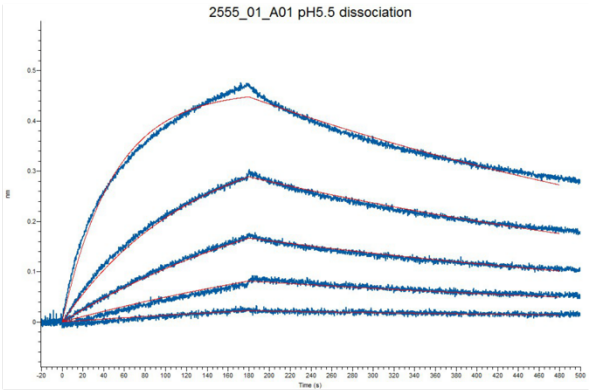

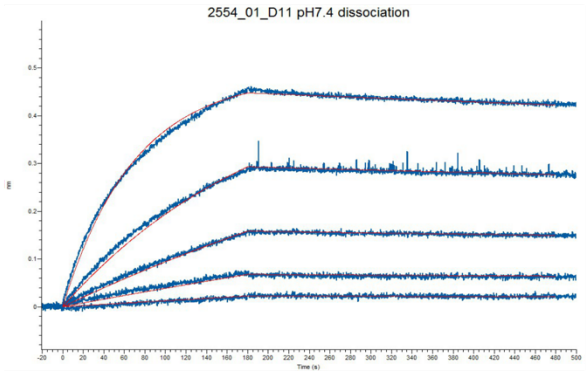

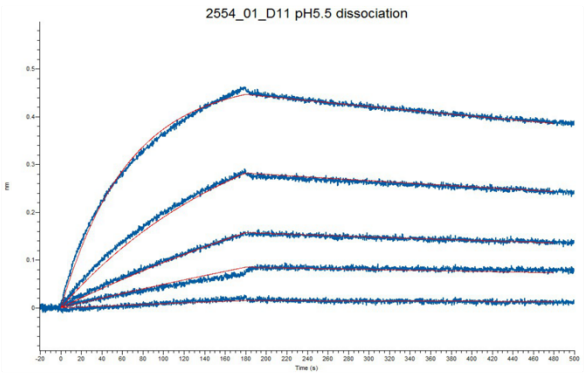

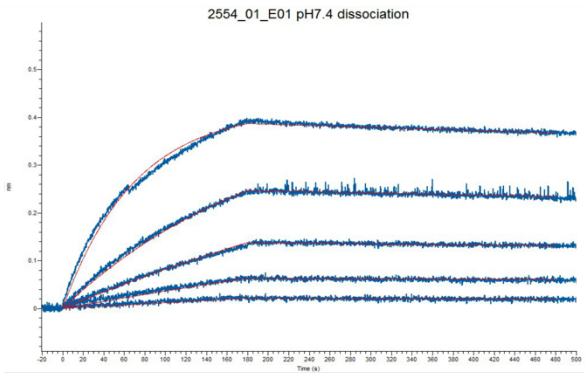

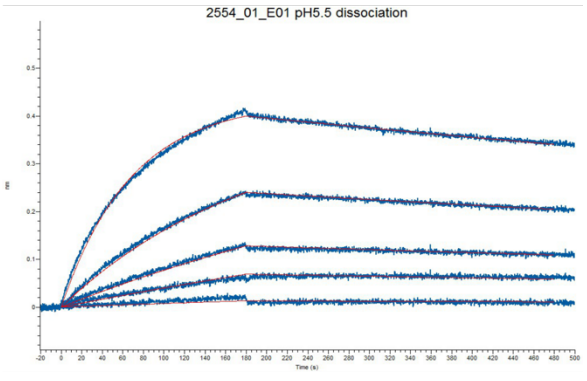

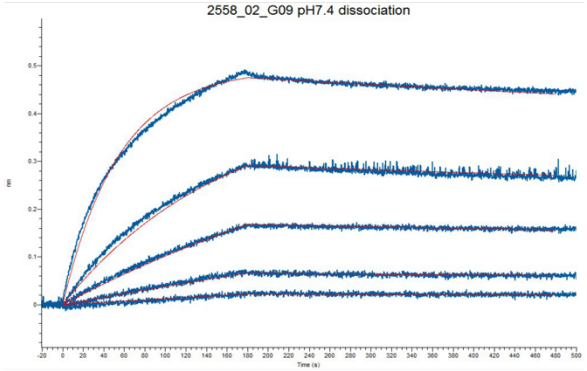

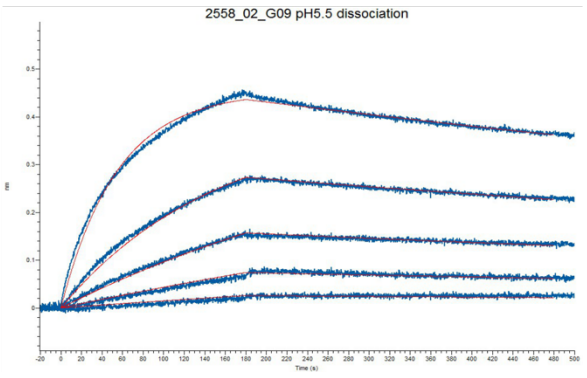

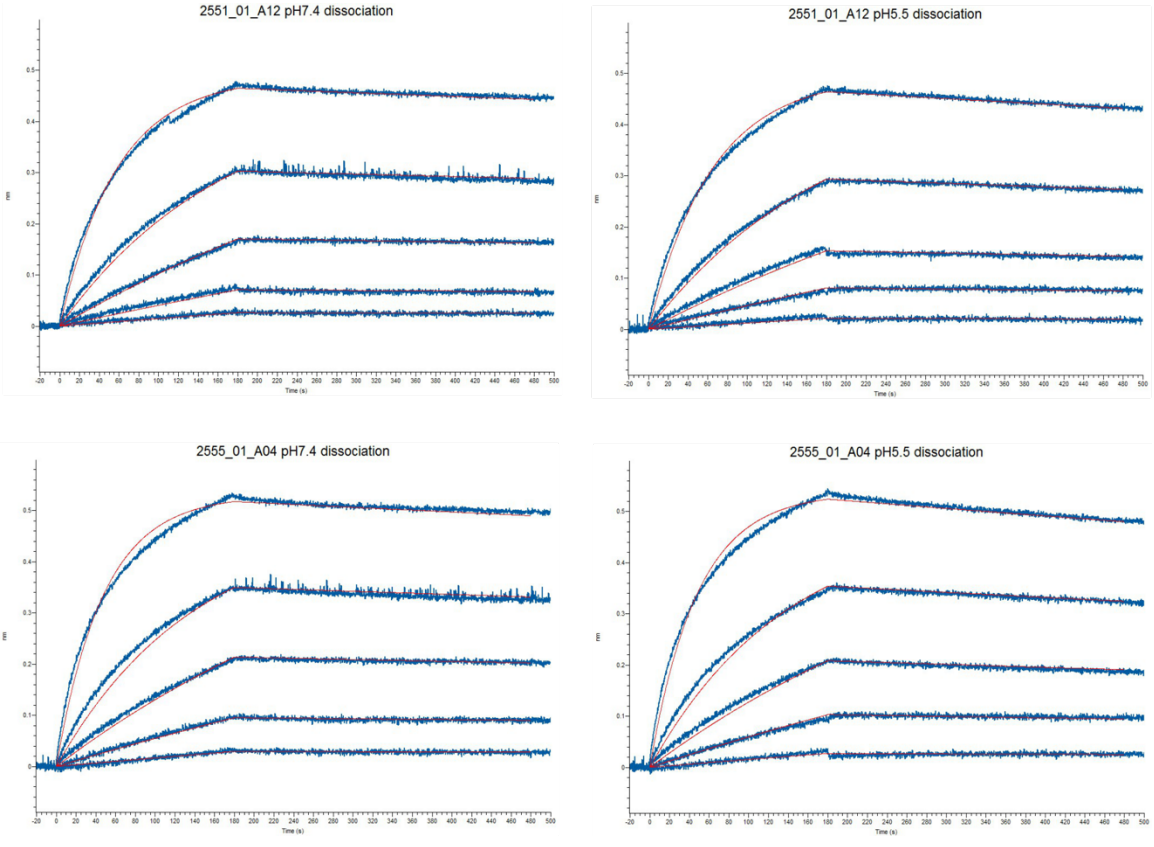

Anti-long-chain α-neurotoxin antibodies binding to α-bungarotoxin.

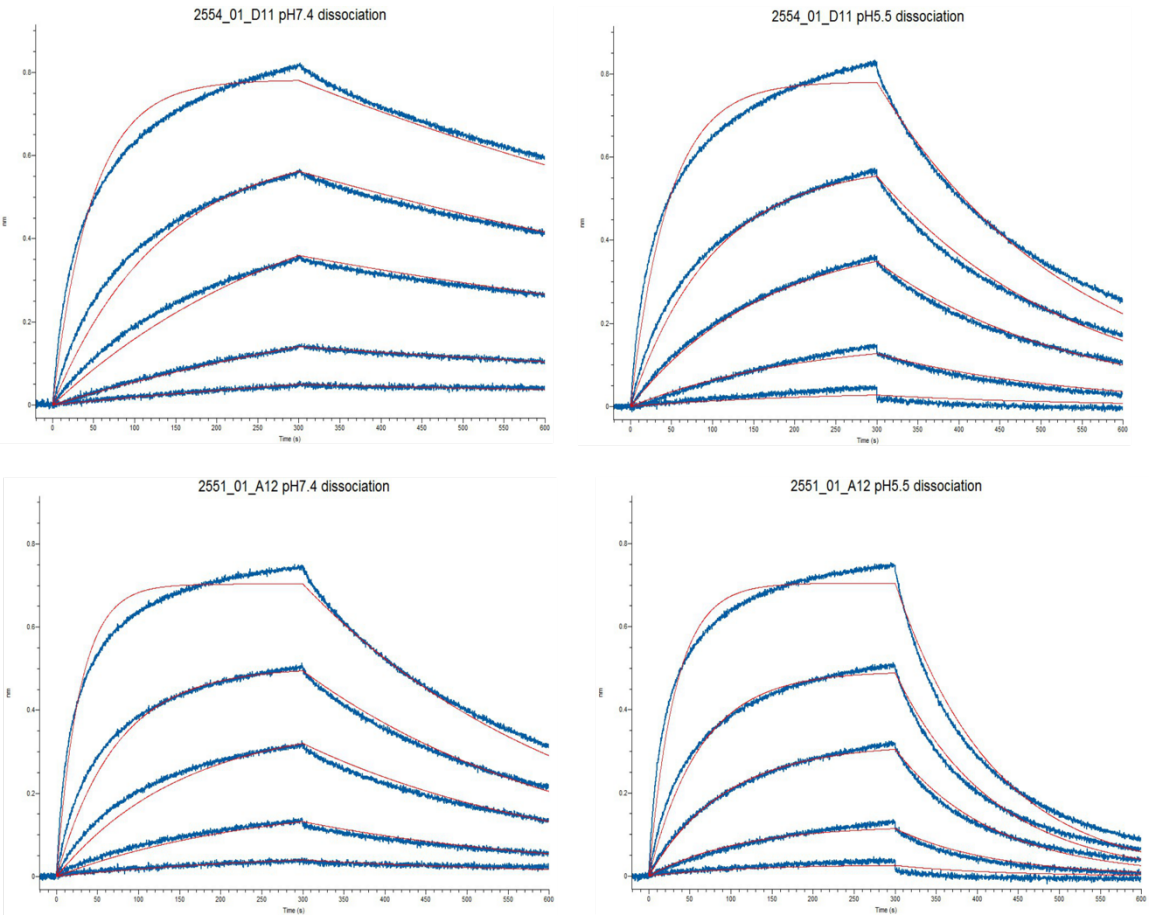

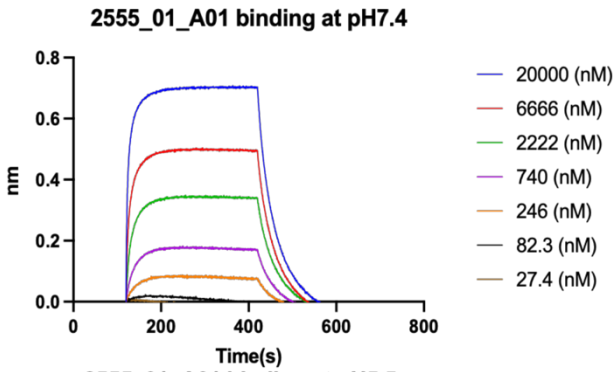
2555_01_A01 binding at pH7.4
nm
Time(s)
20000 (nM)
6666 (nM)
2222 (nM)
740 (nM)
246 (nM)
82.3 (nM)
27.4 (nM)

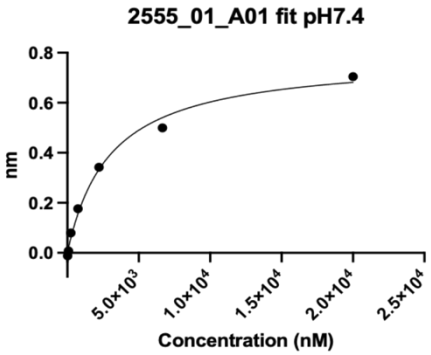
2555_01_A01 fit pH7.4
nm
Concentration (nM)

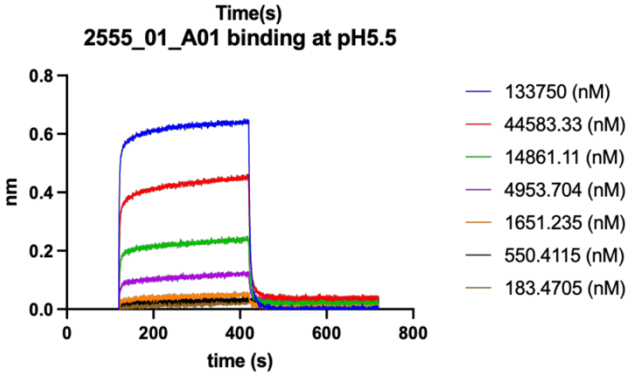
2555_01_A01 binding at pH5.5
nm
time (s)
133750 (nM)
44583.33 (nM)
14861.11 (nM)
4953.704 (nM)
1651.235 (nM)
550.4115 (nM)
183.4705 (nM)

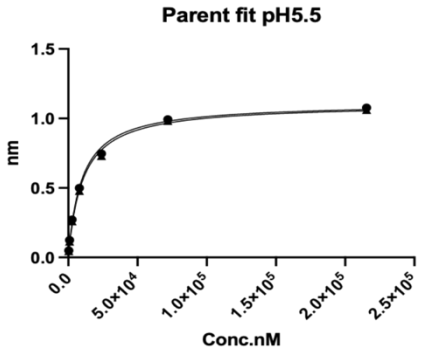
Parent fit pH5.5
nm
Conc.nM

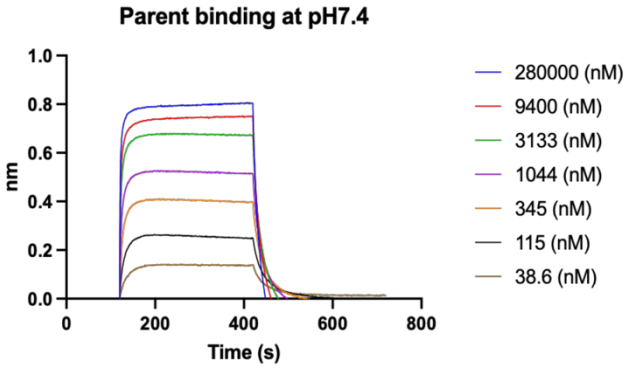
Parent binding at pH7.4
nm
Time (s)
280000 (nM)
9400 (nM)
3133 (nM)
1044 (nM)
345 (nM)
115 (nM)
38.6 (nM)

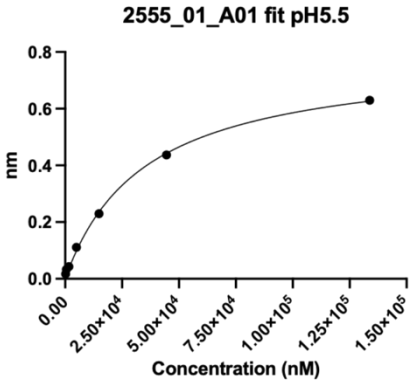
2555_01_A01 fit pH5.5
nm
Concentration (nM)

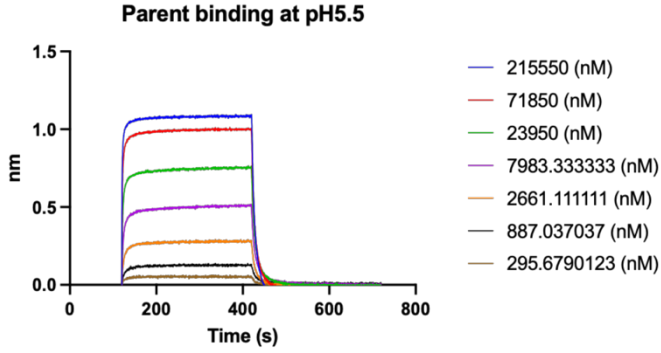
Parent binding at pH5.5
nm
Time (s)
215550 (nM)
71850 (nM)
23950 (nM)
7983.333333 (nM)
2661.111111 (nM)
887.037037 (nM)
295.6790123 (nM)

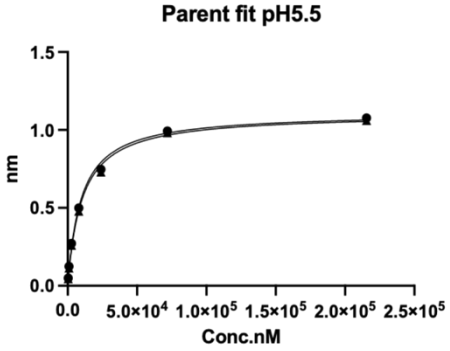
Parent fit pH5.5
nm
Conc.nM

Table Anti-Long-chain alpha-neurotoxin antibodies binding to bungarotoxin, steady-state analysis, one site-specific binding

	pH	*Rmax*	*Kd (nM)*	*Rmax*	*Kd (nM)*	*Degrees of Freedom*
Parent	7.4	0.7585	2934	0.6777 to 0.8455	1600 to 5252	5
Parent	5.5	1.111	9650	1.041 to 1.186	7363 to 12599	5
2555_01_A01	7.4	0.7833	2991	0.6851 to 0.9047	1931 to 4668	5
2555_01_A01	5.5	0.7902	34958	0.7213 to 0.8714	27186 to 45230	5
2555_01_A04	7.4	0.7823	1346	0.6685 to 0.9233	759.0 to 2391	4
2558_02_G09	7.4	0.6273	2385	0.5498 to 0.7242	1586 to 3623	5
2551_01_B11	7.4	0.6406	3583	0.5500 to 0.7638	2376 to 5537	5

Table Affinity kinetics of 2555_01_A01 antibody binding to cobratoxin n=1

Conc. (nM)	*Dissociation pH*	*Response*	*KD (M)*	*KD Error*	*kon(1/Ms)*	*kon Error*	*kdis(1/s)*	*kdis Error*	*RMax*	*RMax Error*	*Req*	*Req/Rmax(%)*	*Full X^2*	*Full R^2*
9.	7.4	0.0074	1.338E-08	2.687E-11	4.254E04	7.685E01	5.691E-04	4.997E-07	0.1503	0.0046	0.0605	40.2	8.2551	0.9988
81.	7.4	0.5685	1.338E-08	2.687E-11	4.254E04	7.685E01	5.691E-04	4.997E-07	1.3095	0.002	1.1239	85.8	8.2551	0.9988
27.	7.4	0.0995	1.338E-08	2.687E-11	4.254E04	7.685E01	5.691E-04	4.997E-07	0.5648	0.0019	0.3777	66.9	8.2551	0.9988
243.	7.4	1.1684	1.338E-08	2.687E-11	4.254E04	7.685E01	5.691E-04	4.997E-07	1.4293	0.0012	1.3547	94.8	8.2551	0.9988
730.	7.4	1.5815	1.338E-08	2.687E-11	4.254E04	7.685E01	5.691E-04	4.997E-07	1.5565	0.0005	1.5285	98.2	8.2551	0.9988
9.	5.5	0.0106	8.065E-07	5.379E-09	2.082E04	1.338E02	1.679E-02	2.991E-05	1.3889	0.149	0.0153	1.1	59.1936	0.9897
2200.	5.5	2.0827	8.065E-07	5.379E-09	2.082E04	1.338E02	1.679E-02	2.991E-05	2.676	0.0064	1.9582	73.2	59.1936	0.9897
730.	5.5	1.5771	8.065E-07	5.379E-09	2.082E04	1.338E02	1.679E-02	2.991E-05	3.1415	0.0136	1.4926	47.5	59.1936	0.9897
27.	5.5	0.1086	8.065E-07	5.379E-09	2.082E04	1.338E02	1.679E-02	2.991E-05	3.0974	0.0547	0.1003	3.2	59.1936	0.9897
243.	5.5	1.1443	8.065E-07	5.379E-09	2.082E04	1.338E02	1.679E-02	2.991E-05	4.6279	0.0277	1.0716	23.2	59.1936	0.9897
81.	5.5	0.565	8.065E-07	5.379E-09	2.082E04	1.338E02	1.679E-02	2.991E-05	5.5683	0.0407	1.848E-02	4.075E-05	59.1936	0.9897

Table Affinity kinetics of 2555_01_A01 antibody binding to cobratoxin n=2

Conc. (nM)	Cycle	*Response*	*KD (M)*	*KD Error*	*ka (1/Ms)*	*ka Error*	*kdis (1/s)*	*kdis Error*	*Rmax*	*Rmax Error*	*Req*	*Req/Rmax(%)*	*Full X^2*	*Full R^2*
9	7.4	0.1636	8.94E-10	3.38E-12	2.35E+05	5.94E+02	2.10E-04	5.88E-07	0.5339	0.0012	0.4856	91	1.2364	0.9979
3	7.4	0.0754	8.94E-10	3.38E-12	2.35E+05	5.94E+02	2.10E-04	5.88E-07	0.5859	0.0017	0.4514	77	1.2364	0.9979
81	7.4	0.4599	8.94E-10	3.38E-12	2.35E+05	5.94E+02	2.10E-04	5.88E-07	0.4735	0.0003	0.4684	98.9	1.2364	0.9979
27	7.4	0.281	8.94E-10	3.38E-12	2.35E+05	5.94E+02	2.10E-04	5.88E-07	0.4108	0.0006	0.3976	96.8	1.2364	0.9979
1	7.4	0.0239	8.94E-10	3.38E-12	2.35E+05	5.94E+02	2.10E-04	5.88E-07	0.481	0.0027	0.2539	52.8	1.2364	0.9979
3	5.5	0.0732	7.22E-09	2.56E-11	2.29E+05	6.68E+02	1.66E-03	3.34E-06	0.8067	0.003	0.2368	29.4	0.4313	0.9978
27	5.5	0.284	7.22E-09	2.56E-11	2.29E+05	6.68E+02	1.66E-03	3.34E-06	0.484	0.001	0.3819	78.9	0.4313	0.9978
81	5.5	0.467	7.22E-09	2.56E-11	2.29E+05	6.68E+02	1.66E-03	3.34E-06	0.5013	0.0005	0.4603	91.8	0.4313	0.9978
9	5.5	0.165	7.22E-09	2.56E-11	2.29E+05	6.68E+02	1.66E-03	3.34E-06	0.6165	0.0018	0.3421	55.5	0.4313	0.9978
1	5.5	0.0236	7.22E-09	2.56E-11	2.29E+05	6.68E+02	1.66E-03	3.34E-06	0.6388	0.0052	0.0777	12.2	0.4313	0.9978

Table Affinity kinetics of 2555_01_A01 antibody binding to elapitoxin n=1

Conc. (nM)	*Dissociation pH*	*Response*	*KD (M)*	*KD Error*	*kon(1/Ms)*	*kon Error*	*kdis(1/s)*	*kdis Error*	*RMax*	*RMax Error*	*Req/Rmax(%)*	*Full X^2*	*Full R^2*
9	7.4	0.0411	3.38E-08	1.84E-10	1.44E+04	6.94E+01	4.86E-04	1.23E-06	1.9281	0.0272	21.1	1.5744	0.9979
240	7.4	0.5589	3.38E-08	1.84E-10	1.44E+04	6.94E+01	4.86E-04	1.23E-06	1.2899	0.005	87.7	1.5744	0.9979
27	7.4	0.1088	3.38E-08	1.84E-10	1.44E+04	6.94E+01	4.86E-04	1.23E-06	1.77	0.0122	44.4	1.5744	0.9979
730	7.4	0.8641	3.38E-08	1.84E-10	1.44E+04	6.94E+01	4.86E-04	1.23E-06	1.0447	0.0022	95.6	1.5744	0.9979
2200	7.4	1.1566	3.38E-08	1.84E-10	1.44E+04	6.94E+01	4.86E-04	1.23E-06	1.145	0.0009	98.5	1.5744	0.9979
81	7.4	0.2573	3.38E-08	1.84E-10	1.44E+04	6.94E+01	4.86E-04	1.23E-06	1.519	0.0076	70.6	1.5744	0.9979
9	5.5	0.0388	5.25E-07	5.82E-09	1.18E+04	1.26E+02	6.18E-03	1.70E-05	2.6426	0.1521	1.7	1.8761	0.9929
730	5.5	0.8431	5.25E-07	5.82E-09	1.18E+04	1.26E+02	6.18E-03	1.70E-05	1.5082	0.011	58.2	1.8761	0.9929
81	5.5	0.2528	5.25E-07	5.82E-09	1.18E+04	1.26E+02	6.18E-03	1.70E-05	2.6451	0.0337	13.4	1.8761	0.9929
240	5.5	0.5493	5.25E-07	5.82E-09	1.18E+04	1.26E+02	6.18E-03	1.70E-05	2.1786	0.0222	31.4	1.8761	0.9929
27	5.5	0.1043	5.25E-07	5.82E-09	1.18E+04	1.26E+02	6.18E-03	1.70E-05	2.8706	0.0599	4.9	1.8761	0.9929
2200	5.5	1.1272	5.25E-07	5.82E-09	1.18E+04	1.26E+02	6.18E-03	1.70E-05	1.3102	0.005	80.7	1.8761	0.9929

Table Affinity kinetics of 2554_01_D11 antibody binding to cobratoxin n=1

Conc. (nM)	Dissociation pH	Response	KD (M)	KD Error	kon(1/Ms)	kon Error	kdis(1/s)	kdis Error	RMax	RMax Error	Req/Rmax(%)	Full X^2	Full R^2
3	5.5	0.0508	3.93E-09	1.43E-11	1.01E+05	3.25E+02	3.96E-04	6.65E-07	1.7653	0.0099	43.3	0.3247	0.9995
9	5.5	0.142	3.93E-09	1.43E-11	1.01E+05	3.25E+02	3.96E-04	6.65E-07	1.6038	0.0058	69.6	0.3247	0.9995
240	5.5	1.1722	3.93E-09	1.43E-11	1.01E+05	3.25E+02	3.96E-04	6.65E-07	1.2723	0.001	98.4	0.3247	0.9995
27	5.5	0.3033	3.93E-09	1.43E-11	1.01E+05	3.25E+02	3.96E-04	6.65E-07	1.209	0.0036	87.3	0.3247	0.9995
81	5.5	0.7404	3.93E-09	1.43E-11	1.01E+05	3.25E+02	3.96E-04	6.65E-07	1.2575	0.0026	95.4	0.3247	0.9995
0.33	7.4	0.0072	2.91E-09	1.18E-11	7.48E+04	2.40E+02	2.18E-04	5.43E-07	3.3448	0.0453	10.2	0.094	0.9997
1	7.4	0.0171	2.91E-09	1.18E-11	7.48E+04	2.40E+02	2.18E-04	5.43E-07	2.2007	0.0162	25.6	0.094	0.9997
3	7.4	0.0508	2.91E-09	1.18E-11	7.48E+04	2.40E+02	2.18E-04	5.43E-07	2.1721	0.0086	50.7	0.094	0.9997
9	7.4	0.081	2.91E-09	1.18E-11	7.48E+04	2.40E+02	2.18E-04	5.43E-07	1.1028	0.0039	75.5	0.094	0.9997
240	7.4	0.6848	2.91E-09	1.18E-11	7.48E+04	2.40E+02	2.18E-04	5.43E-07	0.8022	0.0009	98.8	0.094	0.9997
27	7.4	0.352	2.91E-09	1.18E-11	7.48E+04	2.40E+02	2.18E-04	5.43E-07	1.8198	0.0054	90.3	0.094	0.9997

Table Affinity kinetics of 2554_01_D11 antibody binding to elapitoxin n=1

Conc. (nM)	Dissociation pH	Response	KD (M)	KD Error	ka (1/Ms)	ka Error	kdis (1/s)	kdis Error	Rmax	Rmax Error	Req	Req/Rmax(%)	Full X^2	Full R^2
3	7.4	0.0695	7.83E-10	2.57E-12	1.81E+05	3.42E+02	1.42E-04	3.82E-07	0.7375	0.0015	0.5849	79.3	0.5461	0.9991
3	5.5	0.0682	1.65E-09	5.21E-12	2.04E+05	5.31E+02	3.37E-04	6.04E-07	0.8802	0.0025	0.5679	64.5	1.0783	0.9978
1	7.4	0.0203	7.83E-10	2.57E-12	1.81E+05	3.42E+02	1.42E-04	3.82E-07	0.7055	0.0024	0.3957	56.1	0.5461	0.9991
9	7.4	0.1505	7.83E-10	2.57E-12	1.81E+05	3.42E+02	1.42E-04	3.82E-07	0.6284	0.0011	0.5781	92	0.5461	0.9991
1	5.5	0.0196	1.65E-09	5.21E-12	2.04E+05	5.31E+02	3.37E-04	6.04E-07	0.3667	0.0029	0.1384	37.7	1.0783	0.9978
81	7.4	0.4481	7.83E-10	2.57E-12	1.81E+05	3.42E+02	1.42E-04	3.82E-07	0.4824	0.0003	0.4778	99	0.5461	0.9991
27	5.5	0.2778	1.65E-09	5.21E-12	2.04E+05	5.31E+02	3.37E-04	6.04E-07	0.4442	0.0008	0.4186	94.2	1.0783	0.9978
27	7.4	0.2811	7.83E-10	2.57E-12	1.81E+05	3.42E+02	1.42E-04	3.82E-07	0.501	0.0006	0.4869	97.2	0.5461	0.9991
9	5.5	0.1495	1.65E-09	5.21E-12	2.04E+05	5.31E+02	3.37E-04	6.04E-07	0.5645	0.0014	0.477	84.5	1.0783	0.9978
81	5.5	0.4529	1.65E-09	5.21E-12	2.04E+05	5.31E+02	3.37E-04	6.04E-07	0.4673	0.0003	0.458	98	1.0783	0.9978
3	5.5	0.0613	2.21E-09	7.22E-12	1.85E+05	5.06E+02	4.10E-04	7.34E-07	0.7802	0.0023	0.4491	57.6	0.3157	0.9985
81	5.5	0.4064	2.21E-09	7.22E-12	1.85E+05	5.06E+02	4.10E-04	7.34E-07	0.4295	0.0004	1.54E-02	97.3	0.3157	0.9985

81	7.4	0.388	9.31E-10	5.08E-12	1.74E+05	5.75E+02	1.62E-04	7.00E-07	0.4271	0.0004	1.42E-02	98.9	0.4829	0.9941
27	7.4	0.2383	9.31E-10	5.08E-12	1.74E+05	5.75E+02	1.62E-04	7.00E-07	0.4293	0.001	4.85E-03	96.7	0.4829	0.9941

Table Affinity kinetics of 2554_01_D11 antibody binding to bungarotoxin n=1

Conc. (nM)	Dissociation pH	Response	KD (M)	KD Error	ka (1/Ms)	ka Error	kdis (1/s)	kdis Error	Rmax	Rmax Error	Req	Req/Rmax(%)	Full X^2	Full R^2
2200	7.4	0.78293	1.22E-07	7.02E-10	9.46E+03	36.75318	1.16E-03	4.89E-06	0.79743	0.000808	0.755402	94.72954	7.250811	0.994266
3	5.5	-0.01463	4.78E-07	1.57E-09	8.11E+03	24.71515	3.88E-03	4.78E-06	1.15E-14	0.081645	7.19E-17	0.623661	3.203904	0.996896
3	7.4	-0.02466	1.22E-07	7.02E-10	9.46E+03	36.75318	1.16E-03	4.89E-06	2.23E-14	0.064275	5.34E-16	2.39232	7.250811	0.994266
9	5.5	-0.01301	4.78E-07	1.57E-09	8.11E+03	24.71515	3.88E-03	4.78E-06	7.87E-16	0.027354	1.45E-17	1.847934	3.203904	0.996896
9	7.4	-0.01599	1.22E-07	7.02E-10	9.46E+03	36.75318	1.16E-03	4.89E-06	2.23E-14	0.021582	1.53E-15	6.849249	7.250811	0.994266
27	5.5	0.0276	4.78E-07	1.57E-09	8.11E+03	24.71515	3.88E-03	4.78E-06	0.773283	0.009613	0.041341	5.346213	3.203904	0.996896
27	7.4	0.017039	1.22E-07	7.02E-10	9.46E+03	36.75318	1.16E-03	4.89E-06	0.192282	0.0074	0.034749	18.07214	7.250811	0.994266
81	5.5	0.107383	1.22E-07	7.02E-10	9.46E+03	36.75318	1.16E-03	4.89E-06	0.596012	0.003577	0.237348	39.82276	7.250811	0.994266
240	5.5	0.338879	4.78E-07	1.57E-09	8.11E+03	24.71515	3.88E-03	4.78E-06	1.260086	0.003781	0.421181	33.42477	3.203904	0.996896
81	5.5	0.125576	4.78E-07	1.57E-09	8.11E+03	24.71515	3.88E-03	4.78E-06	1.188259	0.004995	0.172171	14.48937	3.203904	0.996896
2200	5.5	0.806493	4.78E-07	1.57E-09	8.11E+03	24.71515	3.88E-03	4.78E-06	0.941964	0.00101	0.773823	82.14993	3.203904	0.996896
730	7.4	0.525642	1.22E-07	7.02E-10	9.46E+03	36.75318	1.16E-03	4.89E-06	0.681826	0.001526	0.583918	85.64042	7.250811	0.994266
730	5.5	0.54786	4.78E-07	1.57E-09	8.11E+03	24.71515	3.88E-03	4.78E-06	0.961063	0.002012	0.58076	60.42894	3.203904	0.996896

Table Affinity kinetics of 2551_01_A12 antibody binding to cobratoxin n=1

Conc. (nM)	Cycle	Response	KD (M)	KD Error	kon(1/Ms)	kon Error	kdis(1/s)	kdis Error	RMax	RMax Error	Req	Req/Rmax(%)	Full X^2	Full R^2
27	7.4	0.3789	4.19E-09	2.26E-11	9.19E+04	4.39E+02	3.85E-04	9.59E-07	1.6551	0.0071	1.4329	86.6	0.1808	0.9992
3	7.4	0.0503	4.19E-09	2.26E-11	9.19E+04	4.39E+02	3.85E-04	9.59E-07	1.7747	0.0113	0.7407	41.7	0.1808	0.9992
240	7.4	0.7174	4.19E-09	2.26E-11	9.19E+04	4.39E+02	3.85E-04	9.59E-07	0.7885	0.001	0.775	98.3	0.1808	0.9992
9	7.4	0.0946	4.19E-09	2.26E-11	9.19E+04	4.39E+02	3.85E-04	9.59E-07	1.0849	0.0057	0.7404	68.2	0.1808	0.9992
27	5.5	0.3392	6.17E-09	2.48E-11	1.15E+05	4.35E+02	7.07E-04	9.30E-07	1.2105	0.0042	0.9855	81.4	0.4844	0.9992
3	5.5	0.0547	6.17E-09	2.48E-11	1.15E+05	4.35E+02	7.07E-04	9.30E-07	1.6048	0.0117	0.5253	32.7	0.4844	0.9992
81	5.5	0.7921	6.17E-09	2.48E-11	1.15E+05	4.35E+02	7.07E-04	9.30E-07	1.2505	0.0029	1.162	92.9	0.4844	0.9992
240	5.5	1.184	6.17E-09	2.48E-11	1.15E+05	4.35E+02	7.07E-04	9.30E-07	1.2578	0.0011	1.2263	97.5	0.4844	0.9992
9	5.5	0.1558	6.17E-09	2.48E-11	1.15E+05	4.35E+02	7.07E-04	9.30E-07	1.5331	0.0067	0.9098	59.3	0.4844	0.9992

Table Affinity kinetics of 2551_01_A12 antibody binding to elapitoxin n=1

Conc. (nM)	Dissociation pH	Response	KD (M)	KD Error	ka (1/Ms)	ka Error	kdis (1/s)	kdis Error	Rmax	Rmax Error	Req	Req/Rmax(%)	Full X^2	Full R^2
1	5.5	0.026	9.73E-10	3.25E-12	1.96E+05	4.32E+02	1.91E-04	4.78E-07	0.5303	0.0027	0.2688	50.7	0.8545	0.9986
27	5.5	0.2821	9.73E-10	3.25E-12	1.96E+05	4.32E+02	1.91E-04	4.78E-07	0.4759	0.0007	0.4593	96.5	0.8545	0.9986
9	7.4	0.1601	5.58E-10	2.39E-12	2.15E+05	4.47E+02	1.20E-04	4.50E-07	0.5873	0.0011	0.553	94.2	0.8467	0.9987
1	7.4	0.0263	5.58E-10	2.39E-12	2.15E+05	4.47E+02	1.20E-04	4.50E-07	0.6992	0.0026	0.4487	64.2	0.8467	0.9987
9	5.5	0.1554	9.73E-10	3.25E-12	1.96E+05	4.32E+02	1.91E-04	4.78E-07	0.5571	0.0011	0.5028	90.2	0.8545	0.9986
3	7.4	0.0731	5.58E-10	2.39E-12	2.15E+05	4.47E+02	1.20E-04	4.50E-07	0.6515	0.0015	0.5493	84.3	0.8467	0.9987
81	5.5	0.4646	9.73E-10	3.25E-12	1.96E+05	4.32E+02	1.91E-04	4.78E-07	0.4947	0.0003	0.4888	98.8	0.8545	0.9986
81	7.4	0.4661	5.58E-10	2.39E-12	2.15E+05	4.47E+02	1.20E-04	4.50E-07	0.4899	0.0002	0.4866	99.3	0.8467	0.9987
3	5.5	0.0721	9.73E-10	3.25E-12	1.96E+05	4.32E+02	1.91E-04	4.78E-07	0.8192	0.002	0.6186	75.5	0.8545	0.9986

Table Affinity kinetics of 2551_01_A12 antibody binding to bungarotoxin n=1

Conc. (nM)	Cycle	Response	KD (M)	KD Error	ka (1/Ms)	ka Error	kdis (1/s)	kdis Error	Rmax	Rmax Error	Req	Req/Rmax(%)	Full X^2	Full R^2
240.	7.4	0.2932	2.108E-07	9.161E-10	1.504E04	5.893E01	3.171E-03	5.969E-06	0.6472	0.0022	0.3446	53.2	5.047	0.9945
2200.	7.4	0.7221	2.108E-07	9.161E-10	1.504E04	5.893E01	3.171E-03	5.969E-06	0.7556	0.0007	0.6895	91.3	5.047	0.9945
9.	5.5	-1.068E-02	6.437E-07	2.544E-09	1.139E04	4.293E01	7.333E-03	8.758E-06	0.	0.0288	0.	1.4	2.9791	0.9963
9.	7.4	-1.798E-02	2.108E-07	9.161E-10	1.504E04	5.893E01	3.171E-03	5.969E-06	0.	0.0167	0.	4.1	5.047	0.9945
2200.	5.5	0.7261	6.437E-07	2.544E-09	1.139E04	4.293E01	7.333E-03	8.758E-06	0.8932	0.0012	0.691	77.4	2.9791	0.9963
27.	7.4	0.0171	2.108E-07	9.161E-10	1.504E04	5.893E01	3.171E-03	5.969E-06	0.2111	0.0058	0.024	11.4	5.047	0.9945
730.	5.5	0.4811	2.108E-07	9.161E-10	1.504E04	5.893E01	3.171E-03	5.969E-06	0.6235	0.0012	0.4838	77.6	5.047	0.9945
81.	5.5	0.1094	6.437E-07	2.544E-09	1.139E04	4.293E01	7.333E-03	8.758E-06	1.0876	0.0054	0.1216	11.2	2.9791	0.9963
81.	7.4	0.1122	2.108E-07	9.161E-10	1.504E04	5.893E01	3.171E-03	5.969E-06	0.536	0.0029	0.1488	27.8	5.047	0.9945
3.	7.4	-1.674E-02	2.108E-07	9.161E-10	1.504E04	5.893E01	3.171E-03	5.969E-06	0.	0.0495	0.	1.4	5.047	0.9945
730.	5.5	0.4861	6.437E-07	2.544E-09	1.139E04	4.293E01	7.333E-03	8.758E-06	0.911	0.0023	0.4841	53.1	2.9791	0.9963
240.	5.5	0.2971	6.437E-07	2.544E-09	1.139E04	4.293E01	7.333E-03	8.758E-06	1.1633	0.0042	0.316	27.2	2.9791	0.9963
27.	5.5	0.0166	6.437E-07	2.544E-09	1.139E04	4.293E01	7.333E-03	8.758E-06	0.6337	0.0101	0.0255	4.0	2.9791	0.9963
3.	5.5	-1.248E-02	6.437E-07	2.544E-09	1.139E04	4.293E01	7.333E-03	8.758E-06	0.	0.0859	0.	0.5	2.9791	0.9963

Table Affinity kinetics of 2555_01_A04 antibody binding to cobratoxin n=1

Conc. (nM)	Dissociation pH	Response	KD (M)	KD Error	kon(1/Ms)	kon Error	kdis(1/s)	kdis Error	RMax	RMax Error	Req	Req/Rmax(%)	Full X^2	Full R^2
730	7.4	0.915	3.19E-08	1.76E-10	1.55E+04	7.57E+01	4.92E-04	1.24E-06	1.0787	0.0022	1.0335	95.8	1.7507	0.9978
2200	7.4	1.1912	3.19E-08	1.76E-10	1.55E+04	7.57E+01	4.92E-04	1.24E-06	1.1741	0.0009	1.1574	98.6	1.7507	0.9978
240	7.4	0.6063	3.19E-08	1.76E-10	1.55E+04	7.57E+01	4.92E-04	1.24E-06	1.3335	0.0051	1.1772	88.3	1.7507	0.9978
27	7.4	0.1128	3.19E-08	1.76E-10	1.55E+04	7.57E+01	4.92E-04	1.24E-06	1.8126	0.0124	0.8314	45.9	1.7507	0.9978
9	7.4	0.0416	3.19E-08	1.76E-10	1.55E+04	7.57E+01	4.92E-04	1.24E-06	1.9853	0.0271	0.4372	22	1.7507	0.9978
81	7.4	0.2778	3.19E-08	1.76E-10	1.55E+04	7.57E+01	4.92E-04	1.24E-06	1.5428	0.0077	1.1072	71.8	1.7507	0.9978
27	5.5	0.1118	1.48E-07	1.27E-09	1.65E+04	1.38E+02	2.43E-03	4.83E-06	1.9688	0.0277	0.3045	15.5	3.6746	0.9918
2200	5.5	1.1884	1.48E-07	1.27E-09	1.65E+04	1.38E+02	2.43E-03	4.83E-06	1.1785	0.0021	1.1044	93.7	3.6746	0.9918
81	5.5	0.2764	1.48E-07	1.27E-09	1.65E+04	1.38E+02	2.43E-03	4.83E-06	1.7002	0.0157	0.6025	35.4	3.6746	0.9918
240	5.5	0.6041	1.48E-07	1.27E-09	1.65E+04	1.38E+02	2.43E-03	4.83E-06	1.4643	0.0101	0.9067	61.9	3.6746	0.9918
9	5.5	0.0414	1.48E-07	1.27E-09	1.65E+04	1.38E+02	2.43E-03	4.83E-06	1.337	0.0658	0.0768	5.7	3.6746	0.9918
730	5.5	0.913	1.48E-07	1.27E-09	1.65E+04	1.38E+02	2.43E-03	4.83E-06	1.1297	0.0045	0.9397	83.2	3.6746	0.9918

Table Affinity kinetics of 2555_01_A04 antibody binding to elapitoxin n=1

Conc. (nM)	Dissociation pH	Response	KD (M)	KD Error	ka (1/Ms)	ka Error	kdis (1/s)	kdis Error	Rmax	Rmax Error	Req	Req/Rmax(%)	Full X^2	Full R^2
81	5.5	0.5294	9.49E-10	2.44E-12	2.61E+05	4.87E+02	2.48E-04	4.40E-07	0.5389	0.0002	0.5326	98.8	0.9559	0.9987
1	5.5	0.0301	9.49E-10	2.44E-12	2.61E+05	4.87E+02	2.48E-04	4.40E-07	0.5967	0.0023	0.3062	51.3	0.9559	0.9987
1	7.4	0.0309	4.38E-10	2.19E-12	2.64E+05	6.04E+02	1.15E-04	5.13E-07	0.6269	0.0027	0.436	69.5	1.4463	0.9982
81	7.4	0.5251	4.38E-10	2.19E-12	2.64E+05	6.04E+02	1.15E-04	5.13E-07	0.5318	0.0002	0.5289	99.5	1.4463	0.9982
27	7.4	0.3441	4.38E-10	2.19E-12	2.64E+05	6.04E+02	1.15E-04	5.13E-07	0.4715	0.0006	0.464	98.4	1.4463	0.9982
3	7.4	0.093	4.38E-10	2.19E-12	2.64E+05	6.04E+02	1.15E-04	5.13E-07	0.7254	0.0018	0.633	87.3	1.4463	0.9982
3	5.5	0.092	9.49E-10	2.44E-12	2.61E+05	4.87E+02	2.48E-04	4.40E-07	0.8202	0.0016	0.6231	76	0.9559	0.9987
9	5.5	0.2011	9.49E-10	2.44E-12	2.61E+05	4.87E+02	2.48E-04	4.40E-07	0.6053	0.001	0.5476	90.5	0.9559	0.9987
9	7.4	0.203	4.38E-10	2.19E-12	2.64E+05	6.04E+02	1.15E-04	5.13E-07	0.6206	0.0012	0.5918	95.4	1.4463	0.9982
27	5.5	0.3387	9.49E-10	2.44E-12	2.61E+05	4.87E+02	2.48E-04	4.40E-07	0.4966	0.0005	1.36E-05	96.6	0.9559	0.9987

Table Affinity kinetics of 2551_01_B11 antibody binding to cobratoxin n=1

Conc. (nM)	Dissociation pH	Response	KD (M)	KD Error	kon(1/Ms)	kon Error	kdis(1/s)	kdis Error	RMax	RMax Error	Req	Req/Rmax(%)	Full X^2	Full R^2
9	5.5	0.1144	1.77E-08	9.81E-11	9.67E+04	5.23E+02	1.71E-03	2.00E-06	1.3822	0.0095	0.4655	33.7	0.6331	0.998
81	5.5	0.6283	1.77E-08	9.81E-11	9.67E+04	5.23E+02	1.71E-03	2.00E-06	1.1295	0.0042	0.9267	82	0.6331	0.998
3	5.5	0.0393	1.77E-08	9.81E-11	9.67E+04	5.23E+02	1.71E-03	2.00E-06	1.4934	0.0192	0.2162	14.5	0.6331	0.998
1	5.5	0.0144	1.77E-08	9.81E-11	9.67E+04	5.23E+02	1.71E-03	2.00E-06	1.8554	0.0526	0.0991	5.3	0.6331	0.998
240	5.5	1.014	1.77E-08	9.81E-11	9.67E+04	5.23E+02	1.71E-03	2.00E-06	1.1205	0.0019	1.0435	93.1	0.6331	0.998
27	5.5	0.2449	1.77E-08	9.81E-11	9.67E+04	5.23E+02	1.71E-03	2.00E-06	1.0524	0.0056	0.6353	60.4	0.6331	0.998
0.33	7.4	0.004	6.85E-09	3.81E-11	6.76E+04	3.51E+02	4.62E-04	9.23E-07	0.1711	0.0649	0.0079	4.6	0.1106	0.9993
9	7.4	0.0557	6.85E-09	3.81E-11	6.76E+04	3.51E+02	4.62E-04	9.23E-07	0.8751	0.0051	0.497	56.8	0.1106	0.9993
3	7.4	0.0352	6.85E-09	3.81E-11	6.76E+04	3.51E+02	4.62E-04	9.23E-07	1.602	0.0111	0.4881	30.5	0.1106	0.9993
240	7.4	0.5442	6.85E-09	3.81E-11	6.76E+04	3.51E+02	4.62E-04	9.23E-07	0.6629	0.0013	0.6445	97.2	0.1106	0.9993
27	7.4	0.2748	6.85E-09	3.81E-11	6.76E+04	3.51E+02	4.62E-04	9.23E-07	1.5911	0.0077	1.2692	79.8	0.1106	0.9993

Table Affinity kinetics of 2554_01_E01 antibody binding to cobratoxin n=1

Conc. (nM)	Dissocition pH	Response	KD (M)	KD Error	kon(1/Ms)	kon Error	kdis(1/s)	kdis Error	RMax	RMax Error	Req	Req/Rmax(%)	Full X^2	Full R^2
81	7.4	0.5624	7.75E-09	4.54E-11	3.50E+04	1.56E+02	2.71E-04	1.03E-06	1.4936	0.0056	1.3632	91.3	1.1514	0.9983
27	7.4	0.2652	7.75E-09	4.54E-11	3.50E+04	1.56E+02	2.71E-04	1.03E-06	1.8323	0.0085	1.4237	77.7	1.1514	0.9983
729	7.4	1.1446	7.75E-09	4.54E-11	3.50E+04	1.56E+02	2.71E-04	1.03E-06	1.1575	0.0009	1.1453	98.9	1.1514	0.9983
9	7.4	0.104	7.75E-09	4.54E-11	3.50E+04	1.56E+02	2.71E-04	1.03E-06	2.1203	0.0132	1.1394	53.7	1.1514	0.9983
243	7.4	0.8627	7.75E-09	4.54E-11	3.50E+04	1.56E+02	2.71E-04	1.03E-06	1.1406	0.0026	1.1053	96.9	1.1514	0.9983
27	5.5	0.256	2.70E-08	1.43E-10	3.58E+04	1.81E+02	9.65E-04	1.57E-06	2.0021	0.0108	1.0017	50	1.5477	0.9973
81	5.5	0.5544	2.70E-08	1.43E-10	3.58E+04	1.81E+02	9.65E-04	1.57E-06	1.5854	0.0068	1.1894	75	1.5477	0.9973
9	5.5	0.102	2.70E-08	1.43E-10	3.58E+04	1.81E+02	9.65E-04	1.57E-06	2.2002	0.017	0.5506	25	1.5477	0.9973
243	5.5	0.853	2.70E-08	1.43E-10	3.58E+04	1.81E+02	9.65E-04	1.57E-06	1.1458	0.0031	1.0314	90	1.5477	0.9973
3	5.5	0.0372	2.70E-08	1.43E-10	3.58E+04	1.81E+02	9.65E-04	1.57E-06	2.2326	0.0392	0.2235	10	1.5477	0.9973
729	5.5	1.1394	2.70E-08	1.43E-10	3.58E+04	1.81E+02	9.65E-04	1.57E-06	1.1609	0.0012	1.1195	96.4	1.5477	0.9973

Table Affinity kinetics of 2554_01_E01 antibody binding to elapitoxin n=1

Conc. (nM)	Dissocition pH	Response	KD (M)	KD Error	ka (1/Ms)	ka Error	kdis (1/s)	kdis Error	Rmax	Rmax Error	Req	Req/Rmax(%)	Full X^2	Full R^2	SSG KD	SSG Rmax	SSG R^2
9	7.4	0.1285	8.90E-10	3.66E-12	1.75E+05	4.41E+02	1.56E-04	5.08E-07	0.5728	0.0013	0.5213	91	0.7118	0.9984	6.19E-10	0.5207	0.3912
3	5.5	0.0613	2.21E-09	5.95E-12	1.89E+05	4.42E+02	4.18E-04	5.53E-07	0.7693	0.002	0.4429	57.6	0.648	0.9983	6.19E-10	0.5207	0.3912
81	5.5	0.4064	2.21E-09	5.95E-12	1.89E+05	4.42E+02	4.18E-04	5.53E-07	0.4291	0.0003	0.4177	97.3	0.648	0.9983	6.19E-10	0.5207	0.3912
81	1	0.388	8.90E-10	3.66E-12	1.75E+05	4.41E+02	1.56E-04	5.08E-07	0.4249	0.0003	0.4203	98.9	0.7118	0.9984	6.19E-10	0.5207	0.3912
27	1	0.2383	8.90E-10	3.66E-12	1.75E+05	4.41E+02	1.56E-04	5.08E-07	0.4253	0.0007	0.4118	96.8	0.7118	0.9984	6.19E-10	0.5207	0.3912
1	7.4	0.0204	2.21E-09	5.95E-12	1.89E+05	4.42E+02	4.18E-04	5.53E-07	0.2869	0.0025	0.0893	31.1	0.648	0.9983	6.19E-10	0.5207	0.3912
1	7.4	0.0228	8.90E-10	3.66E-12	1.75E+05	4.41E+02	1.56E-04	5.08E-07	0.6927	0.003	0.3664	52.9	0.7118	0.9984	6.19E-10	0.5207	0.3912
9	5.5	0.1271	2.21E-09	5.95E-12	1.89E+05	4.42E+02	4.18E-04	5.53E-07	0.4962	0.0011	0.3984	80.3	0.648	0.9983	6.19E-10	0.5207	0.3912
3	7.4	0.0624	8.90E-10	3.66E-12	1.75E+05	4.41E+02	1.56E-04	5.08E-07	0.7263	0.002	0.5601	77.1	0.7118	0.9984	6.19E-10	0.5207	0.3912
27	5.5	0.2348	2.21E-09	5.95E-12	1.89E+05	4.42E+02	4.18E-04	5.53E-07	0.4035	0.0006	0.3729	92.4	0.648	0.9983	6.19E-10	0.5207	0.3912

Table Affinity kinetics of 2558_2_G09 antibody binding to cobratoxin n=1

Conc. (nM)	Dissociation pH	Response	KD (M)	KD Error	kon(1/Ms)	kon Error	kdis(1/s)	kdis Error	RMax	RMax Error	Req	Req/Rmax(%)	Full X^2	Full R^2
0.33	7.4	0.0047	3.41E-09	1.43E-11	1.10E+05	4.01E+02	3.73E-04	7.67E-07	1.8703	0.0479	0.1652	8.8	0.2015	0.9994
1	7.4	0.0212	3.41E-09	1.43E-11	1.10E+05	4.01E+02	3.73E-04	7.67E-07	1.8287	0.0171	0.4149	22.7	0.2015	0.9994
240	7.4	0.7516	3.41E-09	1.43E-11	1.10E+05	4.01E+02	3.73E-04	7.67E-07	0.7975	0.0006	0.7863	98.6	0.2015	0.9994
3	7.4	0.0591	3.41E-09	1.43E-11	1.10E+05	4.01E+02	3.73E-04	7.67E-07	1.8448	0.0087	0.8638	46.8	0.2015	0.9994
9	7.4	0.1109	3.41E-09	1.43E-11	1.10E+05	4.01E+02	3.73E-04	7.67E-07	1.1293	0.0044	0.8192	72.5	0.2015	0.9994
27	7.4	0.4293	3.41E-09	1.43E-11	1.10E+05	4.01E+02	3.73E-04	7.67E-07	1.5936	0.0051	1.415	88.8	0.2015	0.9994
1	5.5	0.0244	8.51E-09	5.30E-11	1.58E+05	9.56E+02	1.35E-03	2.07E-06	1.6577	0.0475	0.1743	10.5	1.6919	0.997
240	5.5	1.2709	8.51E-09	5.30E-11	1.58E+05	9.56E+02	1.35E-03	2.07E-06	1.2694	0.0015	1.2259	96.6	1.6919	0.997
3	5.5	0.0609	8.51E-09	5.30E-11	1.58E+05	9.56E+02	1.35E-03	2.07E-06	1.4233	0.018	1.82E-03	0.371	26.1	0.997
81	5.5	0.8982	8.51E-09	5.30E-11	1.58E+05	9.56E+02	1.35E-03	2.07E-06	1.1976	0.0038	1.42E-02	1.0837	90.5	0.997
9	5.5	0.1843	8.51E-09	5.30E-11	1.58E+05	9.56E+02	1.35E-03	2.07E-06	1.3754	0.0097	2.77E-03	0.707	51.4	0.997
27	5.5	0.4106	8.51E-09	5.30E-11	1.58E+05	9.56E+02	1.35E-03	2.07E-06	1.1374	0.006	5.62E-03	0.8649	76	0.997

Table Affinity kinetics of 2558_2_G09 antibody binding to elapitoxin n=1

Conc. (nM)	Dissociation pH	Response	KD (M)	KD Error	ka (1/Ms)	ka Error	kdis (1/s)	kdis Error	Rmax	RMax Error	Req	Req/Rmax(%)	Full X^2	Full R^2
27	5.5	0.2629	1.99E-09	4.69E-12	2.39E+05	4.95E+02	4.76E-04	5.35E-07	0.405	0.0005	0.3772	93.1	0.7138	0.9983
3	7.4	0.0665	6.20E-10	2.51E-12	2.34E+05	5.11E+02	1.45E-04	4.96E-07	0.5562	0.0014	0.4609	82.9	0.995	0.9985
9	5.5	0.1509	1.99E-09	4.69E-12	2.39E+05	4.95E+02	4.76E-04	5.35E-07	0.5062	0.001	0.4145	81.9	0.7138	0.9983
9	7.4	0.1603	6.20E-10	2.51E-12	2.34E+05	5.11E+02	1.45E-04	4.96E-07	0.5396	0.0011	0.5048	93.6	0.995	0.9985
1	5.5	0.0209	6.20E-10	2.51E-12	2.34E+05	5.11E+02	1.45E-04	4.96E-07	0.5475	0.0024	0.338	61.7	0.995	0.9985
27	7.4	0.2856	6.20E-10	2.51E-12	2.34E+05	5.11E+02	1.45E-04	4.96E-07	0.4168	0.0006	0.4074	97.8	0.995	0.9985
81	5.5	0.447	1.99E-09	4.69E-12	2.39E+05	4.95E+02	4.76E-04	5.35E-07	0.4493	0.0002	0.4385	97.6	0.7138	0.9983
81	7.4	0.4833	6.20E-10	2.51E-12	2.34E+05	5.11E+02	1.45E-04	4.96E-07	0.4909	0.0002	0.4871	99.2	0.995	0.9985
3	5.5	0.0644	1.99E-09	4.69E-12	2.39E+05	4.95E+02	4.76E-04	5.35E-07	0.639	0.0015	0.3841	60.1	0.7138	0.9983
1	7.4	0.0195	1.99E-09	4.69E-12	2.39E+05	4.95E+02	4.76E-04	5.35E-07	0.7335	0.0026	0.2452	33.4	0.7138	0.9983